
University of Southern Queensland

Faculty of Engineering & Surveying

**PHD DISSERTATION**

# WIRELESS NETWORK CODING FOR MULTI-HOP RELAY CHANNELS

Gengkun Wang

Student Number: 0061003974

**Principal Supervisor**

A/Prof. Wei Xiang

**Co-Supervisor**

A/Prof. Paul Wen

March, 2013

# Abstract

Future wireless communication systems are required to meet growing demands for high spectral efficiency, low energy consumption and high mobility. The advent of wireless network coding (WNC) has offered a new opportunity to improve network throughput and transmission reliability by exploiting interference in intermediate relays. Combined with network coding and self-information cancelation, WNC for two-way relay channels (TWRCs) has come to the forefront.

This dissertation focuses on exploiting WNC in multi-hop two-way relay channels (MH-TRCs). Particularly, a multi-hop wireless network coding (MH-WNC) scheme is designed for the generalized $L$-node $K$-message MH-TRC. Theoretical studies on the network throughput and performance bounds achieved by the MH-WNC scheme with different relaying strategies (i.e., amplify-and-forward (AF) and compute-and-forward (CPF)) are carried out. Furthermore, by introducing different numbers of transmission time intervals into the MH-WNC, a multiple-time-interval (Multi-TI) MH-WNC is proposed to determine an optimal MH-WNC which can achieve the best outage performance for all-scale MH-TRCs. Finally, this study extends the research on WNC one step forward from two-user networks to multi-user networks. An extended CPF joint with a dominated solution for maximizing the overall computation rate is proposed for the multi-way relay channel (mRC) in the last chapter.

The contributions of this dissertation are multifold. First, the proposed MH-WNC scheme with fixed two transmission time intervals can achieve a significantly improved network throughput compared to the non-network coding (Non-NC) scheme in the generalized $L$-node $K$-message MH-TRC. Theoretical results are derived for both multi-hop analog network coding (MH-ANC) and multi-hop compute-and-forward (MH-CPF). Moreover, both theoretical and numerical re-

sults demonstrate that the two MH-WNC schemes can be applied to different scale MH-TRCs to achieve a better outage performance compared to the conventional Non-NC scheme (i.e., MH-ANC for the non-regenerative MH-TRC with a small number of nodes, and MH-CPF for the regenerative MH-TRC with a large number of nodes.). Furthermore, a Multi-TI MH-WNC scheme is generalized with a special binary-tree model and characteristic matrix. The determined optimal MH-WNC scheme is able to provide the best outage performance and outperform the Non-NC scheme in all scale MH-TRCs. Last but not least, this dissertation provides a preliminary investigation of WNC in mRCs. The proposed dominated solution for maximizing the overall computation rate can ensure that all the nodes in the mRC successfully recover their required messages. Moreover, the extended CPF strategy is proven superior to Non-NC in the mRC with a small number of users.

# Certification of Dissertation

I certify that the ideas, designs and experimental work, results, analyses and conclusions set out in this dissertation are entirely my own effort, except where otherwise indicated and acknowledged.
I further certify that the work is original and has not been previously submitted for assessment in any other course or institution, except where specifically stated.

_____ / /

Gengkun Wang, Candidate

_____ / /

A/Prof. Wei Xiang, Principal supervisor

_____ / /

A/Prof. Peng(Paul) Wen, Associate supervisor

# Acknowledgments

First, I would like to express my deepest gratitude to A/Prof. Wei Xiang, my principal supervisor for his endless commitment to directing the research and invaluable guidance. Without his continuous support, this thesis would not have been completed.

I am also thankful to Prof. Jinhong Yuan from UNSW, for his instructive discussions and constructive suggestions to my thesis. I would also like to thank A/Prof. Peng (Paul) Wen, my associate supervisor, for his support during my PhD research.

I would like thank the Chinese Scholarship Council for supporting my study at USQ during these three years. In addition, a special thank to all my friends and colleagues at USQ.

Last but no least, I would like to dedicate this work to my parents. I am greatly indebted to them for their unconditional support, love and encouragement.

Gengkun Wang

*University of Southern Queensland*

*March 2013*

# List of publications

The following publications were produced during the period of candidature:

[1] Gengkun Wang, Wei Xiang, Jinhong Yuan, and Tao Huang, "Outage performance of Analog Network Coding in Generalized Two-Way Multi-Hop Networks," in *Proc. IEEE Wireless Communications and Networking Conference*, Cancun, Mexico, Mar. 2011, pp. 759-764.

This paper was awarded the Best Paper Award by IEEE WCNC 2011, which is one of world's three most prestigious conferences in communication technologies.

[2] Gengkun Wang, Wei Xiang, Jinhong Yuan, and Tao Huang, "Outage Analysis of Non-Regenerative Analog Network Coding for Two-Way Multi-Hop Networks," *IEEE Commun. Lett.*, vol. 15, pp. 662 - 664, May 2011.

The work in the paper is presented in Chapter 4.

[3] Gengkun Wang, Wei Xiang, and Jinhong Yuan, "Multi-Hop Compute-and-Forward for Generalized Two-Way Relay Channels," accepted by *Trans. Emerging Tel. Tech. (formerly known as European Transactions on Telecommunications (ETT)).*

The work in the paper is presented in Chapter 5.

[4] Gengkun Wang, Wei Xiang, and Jinhong Yuan, "Outage Performance for Compute-and-Forward in Generalized Multi-Way Relay Channels," *IEEE Commun. Lett.*, vol. 16, pp. 2099 - 2102, Dec 2012.

The work in the paper is presented in Chapter 7.

# Contents

# List of Figures

# List of Tables

# Acronyms & Abbreviations

| | |
|---|---|
| AF | Amplify-and-forward |
| ANC | Analog network coding |
| AWGN | Additive white Gaussian noise |
| BER | Bit-error-rate |
| BPSK | Binary phase-shift keying |
| BS | Base station |
| BSC | Binary symmetric channel |
| CDMA | Code division multiple access |
| CDNC | Channel decoding network coding |
| CF | Compress-and-forward |
| CPF | Compute-and-forward |
| CSI | Channel state information |
| DF | Decode-and-forward |
| EF | Estimate-and-forward |
| FDMA | Frequency division multiple access |
| FFNC | Finite field network coding |
| GF | Galois field |
| LDPC | Low-density parity-check |
| LLL | Lenstra-Lenstra-Lovsz |
| LNC | Linear network coding |
| LTE | Long-term evolution |
| MAC | Multiple-access channel |
| MH-ANC | Multi-hop analog network coding |
| MH-CPF | Multi-hop compute-and-forward |

| | |
|---|---|
| MH-TRC | Multi-hop two-way relay channel |
| MH-WNC | Multi-hop wireless network coding |
| MIMO | Multi-input multi-output |
| ML | Maximum likelihood |
| mRC | Multi-way relay channel |
| MS | Mobile station |
| NC | Network coding |
| Non-NC | Non-network coding |
| P2P | Peer-to-peer |
| PNC | Physical-layer network coding |
| QPSK | Quadrature phase-shift keying |
| RA | Repeat accumulate |
| RLNC | Random linear network coding |
| SNR | Signal-noise-ratio |
| SVP | Shortest vector problem |
| TDMA | Time division multiple access |
| TI | Transmission time interval |
| TWRC | Two-way relay channel |
| WNC | Wireless network coding |
| XOR | Exclusive or |

# Chapter 1

# Introduction

Wireless communications are increasingly dominating communication technologies in their various forms. They provide the advantages of mobility, global internet connectivity, distributed sensing, and so on. Future mobile and wireless communication systems are required to meet the needs, requirements and interests of users and society as a whole [1]. This will require an increase in spectral efficiency, energy consumption and mobility far beyond those of second or third generation systems.

Much research has been carried out to enhance the spectral efficiency and data rate of next-generation wireless communication systems. Among all these approaches, relay-based wireless communication systems have attracted a great deal of attention thanks to their potential in extending cell coverage and reducing power consumption [2]. In the last few decades, multi-hop networks, such as wireless sensor networks [3], wireless mesh networks [4], mobile ad hoc networks [5], vehicular ad hoc networks [6], have emerged as promising approaches to provide more convenient wireless communications due to their extended cover range, easy deployment and low costs.

Relaying is one of the features being proposed for the fourth generation (4G) long-term evolution (LTE) advanced system [7] [8] [9]. Unlike the use of a repeater which re-broadcasts the signal, LTE relays actually receive, demodulate and decode the data, apply any error correction to it and then re-transmitting a new signal. The LTE relay is a fixed relay, that relays messages between the base station (BS) and mobile stations (MSs) through multi-hop communications [10].

There are a number of scenarios where the LTE relay will be advantageous, such as increasing network density, network coverage extension, and rapid network roll-out. However, despite these advantages, multi-hop wireless relay communications require an increase of time slots to transmit data in a multi-hop manner [11]. Most significant of these is the time resource. For example, in a two-hop relay network, two time slots are required to transmit a message via the relay. In wireless multi-hop relay communications, information is conveyed through a series of intermediate relays in a conventional hop-by-hop and message-by-message manner, which limits the network throughput, and thus the data rate of the system.

Recently, the advent of network coding (NC) has offered a new opportunity to improve network throughput and transmission reliability by exploiting interference in intermediate relays. The concept of NC was originally introduced in [12] in 2000, when a simple but important discovery was made. It was observed that relays can not only forward but also combine the incoming messages for generating the message on the outgoing links. The idea was first used in wired networks, and then exploited to wireless networks as wireless network coding (WNC) [13–15].

This study focuses on exploiting WNC in multi-hop relay channels and multi-way relay channels, along with a generalized transmission scheme and theoretical studies. The research outcome of this project can be further implemented to improve the network throughput, outage performance and data rate of next-generation mobile and wireless communication systems.

In the next sections, the motivations of this project, and the primary contributions in this dissertation are presented.

## 1.1 Motivations

Combined with network coding and self-information cancelation, WNC for the two-way relay channel (TWRC) has come to the forefront [16–19]. WNC has been proven to double the system capacity [20] achieved by Non-NC in the single relay TWRC. There has been a large body of work on WNC and its applications in other wireless relay networks, such as multi-hop relay networks [13], multiple

access channels [21], and multi-cast channels [22]. The performance (including outage probability, bit-error-rate (BER) and maximum sum-rate) of WNC in the single relay TWRC has been widely studied [23–26].

Multi-hop two-way relay networks are wireless networks using two or more wireless hops to exchange messages between two end users. These can be considered as the generalized TWRC. The use of time or frequency in this type of network is different from that of single-hop networks because the time or frequency that each hop uses generally does not overlap and interfere. Messages are transmitted hop-by-hop in the multi-hop network, causing delays [27,28] and reducing the spectrum efficiency of message delivery. The traditional hop-by-hop and message-by-message transmission scheme suffers from severe low spectrum efficiency with the increased number of nodes and messages.

Inspired by the significant improvement of WNC in network throughput in the canonical single relay TWRC, this study exploits WNC into the generalized multi-hop two-way relay channel (MH-TRC) to improve the spectrum efficiency and reduce communication delays. Moreover, according to different strategies applied at the relay, WNC can be categorized into analog network coding (ANC) [29,30] and physical-layer network coding (PNC) [20]. Therefore, the MH-WNC schemes corresponding to the non-regenerative and regenerative MH-TRCs are designed in this research. The performance of the proposed MH-WNC schemes will be analyzed to demonstrate their superiority to the non-network coding (Non-NC) scheme.

Recently, Nazer and Gastpar proposed a new compute-and-forward (CPF) scheme for reliable PNC [31], where relays compute and forward linear combinations of user messages to destinations. Given a sufficient number of linear combinations, the destinations can solve for their desired messages. The established "computation rate" is proven to achieve significant improvements over conventional relaying schemes in the multiple-access channel (MAC). There have been a number of works on CPF and its implementation [32–34], however there are no published research results on the implementation of CPF to the TWRC, let alone the MH-TRC. Inspired by the advantage of the computation rate, in this study, CPF is implemented to the generalized MH-TRC to improve the achievable rate

of the network, thus improving the outage performance.

The work published in [35] and [36] showed that the multi-hop wireless network coding (MH-WNC) scheme with fixed two transmission time intervals is unable to outperform Non-NC for all-scale MH-TRCs, i.e., the multi-hop analog network coding (MH-ANC) [35] can only outperform Non-NC in small scale MH-TRCs, while the multi-hop compute-and-forward (MH-CPF) [36] has better outage performance than Non-NC in the MH-TRCs with a large number of nodes. In view of this fact, by generalizing the number of transmission time intervals, a Multi-TI MH-WNC scheme is proposed to investigate the relationship between the number of time intervals and outage performance. The aim of this work is to determine an optimal MH-WNC scheme which can achieve the best outage performance for all-scale MH-TRCs.

On the application of WNC to wireless relay channels, the two-user two-way relay channel is the simplest and most popular network. However, when extending the two-user case to the multi-user case, most exiting WNC schemes are not directly applicable (such as ANC, "standard" PNC). The proposed CPF in [31] offered a solution for a reliable WNC in multi-user multi-relay networks, where the relay can decode successive linear equations and pass them to the destination. In view of this fact, this research extends the original CPF to multi-user relay networks, such as the multi-way relay channel (mRC).

The idea of the mRC was first introduced by Gunduz *et al* in [37], in which multiple users exchanged messages with the help of one relay terminal. Traditionally, the relay conveys seperate messages for each pair of users. For example, the relay conveys the message from user $U_1$ to user $U_2$ in the first two time slots, then convey the message from user $U_2$ to user $U_1$ in the next two time slots, and so forth. This relaying scheme requires significant amounts of time resource, and limits the channel use rate. By extending the original CPF to the mRC, it is able to improve the network throughput and channel use rate. However, different from the multi-user multi-relay network on which the original CPF was based, there is only one relay in the mRC. In the application of CPF to mRC, there comes the issue of how to ensure the linear independent condition while maximizing the overall computation rate upon one reception. Therefore, the extended CPF

joined with a novel dominated solution will be designed to realize the application of CPF in the mRC and improve the outage performance.

## 1.2 Contributions

The key idea underlying this design is to extend wireless network coding from the canonical single relay two-way relay network and MAC to multi-hop and multi-user relay-based wireless networks. This project proposes new designs of WNC to achieve higher performance in the MH-TRC, and further the mRC. Specifically, the contributions in this project can be summarized as follows:

- **Wireless Network Coding for Multi-Hop Two-Way Relay Networks:** A general MH-WNC scheme for the generalized $L$-node $K$-message MH-TRC is designed. It is proven to significantly improve the network throughput compared to the Non-NC scheme. Specifically, the transmission scheme is generalized with detailed transmission events at each node in different time slots. The transmission pattern is presented by a designed grid chart in Chapter 3.

- **Multi-Hop Analog Network Coding:** The MH-ANC scheme, where the AF strategy is applied at relay nodes, is analyzed in Chapter 4. The performance of MH-ANC lies on the end-to-end signal-noise-ratio (SNR) of the system. However, due to the bi-directional transmission, the noise propagation increases exponentially with the increase in the numbers of nodes and messages. In order to overcome the complexity issue, two different recursive approaches are proposed to obtain the received SNR of each message. More precisely, the forward recursive approach is designed for the MH-TRC with relatively small numbers of nodes and messages, while the backward recursive approach can be applied to the large scale MH-TRCs. The closed-form expressions of outage probabilities for both Non-NC and MH-ANC schemes are derived. Numerical results demonstrate that the proposed MH-ANC has better outage performance than the Non-NC scheme in the MH-TRC where the number of nodes is relatively small.

- **Multi-Hop Compute-and-Forward:** The MH-CPF scheme, where the CPF scheme is applied at relay nodes, is analyzed in Chapter 5. The similar recursive approaches for deriving the received SNR in the MH-ANC is designed to obtain the received linear combinations at the user nodes to overcome the complexity issue when the numbers of nodes and messages are large. Moreover, a two-dimension complex lattice reduction algorithm is designed to find the best coefficients that maximizes the computation rate. The outage probabilities for both Non-NC and MH-ANC schemes are derived. The numerical results demonstrate that the proposed MH-CPF has better outage performance than Non-NC in large scale MH-TRCs.

- **Optimal Multi-Hop Wireless Network Coding.** The Multi-TI MH-WNC scheme is proposed in Chapter 6. To generalize the performance analysis, the transmission pattern of the Multi-TI MH-WNC scheme is converted to a binary tree model. Specifically, the end-to-end SNR of Multi-TI MH-ANC is solved with a proposed postorder traversal approach, and the outage probability of Multi-TI MH-CPF is obtained with the converted transmission matrix. It is demonstrated that there exists an optimal MH-WNC scheme which can achieve the best outage performance for all-scale MH-TRCs. Although the optimal MH-WNC is poorer than the 2-TI MH-WNC scheme in network throughput, the former is proven to be superior to the latter in outage performance. Furthermore, the optimal MH-WNC scheme for different scale MH-TRCs is generalized, and the numerical results prove that it can achieve better outage performance than Non-NC in all scale MH-TRCs.

- **Multi-Way Compute-and-Forward:** The original CPF is extended to the mRC with the generalized transmission scheme. In Chapter 7, a dominated solution is proposed to overcome the issue of ensuring the linear independent condition while maximizing the overall computation rate upon one reception. The outage performance of the proposed CPF scheme is analyzed, and the numerical results show that the extended CPF scheme joined with the proposed dominated solution has better outage performance than the Non-NC scheme in the mRC with relatively a small number of users.

## 1.3 Organization

The dissertation begins with a review of network coding in relay based networks in Chapter 2. Chapter 3 develops a generalized MH-WNC for the $L$-node $K$-message MH-TRC.

The MH-ANC scheme for the generalized non-regenerative MH-TRC is analyzed in Chapter 4. Two recursive approaches for deriving the received SNR of each message are presented in Section 4.4. The outage performance and maximum sum-rate of MH-ANC is analyzed and closed-form expressions are presented in the following sections. Finally, the comparison between the Non-NC and MH-ANC schemes is presented in Section 4.9.

The MH-CPF scheme for the generalized $L$-node $K$-message MH-TRC is analyzed in Chapter 5. The algorithm for maximizing the computation rate is discussed in Section 5.5. The outage probability for MH-CPF is derived in Section 5.7. The numerical results and discussion are presented in Section 5.9.

Chapter 6 looks at the optimal MH-WNC for all-scale MH-TRCs. In Section 6.4, the model of Multi-TI MH-WNC for the generalized MH-TRC is built. The methodologies for analyzing the performance of Multi-TI MH-WNC are discussed in Section 6.5. The optimum MH-ANC and MH-CPF for different scale MH-TRCs are obtained through numerical simulations in Section 6.6. The findings are discussed in Section 6.7.

In Chapter 7, the research is moved from two-way channels to multi-way channels. The system model and CPF scheme for the mRC are presented in Section 7.3. The dominated solution for maximizing the overall computation rate in the mRC is described in Section 7.4. Outage performance analysis of the proposed CPF for the mRC is presented in Section 7.5 and numerical results are given in Section 7.6.

Finally, Chapter 8 summarizes the results and future directions for this line of work.

# Chapter 2

# Background

This chapter provides an overview of network coding and its applications in relay-based networks. It begins in Section 2.1 presenting some preliminary knowledge of relay-based network and two prominent relaying strategies. Section 2.2 and Section 2.3 discuss network coding and its application in wireless communication systems. Section 2.4 discusses prior work in network coding relevant to this dissertation. The specific differences with the components in this dissertation will be discussed in the corresponding chapters.

## 2.1 Relay Networks

Relay networks refer to a class of network topology commonly used in wireless networks. In such a network, the source and destination are unable to communicate with each other directly because the distance between them is greater than the transmission range [38]. Therefore, the source and destination are interconnected by means of intermediate nodes [39–41].

As is well documented throughout the available literature, there are two different types of relaying strategies existing, i.e., non-regenerative and regenerative relaying strategies [42, 43].

- **Non-regenerative relaying strategy:** Non-regenerative relaying strategies (also known as transparent relaying strategies) imply that relays do not modify the information represented by a waveform, and no digital operations are performed. Very simple operations are usually performed, such as

simple amplification, phase rotation. One of the simplest example strategies belonging to non-regenerative relaying strategies is amplify-and-forward (AF), where the received signal is amplified and retransmitted. There are no complicated operations at the relay, but noise builds with the transmission [44–47].

- **Regenerative relaying strategy:** Regenerative relaying strategies, on the other hand, require relays to change the waveform and/or the information contents by performing some processing in a digital domain. Unlike the non-regenerative relaying strategy, this requires digital operations, thus more powerful hardware. Therefore, regenerative relays usually outperform non-regenerative relays. The most prominent examples of regenerative relaying strategies are estimate and forward (EF) [48], compress and forward (CF) [49,50], and decode and forward (DF) [51,52]. Although the decoding process in regenerative relaying strategies eliminates the noise propagation, however decoding errors accumulate via transmissions.

## 2.2 Network Coding

A basic assumption in all communication networks today is that information is separate. Therefore, the information transmitted in the internet or phone network operates the same way as cars sharing a highway. Only recently made with the advent of NC [12] is a simple but important observation that in communication networks, relays can not only transmit but also combine the received packets for generating encoded packets on the outgoing links. At the network layer for example, relays can perform the binary addition of independent bit streams. In other words, data streams that are independently produced and consumed do not necessarily need to be kept separate when they are transmitted throughout the network. There are ways to combine and later extract independent information [53].

Network coding is best demonstrated via the famous butterfly example shown in Figure 2.1. All links are assumed to have the same capacity of one message per time unit. Without network coding, 10 time units are required for the two

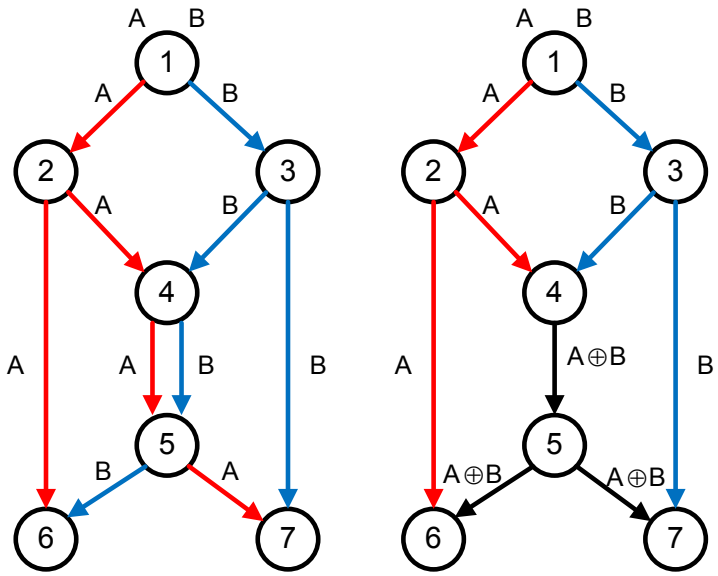


**(a)** ***Without network coding.*** **(b)** ***With network coding.***

Figure 2.1: The butterfly example.

end nodes 6 and 7 to receive both messages, as shown in Figure 2.1(a). The network throughput without network coding is 1/5 message/time unit. However, by sending the bitwise exclusive OR (XOR) of messages $A$ and $B$ in the middle links, two messages can be delivered per time unit to both receivers. As a result, the number of time units can be reduced to 8 and the network throughput is improved to 1/4 message/time unit, i.e., with a 25% improvement.

Following the seminal work of [12], Li *et al.* [54] showed that a linear coding mechanism is sufficient for the achievement of the multi-cast capacity. The proposed linear network coding (LNC) refers to the linear combination at a relay, where the output flow at this node is the linear combination of its input flows. The coefficients of the combination are selected from a finite field. Note that the operation is computed in a finite field, thus the generated message has the same length as the original message. Sink nodes receive these network coded messages, and collect them in a matrix. The original messages can be recovered by any node as long as the matrix has a full rank.

While the network topology in wireless communication networks is dynamic

and/or unknown, the deterministic network coding is difficult to realize. In this case, random linear network coding (RLNC) is an efficient approach to apply network coding to such communication networks [55–57]. The main idea of RLNC is to select the linear coefficients in a finite field $\mathbb{F}$ in a random way. Therefore, each node sends out packets obtained as a random linear combination stored in its buffer. One prominent result of [55] is that: if the source information is divided into $k$ original packets, each receiver could recover the whole information form any $k$ received network coded packets with probability $1 - 1/|\mathbb{F}|$. For a sufficiently large finite field, this probability is close to 1. Lun *et al.* [58] showed that RLNC could approximately achieve the network throughput for both unicast and multi-cast sessions in wireless communication networks.

## 2.3 Wireless Network Coding

Since its inception in information theory in 2000, network coding has attracted a significant amount of research attention [59]. After the initial theoretical studies in wired networks, the applicability of network coding for wireless networks was soon identified and investigated extensively [60]. However, wireless links have higher error rates than wired links which are more reliable and predictable, and wireless links vary over short time scales [61]. Moreover, a major distinguishing feature of wireless networks with wired networks is their multi-cast nature [62,63]. Transmissions in wired network do not interfere with each other, while interference is unavoidable in MACs. Traditionally, channel-access schemes [64], such as time division multiple access (TDMA) [65], frequency division multiple access (FDMA) [66, 67], and code division multiple access (CDMA) [68] are applied to avoid interference.

Albeit with totally different characteristics, the multi-cast feature of wireless networks provides an opportunity to apply network coding. When a transmitter broadcasts a message, it is likely that all neighboring receivers within the transmission range will receive it. Then, utilizing the idea of network coding, these receivers can then transmit the function of overhearing messages to the next hop.

In view of this fact, WNC [69–72] was proposed to improve the throughput in

wireless networks [15]. To date, prominent applications of WNC include TWRCs [14, 19, 73], multi-hop networks [13], multiple access channels [21], and multi-cast channels [22].

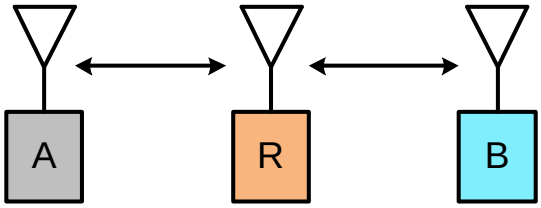


Figure 2.2: A single relay two-way relay channel.

The WNC scheme can be illustrated through a very simple single relay TWRC shown in Figure 2.2. In this network, two users exchange messages over a shared wireless half-duplex channel [74] via one intermediate relay.

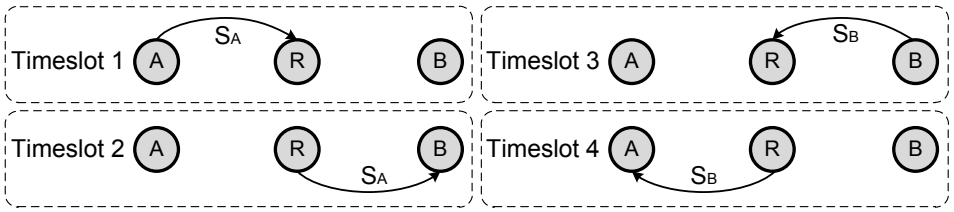


Figure 2.3: Traditional straightforward scheme.

Traditionally, interference is avoided by prohibiting the overlapping of signals from users $A$ and $B$ to relay $R$ at the same time slot. Let $S_A$ and $S_B$ denote the messages initiated by user $A$ and $B$, separately. The straightforward transmission scheme can be illustrated by Figure 2.3. It can be seen from the figure, that a number of four time slots are required to complete message exchange between the two users.

On the other hand, Figure 2.4 shows the network coding in the single relay TWRC. In the first and second time slot, users $A$ and $B$ send their messages $S_A$ and $S_B$ to relay $R$, separately. Instead of forwarding their messages individually,

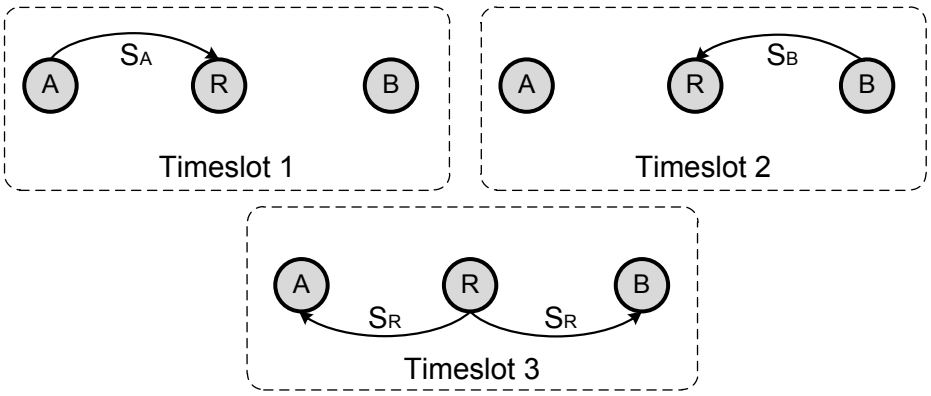


Figure 2.4: Network Coding.

relay $R$ constructs a network-coded message $S_R$ as

$$S_R = S_A \oplus S_B, \tag{2.1}$$

where $\oplus$ denotes XOR operation being applied over the entire messages of $S_A$ and $S_B$. In the third time slot, relay $R$ broadcasts $S_R$ to both users $A$ and $B$. Upon reception, user $A$ can extract $S_B$ from $S_R$ as follows

$$S_A \oplus S_R = S_A \oplus (S_A \oplus S_B) = S_B. \tag{2.2}$$

A similar operation can be applied at user $B$ to recover $S_A$. Only three time slots are required with network coding, representing a 50% network throughput improvement over the traditional straightforward scheme.

### 2.3.1 Analog Network Coding

In [13], Katti *et al.* embraced interference into two-way relay channels, and proposed analog network coding. The proposed ANC scheme was performed in signal-level rather than bit-level.

The ANC scheme for the single relay TWRC can be divided into two phases, i.e., multi-access (MA) and broadcast phases, as shown in Figure 2.5.

In the MA phase, both users transmit their modulated signals to relay $R$ simultaneously. The received signal at the relay is

$$y_R = \sqrt{P_A} h_{A,R} x_A + \sqrt{P_B} h_{B,R} x_B + n_R, \tag{2.3}$$

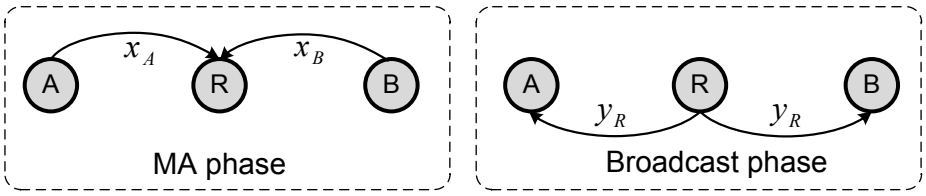


Figure 2.5: Analog network coding.

where $n_R$ is the received noise at relay $R$, $\sqrt{P_A}$ and $\sqrt{P_B}$ are the transmission powers, and $x_A$ and $x_B$ are the transmitted signals at user $A$ and $B$, separately. $h_{A,R}$ and $h_{B,R}$ are the channel coefficients of link $A-R$ and $B-R$, separately.

The AF relaying strategy is applied at the relay. Therefore, the relay amplifies and forwards the received signal to both users in the broadcast phase. For example, the received signal at user $A$ is

$$\begin{aligned} y_A=&G\sqrt{P_R}h_{A,R}y_R + n_A \\ =&G\sqrt{P_R}\sqrt{P_A}h_{A,R}h_{A,R}x_A + G\sqrt{P_R}\sqrt{P_B}h_{A,R}h_{B,R}x_B + G\sqrt{P_R}h_{A,R}n_R + n_A, \end{aligned}$$

where $G$ is the gain at the relay given by

$$G = \sqrt{\frac{1}{P_A|h_{A,R}|^2 + P_B|h_{B,R}|^2 + \sigma^2}},$$

where $\sigma^2$ is the noise variance of the received noise $n_R$. Since user $A$ has the knowledge of its own transmitted signal $x_A$, the resulting signals after cancelling interference can be written as

$$y_A^*=G\sqrt{P_R}\sqrt{P_B}h_{A,R}h_{B,R}x_B + G\sqrt{P_R}h_{A,R}n_R + n_A. \tag{2.4}$$

The received SNR for message $x_B$ can then be calculated as

$$\gamma_B = \frac{G^2P_RP_B|h_{A,R}|^2|h_{B,R}|^2}{G^2P_R|h_{A,R}|^2\sigma^2 + \sigma^2}. \tag{2.5}$$

Only two time slots are required to exchange the two messages, therefore a doubled network throughput is achieved by ANC. Moreover, only simple operations are required at both relay and user nodes. However, noise builds as messages traverse, as can be observed from the received SNR given by (2.5).

### 2.3.2 Physical-Layer Network Coding

In PNC [14], the received signal is decoded to the modular-2 summation of the transmitted messages. Considering a single relay TWRC with binary symmetric channels (BSCs) [75], the two messages sent from the two users are $S_A$ and $S_B$, which are either 1 or 0. The two modulated signals after binary phase-shift keying (BPSK) modulation are either $X = 1(S = 1)$ or $X = -1(S = 0)$. Similar to ANC, two phases are required for the PNC scheme. During the MA phase, the relay receives a combination of two modulated signals $Y_R$. The aim of PNC is to decode the XOR combination of the two codewords, i.e., $S_R = S_A \oplus S_B$. Table 2.1 shows the PNC mapping [76] process at the relay.

Table 2.1: PNC mapping.

| **Modulation at users** | | | | **Demodulation and Modulation at the relay** | | |
|---|---|---|---|---|---|---|
| **Message** | | **Signal** | | **Rec. Signal** | **Demodulated Combination** | **Trans. Signal** |
| $S_A$ | $S_B$ | $X_A$ | $X_B$ | $Y_R$ | $S_R = S_A \oplus S_B$ | $X_R$ |
| 0 | 0 | $-1$ | $-1$ | $-2$ | 0 | $-1$ |
| 0 | 1 | $-1$ | 1 | 0 | 1 | 1 |
| 1 | 0 | 1 | $-1$ | 0 | 1 | 1 |
| 1 | 1 | 1 | 1 | 2 | 0 | $-1$ |

The signal constellation can be expressed as the following Figure 2.6, where

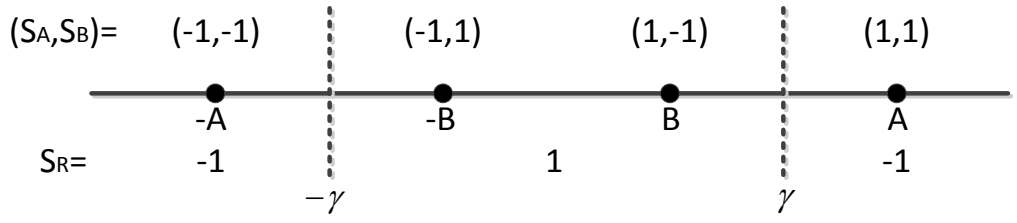


Figure 2.6: Signal constellation of the received signal at the relay node.

$-\gamma$ and $\gamma$ are two decision boundaries. For AWGN channels, $A = B = 1$, and $A = ||h_{A,R}|\sqrt{P_A} + |h_{B,R}|\sqrt{P_B}|$ and $B = ||h_{A,R}|\sqrt{P_A} - |h_{B,R}|\sqrt{P_B}|$ for fading channels [77, 78]. In the broadcast phase, relay $R$ broadcasts $S_R$ to both user $A$ and $B$, and they can extract required messages simply by subtracting their own

messages.

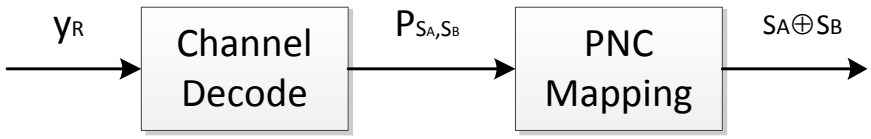


Figure 2.7: Channel decoding network coding.

When PNC is applied in channel-coded channels, a critical process at the relay is to transform the superimposed channel-coded packets received from two source nodes, i.e., $y_R = x_A + x_B + n_R$, to the network-coded combination of the source packets, i.e., $S_R = S_A \oplus S_B$. In the traditional multiple access problem, the relay decodes $S_A$ and $S_B$ separately and uses network coding to obtain $S_R$. However, the only interested network-coded information is $S_A \oplus S_B$g. In [79], Zhang *et al.* proposed a new channel decoding network coding (CDNC) for the procedure of $y_R \rightarrow S_A \oplus S_B$, as shown in Figure 2.7. The relay first decodes $y_R$ to obtain the probability mass function of $S_A + S_B$, denoted by $P_{S_A+S_B}(X) = \Pr(S_A + S_B = X|y_R)$. Then the relay could obtain the target information $S_R = S_A \oplus S_B$ through the PNC mapping.

A new channel decoding scheme for CDNC based on repeat accumulate (RA) codes was proposed in [79]. The decoder at relay $R$ provides the design of such a decoder along the following three steps: (1) construct a virtual encoder corresponding to the decoder; (2) construct the Tanner graph of the virtual code; and (3) design the belief propagation algorithm based on the Tanner graph. Although the process was only applied on regular RA codes [80], extensions to other channel codes, such as low-density parity-check (LDPC) codes and Turbo codes, are straightforward. A joint design of PNC with Turbo codes [81] and LDPC codes [17] has been used to improve the error performance for PNC in the single TWRC.

### 2.3.3 Compute-and-Forward

It is well recognized that random codes are the "optimal" channel codes for achieving Shannon's bound [82, 83]. However, a big step towards disproving this

conjecture was achieved in 1975 [84], and shortly afterwards interest in using bandwidth-efficient modulation codes with new structures, e.g., multi-$h$ codes [85] and lattice codes [86, 87] began.

An $n$-dimensional lattice $\Lambda$ is defined by a set of $n$ basis (column) vectors $\{\mathbf{g}_1, \mathbf{g}_2, ..., \mathbf{g}_n\}$ in $R^n$. The lattice $\Lambda$ is composed of all integral combinations of the basis vectors, i.e.,

$$\Lambda = \{l = G \cdot i, i \in \mathbb{Z}^n\}, \tag{2.6}$$

where $\mathbb{Z} = \{0, \pm 1, \pm 2, ...\}$, and the $n \times n$ generator matrix $G$ is given by $G = [\mathbf{g}_1\ \mathbf{g}_2\ ...\mathbf{g}_n]$. It should be noted that the generator is not unique.

Nested lattices was defined in [88], where a pair of $n$-dimensional lattice $(\Lambda_1, \Lambda_2)$ is called nested if $\Lambda_1 \subset \Lambda_2$, i.e., there exists corresponding generator matrices $G_1$ and $G_2$, such that

$$G_2 = G_1 \cdot \mathbf{J}, \tag{2.7}$$

where $\mathbf{J}$ is an $n \times n$ integer matrix whose determinant is greater than one. The volumes of the Voronoi region [89] of the two nested lattices satisfy

$$V_2 = \det\{J\} \cdot V_1. \tag{2.8}$$

Figure 2.8 shows an example of nested hexagonal lattices with $\mathbf{J} = 3 \cdot I$, where $I$ is the 2 by 2 identity matrix. One key result by Erez and Zamir [90] was that nested lattice codes (combined with lattice decoding) can achieve the capacity of the point-to-point AWGN channel

$$C = \frac{1}{2} \log\left(1 + \mathrm{SNR}\right). \tag{2.9}$$

There is a large body of work on lattice codes and their applications in channel coding [88]. Combined with network coding and lattice codes, the CPF scheme was proposed by Nazer *et al.* in [91]. The CPF scheme relies on codes with a linear structure, specifically nested lattice codes. The linearity of the codebook ensures that integer combination of codewords are also codewords, as shown in Figure 2.9.

Considering a two-user MAC, each transmitter maps its finite-field message into an element of the nested lattice code and sends the codeword to the relay

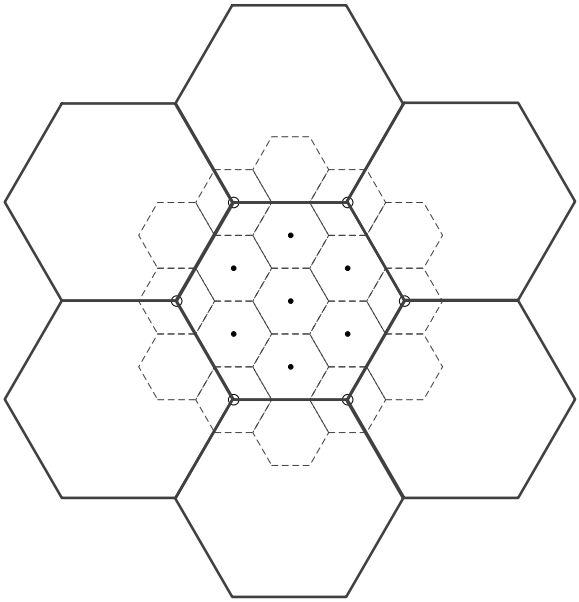

Figure 2.8: Nested lattice.

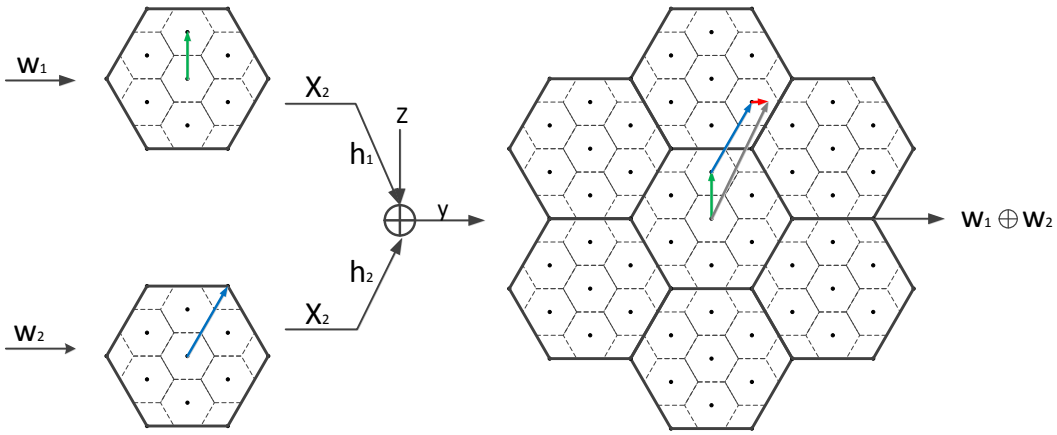


Figure 2.9: A simple example of compute-and-forward.

through the MAC. Assuming that the channel coefficients $h_1$ and $h_2$ are both equal to 1, the received signal at the relay can then be given by

$$y_R = x_1 + x_2 + n_R. \tag{2.10}$$

The relay observes a noisy sum of the transmitted codewords and determines the closest lattice point. After taking a modulo operation with respect to the coarse lattice ($\Lambda_2$), the receiver can invert the mapping and determine the modulo sum of the original messages. For the above case, both channel coefficients are

equivalent to 1, the two coefficients are also chosen as 1. For fading channels, instead of trying to decode the sum of the codewords, the relay aims to decode an integer combination of the codewords (modulo the coarse lattice)

$$v = [a_1 x_1 + a_2 x_2] \bmod \Lambda. \tag{2.11}$$

This combination is also a codeword due to the linear structure of the nested lattice code. If the integer coefficients are close enough to the channel coefficients, then it seems plausible that the relay can decode the function successfully. In other words, the relay can recover the integer combination of codewords as long as the rate of the nested lattice code is at most the computation rate [92]

$$R_{\text{COMP}}(\mathbf{h}, \mathbf{a}) = \max_{\mathbf{a} \neq \mathbf{0}} \log^+ \left( ||\mathbf{a}||^2 - \frac{P|\mathbf{a}\mathbf{h}^\dagger|^2}{1 + P||\mathbf{h}||^2} \right)^{-1}, \tag{2.12}$$

where $\log^+(x) \triangleq \max\big(\log(x), 0\big)$, $\mathbf{a} = [a_1 \ a_2]$ and $\mathbf{h} = [h_1 \ h_2]$. The established computation rate is proven to have significant improvements than conventional relaying strategies in the MAC.

## 2.4 Other Recent Work

Subsequent growth in wireless network coding has been explosive. The benefits of combining network coding with broadcasting have been investigated in [93,94]. Since the proposed PNC scheme in [14] requires perfect synchronization of the two users, many previous works [14, 20, 95, 96] found that symbol misalignment will result in appreciable performance penalties. Zhang *et al.* [14] showed that the BER performance penalties due to symbol offset is 3 dB worse for BPSK modulation, and 6 dB for quadrature phase shift keying (QPSK) modulation. In [97], the authors proposed a practical PNC which removed the synchronization assumption in the original PNC scheme. Most recently, Lu *et al.* in [98] used a belief propagation algorithm in channel-coded PNC, and reduced the penalties caused by the symbol misalignment in asynchronous PNC.

COPE was designed by Katti *et al.* in [15], where the two-way transmission was finished in three time slots in comparison to the traditional four time slot scheme. In [13], where Katti *et al.* embrace interference into two-way relay channels, the network coding was performed in signal-level rather than bit-level. The

follow-up work by Louie *et al.* showed that ANC can achieve higher maximum sum-rates than the conventional four time slot transmission scheme in the single relay TWRC.

There has been much interest in applying wireless network coding in various relay networks. In [99], Wang *et al.* proposed network coding schemes for cooperative relay networks and user cooperation networks. Relay selection was integrated with network coding in [100, 101] for multi-relay networks. Park *et al.* [102] proposed a hierarchically modulated network coding scheme for asymmetric two-way relay channels. Similar work with network-coded modulation was carried out in [103]. In [104,105], Xiao *et al.* proposed a new finite-field network coding for the multi-user multi-relay network, which showed better performance than superposition coding in binary field.

Furthermore, You *et al.* extended the analog network coding from two-hop to multi-hop in [106], which is shown to have significant improvement in network throughput. However, the work in [106] is different from the MH-TRC proposed in this dissertation. The difference will be discussed in the corresponding chapter. Most recently, much researchers have tried to integrate wireless network coding with multi-antenna technology to improve network throughput and/or reduce processing complexity [107–110].

Additionally, when channel coding and decoding are applied for the two-way relay network, a critical process at the relay is to transform the superimposed channel-coded packets received from two source nodes to the network-coded combination of the source packets. In contrast to the traditional network coding scheme where network coding is performed after channel decoding, Zhang *et al.* [111] proposed a new scheme where network coding is performed prior to channel decoding processing by directly combining the soft/hard decisions. Joint designs of PNC with RA codes [79], Turbo codes [81], and LDPC codes [17] have been designed to improve the error performance for two-way relay channels. Rateless codes [112–114] combined with network coding was investigated in [115], and the result showed that the proposed scheme can reduce the startup and playback delay in peer-to-peer (P2P) video streaming [116]. In [117,118], the authors proposed a novel transmission scheme for rateless codes over cooperative relay

networks with multiple relay nodes, where the scheme combines network coding to allow source nodes transmitting partial information about the next message block during the current block transmission. The network coding with rateless code design yields an increase in the overall throughput, thereby improving the spectral efficiency.

# Chapter 3

# Wireless Network Coding for Multi-Hop Two-Way Relay Channels

## 3.1 Introduction

Multi-hop two-way relay channels are wireless channels that two users employ to exchange their messages through two or more relays. The traditional straightforward hop-by-hop transmission scheme suffers long delays, low packet delivery efficiency and spectrum efficiency. Recently, the advent of WNC has offered a new opportunity to improve the network throughput and transmission reliability by exploiting interference in intermediate relays. It has been proven that WNC can double the system capacity in a single relay TWRC [20].

In this chapter, the WNC in the single TWRC is extended to the generalized $L$-node $K$-message MH-TRC, and a novel MH-WNC is designed. More specifically, the generalized $L$-node $K$-message MH-TRC model is presented. In this model, $K$-pair messages from two user nodes are exchanged through $L-1$ hops. Two exchange patterns are defined for the multi-message exchange, i.e., non-symmetrical and symmetrical exchange patterns. In order to set a benchmark for the network throughput, communication delays and performance analysis, two different Non-NC schemes with different exchange patterns are briefly described. That is, the traditional straightforward transmission scheme with the symmetrical

exchange pattern, and the optimized scheme with the non-symmetrical exchange pattern.

The WNC scheme for the single relay TWRC has been widely studied [14, 19, 73]. The principle of WNC is a network-coded message working with self information cancelation. In the single relay TWRC, the network-coded message is generated at the only relay node, and the self information cancelation is performed at the two user nodes. However, it should be noted that for the MH-TRC, network-coded messages are generated when the packets from two neighboring nodes collide. Therefore, the self information cancelation can be performed on the relay nodes at each reception, or on user nodes at the end of the transmission.

For the proposed MH-WNC in this dissertation, self information cancelation is applied only at the user nodes, which leads to less complexity for the relay node compared to the information cancelation at relay nodes upon each reception. This chapter presents a general transmission strategy of the MH-WNC scheme. The system model and transmission strategy in this chapter provide a platform for the performance analysis discussed in the following chapters.

The contributions in this chapter can be summarized as follows:

1. The transmission scheme of MH-WNC for the $L$-node $K$-message MH-TRC is generalized, and the transmission pattern and transmission events at each node in different time slots are presented;

2. A simulation platform for analyzing the MH-WNC schemes for different scale MH-TRCs is built, and the generalized transmission pattern is illustrated with grid charts; and

3. The network throughput and communication delays for different schemes in the generalized MH-TRC are evaluated, and the comparison results are summarized.

## 3.2 Related Work

There has been some work in the application of WNC to multi-hop relay networks. Zhang *et al.* [14] described PNC for general uni-directional and bi-directional

linear networks, where the self information cancelation is performed on the relay nodes at each reception. In the proposed scheme, each relay stores a copy of the message it sends. It then "adds" the inverse of this stored message to the message it receives from the neighboring nodes in the next time slot to recover the new message being forwarded. The results in [14] showed that PNC can achieve the upper-bound capacity, 0.5 frame/time slot in each direction for bi-directional transmissions between the two end nodes [119]. Their scheme was built on the BSC, however the PNC scheme in noisy and fading channels requires perfect decoding. Moreover, the decoding error propagates throughout the transmission.

The relay-aid network coding (RANC) in multi-hop wireless networks was investigated in [120], and the authors exploited PNC into wireless ad hoc networks. In the proposed scheme, nodes are divided into native nodes and relay nodes, where the native node only transmits its own message and the relay node transmits the XOR combination of the received messages and its own message. The simulation results showed that the proposed RANC can significantly improve the network throughput over COPE [15].

Combined with multiple antennas technology, Ono *et al.* proposed an architecture of multi-input and multi-output (MIMO) mesh network incorporated with network coding in [121, 122]. By introducing multiple antennas into multi-hop networks, co-channel interference cancelation and bi-directional transmission can be realized at the same time. The numerical analysis showed that the proposed architecture can achieve significantly higher channel capacity and reliability than that of conventional schemes for the MH-TRC.

Most recently, You *et al.* applied ANC to the MH-TRC in [106], where two different ANC schemes for MH-TRC were proposed. That is, the AF-ANC-Central scheme, where ANC was only utilized at the central node, and the AF-ANC-Even scheme, where the even relays perform ANC and odd relays only perform substraction and AF. The proposed AF-ANC-Central scheme can achieve only a doubled network throughput compared to the Non-NC scheme. The AF-ANC-Even scheme can further improve the network throughput, but the self information cancelation was performed on relay nodes at each reception. This additional operation increased the complexity of relay nodes and required more powerful

hardware. Moreover, the authors did not generalize a transmission scheme for all scale MH-TRCs and there was no outage performance analysis in the published work.

## 3.3 System Model

Consider a MH-TRC with $L$ nodes $\{N_l\}_{l=1}^{L}$ as illustrated in Figure 3.1. User nodes $N_1$ and $N_L$ wish to exchange their messages through intermediate relay nodes $\{N_l\}_{l=2}^{L-1}$. The message sequences to be transmitted by $N_1$ and $N_L$ are noted as $\mathbf{U} = \{u_k\}_{k=1}^{K}$ and $\mathbf{V} = \{v_k\}_{k=1}^{K}$, respectively. It is assumed that only immediately neighboring nodes are within the transmission range in this network, and signals received from non-neighboring nodes are negligible due to signal attenuation. All the links between two nodes are assumed to have the same capacity of one message per channel per time unit.

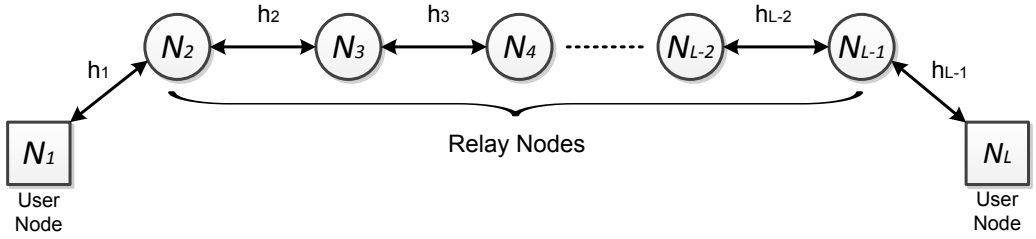


Figure 3.1: The $L$-node $K$-message multi-hop two-way relay network.

### 3.3.1 Message Exchange Pattern

Different from the traditional MH-TRC where only one pair of messages are exchanged between the two user nodes, the $K$-pair messages can be exchanged via different patterns, such as $\{u_1, v_1, u_2, v_2, ..., u_K, v_K\}$ (one message to $N_L$, one message to $N_1$, and so forth), or $\{u_1, u_2, v_1, v_2, ..., v_{K-1}, v_K\}$ (two messages to $N_L$, two messages to $N_1$, and so forth). In this section, two general types of transmission patterns are considered, i.e., symmetrical and non-symmetrical exchange patterns.

- **Symmetrical exchange pattern:** The symmetrical exchange pattern, as

the name suggests, is the message exchange pattern where message exchange between the two users is symmetrical. That is, the two users exchange their messages one by one at an equal rate.

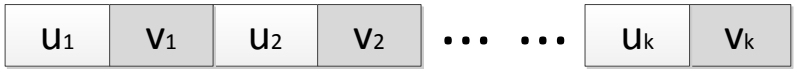


Figure 3.2: Symmetrical exchange pattern.

For the traditional straightforward relaying scheme, the two user nodes swap messages every $L-1$ time slots, i.e., user node $N_L$ sends message $v_1$ once it receives message $u_1$ from the other end, and so forth. As can be observed in Figure 3.2, the message sequence exchanged with this pattern is $\{(u_1, v_1), (u_2, v_2), ..., (u_K, v_K)\}$. The message transmission with this transmission pattern is similar to the situation where two people swap words in a telephone conversion.

- **Non-symmetrical exchange pattern:** The non-symmetrical message exchange pattern refers to the pattern of the message exchange between the two users that is not symmetrical, i.e., the exchange sequence is $\{(u_1, u_2, ..., u_K), (v_1, v_2, ..., v_K)\}$, as shown in Figure 3.3.

  That is, user node $N_1$ sends its messages continuously every $L-1$ time slots, and user node $N_L$ starts sending its messages after receiving all the $K$ messages from user node $N_1$.

  This type of transmission is like the car flow on a highway with traffic control, where only one lane is opened for bi-directional traffic. Therefore, when the number of cars in one direction accumulates to a certain point


Figure 3.3: Non-symmetrical exchange pattern.

(similar to the number of messages $K$ in the MH-TRC), all the cars in this direction are released at once, while the cars traveling in the other direction are kept waiting.

### 3.3.2 Communication Delays

The efficiency of message delivery and delay have been the widely studied research topics in multi-hop networks in recent years (see, e.g. [27, 28]). An important factor in the performance measurement of a communication system is communication delays, which are usually caused by the long distance between transmitters and receivers. For example, the communication delay between the probe on Mars and control center on the Earth is approximately $3 \sim 21$ minutes.

Similarly, it is assumed that the distances between two neighboring nodes in the MH-TRC are identical to each other, and each transmission between two nodes takes one time unit (disregarding the time between the relay node receiving and transmiting the message). It takes $L-1$ time units for one message to reach the other end in the $L$-node MH-TRC. Therefore, the communication delay is $L-1$ time unit.

The communication delay can be decreased by reducing the distance between two user nodes or applying advanced communication technologies. However, the focus of this dissertation is to improve the network throughput and communication delays with the network coding technique. As can be observed, the $L-1$ time unit communication delays between the two user nodes cannot be reduced with neither the routing or scheduling schemes, nor the network coding scheme. Therefore, for the performance analysis in the following sections, this type communication delay is not considered. On the other hand, two types of other communication delays will be analyzed for the schemes with and without network coding in the following sections:

- $t_1$, the delay between one user node sending the first outgoing message and receiveing the first incoming message; and

- $t_2$, the delay between one user receiving the two messages.

## 3.4 Non-Network Coding

The Non-NC scheme, opposite to the network coding scheme, is specified to the transmission scheme that avoids interference. This type of schemes usually uses time division techniques to schedule the transmission at each hop. In the following sections, two types of Non-NC schemes corresponding to different exchange patterns are discussed.

### 3.4.1 Straightforward Scheme

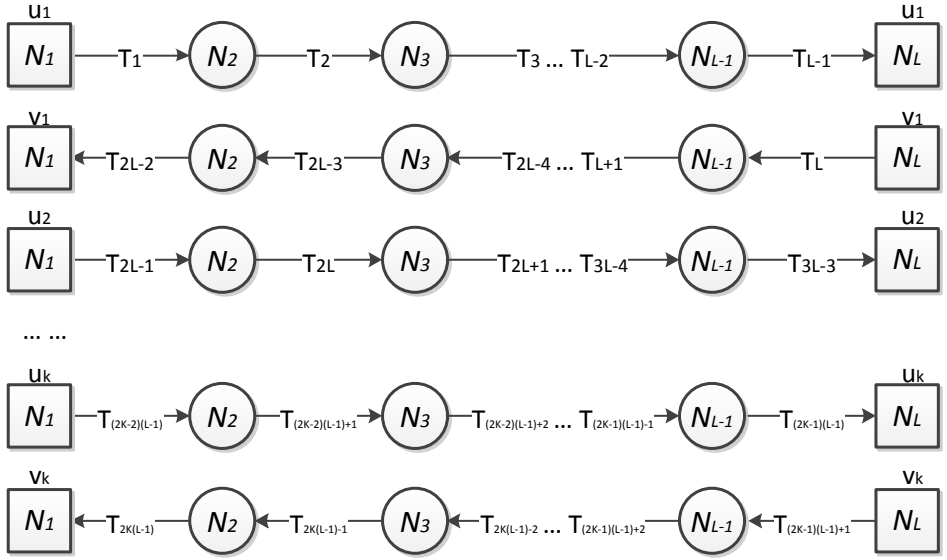


Figure 3.4: The straightforward scheme for the MH-TRC.

In the straightforward scheme, to avoid signal colliding [64], intermediate terminals relay the signal from one hop to the next, as shown in Figure 3.4. For non-regenerative systems, relays may amplify and forward the received signal from the previous node, while these relays decode the signal and re-encode it prior to retransmission in regenerative systems. Under this scheme, it takes $L-1$ time slots to forward one message from $N_1$ to $N_L$, and a total of $\mathcal{T}_{\mathrm{SF}} = 2K(L-1)$ time slots are required to complete the message sequence exchange.

The network throughput is defined as the number of messages transmitted in one time unit, thus the network throughput of the straightforward scheme can

be given by

$$C_{\mathrm{SF}} = \frac{2K}{2K(L-1)} = \frac{1}{L-1} \quad \text{(message/time slot)}. \tag{3.1}$$

For the symmetrical message exchange pattern, users node $N_1$ and $N_L$ take turns to transmit their messages until the end of the exchange process. The number of time slots for message $u_k$ to reach $N_L$ is $L-1$, and the number of time slots for message $v_k$ to reach $N_1$ is also $L-1$. Therefore, the communication delay between user $N_1$ sending its first message and receiving its first message is $t_1 = 2(L-1)$. Similarly, the delay between receiving two messages is $t_2 = 2(L-1)$.

### 3.4.2 Optimized Scheme

For the above straightforward scheme, each user sends its message every $L-1$ time slots. Thus, each node in the network only works once every $L-1$ time slots. Consequently, this scheme has low network throughput and channel use rate.

On the other hand, it is noted that each node is only able to receive the signal from its neighboring nodes. For example, as relay node $N_2$ cannot receive the signal from relay node $N_4$, the idle channels can be utilized for transmission without causing any interference.

By rescheduling the transmission strategy, an optimized scheme is designed as shown in Figure 3.5. With this scheme, user node $N_1$ transmits a new message every 3 time slots. For example, when node $N_4$ transmits message $u_1$ to $N_5$ in the fourth time slot, node $N_1$ sends $u_2$ to $N_2$ at the same time. Under this scheme, each node in the MH-TRC forwards the received signal to the next neighboring node every 3 time slots, and the transmissions do not overlap with each other due to the two-hop intervals between them. It can be deduced that the total number of time slots required for this optimized scheme is $2[(L-1)+3(K-1)]$, and the network throughput is given by

$$C_{\mathrm{OP}} = \frac{K}{(L-1)+3(K-1)} \quad \text{(message/time slot)}. \tag{3.2}$$

When the number of messages $K$ is far larger than the number of nodes $L$, an upper limit of $C_{\mathrm{OP}}$ can be obtained as

$$\hat{C}_{\mathrm{OP}} = \lim_{K>>L} \frac{K}{(L-1)+3(K-1)} = \frac{1}{3} \quad \text{(message/time slot)}. \tag{3.3}$$

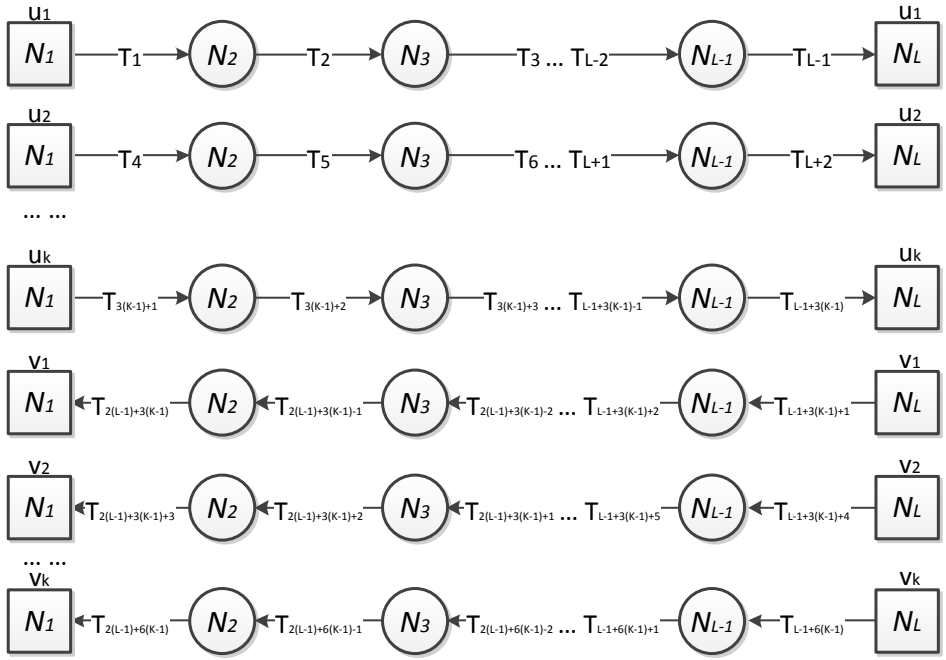


Figure 3.5: The optimized scheme for the MH-TRC.

In comparison with the straightforward scheme, the optimized scheme significantly improves the network throughput when the number of message is large. However, this optimized scheme cannot work when the symmetrical exchange pattern is required. Under this scheme, one user node does not start sending its messages until it receives all the messages from the counterpart user. Therefore, the communication delays with this optimized scheme are $t_1 = K(L-1)$ and $t_2 = 3$. Although the waiting time delay $t_2$ is relatively short compared to the straightforward scheme, it can be found out that the time delay $t_1$ is extremely long when the number of messages is large, meaning the user has to wait an extremely long period to receive its first message.

## 3.5 Wireless Network Coding

In order to improve the network throughput of the MH-TRC, WNC is now introduced into the $L$-node $K$-message MH-TRC. Without loss of generality, only the MH-TRC with odd number of nodes is considered in this dissertation, while

the case of even $L$ can also be extrapolated from the same procedure presented in this section. Note that only the transmission pattern and the simulation platform for MH-WNC are discussed in this chapter, the MH-WNC corresponding to the non-regenerative and regenerative relaying strategies will be analyzed in the two following chapters.

First, time slots are divided into two types, i.e., the odd and even time slots. In an odd time slot, odd-numbered nodes broadcast signals to their neighboring nodes, while in an even time slot, even-numbered nodes broadcast signals to neighboring nodes. The two user nodes $N_1$ and $N_L$ send one message every two time slots simultaneously, and the message sent by $N_1$ and $N_L$ in time slot $j \in \{1, 3, ..., 2K-1\}$ are

$$u_{(j+1)/2} \quad \text{and} \quad v_{(j+1)/2},$$

respectively. A total number of $2K-1$ time slots are required for the two user nodes to complete sending the message sequences.

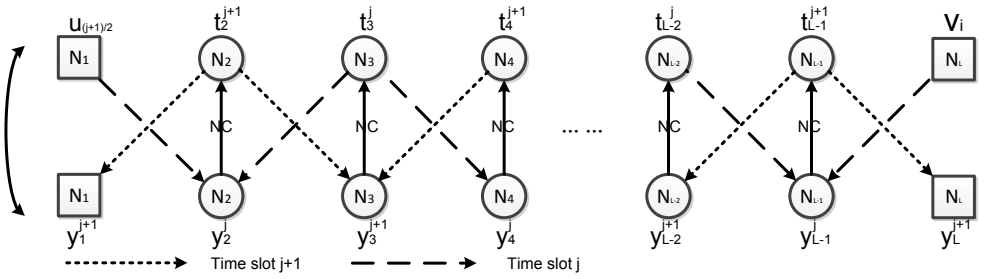


Figure 3.6: Wireless network coding for the $L$-node $K$-message MH-TRC.

Similar to the WNC scheme for the single relay TWRC, the relay nodes network-codes the received signal and broadcast the network-coded message to the neighboring nodes in the next transmission time slot, as shown in Figure 3.6. The figure only plots the transmission schedule for two time slots $j$ and $j+1$, while the general transmission schedule can be intuitively deduced. The "NC" operation in the figure represents the network-coding operation at the relay, which is either simple amplification in non-regenerative systems, or decoding the received signal to obtain a network-coded codeword in regenerative networks.

The received signal at relay node $N_l$ in time slot $j$ can be given by

$$y_l^j = h_{l-1} t_{l-1}^j + h_{l+1} t_{l+1}^j + w_l^j, \tag{3.4}$$

where $t_l^j$ is the transmitted signal by relay node $N_l$ in time slot $j$, $w_l^j$ denotes the received noise at node $N_l$ in time slot $j$. For non-regenerative relaying strategies, the transmitted signal $t_l^j$ is simply a scaled version of the received signal from the previous time slot $y_l^{j-1}$, which is illustrated in Chapter 4. For regenerative relaying strategies, the transmitted signal $t_l^j$ is the network-coded codeword decoded from $y_l^{j-1}$ (an XORed message with "standard" PNC, or a linear combination with CPF), which is discussed in Chapter 5.

After time slot $L-1$, the two user nodes will receive the signal containing the messages from the counterpart user node every two time slots. Knowing its own messages, the user nodes can extract the required messages. The user nodes cancel the own signals in the analog field and decode the required messages in MH-ANC, as will be explained in Chapter 4. On the other hand, the user nodes decode the linear combination of outgoing and incoming messages, and solve the linear eqnarrays for the required messages, as will be explained in Chapter 5.

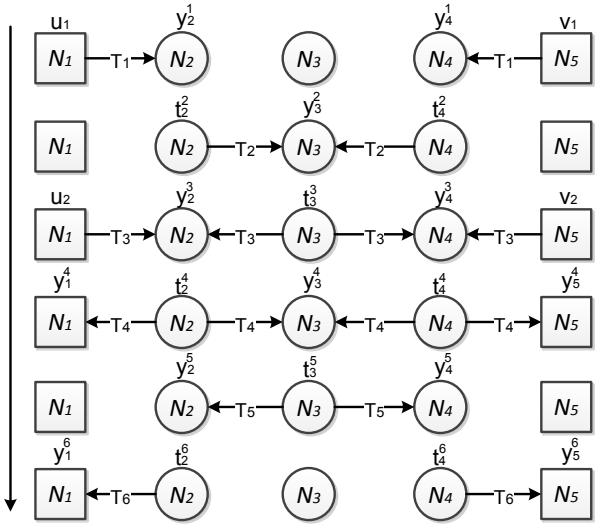


Figure 3.7: Transmission scheme of MH-WNC for the 5-node 2-message MH-TRC.

**Transmission scheme of MH-WNC for a 5-node 2-message MH-TRC:** A total number of 6 time slots are required to complete messages exchange with MH-WNC in the 5-node 2-message MH-TRC. The transmission scheme of

Table 3.1: Transmission events of MH-WNC for the 5-node 2-message MH-TRC.

| **Time slot** | **Node** | **Event** | **Received signal** |
|---|---|---|---|
| 1 | $N_2$ | $N_1 \xrightarrow{u_1} N_2$ | $y_2^1 = h_1 u_1 + w_2^1$ |
| | $N_4$ | $N_4 \xleftarrow{v_1} N_5$ | $y_5^1 = h_4 v_1 + w_5^1$ |
| 2 | $N_3$ | $N_2 \xrightarrow{t_2^2} N_3 \xleftarrow{t_4^2} N_4$ | $y_3^2 = h_2 t_2^2 + h_3 t_4^2 + w_3^2$ |
| 3 | $N_2$ | $N_1 \xrightarrow{u_2} N_2 \xleftarrow{t_3^3} N_3$ | $y_2^3 = h_1 u_2 + h_2 t_3^3 + w_2^3$ |
| | $N_4$ | $N_3 \xrightarrow{t_3^3} N_4 \xleftarrow{v_2} N_5$ | $y_4^3 = h_3 t_3^3 + h_4 v_2 + w_4^3$ |
| 4 | $N_1$ | $N_1 \xleftarrow{t_2^4} N_2$ | $y_1^4 = h_2 t_2^4 + w_1^4$ |
| | $N_3$ | $N_2 \xrightarrow{t_2^4} N_3 \xleftarrow{t_4^4} N_4$ | $y_3^4 = h_2 t_2^4 + h_3 t_4^4 + w_3^4$ |
| | $N_5$ | $N_4 \xrightarrow{t_4^4} N_5$ | $y_5^4 = h_4 t_4^4 + w_5^4$ |
| 5 | $N_2$ | $N_2 \xleftarrow{t_3^5} N_3$ | $y_2^5 = h_2 t_3^5 + w_2^5$ |
| | $N_4$ | $N_3 \xrightarrow{t_3^5} N_4$ | $y_4^5 = h_3 t_3^5 + w_4^5$ |
| 6 | $N_1$ | $N_1 \xleftarrow{t_2^6} N_2$ | $y_1^6 = h_1 t_2^6 + w_1^6$ |
| | $N_5$ | $N_4 \xrightarrow{t_4^6} N_5$ | $y_5^6 = h_4 t_4^6 + w_5^6$ |

$A \xrightarrow{x} B$ – node $A$ transmits message $x$ to $B$,

$A \xleftarrow{x} B$ – node $A$ receives message $x$ from $B$,

$A \xrightarrow{x} B \xleftarrow{y} C$ – node $B$ receives messages $x$ and $y$ from nodes $A$ and $C$ simultaneously in a multiple-access phase,

$A \xleftarrow{x} B \xrightarrow{x} C$ – node $B$ broadcasts message $x$ to nodes $A$ and $C$ in a broadcast phase.

MH-WNC for a 5-node 2-message MH-TRC is illustrated in Figure 3.7 and Table 3.1.

It should be noted that the transmission events at each node depend on the total number of nodes and messages. For example, the number of time slots required for sending all the $K$ messages is less than the number of hops, i.e., $\big(2K-1 < L-1\big)$. In other words, the two user nodes have completed sending all their messages before the first message from the other end arrives. In this case, the user nodes remain silent until the first message from the other end arrives in time slot $L-1$, and the relay nodes remain silent when there are no new messages coming from the neighboring nodes.

For the general case of $2K - 1 < L - 1$, the transmission events of all of the nodes are summarized in Table 3.2 (on the next page), and the transmission

Table 3.2: Transmission events of MH-WNC in the $L$-node $K$-message MH-TRC ($2K-1<L-1$).

| **Node** | **Set of time slots ($\Omega$)** | **Event in the set of time slot $j$, $j\in\Omega$** |
|---|---|---|
| $N_1$ | $\{1,3,5,...,2K-1\}$ | $N_1 \overset{u_{j+1/2}}{\longrightarrow} N_2$ |
| | $\{2K+1,2K+3,2K+5,...,L+2K-4\}$ | $\ominus$ |
| | $\{L-1,L+1,...,L-1+2(K-1)\}$ | $N_1 \overset{t_2^j}{\longleftarrow} N_2$ |
| $N_L$ | $\{1,3,5,...,2K-1\}$ | $N_{L-1} \overset{v_{j+1/2}}{\longleftarrow} N_L$ |
| | $\{2K+1,2K+3,2K+5,...,L+2K-4\}$ | $\ominus$ |
| | $\{L-1,L+1,...,L-1+2(K-1)\}$ | $N_{L-1} \overset{t_{L-1}^j}{\longrightarrow} N_L$ |
| $N_2$ | $\{1\}$ | $N_1 \overset{u_1}{\longrightarrow} N_2$ |
| | $\{3,5,...,2K-1\}$ | $N_1 \overset{u_{(j+1)/2}}{\longrightarrow} N_2 \overset{t_2^j}{\longleftarrow} N_3$ |
| | $\{2K+1,2K+3,2K+5,...,L+2K-4\}$ | $N_2 \overset{t_3^j}{\longleftarrow} N_3$ |
| | $\{2,4,...,L+2K-5\}$ | $N_1 \overset{t_2^j}{\longleftarrow} N_2 \overset{t_2^j}{\longrightarrow} N_3$ |
| | $L-1+2(K-1)$ | $N_1 \overset{t_2^j}{\longleftarrow} N_2$ |
| $N_{L-1}$ | $\{1\}$ | $N_{L-1} \overset{v_1}{\longleftarrow} N_L$ |
| | $\{3,5,...,2K-1\}$ | $N_{L-2} \overset{t_{L-2}^j}{\longrightarrow} N_{L-1} \overset{v_{(j+1)/2}}{\longleftarrow} N_L$ |
| | $\{2K+1,2K+3,2K+5,...,L+2K-4\}$ | $N_{L-2} \overset{t_{L-2}^j}{\longrightarrow} N_{L-1}$ |
| | $\{2,4,...,L+2K-5\}$ | $N_{L-2} \overset{t_{L-1}^j}{\longleftarrow} N_{L-1} \overset{t_{L-1}^j}{\longrightarrow} N_L$ |
| | $L-1+2(K-1)$ | $N_{L-1} \overset{t_{L-1}^j}{\longrightarrow} N_L$ |
| $\{N_l\}_{l=3}^{(L-3)/2}$ | $\{1,2,...,l-1\}\bigcup\{L+2K-l,...,\mathcal{T}_K\}$ | $\ominus$ |
| | $\{l\}$ | $N_{l-1} \overset{v_{l-1}^j}{\longrightarrow} N_l$ |
| | $\{l+2,l+4,...,L-1+2(K-1)-l\}$ | $N_{l-1} \overset{t_{l-1}^j}{\longrightarrow} N_l \overset{t_{l+1}^j}{\longleftarrow} N_{l+1}$ |
| | $\{l+1,l+3,...,L-1+2(K-1)-2(l-1)\}$ | $N_{l-1} \overset{t_l^j}{\longleftarrow} N_l \overset{t_l^j}{\longrightarrow} N_{l+1}$ |
| | $L-1+2(K-1)-2(l-2)$ | $N_{l-1} \overset{t_l^j}{\longleftarrow} N_l$ |
| $\{N_l\}_{l=(L+1)/2}^{L-2}$ | $\{1,2,...,L-l-2\}\bigcup\{2K+l,...,\mathcal{T}_K\}$ | $\ominus$ |
| | $\{L-1-l\}$ | $N_l \overset{t_{l+1}^j}{\longleftarrow} N_{l+1}$ |
| | $\{L-l+1,L-l+3,...,2(K-1)+l\}$ | $N_{l-1} \overset{t_{l-1}^j}{\longrightarrow} N_l \overset{t_{l+1}^j}{\longleftarrow} N_{l+1}$ |
| | $\{L-l,L-l+2,...,2(K-1)+l-1\}$ | $N_{l-1} \overset{t_l^j}{\longleftarrow} N_l \overset{t_l^j}{\longrightarrow} N_{l+1}$ |
| | $2(K-1)+l+1$ | $R_l \overset{t_l^j}{\longrightarrow} N_{l+1}$ |
| $N_{(L-1)/2}$ | $\{1,2,...,(L-3)/2\}\bigcup\{2K+(L-5)/2,...,\mathcal{T}_K\}$ | $\ominus$ |
| | $\{(L-1)/2,(L+1)/2,...,2(K-1)+(L-1)/2\}$ | $N_{(L-3)/2} \overset{t_{(L-3)/2}^j}{\longrightarrow} N_{(L-1)/2} \overset{t_{(L+1)/2}^j}{\longleftarrow} N_{(L+1)/2}$ |
| | $\{N/2+1,N/2+3,...,2(K-1)+N/2-1\}$ | $N_{(L-3)/2} \overset{t_{(L-1)/2}^j}{\longleftarrow} N_{(L-1)/2} \overset{t_{(L-1)/2}^j}{\longrightarrow} N_{(L+1)/2}$ |

$\mathcal{T}_K = L-1+2(K-1)$ – the total number of time slots.

events for the case of $2K-1 \geqslant L-1$ can be similarly extrapolated.

The total number of time slots required for the generalized $L$-node $K$-message MH-TRC with MH-WNC is $\mathcal{T}_{\text{MH-WNC}} = L-1+2(K-1)$, and the network throughput is

$$C_{\text{MH-WNC}} = \frac{2K}{L-1+2(K-1)} \quad \text{(message/time slot)}. \tag{3.5}$$

The upper limit of $C_{\text{MH-WNC}}$ when the number of messages $K$ is far larger than the number of nodes $L$ can be obtained as

$$\hat{C}_{\text{MH-WNC}} = \lim_{K>>L} \frac{2K}{L-1+2(K-1)} = 1 \quad \text{(message/time slot)}. \tag{3.6}$$

In comparison with Non-NC, MH-WNC significantly improves the network throughput. That is, $L-1$ times better than the straightforward scheme and $(L-1)/3$ times better than the optimized scheme.

The messages of the two user nodes are transmitted simultaneously, and both user nodes receive messages from the counterpart user node at the same time slot. Each message needs $L-1$ time slot to traverse the entire $L-1$ hops, so the communication delay between one user node sending out its first message and receiving its first message is $t_1 = L-1$. Moreover, since the message is transmitted every two time slots, both user nodes will receive a new message from the counterpart user node every two time slots after the first message arrives. The communication delay between receiving two messages is $t_2 = 2$. In comparison with the Non-NC scheme, the MH-WNC gives significant improvement in both communication delays.

## 3.6 Simulation Platform

The transmission pattern for WNC in the single relay TWRC is quite straightforward and intuitively understood. It only consists of two phases, i.e., the multiple access and broadcast phases. The transmission of each pair of messages is independent, and the transmission of previous messages does not affect that of subsequent messages.

Similarly, the proposed MH-WNC is made up of a series of multiple access and broadcast phases. However, since each node works every two time slots, the

transmission of different messages are overlapped. Therefore, a simulation platform is built to show the detailed transmission pattern and transmission events at each node of MH-WNC for different scale MH-TRCs. The established simulation platform can also be used to analyze the performance of MH-WNC in Chapters 4 and 5.

Following the transmission scheme, the transmission scenario for MH-WNC can be extrapolated as follows

- User nodes send their messages every two time slots in odd time slots, until they have finished sending all the $K$ messages. They start to receive messages from their neighboring relay nodes from time slot $L-1$ every two time slots in even time slots until the end of the entire exchange process. They remain silent in the rest time slots; and

- Relay nodes transmit the forward and backward messages once every two time slots.

Denote by $\mathbb{R}$, $\mathbb{T}$ and $\ominus$ the receiving, sending and silent modes of the node in the MH-WNC, respectively. Let $\mathbb{S}_l^j$ be the operation mode for node $N_l$ in time slot $j$. Following the above transmission scenario, the transmission modes for each node in different time slots can be summarized as:

- For user nodes $N_1$ and $N_L$,
  $\mathbb{S}_1^j = \mathbb{S}_L^j = \mathbb{T}$, $j \in \{1, 3, 5, ..., 2(K-1)+1\}$.
  $\mathbb{S}_1^j = \mathbb{S}_L^j = \mathbb{R}$, $j \in \{L-1, L-1+2, L-1+4, ..., L-1+2(K-1)\}$.
  $\mathbb{S}_1^j = \mathbb{S}_L^j = \ominus$, other.

- For relay nodes $\{N_l\}_{l=2}^{L-1}$,
  $\mathbb{S}_l^j = \mathbb{T}$, $j \in \{L-l+1, L-l+2+1, L-l+4+1, ..., L-l+2(K-1)+1\} \cup \{l+1, l+2+1, l+4+1, ..., l+2(K-1)+1\}$.
  $\mathbb{S}_l^j = \mathbb{R}$, if $\mathbb{S}_{l-1}^j = \mathbb{T} \cup \mathbb{S}_{l+1}^j = \mathbb{T}$.
  $\mathbb{S}_1^j = \ominus$, other.

Let $-1$ represent the receiving mode, 1 represent the sending mode, 0 represent the silent mode, and $-2$ represent receiving signals from both neighboring nodes.

The transmission pattern can be represented with a $\mathcal{T}$ (the number of time slots) by $L$ (the number of nodes) transmission matrix $\mathbf{T}$.

For example, the transmission matrix of MH-WNC for the 5-node 2-message MH-TRC can be expressed as

$$\mathbf{T}_{52}^{2} = \begin{bmatrix} 1 & -1 & 0 & -1 & 1 \\ 0 & 1 & -2 & 1 & 0 \\ 1 & -2 & 1 & -2 & 1 \\ -1 & 1 & -2 & 1 & -1 \\ 0 & -1 & 1 & -1 & 0 \\ -1 & 1 & 0 & 1 & -1 \end{bmatrix}. \tag{3.7}$$

With the matrix, the transmission pattern of the MH-WNC scheme for different scale MH-TRCs can be illustrated. A grid chart is designed to display the transmission pattern of the MH-WNC. For example, the grid charts for the 5-node 3-message MH-TRC and 11-node 3-message MH-TRCs with MH-WNC are illustrated by Figure 3.8.

The horizontal grids represent the $L$ nodes in the network, and the vertical grids represent the $\mathcal{T}$ time slots. Each grid represents the operation mode of the corresponding node in a specific time slot. The black grid represents the transmission mode, the dark gray grid represents the node receiving two signals from two neighboring nodes, the ash grey grid represents the node receiving only one signal from one of its neighboring nodes, and the white grid represents the silent mode.

It can be observed that the shape of the transmission pattern of the MH-WNC in Figure 3.8(b) is like the letter $X$. All the relay nodes remain silent before the first signal reaches, and after sending out the last message. Moreover, after initial stages, all the relay nodes receive bi-directional signals from both neighboring nodes. When there are no more new messages from user nodes, the relay node only transmits when there is a new message coming from the other nodes.

Given the numbers of nodes $L$ and messages $K$, the grid chart of the transmission pattern of the MH-WNC for different scale MH-TRCs can be plotted with

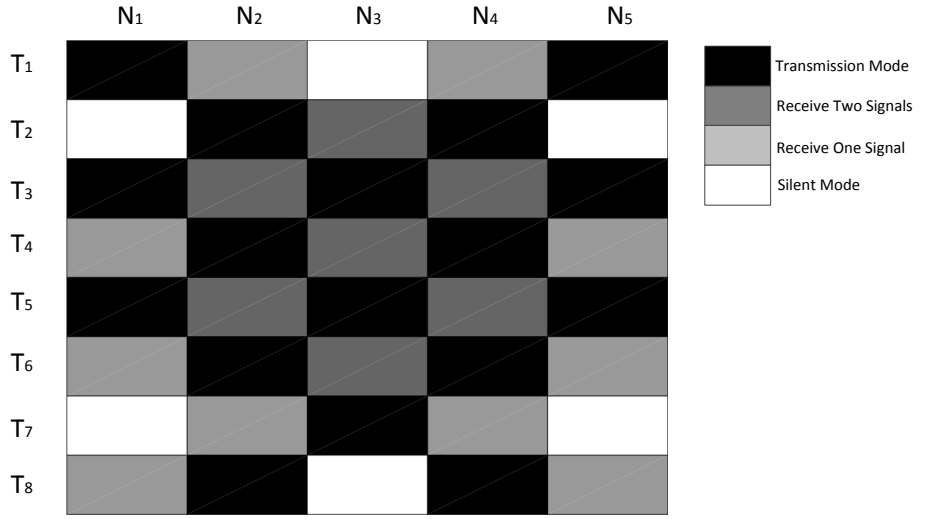


**(a)** 5-***node*** 3-***message MH-TRC.***

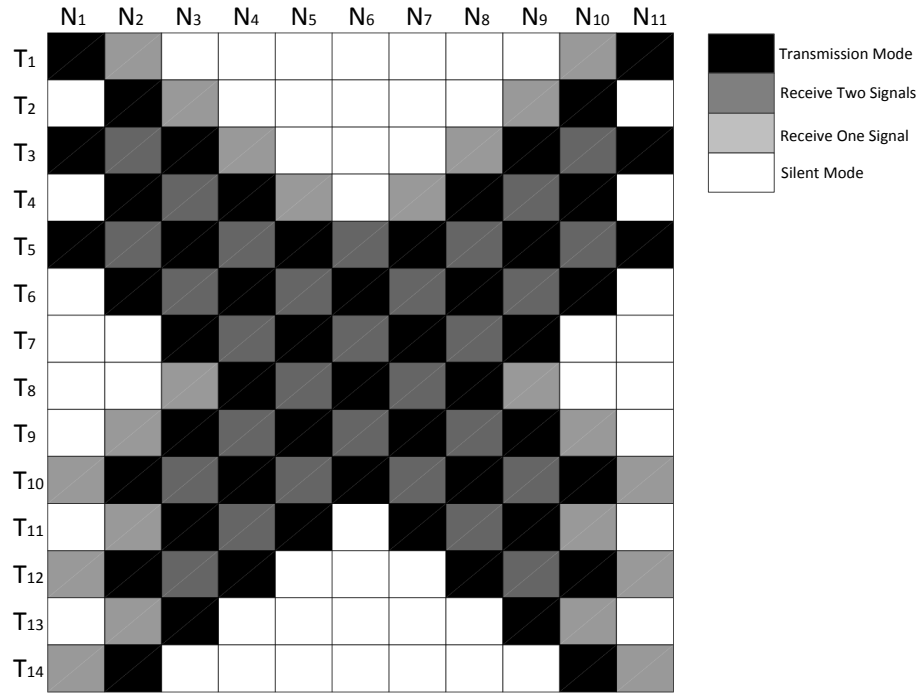


**(b)** 11-***node*** 3-***message MH-TRC.***

Figure 3.8: Grid charts of the transmission pattern of MH-WNC for different scale MH-TRCs.

the above simulation platform.

## 3.7 Summary

In summary, a novel MH-WNC scheme for the generalized $L$-node $K$-message MH-TRC is designed in this chapter. The transmission events of each user node in different time slots are specialized. A simulation platform is built to express the transmission pattern of MH-WNC for the generalized MH-TRC, and will be further used for performance analysis in the following chapters. The proposed MH-WNC scheme can significantly improve the network throughput in comparison with the Non-NC schemes. Specifically, the schemes discussed in this chapter are summarized in the following Table 3.3.

Table 3.3: Different transmission schemes for the generalized $L$-node $K$-message MH-TRC

| **Scheme** | $t_1$ | $t_2$ | **Network throughput** | **Network Throughput Upper limit** | **Exchange pattern** |
|---|---|---|---|---|---|
| **Straightforward** | $2(L-1)$ | $2(L-1)$ | $\frac{1}{L-1}$ | $\frac{1}{L-1}$ | Symmetrical |
| **Optimized** | $(K+1)(L-1)$ | 3 | $\frac{K}{L-1+3(K-1)}$ | $\frac{1}{3}$ | Non-symmetrical |
| **MH-WNC** | $L-1$ | 2 | $\frac{2K}{L-1+2(K-1)}$ | 1 | Symmetrical |

It is found that, for the symmetrical message exchange pattern, MH-WNC can achieve the best network throughput of the three schemes. The network throughput improvement over the straightforward scheme is $L-1$ times when the number of messages is large. Moreover, the communication delays $t_1$ and $t_2$ of MH-WNC are the shortest of these schemes. It can also be observed that the straightforward scheme without interference takes the most number of time slots to complete the whole message sequence exchange. Although the communication delay between receiving the two messages $t_2$ is rather short in the optimized scheme, the communication delay $t_1$ is the longest of these three schemes. Due to the asymmetry message rate between the two users, the non-symmetrical transmission pattern is only applicable in some special communication systems.

To sum up, the proposed MH-WNC scheme can not only achieve a significant network throughput improvement over the Non-NC scheme in the generalized MH-TRC, but it also has the shortest communication delays. In the following

two chapters, the outage performance of the proposed MH-WNC scheme with two different relaying strategies will be analyzed to demonstrate that the superiority of the MH-WNC scheme to the Non-NC schemes is not only in the network throughput, but also in the outage performance.

# Chapter 4

# Analog Network Coding for Non-Regenerative Multi-Hop Two-Way Channels

## 4.1 Introduction

In the last chapter, a general MH-WNC for the generalized $L$-node $K$-message MH-TRC was proposed, and in this chapter immediately following the results, the MH-WNC for the generalized non-regenerative MH-TRC will be investigated. Katti *et al.* [13] embraced interference into two-way relay channels and proposed analog network coding where the relay simply acted as a repeater and transmits a scaled version of its observation, and source nodes extract the required signal by canceling its own signal. The proposed ANC scheme is performed in signal-level not bit-level and only requires simple operations at both relay and user nodes.

In this chapter, a MH-WNC scheme with the AF relaying strategy for the generalized non-regenerative MH-TRC is proposed. It is refereed to as the MH-ANC scheme. Due to the bidirectional transmission, each message propagates through a series of intermediate relay nodes until it reaches the user nodes. As a result, the received signal at the user nodes consists of the combination of outgoing and incoming messages, plus the propagated received noise at each relay node. Different from the ANC scheme for the MH-TRC in the previous work [106], the self information cancelation is performed at the user nodes. Therefore, the received

signal at the user nodes should be derived to perform self information cancelation. Moreover, the performance analysis of MH-ANC lies on the received signal-to-noise-ratio (SNR) of each message, so a closed-form received SNR expression is derived for the outage and sum-rate analysis.

This chapter tackles these challenges and makes the following contributions:

1. The MH-ANC scheme for the generalized non-regenerative MH-TRC is proposed, and the received signals at the user nodes;

2. To overcome the exponentially increased complexity with the increased number of nodes and messages, two novel recursive approaches are proposed to derive the received SNR;

3. The bound of the end-to-end SNR is analyzed, and a very tight upper bound in high SNR regions is obtained. The upper-bound outage probability and maximum sum-rate are established; and

4. The corresponding received SNR and outage probability analysis for Non-NC in the MH-TRC are derived as benchmarks for comparison. When the number of messages is far larger than the number of nodes, both numerical and analytical results demonstrate that MH-ANC is superior to Non-NC in outage probability in small scale MH-TRCs. Moreover, when the number of nodes is relatively small in high SNR regions, the results clearly demonstrate that the maximum sum-rate of MH-ANC is significantly better than that of Non-NC .

## 4.2 Related Work

There is a large body of work on the performance analysis of the traditional AF scheme in multi-hop relay networks. Hasna *et al.* [123] derived the analytical expressions of the harmonic mean and cumulative density function of the end-to-end SNR for two-hop relay networks, which can be applied to outage performance and average BER analysis. Moreover, they also provided a tight upper bound for the end-to-end SNR at high SNR regions. Later on, they analyzed the outage probability of a two-hop relay network with fixed gain and over Rayleigh-fading

channels in [124] and [125], separately. Following their previous work, they generalized the outage probability of the multi-hop relay network over Nakagami fading channels in [126], and derived the average BER of the multi-hop relay network over fading channels in [127]. In [128], Zhao *et al.* also analyzed the outage probability of the multi-hop system over shadowed Nakagami-$m$ fading channels. Conne *et al.* analyzed the outage probability of multi-hop amplify-and-forward multiple relay system in [129], where tight lower and upper bounds are derived for the system. In this chapter, this previous work in the non-regenerative multi-hop relay network will be used as a benchmark in the outage performance comparison with the Non-NC scheme.

Following the work of Katti in 2007, much interest has been moved to the application and performance analysis of ANC in different types of wireless relay networks. In [24], the authors analyzed the performance of ANC in a single relay TWRC. Closed-form expressions of the end-to-end SNR, outage probability, sum-bit-error-rate (Sum-BER) and maximum sum-rate for the traditional straightforward scheme, three time slot network coding scheme and ANC scheme were derived. The numerical results in this paper showed that ANC can achieve a higher maximum sum-rate over the traditional straightforward transmission scheme.

The asymptotic optimality of ANC in high SNR regions was recently studied in [130–132], where the authors investigated the performance of ANC in high SNR regions and derived tight upper and lower bounds. Wang *et al.* [133] proposed a rate adaptation scheme for ANC, and found the optimal transmission power that maximizes the achievable rate. The authors in [134, 135] proposed a solution to overcome the synchronization issue in ANC, which was proven to achieve full diversity.

Most recently, You *et al.* applied ANC to the MH-TRC in [106], where the proposed AF-ANC-Central scheme achieves a doubled throughput without any SNR loss compared to the Non-NC scheme. Although this work is similar to the work presented in this dissertation at first glance, there are some fundamental differences. First, the proposed AF-ANC-Central scheme can a only achieve doubled network throughput over the Non-NC scheme, while the number of mes-

sages is large the proposed MH-WNC in this project can achieve a $L-1$ times better network throughput improvement. Although the AF-ANC-Even scheme described in the paper is able to further improve the network throughput, the self information cancelation performed on relay nodes at each reception increases the complexity of relay nodes and requires more powerful hardware. Moreover, there was no outage performance analysis in the published paper.

## 4.3 System Model

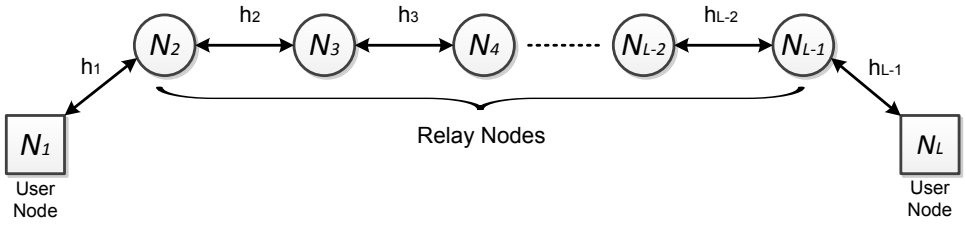


Figure 4.1: The $L$-node $K$-message multi-hop two-way relay network.

The $L$-node $K$-message MH-TRC is shown in Figure 4.1, where user nodes $N_1$ and $N_L$ wish to exchange their messages through intermediate relay nodes $\{N_l\}_{i=2}^{L-1}$. The message sequences to be transmitted by $N_1$ and $N_L$ are noted as $\mathbf{U} = \{u_k\}_{k=1}^{K}$ and $\mathbf{V} = \{v_k\}_{k=1}^{K}$, respectively. Assuming that BPSK modulation is applied at all the nodes, the modulated signal sequences initiated by $N_1$ and $N_L$ are noted as $\hat{\mathbf{U}} = \{\hat{u}_k\}_{k=1}^{K}$ and $\hat{\mathbf{V}} = \{\hat{v}_k\}_{k=1}^{K}$. The user nodes transmit one message every two time slots, and the modulated signals sent by $N_1$ and $N_L$ in time slot $j \in \{1, 3, ..., 2K-1\}$ are

$$\hat{u}_{(j+1)/2} \quad \text{and} \quad \hat{v}_{(j+1)/2}.$$

The channel coefficient between node $N_l$ and $N_{l+1}$ is denoted by $\{h_l\}_{l=1}^{L-1}$, which is considered quasi-static and reciprocal in bi-direction. For Rayleigh fading channels, $h_l \sim \mathcal{CN}(0, 2\alpha_l^2)$ is modeled as a zero mean, independent, circularly symmetric complex Gaussian random variable with variance $\alpha_l^2$ per dimension. $\{\omega_l\}_{l=1}^{L}$ is the received noise at node $N_l$, which is a zero mean, independent, circularly symmetric, complex Gaussian random variable with the variance of $\sigma^2$.

$\gamma'_l = \frac{|h_l|^2}{\sigma^2}$ is the SNR of hop $l$, which is exponentially distributed with parameter $1/\bar{\gamma}'_l$, where $\bar{\gamma}'_l = \frac{2\alpha_l^2}{\sigma^2}$ denotes the average SNR of the channel. For simplicity, it is assumed that the power per transmission per node for all the nodes are identical, and equalized to 1.

### 4.3.1 Non-Network Coding

As described in the last chapter, the Non-NC scheme includes the straightforward scheme with the symmetrical exchange pattern and the optimized scheme with the non-symmetrical exchange pattern. It should be noted that the transmission procedure of each message in the optimized scheme is the same as that in the straightforward scheme, therefore the received SNR of each message is the same for both schemes. Furthermore, the non-symmetrical exchange pattern in the optimized scheme is different from the straightforward and MH-WNC schemes. Therefore, in this and the following chapters, the performance analysis for the optimized scheme is omitted. Interested readers can derive the received SNR and outage performance with the same procedure for the straightforward scheme provided in this chapter.

In the following parts of the dissertation, the Non-NC scheme represents the traditional straightforward scheme described in Section 3.4.1.

For the Non-NC scheme, relays amplify and forward the received signals from the previous nodes. The received signal at relay $N_l, l = 3, 4, ..., n-2$ in time slot $j$ can be written as

$$\begin{aligned} y_l^j &= G_{l-1} h_{l-1} t_{l-1}^j + \omega_l^j, \quad N_1 \rightarrow N_L, \\ y_l^j &= G_{l+1} h_l t_{l+1}^j + \omega_i^j, \quad N_L \rightarrow N_1. \end{aligned}$$

where $G_l$ represents the gain at relay nodes $N_l$. In order to satisfy the average power constrain on relay nodes [136], $G_l$ is set to

$$\overleftarrow{G}_l = \sqrt{\frac{1}{|h_l|^2 + \sigma^2}}, \quad N_l \xleftarrow{t_{l+1}^j} N_{l+1}, \tag{4.1}$$

$$\vec{G}_l = \sqrt{\frac{1}{|h_{l-1}|^2 + \sigma^2}}, \quad N_{l-1} \xrightarrow{t_{l-1}^j} N_l. \tag{4.2}$$

For the relay nodes $N_2$ and $N_{L-1}$, $y_l^j$ is given by

$$y_2^j = h_1 t_1^j + \omega_2^j, \quad N_1 \to N_2,$$
$$y_{L-1}^j = h_{L-1} t_L^j + \omega_{L-1}^j, \quad N_L \to N_{L-1}.$$

Therefore, the received signal at node $N_1$ in time slot $j \in \{L-1, 3(L-1), ..., (2K-1)(L-1)\}$ can be derived as

$$y_1^{L-1} = \prod_{l=1}^{L-1} h_l \prod_{l=2}^{L-1} \overleftarrow{G}_l \hat{v}_1 + \sum_{l=1}^{L-1} \omega_l^{L-1-l+1} \prod_{z=1}^{l-1} h_{z-1} \prod_{z=2}^{l} \overleftarrow{G}_z,$$
$$y_1^{3(L-1)} = \prod_{l=1}^{L-1} h_l \prod_{l=2}^{L-1} \overleftarrow{G}_l \hat{v}_2 + \sum_{l=1}^{L-1} \omega_l^{2(L-1)-l+1} \prod_{z=1}^{l-1} h_{z-1} \prod_{z=2}^{l} \overleftarrow{G}_z,$$
$$...$$
$$y_{\hat{v}_k} = y_1^{(2k-1)(L-1)} = \prod_{l=1}^{L-1} h_l \prod_{l=2}^{L-1} \overleftarrow{G}_l \hat{v}_k + \sum_{l=1}^{L-1} \omega_l^{(2k-1)(L-1)-l+1} \prod_{z=1}^{l-1} h_{z-1} \prod_{z=2}^{l} \overleftarrow{G}_z. \quad (4.3)$$

Following (4.3), the received SNR of $\hat{v}_k$ can be written as

$$\gamma_{\hat{v}_k} = \frac{\mathcal{S}_{y_{\hat{v}_k}}}{\mathcal{N}_{y_{\hat{v}_k}}}, \quad (4.4)$$

where $\mathcal{S}_{y_{\hat{v}_k}}$ and $\mathcal{N}_{y_{\hat{v}_k}}$ are the signal and noise powers, respectively.

The signal power $\mathcal{S}_{y_{\hat{v}_k}}$ can be given by

$$\mathcal{S}_{y_{\hat{v}_k}} = \left| \prod_{l=1}^{L-1} h_l \prod_{l=2}^{L-1} \overleftarrow{G}_l \hat{v}_k \right|^2 = \prod_{l=1}^{L-1} |h_l|^2 \prod_{l=2}^{L-1} \overleftarrow{G}_l^2, \quad (4.5)$$

and the noise power $\mathcal{N}_{y_{\hat{v}_k}}$ can be obtained as

$$\mathcal{N}_{y_{\hat{v}_k}} = \left| \sum_{l=1}^{L-1} \omega_l^{(2k-1)(L-1)-l+1} \prod_{z=1}^{l-1} h_{z-1} \prod_{z=2}^{l} \overleftarrow{G}_z \right|^2 = \sum_{l=1}^{L-1} \sigma^2 \prod_{z=1}^{l-1} |h_z|^2 \prod_{z=2}^{l} \overleftarrow{G}_z^2. \quad (4.6)$$

The received SNRs of each message are identical to each other due to the same transmission procedure in the two-way relay network. Thus, the end-to-end SNR of the Non-NC scheme is equivalent to the received SNR of $\hat{v}_k$, given by

$$\gamma_{\text{Non-NC}} = \gamma_{\hat{v}_k} = \frac{\prod_{l=1}^{L-1} |h_l|^2 \prod_{l=2}^{L-1} \overleftarrow{G}_l^2}{\sum_{l=1}^{L-1} \sigma^2 \prod_{z=1}^{i-1} |h_z|^2 \prod_{z=2}^{i} \overleftarrow{G}_z^2}. \quad (4.7)$$

The end-to-end SNR given by (4.7) can be simplified as

$$\gamma_{\text{Non-NC}} = \left[ \prod_{l=1}^{L-1} \left( 1 + \frac{1}{\gamma'_l} \right) - 1 \right]^{-1}, \quad (4.8)$$

as proven in Appendix (A.1).

The expansion of (4.8) results in the polynomials of $\frac{1}{\gamma'_l}$, and the upper bound of end-to-end SNR of $\gamma_{\text{Non-NC}}$ at high SNR regions can be evaluated by canceling the high-order product term of $\frac{1}{\gamma'_l}$ in (4.8) as

$$\hat{\gamma}_{\text{Non-NC}} = \left[\sum_{l=1}^{L-1} \frac{1}{\gamma'_l}\right]^{-1}. \tag{4.9}$$

### 4.3.2 Multi-Hop Analog Network Coding

The transmission scheme of MH-WNC for the MH-TRC was generalized in the last chapter (refer to Section 3.5 and Section 3.6).

The ANC strategy is applied at each relay for MH-ANC, and the transmitted signal of relay node $N_l$ in time slot $j$ is a scaled version of the received signal in the previous time slot, given by

$$t_l^j = G_l y_l^{j-1}, \tag{4.10}$$

where $G_l$ represents the gain at relay nodes $N_l$, which is set to

$$G_l = \sqrt{\frac{1}{|h_{l-1}|^2 + |h_l|^2 + \sigma^2}}, \quad N_{l-1} \xrightarrow{t_{l-1}^j} N_l \xleftarrow{t_{l+1}^j} N_{l+1}. \tag{4.11}$$

In the MH-ANC scheme, the signal is transmitted bi-directionally throughout the process. The received signal at relay $N_l, l = \{3, 4, ..., L-2\}$ in time slot $j$ can be obtained as

$$y_l^j = G_{l-1} h_{l-1} t_{l-1}^j + G_{l+1} h_l t_{l+1}^j + \omega_i^j,$$

and for the relay nodes $N_2$ and $N_{L-1}$, $y_l^j$ is given by

$$\begin{aligned} y_2^j &= h_1 \hat{u}_{j+1/2} + G_3 h_2 t_3^j + \omega_2^j, \\ y_{L-1}^j &= h_{L-1} \hat{v}_{j+1/2} + G_{L-2} h_{L-2} t_{L-2}^j + \omega_{L-1}^j. \end{aligned}$$

For example, the received signal at user node $N_1$ in time slot 4 and 6 in a

5-node 2-message MH-TRC can be derived as

$$
\begin{aligned}
y_1^4=&h_1t_2^4+\omega_1^4\\
=&h_1\left(G_2y_2^3\right)+\omega_1^4\\
=&h_1\left(G_2\left(h_1\hat{u}_2+h_2t_3^3+\omega_2^3\right)\right)+\omega_1^4\\
=&h_1\left(G_2\left(h_1\hat{u}_2+h_2G_3y_3^2+\omega_2^3\right)\right)+\omega_1^4\\
=&h_1\left(G_2\left(h_1\hat{u}_2+h_2G_3y_3^2+\omega_2^3\right)\right)+\omega_1^4\\
=&h_1\left(G_2\left(h_1\hat{u}_2+h_2G_3\left(h_2t_2^2+h_3t_4^2+\omega_3^2\right)+\omega_2^3\right)\right)+\omega_1^4\\
=&h_1\left(G_2\left(h_1\hat{u}_2+h_2G_3\left(h_2G_2y_2^1+h_3G_4y_4^1+\omega_3^2\right)+\omega_2^3\right)\right)+\omega_1^4\\
=&h_1\left(G_2\left(h_1\hat{u}_2+h_2G_3\left(h_2G_2\left(h_1\hat{u}_1+\omega_2^1\right)+h_3G_4\left(h_4\hat{v}_1+\omega_4^1\right)+\omega_3^2\right)+\omega_2^3\right)\right)+\omega_1^4\\
=&h_1^2G_2\hat{u}_2+h_2^2h_1^2G_2^2G_3\hat{u}_1+h_4h_3h_2h_1G_4G_3G_2\hat{v}_1\\
&+\omega_1^4+\omega_2^3h_1G_2+\omega_3^2h_2G_3h_1G_2+\omega_2^1h_2G_2h_2G_3h_1G_2+\omega_4^1h_3G_4h_2G_3h_1G_2,\\
y_1^6=&h_1t_2^6+\omega_1^6\\
=&h_1\left(G_2y_2^5\right)+\omega_1^6\\
=&h_1\left(G_2\left(h_2t_3^5+\omega_2^5\right)\right)+\omega_1^6\\
=&...\\
=&h_1^2h_2^2G_2^2G_3\hat{u}_2+h_1h_2h_3h_4G_2G_3G_4\hat{v}_2+\\
&(h_1^2G_2^3h_2^4G_3^2+h_1^2G_2^2h_2^2G_3^2h_3^2G_4)\hat{u}_1+(h_1G_2^2h_2^3G_3^2h_3G_4h_4+h_1G_2h_2G_3^2h_3^3G_4^2h_4)\hat{v}_1+\\
&\omega_1^6+\omega_2^5h_1G_2+\omega_3^4h_1G_2h_2G_3+\omega_4^3h_1G_2h_2G_3h_3G_4+\\
&\omega_2^3h_1G_2^2h_2^2G_3+\omega_3^2(h_1G_2^2h_2^3G_3^2+h_1G_2h_2G_3^2h_3^2G_4)+\\
&\omega_2^1(h_1G_2^3h_2^4G_3^2+h_1G_2^2h_2^2G_3^2h_3^2G_4)+\omega_4^1(h_1G_2^2h_2^3G_3^2h_3G_4+h_1G_2h_2G_3^2h_3^3G_4^2).
\end{aligned}
$$

After time slot $L-1$, the user nodes receive the signals with the counterpart messages from the neighboring relay nodes. For MH-ANC in the generalized $L$-node $K$-message MH-TRC with the case $2K-1\geqslant L-1$, $y_1^j$ can be given by

$$
\begin{aligned}
y_1^j=&\sum_{l=1}^{\frac{j}{2}}\phi_l^j\hat{u}_l+\sum_{l=1}^{\frac{j-(L-1)}{2}}\phi'^j_l\hat{v}_l+\prod_{l=1}^{L-1}h_l\prod_{l=2}^{L-1}G_l\hat{v}_{\frac{j-L+3}{2}}+\sum_{l=1}^{L-1}\sum_{i=1}^{j}\psi_l^i\omega_l^i, \qquad (4.12)\\
&j\in\{L-1,L+1,...,2K-2\}
\end{aligned}
$$

$$
\begin{aligned}
y_1^j=&\sum_{l=1}^{K}\phi_l^j\hat{u}_l+\sum_{l=1}^{\frac{j-(L-1)}{2}}\phi'^j_l\hat{v}_l+\prod_{l=1}^{L-1}h_l\prod_{l=2}^{L-1}G_l\hat{v}_{\frac{j-L+3}{2}}+\sum_{l=1}^{L-1}\sum_{i=1}^{j}\psi_l^i\omega_l^i, \qquad (4.13)\\
&j\in\{2K,2K+2,...,\mathcal{T}_{\text{MH-ANC}}\}
\end{aligned}
$$

and for the case $2K-1<L-1$, $y_1^j$ can be given by

$$y_1^j=\sum_{l=1}^{K}\phi_l^j\hat{u}_l+\sum_{l=1}^{\frac{j-(L-1)}{2}}\phi'^j_l\hat{v}_l+\prod_{l=1}^{L-1}h_l\prod_{l=2}^{L-1}G_l\hat{v}_{\frac{j-L+1}{2}+1}+\sum_{l=1}^{L-1}\sum_{i=1}^{j}\psi_l^i\omega_l^i, \quad (4.14)$$
$$j\in\{L-1,L+1,...,\mathcal{T}_{\text{MH-ANC}}\}$$

where $\phi_l^i$, $\phi'^i_l$ and $\psi_l^i$ are two polynomials of $\{h_l\}_{l=1}^{L-1}$ and $\{G_l\}_{l=2}^{L-1}$ in time slot $i$. (4.12) describes the transmission between $\hat{v}_1$ reaches $N_1$ and $\hat{u}_K$ is sent from $N_1$, and (4.13) denotes the transmission after $\hat{u}_K$ is sent from $N_1$ until time slot $\mathcal{T}_{\text{MH-ANC}}$.

At time slot $L-1$, it is shown by (4.13) that $y_1^{L-1}$ contains terms $\{\hat{u}_1,\hat{u}_2,...,\hat{u}_{(L-1)/2}\}$ and $\hat{v}_1$. Assuming that user node $N_1$ has the knowledge of $\phi_l^i$ and $\psi_l^i$, user node $N_1$ can recover $\hat{v}_1$ by canceling terms $\{\hat{u}_1,\hat{u}_2,...,\hat{u}_{(L-1)/2}\}$. In the next receiving time slot $L+1$, $y_1^{L+1}$ contains terms $\{\hat{u}_1,\hat{u}_2,...,\hat{u}_{(L+1)/2}\}$, $\hat{v}_1$ and $\hat{v}_2$. By canceling the terms of its own messages and $\hat{v}_1$ recovered in time slot $L-1$, user node $N_1$ can recover message $\hat{v}_2$. This operation continues until the end of the exchange process.

The received signal of $\hat{v}_k$ at user node $N_1$ in time slot $L-1+2(k-1)$ after canceling the known message terms can be derived as

$$y^*_{\hat{v}_k}=\prod_{l=1}^{L-1}h_l\prod_{l=2}^{L-1}G_l\hat{v}_k+\sum_{l=1}^{L-1}\sum_{i=1}^{L-1+2(k-1)}\psi_l^i\omega_l^i. \quad (4.15)$$

Similarly, the received signal of $\hat{u}_k$ is

$$y^*_{\hat{u}_k}=\prod_{l=1}^{L-1}h_l\prod_{l=2}^{L-1}G_l\hat{u}_k+\sum_{l=2}^{L}\sum_{i=1}^{L-1+2(k-1)}\psi'^i_l\omega_l^i, \quad (4.16)$$

where $\psi'^i_l$ is also the polynomial of $\{h_l\}_{l=1}^{L-1}$ and $\{G_l\}_{l=2}^{L-1}$.

## 4.4 Received SNR

Following (4.15), the received SNR of $\hat{v}_k$ can be given by

$$\gamma_{\text{MH-ANC},\hat{v}_k}=\frac{\mathcal{S}_{\text{MH-ANC},\hat{v}_k}}{\mathcal{N}_{\text{MH-ANC},\hat{v}_k}}=\frac{\prod_{l=1}^{L-1}|h_l|^2\prod_{l=2}^{L-1}G_l^2}{\sum_{l=1}^{L-1}\sum_{i=1}^{L-1+2(k-1)}|\psi_l^i|^2\sigma^2}. \quad (4.17)$$

The only unknown variable in the received SNR given by (4.17) is $\psi_l^i$, which represents the received noise power at each node propagating until the end of the transmission of message $\hat{v}_k$. Due to the bi-directional transmission throughout the process, the complexities of the expressions for $\phi_l^i$, $\psi_l^i$ and $\psi'^i_l$ increase exponentially with the increased number of nodes and messages. It is difficult to derive the expressions of these two polynomials intuitively. In the following sections, two different recursive approaches for the received noise power $\mathcal{N}_{\mathrm{ANC},\hat{v}_k}$ are proposed.

### 4.4.1 Forward Recursive Approach

According to the transmission scenario presented in Section 3.6, the user nodes do not receive any signal before time slot $L-1$. However, to assist the received SNR analysis, "virtual" receive signals at the user nodes $N_1$ before time slot $L-1$ are created, denoted by $\{y_1^j\}_{j=2,4,\ldots,L-1}$. For example, the received signal at user node $N_1$ in time slot 4 and 6 can be given as follows

$$\begin{aligned}
y_1^2=&G_2h_1t_2^1+\omega_1^2\\
=&G_2h_1(h_1\hat{u}_1+\omega_2^1)+\omega_1^2\\
=&G_2h_1h_1\hat{u}_1+G_2h_1\omega_2^1+\omega_1^2, \qquad (4.18)\\
y_1^4=&G_2h_1t_2^3+\omega_1^4\\
=&G_2h_1(h_1t_1^3+G_3h_2t_3^3+\omega_2^3)+\omega_1^4\\
=&G_2h_1(h_1\hat{u}_2+G_3h_2(G_2h_2t_2^2+\omega_3^2)+\omega_2^3)+\omega_1^4\\
=&G_2h_1(h_1\hat{u}_2+G_3h_2(G_2h_2h_1\hat{u}_1+G_2h_2\omega_2^1+\omega_3^2)+\omega_2^3)+\omega_1^4. \qquad (4.19)
\end{aligned}$$

The terms that contains the outgoing signals will be canceled upon the final reception at user nodes. Therefore, the corresponding noise terms in the above two received signals are given by

$$n_1^2=G_2h_1\omega_2^1+\omega_1^2, \qquad (4.20)$$

$$n_1^4=G_2h_1G_3h_2G_2h_2\omega_2^1+G_2h_1G_3h_2\omega_3^2+G_2h_1\omega_2^3+\omega_1^4. \qquad (4.21)$$

The two equations (4.20) and (4.21) are easily understood. The received noise in time slot 2 contains the propagated received noise at relay node $N_2$ in time

slot 1 and the received noise at user node $N_1$ in time slot 2. The received noise in time slot 4 consists of the propagated received noises $\omega_2^1$, $\omega_3^2$, $\omega_2^3$ and $\omega_1^4$.

Denote by $\mathcal{N}_i'$ the received noise power at user node $N_1$ in time slot $i$, the corresponding noise powers for (4.20) and (4.21) are

$$\mathcal{N}_2' = (G_2^2|h_1|^2 + 1)\sigma^2 = (\psi_2^2 + \psi_1^2)\sigma^2, \tag{4.22}$$

$$\begin{aligned}\mathcal{N}_4' &= (G_2^2|h_1|^2 G_3^2|h_2|^2 + G_2^2|h_1|^2 G_3^2|h_2|^2 G_2^2|h_2|^2 + G_2^2|h_1|^2 + 1)\sigma^2 \\ &= (\psi_3^2 + \psi_2^2 + \psi_1^2)\sigma^2.\end{aligned} \tag{4.23}$$

It can be observed that the received noise at the user node consists of the propagated received noise at different relay nodes in different time slots. Therefore, the calculation of the received noise of each message equals the calculation of the received noise at each transmission propagating through different paths to the user nodes.

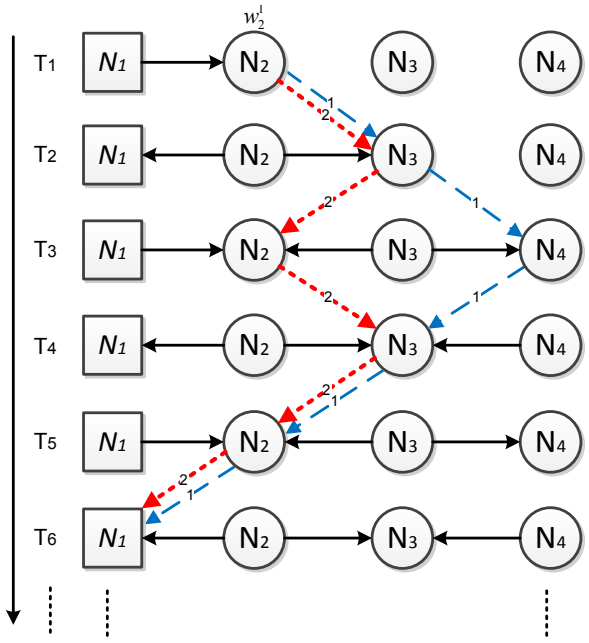


Figure 4.2: Propagation paths of $w_2^1$ in 6 time slots.

Assuming that message $\hat{v}_1$ has not arrived at $N_1$ in time slot 6, a simple example to display the noise propagation can be shown in Figure 4.2. The solid arrows represent the transmission in different time slots, and the dash and dotted arrows indicate the two propagation paths of received noise $\omega_2^1$ to time slot 6. Polynomial $\psi_2^1$ for term $\omega_2^1$ is the summation of the propagations at the two

paths. The noise propagation at each path can be calculated by multiplying the amplification factor at each node along the path. As a result, polynomial $\psi_2^1$ can be obtained as

$$\begin{aligned}\phi_2^1 =& \underbrace{G_2^2|h_2|^2 G_3^2|h_3|^2 G_4^2|h_3|^2 G_3^2|h_2|^2 G_2^2|h_1|^2}_{\text{Path 1}} + \underbrace{G_2^2|h_2|^2 G_3^2|h_2|^2 G_2^2|h_2|^2 G_3^2|h_2|^2 G_2^2|h_1|^2}_{\text{Path 2}} \\ =& \underbrace{G_4^2 G_3^4 G_2^4 |h_3|^4 |h_2|^4 |h_1|^2}_{\text{Path 1}} + \underbrace{G_3^4 G_2^6 |h_2|^8 |h_1|^2}_{\text{Path 2}}. \end{aligned} \tag{4.24}$$

Although there are only two terms in (4.24), and it is easy to deduce the polynomials for other received noise similarly. However, the number of paths to the user node increases quickly with the increased number of time slots.

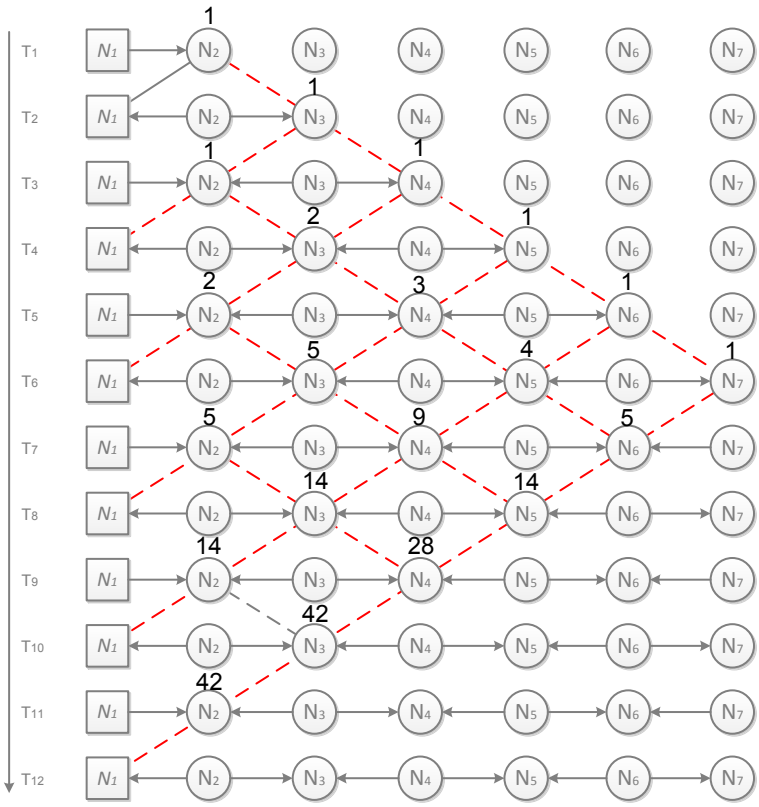


Figure 4.3: The number of propagation paths to each node.

Figure 4.3 shows the numbers of paths to each node in different time slots. As can be seen from the figure, the number of transmission paths to a relay node in time slot $j$ equals the sum of the numbers of transmission paths to the two neighboring relays in the previous time slot $j-1$. For instance, the number of propagation paths of the received noise $\omega_2^1$ is 42 in time slot 11. It can be deduced

that the number of the transmission paths for the received noise $\omega_2^1$ is 286 in time slot 16, and over 1000 in time slot 20. Moreover, after the first message $\hat{v}_1$ arrives at $N_1$, the complexity for deriving $\{\psi_l^i\}_{l=1,\ldots,L-1}^{i=1,\ldots,j}$ is doubled due to the noise term from relay nodes $\{N_l\}_{l=(L+3)/2}^{L-1}$. Therefore, it is computationally intractable to use this forward recursive approach to derive the linear combination $\psi_i^j$ when the number of messages is large.

### 4.4.2 Backward Recursive Approach

In order to circumvent the complexity issue when the numbers of nodes and messages are large, a novel backward recursive approach is proposed to derive the noise power $\mathcal{N}_j'$, as illustrated by Figure 4.4.

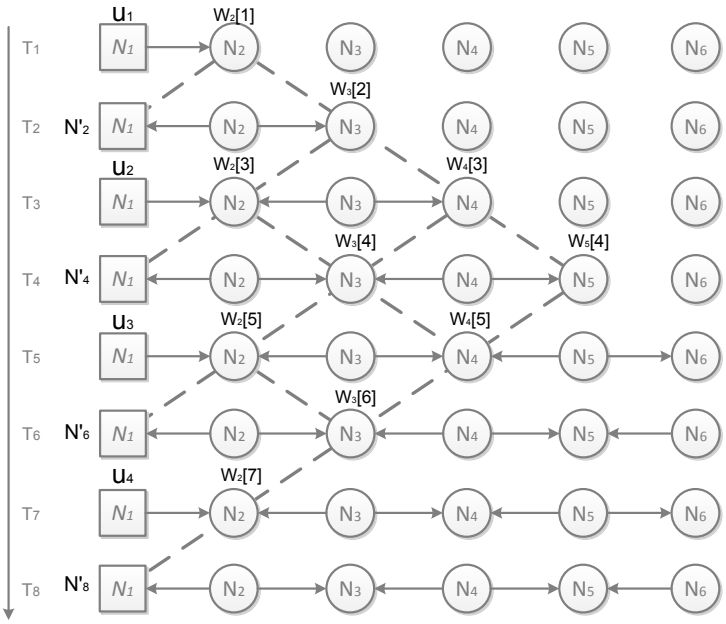


Figure 4.4: Backward recursive approach for the noise power at the user node $N_1$.

In the following derivations, $\sum_{i=a}^{b} \triangleq 0$ when $b < a$, and $\prod_{i=a}^{b} \triangleq 1$ when $b < a$. First, denote by $N_l^j$ the relay node $N_l$ in time slot $j$. Let $w_l[j]$ be the total received noise (including the received noise at this node and the propagation noise from the previous time slots) at $N_l^j$. From Figure 4.4, the following expressions can be

obtained

$$w_2[1]=\frac{\mathcal{N}'_2-\sigma^2}{|h_1|^2G_2^2},\quad w_2[3]=\frac{\mathcal{N}'_4-\sigma^2}{|h_1|^2G_2^2},\quad ...\quad w_2[j]=\frac{\mathcal{N}'_{j+1}-\sigma^2}{|h_1|^2G_2^2}, \tag{4.25}$$

$$w_3[2]=\frac{w_2[3]-\sigma^2}{|h_2|^2G_3^2},\quad w_3[4]=\frac{w_2[5]-\sigma^2}{|h_2|^2G_3^2},\quad ...\quad w_3[j]=\frac{w_2[j+1]-\sigma^2}{|h_2|^2G_3^2}, \tag{4.26}$$

$$w_4[3]=\frac{w_3[4]-w_2[3]|h_2|^2G_2^2}{|h_2|^2G_3^2},\quad w_4[5]=\frac{w_3[6]-w_2[5]|h_2|^2G_2^2}{|h_2|^2G_3^2},$$

$$w_5[4]=\frac{w_4[5]-w_3[4]|h_3|^2G_3^2}{|h_4|^2G_5^2},$$

$$...$$

$$w_l[j]=\frac{w_{i-1}[j+1]-w_{i-2}[j]|h_{i-2}|^2G_{i-2}^2}{|h_{i-1}|^2G_j^2}.\quad \forall i\neq 2,3\forall j \tag{4.27}$$

For example, the received noise power at user node $N_1$ can be recursively given by

$$\begin{aligned}
\mathcal{N}'_2 &= w_2[1]|h_1|^2G_2^2+\sigma^2\\
&= |h_1|^2G_2^2\sigma^2+\sigma^2,\\
\mathcal{N}'_4 &= w_2[3]|h_1|^2G_2^2+\sigma^2\\
&= \left(w_3[2]|h_2|^2G_3^2+\sigma^2\right)|h_1|^2G_2^2+\sigma^2\\
&= \left(\left(w_2[1]|h_2|^2G_2^2+\sigma^2\right)|h_2|^2G_3^2+\sigma^2\right)|h_1|^2G_2^2+\sigma^2\\
&= \left(\left(\frac{\mathcal{N}'_2-\sigma^2}{|h_1|^2G_2^2}|h_2|^2G_2^2+\sigma^2\right)|h_2|^2G_3^2+\sigma^2\right)|h_1|^2G_2^2+\sigma^2\\
&= \left(\mathcal{N}'_2-\sigma^2\right)|h_2|^4G_3^2G_2^2+\left(|h_2|^2G_3^2+|h_2|^2G_3^2|h_1|^2G_2^2+1\right)\sigma^2\\
&= \left(\mathcal{N}'_2-\sigma^2\right)|h_2|^4G_3^2G_2^2+\sum_{j=1}^{3}\sigma^2\prod_{k=2}^{j}|h_{k-1}|^2G_k^2,\\
\mathcal{N}'_6 &= w_2[5]|h_1|^2G_2^2+\sigma^2\\
&= \left(w_3[4]|h_2|^2G_3^2+\sigma^2\right)|h_1|^2G_2^2+\sigma^2\\
&= \left(\left(w_2[3]|h_2|^2G_2^2+w_4[3]|h_3|^2G_4^2+\sigma^2\right)|h_2|^2G_3^2+\sigma^2\right)|h_1|^2G_2^2+\sigma^2\\
&= \left(\left(\frac{\mathcal{N}'_4-\sigma^2}{|h_1|^2G_2^2}|h_2|^2G_2^2+\left(w_3[2]|h_3|^2G_3^2+\sigma^2\right)|h_3|^2G_4^2+\sigma^2\right)|h_2|^2G_3^2+\sigma^2\right)|h_1|^2G_2^2+\sigma^2\\
&= \left(\left(\frac{\mathcal{N}'_4-\sigma^2}{|h_1|^2G_2^2}|h_2|^2G_2^2+\left(\left(\frac{\mathcal{N}'_4-\sigma^2}{|h_1|^2G_2^2}-\sigma^2\right)|h_3|^2G_3^2+\sigma^2\right)|h_3|^2G_4^2+\sigma^2\right)|h_2|^2G_3^2\right.\\
&\quad \left.+\sigma^2\right)|h_1|^2G_2^2+\sigma^2\\
&= \sum_{j=1}^{2}|h_{j+1}|^4G_{j+1}^2G_{j+2}^2\left(\mathcal{N}'_4-\sum_{k=1}^{j}\sigma^2\prod_{l=2}^{k}|h_{l-1}|^2G_l^2\right)+\sum_{j=1}^{4}\sigma^2\prod_{k=2}^{j}|h_{k-1}|^2G_k^2,\\
\mathcal{N}'_8 &= ...
\end{aligned}$$

$$
\begin{aligned}
\mathcal{N}'_l \;=\; & \sum_{j=1}^{\lfloor \frac{i}{4} \rfloor}(-1)^{j-1}\Bigg[\sum_{l_1=1}^{i/2-1}|h_{l_1+1}|^4 G_{l_1+1}^2 G_{l_1+2}^2\Bigg(\sum_{l_2=3}^{l_1}|h_{l_2-1}|^4 G_{l_2-1}^2 G_{l_2+1}^2\Bigg(... \\
& \Bigg(\sum_{l_j=2j-1}^{l_{j-1}}|h_{l_j-(2j-3)}|^4 G_{l_j-(2j-3)}^2 G_{l_j-(2j-4)}^2\Bigg(\mathcal{N}'_{i-2j}-\sum_{m=1}^{l_j-(2j-2)}\sigma^2\prod_{n=2}^{m}|h_{L-1}|^2 G_n^2\Bigg)\Bigg)...\Bigg)\Bigg)\Bigg] \\
& +\sum_{j=1}^{i/2+1}\sigma^2\prod_{k=2}^{j}|h_{k-1}|^2 G_k^2 \\
= & \sum_{j=1}^{\lfloor \frac{i}{4} \rfloor}(-1)^{j-1}\left(\bigotimes_{k=1}^{j}\left(\Phi(k)\prod_{h=j}^{k}\left(\mathcal{N}'_{i-2j}-\sum_{m=1}^{l_j-(2j-2)}\sigma^2\prod_{n=2}^{m}|h_{L-1}|^2 G_n^2\right)\right)\right) \\
& +\sum_{j=1}^{i/2+1}\sigma^2\prod_{k=2}^{j}|h_{k-1}|^2 G_k^2, \\
& i\in\{2,4,...,L-3\}
\end{aligned}
\tag{4.28}
$$

where $\lfloor x \rfloor$ represents taking the integer value of $x$, $\bigotimes_{k=1}^{j}\Phi(k)$ represents $\Phi(1)(\Phi(2)(...(\Phi(j))...))$, and $\Phi(k)=\sum_{l_k=2k-1}^{l_{k-1}}|h_{l_k-(2k-3)}|^4 G_{l_k-(2k-3)}^2 G_{l_k-(2k-4)}^2$, $l_0=i/2-1$.

It can be seen that the received noise for message $\hat{v}_1$ is equivalent to the received noise at user node $N_1$ in time slot $L-1$. Therefore, the received noise for message $\hat{v}_1$ can be given by

$$
\begin{aligned}
& \mathcal{N}_{\text{MH-ANC},\hat{v}_1} \\
& = \mathcal{N}'_{L-1} \\
& = \sum_{j=1}^{\lfloor \frac{L-1}{4} \rfloor}(-1)^{j-1}\left(\bigotimes_{k=1}^{j}\left(\Phi(k)\prod_{h=j}^{k}\left(\mathcal{N}'_{L-1-2j}-\sum_{m=1}^{l_j-(2j-2)}\sigma^2\prod_{n=2}^{m}|h_{L-1}|^2 G_n^2\right)\right)\right) \\
& +\sum_{j=1}^{(L+1)/2}\sigma^2\prod_{k=2}^{j}|h_{k-1}|^2 G_k^2+\underbrace{\sum_{j=(L+3)/2}^{L-1}\sigma^2\prod_{k=2}^{j}|h_{k-1}|^2 G_k^2}_{A},
\end{aligned}
\tag{4.29}
$$

where term $A$ comes from the propagation of the received noises at $\{N_l\}_{l=L+3/2}^{L-1}$. With the same procedure, the noise power of message $\hat{v}_k$ can be calculated as

$$
\begin{aligned}
& \mathcal{N}_{\text{MH-ANC},\hat{v}_k} \\
& =\sum_{j=1}^{\Psi(k)}(-1)^{j-1}\left(\bigotimes_{k=1}^{j}\left(\Phi(k)\prod_{h=j}^{k}\left(\mathcal{N}'_{L-1+2(i-1)-2j}-\sum_{m=1}^{l_j-(2j-2)}\sigma^2\prod_{n=2}^{m}|h_{L-1}|^2 G_n^2\right)\right)\right) \\
& +\sum_{j=1}^{L-1}\sigma^2\prod_{k=2}^{j}|h_{k-1}|^2 G_k^2,
\end{aligned}
\tag{4.30}
$$

and the corresponding received SNR of message $\hat{v}_k$ can be derived as

$$\begin{aligned}
&\gamma_{\text{MH-ANC},\hat{v}_k} \\
&= \frac{\mathcal{S}_{\text{MH-ANC},\hat{v}_k}}{\mathcal{N}_{\text{MH-ANC},\hat{v}_k}} \\
&= \Bigg[ \sum_{j=1}^{L-1} \frac{1}{\gamma'_j} \prod_{k=j+1}^{L-1} \left( 1 + \frac{1}{\gamma'_k} + \frac{\gamma'_{k-1}}{\gamma'_k} \right) \\
&+ \frac{\sum_{j=1}^{\Psi(k)} (-1)^{j-1} \left( \boxtimes_{k=1}^{j} \left( \Phi(k) \prod_{h=j}^{k} \left( \mathcal{N}'_{L+2i-2j-3} - \sum_{m=1}^{l_j-2j+2} \sigma^2 \prod_{n=2}^{m} |h_{L-1}|^2 G_n^2 \right) \right) \right)}{\prod_{j=1}^{L-1} |h_j|^2 \prod_{j=2}^{L-1} G_j^2} \Bigg]^{-1}.
\end{aligned}$$

$$\Psi(k) = \begin{cases} \lfloor \frac{L-2}{2} \rfloor & \frac{L-1+2(k-1)}{2} \geq L-1 \\ \lfloor \frac{L-1}{4} \rfloor + k - 1 & else \end{cases}$$

$$l_0 = L - 3. \tag{4.31}$$

In summary, the received SNR of $\hat{v}_k$ with MH-ANC can be obtained by the forward recursive approach when the numbers of nodes and messages are relatively small, while the backward recursive approach can be used to derive $\gamma_{\text{MH-ANC},\hat{v}_k}$ when the numbers of nodes and messages are large.

## 4.5 End-to-End SNR

The end-to-end SNR for the $L$-node $K$-message MH-TRC is defined as the average received SNR for message sequences $\hat{\mathbf{U}} = \{\hat{u}_1, \hat{u}_2, ..., \hat{u}_K\}$ and $\hat{\mathbf{V}} = \{\hat{v}_1, \hat{v}_2, ..., \hat{v}_K\}$ as

$$\gamma = \frac{1}{2K} \left[ \sum_{k=1}^{K} \gamma_{\hat{u}_k} + \sum_{k=1}^{K} \gamma_{\hat{v}_k} \right], \tag{4.32}$$

where $\gamma_{\hat{u}_k}$ and $\gamma_{\hat{v}_k}$ are the received SNR for message $\hat{u}_k$ and $\hat{v}_k$, respectively. Due to the symmetry of the two-way transmission, $\gamma_{\hat{u}_k} = \gamma_{\hat{v}_k}$. Hence, it follows from (4.32) that

$$\gamma = \frac{1}{K} \sum_{k=1}^{K} \gamma_{\hat{v}_k}. \tag{4.33}$$

**End-to-end SNR of the 5-node 2-message MH-TRC with MH-ANC**: The end-to-end SNR for the special 5-node 2-frame multi-hop network is

$$\gamma^{52}_{\text{MH-ANC}} = \frac{1}{2}\Big(\gamma^{52}_{\text{MH-ANC},\hat{v}_1} + \gamma^{52}_{\text{MH-ANC},\hat{v}_2}\Big). \tag{4.34}$$

With the recursive expressions, the expressions of $\gamma^{52}_{\text{MH-ANC},\hat{v}_1}$ and $\gamma^{52}_{\text{MH-ANC},\hat{v}_2}$ can be readily obtained as

$$\gamma^{52}_{\text{MH-ANC},\hat{v}_1}=\left[\sum_{l=1}^{4}\frac{1}{\gamma'_l}\prod_{j=i+1}^{4}\left(1+\frac{1}{\gamma'_j}+\frac{\gamma'_{j-1}}{\gamma'_j}\right)+\frac{\gamma'_3+\gamma'_4+1}{\gamma'_4(\gamma'_1+\gamma'_2+1)}\right]^{-1}, \tag{4.35}$$

$$\begin{aligned}\gamma^{52}_{\text{MH-ANC},\hat{v}_2}=&\left[\sum_{l=1}^{4}\frac{1}{\gamma'_l}\prod_{j=i+1}^{4}\left(1+\frac{1}{\gamma'_j}+\frac{\gamma'_{j-1}}{\gamma'_j}\right)\right.\\&+\frac{\gamma'_3+\gamma'_4+1}{\gamma'_3\gamma'_4}\left(\frac{\gamma'_2}{\gamma'_1+\gamma'_2+1}+\left(\frac{\gamma'_3}{\gamma'_3+\gamma'_4+1}+\frac{\gamma'_2}{\gamma'_1+\gamma'_2+1}+1\right)\right.\\&\left.\left.\left(\frac{\gamma'^2_3}{(\gamma'_2+\gamma'_3+1)(\gamma'_3+\gamma'_4+1)}+\frac{\gamma'^2_2}{(\gamma'_2+\gamma'_3+1)(\gamma'_1+\gamma'_2+1)}\right)\right)\right]^{-1}\end{aligned} \tag{4.36}$$

Substituting (4.35) and (4.36) into (4.34), the expression for $\gamma^{52}_{\text{MH-ANC}}$ can be obtained. This study aims to derive the closed-form expression of the outage probability, which amounts to the calculation of the cumulative distribution function (CDF) of the end-to-end SNR. However, it can be seen that the expressions in (4.35) and (4.36) are the sum of dependent random variables, some of which are the reciprocal of the product of serval random variables. It is mathematically intractable to derive the CDF of end-to-end SNR $\gamma^{52}_{\text{MH-ANC}}$.

### 4.5.1 Upper Bound

To facilitate the performance analysis, the upper bound analysis for the end-to-end SNR is presented. It is assumed that all the channel coefficients are identically distributed [137], i.e., $\gamma'_l = \gamma'$. Hence, the expression of $\gamma^{52}_{\text{MH-ANC}}$ can be written as

$$\begin{aligned}\gamma^{52}_{\text{MH-ANC}}=&\frac{1}{2}\left[\sum_{l=1}^{4}\frac{1}{\gamma'}\prod_{j=i+1}^{4}\left(2+\frac{1}{\gamma'}\right)+\frac{1}{\gamma'}\right]^{-1}\\&+\frac{1}{2}\left[\sum_{l=1}^{4}\frac{1}{\gamma'}\prod_{j=i+1}^{4}\left(2+\frac{1}{\gamma'}\right)+\frac{1}{\gamma'}\left(\left(\frac{2\gamma'}{2\gamma'+1}\right)^2+\frac{2\gamma'}{2\gamma'+1}+1\right)\right]^{-1}\end{aligned} \tag{4.37}$$

To this end, the expansion of (4.37) is a polynomial of $\frac{1}{\gamma'}$. Thus, the upper bound of $\hat{\gamma}^{52}_{\text{MH-ANC}}$ at high SNR regions can be evaluated by canceling the high-order terms of $\frac{1}{\gamma'}$ as

$$\hat{\gamma}^{52}_{\text{MH-ANC}} = \frac{2}{35}\gamma'. \tag{4.38}$$

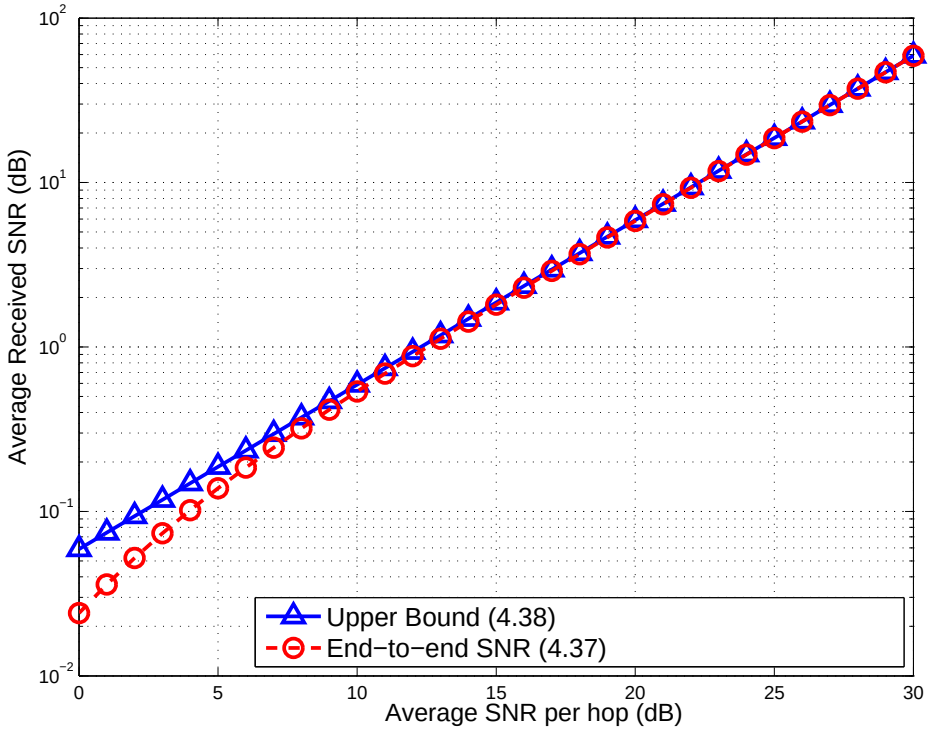


Figure 4.5: End-to-end SNR for the 5-node 2-message MH-TRC.

To verify the tightness of the upper bound, the upper bound given by (4.38) and the end-to-end SNR given by (4.37) are plotted in Figure 4.5. It can be clearly seen that $\hat{\gamma}^{52}_{\text{MH-ANC}}$ given by (4.38) is a very tight upper bound for $\gamma^{52}_{\text{MH-ANC}}$ in high SNR regions.

For the generalized $L$-node $K$-message MH-TRC, a closed-form result for the end-to-end SNR is unable to obtained from the above recursive expressions directly. However, the end-to-end SNR can be obtained via numerical computation. Figure 4.6 shows the end-to-end SNR (measured by the average SNR per channel $\gamma'$) versus the number of messages

As can be seen from the figure, the end-to-end SNR decreases with the increase in the number of messages. The descending rate drops with the increase in the

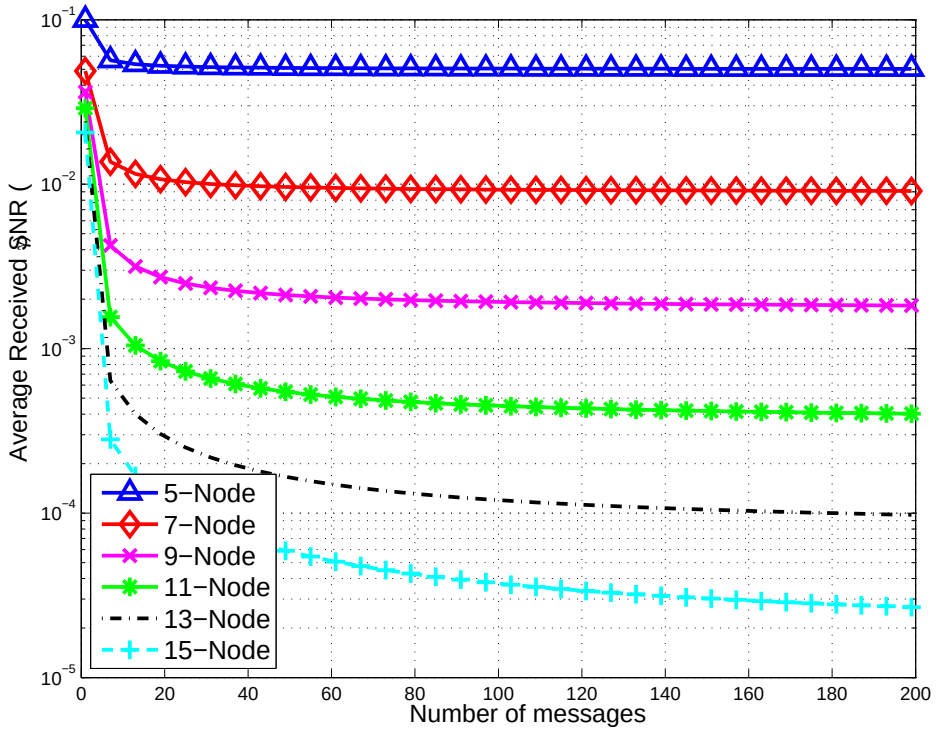


Figure 4.6: End-to-end SNR versus the number of messages for different scale MH-TRCs.

number of messages. The end-to-end SNR curve becomes even when the number of messages reaches a certain value. For the 5-node MH-TRC, when the number of messages is larger than 40, the end-to-end received SNR remains unchanged . Therefore, the end-to-end SNR when $K \gg L$ is estimated, which can be numerically illustrated by Figure 4.7.

As can be seen from Figure 4.7, the end-to-end SNR drops to $10^{-6}$ when the number of nodes is 21. Moreover, as will be demonstrated later, when the number of nodes is larger than 13, the outage probability of the MH-ANC approaches to 1. Therefore, the data in Figure 4.7 can be used to find an approximate function to fit the end-to-end SNR of MH-ANC.

In order to obtain an approximate closed-form expression for the end-to-end SNR of the MH-ANC scheme, the curve fitting tool in Matlab is used to obtain the fitting function of the upper bound end-to-end SNR in Figure 4.7. The procedure of finding the fitting function can be shown as follows:

**Curve fitting for the end-to-end SNR of the generalized MH-TRC:**

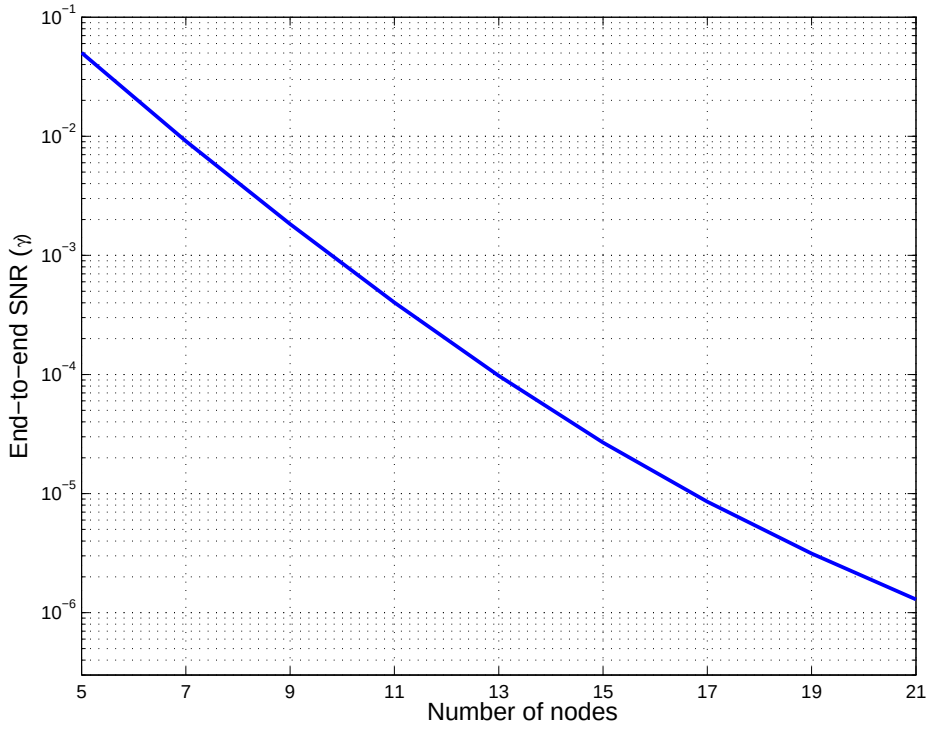


Figure 4.7: The upper bound end-to-end SNR versus the number of nodes.

It can be found from the recursive expressions, that term

$$A = \sum_{j=1}^{L-1} \frac{1}{{\gamma'}_j} \prod_{k=j+1}^{L-1} \left(1 + \frac{1}{{\gamma'}_k} + \frac{{\gamma'}_{k-1}}{{\gamma'}_k}\right) \tag{4.39}$$

in (4.31) is only affected by the number of nodes, which is the noise propagation from transmission path $\{N_L, N_{L-1}, N_{L-2}, ..., N_1\}$. On the other hand, term

$$B = \frac{\sum_{j=1}^{\Psi(k)} (-1)^{j-1} \left( \boxtimes_{k=1}^{j} \left( \Phi(k) \prod_{h=j}^{k} \left( {\mathcal{N}'}_{L+2i-2j-3} - \sum_{m=1}^{l_j-2j+2} \sigma^2 \prod_{n=2}^{m} |h_{L-1}|^2 G_n^2 \right) \right) \right)}{\prod_{j=1}^{L-1} |h_j|^2 \prod_{j=2}^{L-1} G_j^2} \tag{4.40}$$

in (4.31) is affected by both the numbers of nodes and messages. It can be observed from the simulation, that this term becomes trivial compared to term $A$ when the number of messages is large, and remains constant when the number of messages reaches a certain value. The upper bound of term $A$ in high SNR

regions can be simplified as

$$\begin{aligned}
A=&\sum_{j=1}^{L-1}\frac{1}{{\gamma'}_j}\prod_{k=j+1}^{L-1}\left(1+\frac{1}{{\gamma'}_k}+\frac{{\gamma'}_{k-1}}{{\gamma'}_k}\right)\\
=&\sum_{j=1}^{L-1}\frac{1}{\gamma'}\prod_{k=j+1}^{L-1}\left(2+\frac{1}{\gamma'}\right)\\
\overset{a}{\approx}&\sum_{j=1}^{L-1}\frac{1}{\gamma'}\prod_{k=j+1}^{L-1}2\\
=&\frac{1}{\gamma'}\sum_{j=1}^{L-1}\prod_{k=j+1}^{L-1}2\\
=&\frac{1}{\gamma'}\left(2^{L-1}-1\right),
\end{aligned} \tag{4.41}$$

where step $a$ is the approximation where the high-order terms of $\frac{1}{\gamma'}$ are cancelled in high SNR regions.

It should be noted that the above fitting function is not the only function to approximate the upper bound of end-to-end SNR. However, based on the recursive expressions and experiments, the following function is proposed to fit the curve shown in Figure 4.7

$$\left(\frac{(L-a)2^{L-1}}{b}-c\right)^{-1}\gamma', \tag{4.42}$$

where $a$, $b$ and $c$ are three independent parameters in the fitting function. The fitting parameters obtained with the curve fitting tool in Matlab are

$$a=3,\quad b=4,\quad c=1, \tag{4.43}$$

and the statistical results showing the goodness of fit are shown as follows

- Sum squared error (SSE): $3.526e-016$;
- R-square: 0.9983;
- Adjusted R-square: 0.9967; and
- Root-mean-square deviation (RMSE): $8.174e-014$.

It is shown by the statistical results that the result function provides a high accuracy.

To this end, the upper bound of the end-to-end SNR for the generalized $L$-node $K$-message MH-TRC in high SNR regions can be given by

$$\hat{\gamma}_{\text{MH-ANC}} \approx \left(\frac{(L-3)2^{L-1}}{4} - 1\right)^{-1} \gamma'. \tag{4.44}$$

## 4.6 Outage Probability

The maximum average mutual information [75] between the input and output in this case, achieved by independent and identically distributed (i.i.d.) zero-mean, circularly symmetric complex Gaussian inputs, is given as [136]

$$I_{\text{D}} = \log_2(1+\gamma), \tag{4.45}$$

where $\gamma$ is the end-to-end SNR of the system.

In the $L$-node $K$-message MH-TRC, the mutual information is

$$I_{\text{D}} = \frac{2K}{\mathcal{T}} \log_2(1+\gamma), \tag{4.46}$$

where $\mathcal{T}$ is the total time slots used for transmission. The outage event for a target rate $R$ is derived as follows

$$\begin{aligned} p^{out}(R) &= \Pr[I_{\text{D}} < R] \\ &= \Pr\left[\frac{2K}{\mathcal{T}} \log_2(1+\gamma) < R\right] \\ &= \Pr\left[\gamma < 2^{\frac{\mathcal{T}}{2K}R} - 1\right] \\ &= F_\gamma(2^{\frac{\mathcal{T}}{2K}R} - 1), \end{aligned} \tag{4.47}$$

where $F_\gamma(x)$ is the CDF of the end-to-end SNR. In the previous sections, the upper bound of the end-to-end SNR for both Non-NC and MH-ANC schemes is analyzed. Therefore, the upper bound outage probability can be obtained simply by substituting the CDF of the upper bound end-to-end SNR into (4.47).

- **Non-Network Coding**: The upper bound of the end-to-end SNR for the Non-NC scheme is given by eqnarray (4.9) as

$$\hat{\gamma}_{\text{Non-NC}} \approx \left[\sum_{l=1}^{L-1} \frac{1}{\gamma'_l}\right]^{-1}. \tag{4.48}$$

The end-to-end SNR given by the above eqnarray (4.48) is the summation of the reciprocals of the SNR at each hop. The SNR of each hop is exponentially distributed with parameter $1/\bar{\gamma}'_l$.

As shown in Appendix A.2 that the CDF of the end-to-end SNR of the Non-NC scheme given by (4.48) can be derived as

$$F_{\hat{\gamma}_{\text{Non-NC}}}(x) = 1 - \exp\left(-x \sum_{l=1}^{L-1} \frac{1}{\bar{\gamma}'_l}\right). \tag{4.49}$$

The upper bound outage probability for the traditional scheme in the generalized MH-TRC can be derived by substituting (4.49) into (4.47) as follows

$$\begin{aligned}
\hat{p}^{out}_{\text{Non-NC}}(R) \approx & F_{\hat{\gamma}_{\text{Non-NC}}}\left(2^{\frac{\mathcal{T}}{2K}R} - 1\right) \\
= & F_{\hat{\gamma}_{\text{Non-NC}}}\left(2^{\frac{2K(L-1)}{2K}R} - 1\right) \\
= & F_{\hat{\gamma}_{\text{Non-NC}}}\left(2^{(L-1)R} - 1\right) \\
= & 1 - \exp\left(-\left(2^{(L-1)R} - 1\right) \sum_{l=1}^{L-1} \frac{1}{\bar{\gamma}'_l}\right).
\end{aligned} \tag{4.50}$$

- **MH-ANC for the 5-node 2-message MH-TRC**: The upper bound of the end-to-end SNR for MH-ANC is a scaled version of the SNR of each hop $\gamma'$, the CDF of which is

$$F_{\gamma'}(x) = 1 - \exp\left(-\frac{1}{\bar{\gamma}'}x\right). \tag{4.51}$$

Substituting (4.38) and (4.51) into (4.47), the upper bound of the outage probability for the special 5-node 2-message multi-hop network is given as follows

$$\begin{aligned}
\hat{p}^{out}_{\text{ANC-SC}}(R) \approx & F_{\gamma^{52}{}_{\text{ANC-SC}}}\left(2^{\frac{\mathcal{T}}{2K}R} - 1\right) \\
= & F_{\gamma^{52}{}_{\text{ANC-SC}}}\left(2^{\frac{3}{2}R} - 1\right) \\
= & F_{\gamma'}\left(\frac{35}{2}\left(2^{\frac{3}{2}R} - 1\right)\right) \\
= & 1 - \exp\left(-\frac{\left(\frac{35}{2}\left(2^{\frac{3}{2}R} - 1\right)\right)}{\bar{\gamma}'}\right).
\end{aligned} \tag{4.52}$$

- **MH-ANC for the generalized $L$-node $K$-message MH-TRC**: With the upper bound of the end-to-end SNR presented in (4.44), the outage

probability for generalized $L$-node $K$-message MH-TRC can be derived as follows

$$\begin{aligned}\hat{p}^{out}_{\text{MH-ANC}}(R)=&\Pr\left[\gamma_{\text{MH-ANC}}<2^{\frac{L-1+2(K-1)}{2K}R}-1\right]_{|(K>>L)\&(SNR\to\infty)}\\ \approx&\Pr\left[\hat{\gamma}_{\text{MH-ANC}}<2^{R}-1\right]\\ =&\Pr\left[\gamma'<\left(\frac{(L-3)2^{L-1}}{4}-1\right)\left(2^{R}-1\right)\right]\\ =&F_{\gamma'}\left(\left(\frac{(L-3)2^{L-1}}{4}-1\right)\left(2^{R}-1\right)\right)\\ =&1-\exp\left(-\frac{\left(\frac{(L-3)2^{L-1}}{4}-1\right)\left(2^{R}-1\right)}{\bar{\gamma}'}\right).\end{aligned}\tag{4.53}$$

## 4.7 Maximum Sum-Rate

The maximum sum-rate is defined as the summation of the maximum rate at user nodes $N_1$ and $N_L$. The maximum sum-rate of the MH-TRC is defined as

$$R=\frac{K}{\mathcal{T}}\left(E\left[\log_2(1+\gamma_{_{N_1}})\right]+E\left[\log_2(1+\gamma_{_{N_L}})\right]\right),\tag{4.54}$$

where $\gamma_{_{N_1}}$ and $\gamma_{_{N_L}}$ represent the end-to-end SNR at two users. Due to the symmetry of the transmission process, $\gamma_{_{N_1}}$ and $\gamma_{_{N_L}}$ at two users are the same. Thus, the sum-rate given by (4.54) can be simplified to

$$R=\frac{2K}{\mathcal{T}}E\left[\log_2(1+\gamma)\right].\tag{4.55}$$

By integrating by parts [100], (4.55) can be simplified to

$$R=\frac{2K}{\mathcal{T}}\int_0^{\infty}\log_2\left(1+x\right)f_{\gamma}(x)dx\tag{4.56}$$

where $f_{\gamma}(x)$ is the probability density function (PDF) of $\gamma$. Similar to the upper bound outage probability presented in the last section, the upper bound maximum sum-rate can be derived by substituting the PDF of the upper bound end-to-end SNR into (4.56).

- **Non-Network Coding**: The PDF of the end-to-end SNR given by (4.48) can be derived by calculating the derivative of the CDF given by (4.49) as

$$f_{\hat{\gamma}_{\text{Non-NC}}}(x)=\frac{dF_{\hat{\gamma}_{\text{Non-NC}}}(x)}{dx}=\sum_{l=1}^{L-1}\frac{1}{\bar{\gamma}'}\exp\left(-x\sum_{l=1}^{L-1}\frac{1}{\bar{\gamma}'}\right).\tag{4.57}$$

Substituting (4.57) into (4.56), the upper bound of the maximum sum-rate for the Non-NC scheme can be obtained as follows

$$\begin{aligned}\hat{R}_{\text{Non-NC}} \approx & \frac{2K}{2K(L-1)} \int_0^{\infty} \log_2(1+x) f_{\hat{\gamma}_{\text{Non-NC}}}(x) dx \\ = & \frac{1}{(L-1)} \int_0^{\infty} \log_2(1+x) \sum_{l=1}^{L-1} \frac{1}{\bar{\gamma}'} \exp\left(-x \sum_{l=1}^{L-1} \frac{1}{\bar{\gamma}'}\right) dx \\ = & \frac{1}{(L-1)} \frac{1}{\log[2]} \exp\left(\sum_{l=1}^{L-1} \frac{1}{\bar{\gamma}'}\right) \Gamma\left(0, \sum_{l=1}^{L-1} \frac{1}{\bar{\gamma}'}\right), \end{aligned} \tag{4.58}$$

where $\Gamma(s,x)$ is the upper incomplete gamma function $\int_x^{\infty} t^{s-1} e^{-t} dt$.

- **MH-ANC for the 5-node 2-message MH-TRC**: The upper bound of the maximum sum-rate for the the 5-node 2-message MH-TRC with MH-ANC can be derived as

$$\begin{aligned}\hat{R}^{52}_{\text{MH-ANC}} \approx & \frac{4}{6} \int_0^{\infty} \log_2(1+x) f_{\hat{\gamma}^{52}_{\text{MH-ANC}}}(x) dx \\ = & \frac{2}{3} \frac{1}{\log[2]} \exp\left(\frac{35}{2\bar{\gamma}'}\right) \Gamma\left(0, \frac{35}{2\bar{\gamma}'}\right). \end{aligned} \tag{4.59}$$

- **MH-ANC for the generalized $L$-node $K$-message MH-TRC**: Following (4.56), when the number of frames $K \to \infty$, the upper bound of the maximum sum-rate in the generalized multi-hop networks with MH-ANC can be readily derived as

$$\begin{aligned}\hat{R}_{\text{MH-ANC}} \approx & \left[\frac{2K}{(L-1)+2(K-1)} \int_0^{\infty} \log_2(1+x) f_{\hat{\gamma}_{\text{MH-ANC}}}(x) dx\right]_{|m\to\infty} \\ = & \int_0^{\infty} \log_2(1+x) f_{\hat{\gamma}_{\text{MH-ANC}}}(x) dx \\ = & \frac{1}{\log[2]} \exp\left(\frac{\frac{(L-3)2^{L-1}}{4} - 1}{\bar{\gamma}'}\right) \Gamma\left(0, \frac{\frac{(L-3)2^{L-1}}{4} - 1}{\bar{\gamma}'}\right). \end{aligned} \tag{4.60}$$

## 4.8 Effective Network Throughput

In the MH-ANC scheme for the MH-TRC, due the inter-message interference, the outage of one message will affect the outage of the following messages. Hence, in order to measure the actual performance of each scheme, the effective network throughput, defined as the number of message successfully exchanged between

the two user nodes per time slot, can better demonstrate the performance of the scheme. The effective network throughput is defined as

$$C_e \triangleq C(1 - P_b) \tag{4.61}$$

where $P_b$ is the bit-error-rate (BER). Assume that BPSK is used at both user nodes, the BER of MH-ANC can be obtained as

$$P_b = E[\mathcal{Q}(\sqrt{2\gamma_{\text{MH-ANC}}})], \tag{4.62}$$

where $\mathcal{Q}(\cdot)$ is the Gaussian-$\mathcal{Q}$ function defined as $\mathcal{Q}(x) = \frac{1}{\sqrt{2\pi}} \int_x^\infty e^{-\frac{y^2}{2}} dy$ and $E[\cdot]$ is the expectation. After integration by parts [100], (4.62) can be written as

$$P_b = \frac{1}{2\sqrt{\pi}} \int_0^\infty \frac{e^{-x}}{\sqrt{x}} F_{\gamma_{\text{MH-ANC}}}(x) dx.$$

Substituting (4.63) to (4.61), the effective network throughput of the MH-ANC scheme can be derived as

$$C^e = C \left(1 - \frac{1}{2\sqrt{\pi}} \int_0^\infty \frac{e^{-x}}{\sqrt{x}} F_{\gamma_{\text{MH-ANC}}}(x) dx\right). \tag{4.63}$$

- **Non-Network Coding**: Substituting (4.49) into (4.63), the upper bound of the effective network throughput at high SNR regions for the Non-NC scheme can be obtained as follows

$$\begin{aligned} \hat{C}^e_{\text{Non-NC}} \approx & \frac{1}{2\sqrt{\pi}} \int_0^\infty \frac{e^{-x}}{\sqrt{x}} F_{\hat{\gamma}_{\text{Non-NC}}}(x) dx \\ = & \frac{1}{2\sqrt{\pi}} \int_0^\infty \frac{e^{-x}}{\sqrt{x}} \left(1 - \exp\left(-x \sum_{l=1}^{l-1} \frac{1}{\bar{\gamma}'}\right)\right) dx \\ = & \frac{1}{2} - \frac{1}{2\sqrt{1 + \sum_{l=1}^{l-1} \frac{1}{\bar{\gamma}'}}}. \end{aligned} \tag{4.64}$$

- **MH-ANC for the 5-node 2-message MH-TRC**: The upper bound of the effective network throughput for the the 5-node 2-message MH-TRC with MH-ANC can be derived as

$$\hat{C}^e_{\text{MH-ANC},52} \approx \frac{1}{2} - \frac{1}{2\sqrt{1 + \frac{35}{2\bar{\gamma}'}}}. \tag{4.65}$$

- **MH-ANC for the generalized $L$-node $K$-message MH-TRC**: When the number of frames $K \to \infty$, the upper bound of the effective network throughput in the generalized multi-hop networks with MH-ANC can be readily derived as

$$\hat{C}^{e}_{\text{MH-ANC}} \approx \frac{1}{2} - \frac{1}{2\sqrt{1 + \frac{\frac{(L-3)2^{L-1}}{4} - 1}{\bar{\gamma}'}}}. \tag{4.66}$$

## 4.9 Numerical Results

In this section, the outage probability and maximum sum-rate of both Non-NC and MH-ANC schemes in the generalized MH-TRC are compared. The analytical outage results are also validated through Monte Carlo simulations. $R$ is configured to 1 bit/sec/Hz.

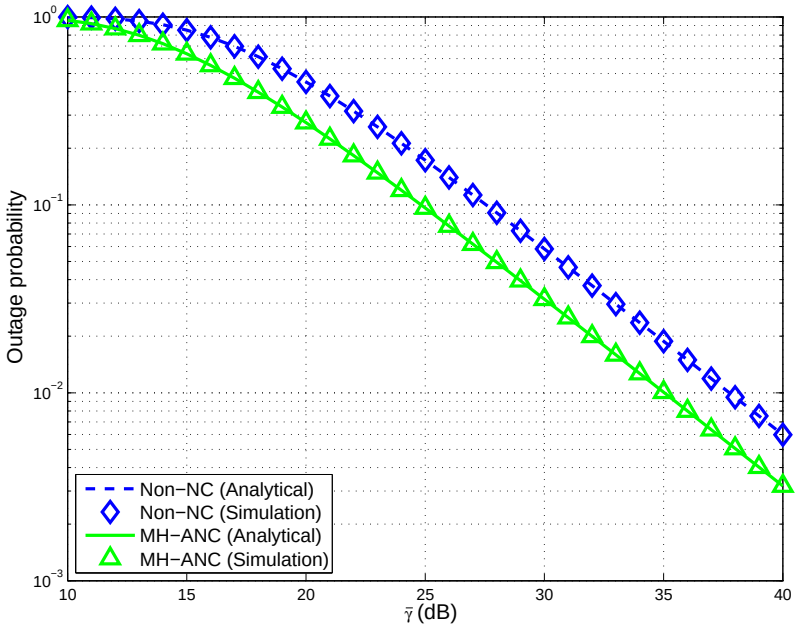


Figure 4.8: Outage probability for the 5-node 2-message MH-TRC.

Figure 4.8 plots the outage probability of both analytical and Monte Carlo simulation results for the special 5-node 2-message MH-TRC . As shown in the figure, the outage performance of the MH-ANC scheme has an approximately 3 dB SNR gain over the Non-NC scheme in this 5-node 2-message MH-TRC, and

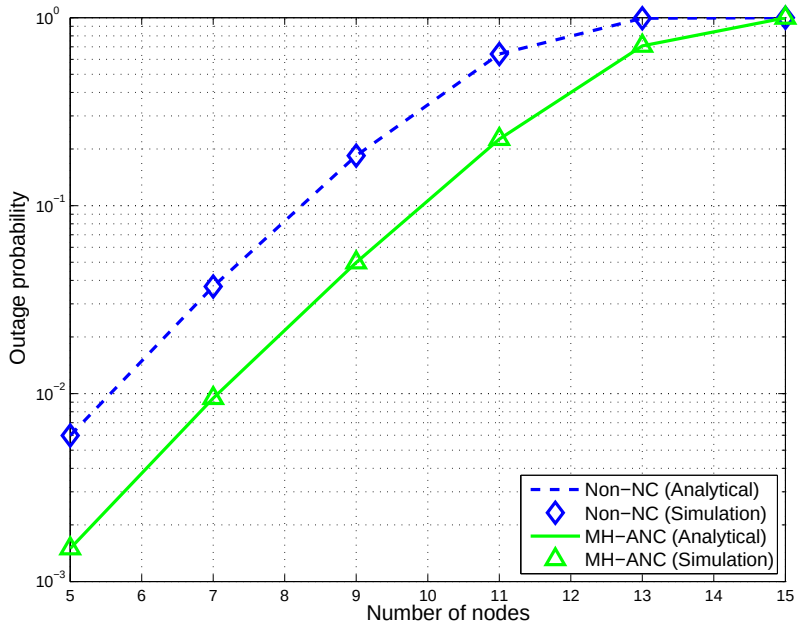


Figure 4.9: Outage probability versus the number of nodes for the generalized MH-TRC.

the experimental result with MH-ANC is in close agreement with the analytical expression given by (4.52).

Figure 4.9 plots the outage probability versus the number of nodes for the generalized MH-TRC with both schemes when the number of messages $K \gg L$. It is assumed that the average SNR per hop $\bar{\gamma}'$ is 40 dB. Both Monte Carlo simulation and analytical results are illustrated in this figure. The figure demonstrates that MH-ANC is able to achieve better performance than the Non-NC scheme. It can seen from the figure that the MH-ANC has a large gain than the Non-NC scheme when the number of nodes in the MH-TRC is small. However, the gain decreases with an increase in the number of nodes. When the number of nodes in the MH-TRC is larger than 15, the outage probabilities for both schemes reach 1, the outage performance gain of the MH-ANC scheme over the Non-NC scheme collapses in large scale MH-TRCs.

Figure 4.10 plots the effective network throughput for the special 5-node 2-message MH-TRC. As shown in the figure, the effective network throughput of the MH-ANC scheme has is significantly better than that of the Non-NC scheme. Moreover, the SNR gain of the MH-ANC scheme relative to the Non-NC scheme

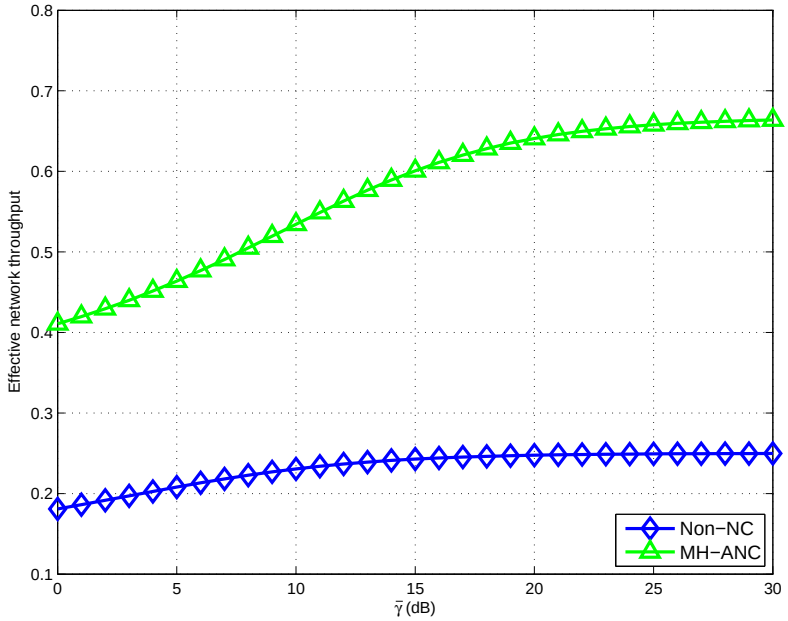


Figure 4.10: Effective network throughput for the 5-node 2-message MH-TRC.

increases with the average SNR per hop.

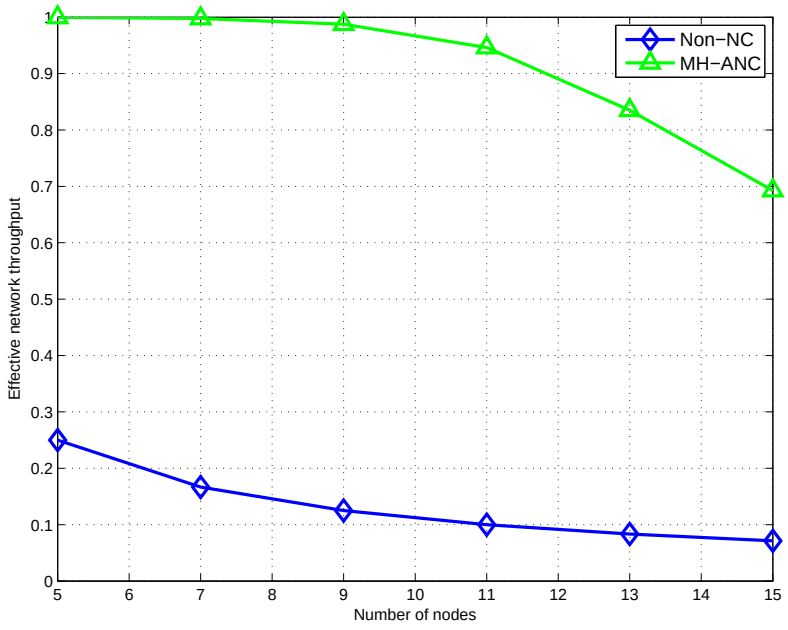


Figure 4.11: Effective network throughput versus the number of nodes for the generalized MH-TRC.

Figure 4.11 plots the effective network throughput for the generalized MH-TRC with both schemes when the number of messages $K \gg L$. It is assumed that the average SNR per hop $\bar{\gamma}'$ is 40 dB. The figure demonstrates that MH-ANC

is able to achieve better effective network throughput than the Non-NC scheme, especially when the number of nodes is small. However, when the number of nodes in the MH-TRC is large, the effective network throughput gain of the MH-ANC scheme over the Non-NC scheme collapses in large scale MH-TRCs.

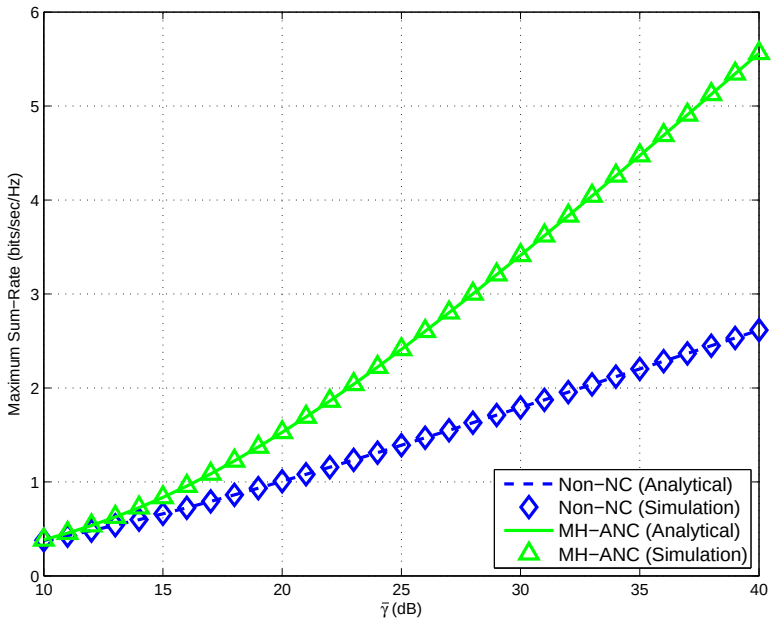


Figure 4.12: Maximum sum-rate for the 5-node 2-message MH-TRC.

Figure 4.12 shows the maximum sum-rate versus the average SNR per hop $\bar{\gamma}'$ for the 5-node 2-message MH-TRC. It can be seen that the maximum sum-rates of both schemes are close to each other in the low SNR regions. However, it is proven that in high SNR regions, the MH-ANC scheme has a significantly better maximum sum-rate over the Non-NC scheme.

Figure 4.13 illustrates the maximum sum-rate versus the number of nodes in the generalized MH-TRC when the number of messages $K \gg L$, and the average SNR per hop is set to 40 dB. As shown in the figure, the maximum sum-rate of MH-ANC is significantly better than the Non-NC scheme when the number of nodes is relatively small. However, the maximum sum-rate for the MH-ANC deteriorates quickly with the increase in the number of nodes, and is poorer than that of Non-NC when the number of nodes is larger than 13.

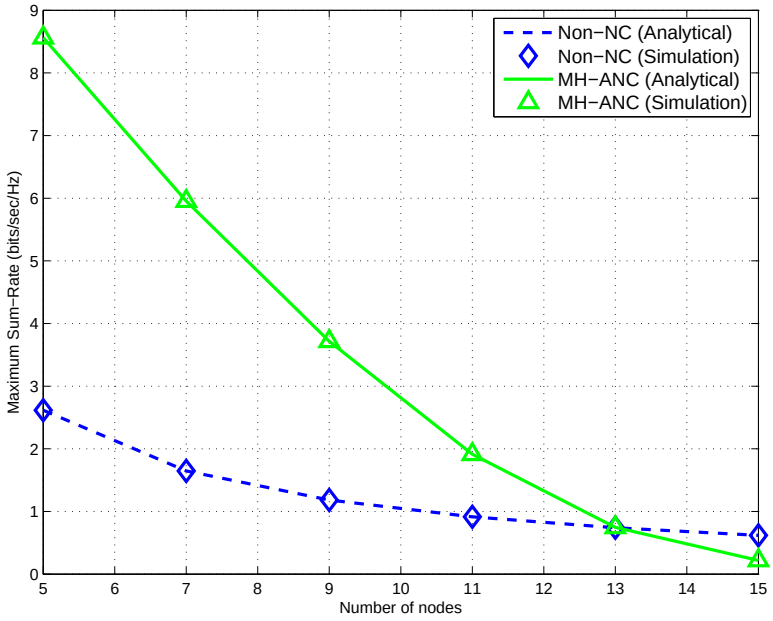


Figure 4.13: Maximum sum-rate versus the number of nodes for the generalized MH-TRC.

## 4.10 Summary

In this chapter, the performance of MH-WNC in the non-regenerative MH-TRC is investigated, including the end-to-end SNR, outage probability and maximum sum-rate. The main contribution is the analytical results of the end-to-end SNR for the MH-ANC in the generalized $L$-node $K$-message MH-TRC, which can be applied to the analysis for outage probability and maximum sum-rate. To circumvent the exponentially increased complexity when the numbers of nodes and messages are large in the MH-TRC, two recursive approaches are proposed in this chapter, i.e., the forward recursive approach for the MH-TRC with a small number of nodes and messages, and the backward recursive approach for the MH-TRC with a large number of nodes and messages.

Moreover, the upper bound end-to-end SNR for the MH-ANC scheme is analyzed. It is proven to be tight in high SNR regions. The approximation of the upper bound end-to-end SNR of the MH-ANC in the generalized MH-TRC is obtained by curve fitting methods, and the fitting function is perfectly fitted to the original data obtained by the recursive approach.

The analytical expressions of the outage probability and maximum sum-rate

are derived by applying the analytical results of the upper bound end-to-end SNR. Both numerical and analytical results demonstrate that MH-ANC is superior to Non-NC in outage probability in small scale MH-TRCs when the number of messages is far larger than the number of nodes. Moreover, the maximum sum-rate results clearly demonstrate that the maximum sum-rate of MH-ANC is significantly better than that of Non-NC when the number of nodes is relatively small in high SNR regions.

To summarize, due to noise propagation in the ANC scheme, the outage probability deteriorates quickly with the number of nodes. As a result, the MH-ANC scheme cannot outperform the conventional Non-NC scheme in outage performance and sum-rate when the number of nodes is relatively large. Therefore, the MH-ANC scheme is more suitable for the MH-TRC with a small number of nodes.

# Chapter 5

# Compute-and-Forward for Regenerative Multi-Hop Two-Way Channels

## 5.1 Introduction

Compute-and-forward was proposed recently to realize reliable PNC [31], where the relays compute and forward linear combinations of user messages to destinations. The established "computation rate" was proven to have significant improvements over conventional relaying strategies in the MAC. Since its establishment in the multi-user multi-relay network [31], there have been some recent efforts on CPF and its implementations in different types of wireless relay networks. As far as the literature review suggests, there is no published work on the implementation of CPF to the TWRC, let alone the MH-TRC.

In this chapter, the original CPF is extended to MH-CPF with application to the generalized regenerative MH-TRC. The relay nodes compute linear combinations of the received signals from two neighboring nodes and broadcast it in their next transmission time slot. Upon receiving the linear combination of the outgoing and incoming messages, the user nodes are able to solve the linear equations for their required messages. Due to the bi-directional transmission, the linear combinations consist of polynomials of outgoing and incoming messages, and the conventional approach for recovering messages in the original CPF scheme cannot

be applied directly into MH-CPF. Therefore, the forward and backward recursive approaches for deriving the noise power in MH-ANC are applied to obtain the received linear combinations at user nodes.

It is well known that the advantage of CPF relies on the maximized computation rate at relay nodes, and the successful realization of MH-CPF depends on the maximization of computation rates at all relay nodes during the entire exchange process. For Rayleigh fading channels, the maximization problem amounts to a complex lattice reduction problem. It should be noted that lattice reduction problem is non-deterministic polynomial-time hard (NP-hard), and there are no analytical solutions for it. However, there has previous been some work in solving complex lattice reduction problems numerically. These can be applied to find the best integer coefficients, thus maximizing the computation rates. To demonstrate the advantage of the proposed MH-CPF, the outage performance of MH-CPF for the generalized MH-TRC will be analyzed.

To sum up, the contributions in the chapter can be given as follows:

1. A MH-CPF scheme for the generalized regenerative MH-TRC is proposed and generalized;

2. The received linear combinations at the user nodes are derived with the proposed forward and backward recursive approaches;

3. To find the best coefficients that maximizes the computation rates at all relay nodes, a complex lattice reduction algorithm is implemented. The maximized computation rate can be obtained within two iterations and the results are perfectly consistent with the maximized computation rate calculated by the greedy search algorithm; and

4. The outage probability for both Non-NC and MH-CPF schemes are evaluated. The numerical results demonstrate that MH-CPF is superior to Non-NC in outage probability in large scale MH-TRCs.

## 5.2 Related Work

In PNC, the relay transforms the interference channel-coded signal into a network-coded message, and the network-coded message is then re-encoded and transmitted to user nodes or destinations. The network-coded message can be either a modular-2 sum of the messages as the "standard" PNC [14], or a combination in finite-field as LNC [54] and finite-field network coding (FFNC) [104], or a linear combination with integer coefficients as CPF [92].

The error performance of PNC was analyzed in [14], where the results showed that the error performance of PNC is a slightly worse than the standard BPSK modulation in low signal-to-noise ratio (SNR) regions, and the penalty of PNC mapping is less than 0.1 dB when the SNR is larger than 10 dB. For fading channels, the ML detection can be applied to estimate the joint symbols as [23,26], i.e, $\hat{S}_R = \arg\min_{(S_1,S_2)} |y_R - h_1 x_1 - h_2 x_2|$.

The PNC scheme for multi-hop networks was proposed in [14], where the authors described the PNC scheme in uni-directional and bi-directional multi-hop networks. The results showed that for the regular linear network, PNC can achieve the upper-bound capacity, 0.5 frame/time slot in each direction, for bi-directional transmission between two end nodes [119]. However, no performance analysis was presented in the paper.

The established "computation rate" in the recent proposed CPF scheme is proven to achieve significant improvements than conventional relaying strategies in the MAC. However, the successful realization of CPF depends of the maximization of computation rates at relay nodes, which amounts to finding the best integer coefficients. In general, the choice of the coefficients $\mathbf{a}$ only depends on the channel coefficients. One simple approach is to choose coefficient vectors with the highest computation rate by a greedy search algorithm [92] .

However, this approach may cause enormous computation complexity. Recently, in [32], the authores converted the maximization problem into the shortest vector problem (SVP). Solving the SVP is known to be non-deterministic polynomial-time hard (NP-hard) such that no closed-form solutions can be given analytically. However, many efficient lattice reduction algorithms were given in [138] to produce a "relatively short vector".

For Rayleigh fading channels, the SVP becomes a complex lattice reduction problem. Traditionally, the Lenstra-Lenstra-Lovsz (LLL) lattice basis reduction algorithm is performed on the real-valued equivalent matrix of the complex matrix [139, 140]. However, such conversion doubles the matrix dimension, requiring extra computations in the detection algorithm [141]. Complex lattice reduction was introduced in [142], which achieves a reduction in complexity of nearly 50% over the traditional LLL algorithm.

The authors in [143] investigated the degree of freedom of the computation capacity, which is defined as the upper bound of the computation rate. Theorem-2 of the paper gave the second-order asymptotics of the computation capacity. However, Remark-2 of the same paper conceded that the given second-order asymptotics are rather poor, especially when $K$ is large. Therefore, deriving tighter approximations for the computation rate and capacity remains an open problem.

There have been a number of works on CPF and its implementation since the proposal of the new relaying scheme. To overcome the difficulty of finding a "good" lattice partition for CPF, an algebraic approach was taken in [34] to study a class of CPF schemes based on practical lattice partitions. In [33], Feng *et al.* generalized the framework by Nazer and Gastpar, and introduced lattice network coding (LaNC).

Moreover, the CPF scheme relies on the awareness of CSI at relay nodes, so that the relay can compute an "optimal" scale factor for decoding. However, the requirement of CSI (even if only at the receivers) may dominate communication when the number of concurrent transmission is large, since channel training is known to effectively reduce the degree of freedom of a wireless link [144]. In [145], the author proposed a blind CPF scheme, where no CSI requirement is necessary.

## 5.3 System Model

The $L$-node $K$-message MH-TRC can be shown in Figure 5.1, where user nodes $N_1$ and $N_L$ wish to exchange their messages through intermediate relay nodes $\{N_l\}_{l=2}^{L-1}$. The message sequences to be transmitted by $N_1$ and $N_L$ are noted as $\mathbf{U} = \{u_k\}_{k=1}^{K}$ and $\mathbf{V} = \{v_k\}_{k=1}^{K}$. Each user node is equipped with a nested lat-

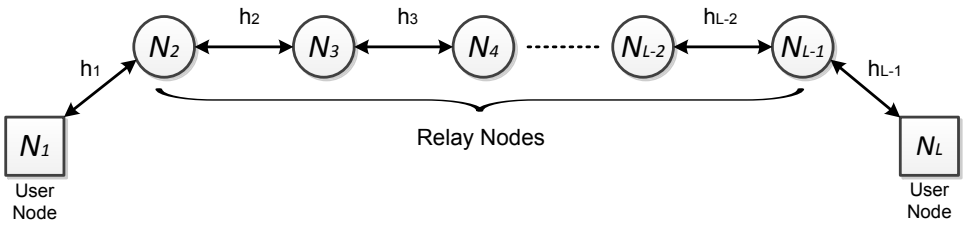


Figure 5.1: The $L$-node $K$-message multi-hop two-way relay network.

tice encoder [92], which maps message $u_k$ ($v_k$) over the finite field to a length-$n$ complex-valued codeword, i.e., $\hat{u}_k = \varepsilon(u_k)$ ($\hat{v}_k = \varepsilon(v_k)$), subject to the power constraint of $||\hat{u}_k||^2 \leqslant nP$ ($||\hat{v}_k||^2 \leqslant nP$). The uplink and downlink (or forward and reverse) channels are assumed to be reciprocal. Denote by $h_l \sim \mathcal{CN}(0, 2\alpha_l^2), l \in \{1, 2, ..., L-1\}$ the channel of hop $l$ between node $N_l$ and $N_{l+1}$, modeled as a zero mean, independent, circularly symmetric complex Gaussian random variable with variance $\alpha_l^2$ per dimension.

In the original CPF scheme, relays compute linear combinations of the messages from users and forward them to the destination. Similarly, with MH-CPF, the relay nodes compute linear combinations of messages from neighboring nodes and broadcast to them in their next transmitting time slots. It is assumed that all the transmission is perfectly synchronized. The received signal at relay node $N_l$ in time slot $j$ can be given by

$$y_l^j = \mathbf{h}_l \begin{bmatrix} t_{l-1}^j & t_{l+1}^j \end{bmatrix}^T + w_l^j, \tag{5.1}$$

where $\mathbf{h}_l = [h_l \ h_{l+1}]$, $t_{l-1}^j$ and $t_{l+1}^j$ are the transmitted signals from neighboring relay nodes $N_{l-1}$ and $N_{l+1}$, which are the decoded linear combinations at the relay nodes in the previous time slot. $w_l^j$ denotes the received noise at node $l$ in time slot $j$, which is a zero mean, independent, circularly symmetric, complex Gaussian random variable with a variance of $\sigma^2$.

After receiving the interference signal, the relay node selects a complex integer coefficient vector $\mathbf{a}_l^j \in \{\mathbb{Z} + \mathbb{Z}i\}^2$ and decodes the following linear combination

$$t_l^j = \mathbf{a}_l^j \begin{bmatrix} t_{l-1}^{j-1} & t_{l+1}^{j-1} \end{bmatrix}^T \tag{5.2}$$

based on the received signal $y_l^j$. In its next transmission time slot, relay node $N_l$ broadcasts the decoded linear combination $t_l^j$ to neighboring nodes $N_{l-1}$ and

$N_{l+1}$.

## 5.4 Computation Rate

The primary goal of MH-CPF is to maximize the computation rates at all relay nodes during the entire exchange process. For the decoded linear combination $t_l^j$, the computation rate at relay node $N_l$ in time slot $j$ is given by [92]

$$R_{\mathrm{COMP},l}\big(\mathbf{h}_l, \mathbf{a}_l^j\big) = \log^+\left(||\mathbf{a}_l^j||^2 - \frac{P|\mathbf{a}_l^j\mathbf{h}_l^\dagger|^2}{\sigma^2 + P||\mathbf{h}_l||^2}\right)^{-1}, \tag{5.3}$$

where $\log^+(x) \triangleq \max\left(\log(x), 0\right)$. For a given $\mathbf{h}_l$, $\hat{\mathbf{a}}_l^j$ is chosen to maximize the above computation rate

$$\hat{\mathbf{a}}_l^j = \arg\max_{\mathbf{a}_l^j \neq 0} R_{\mathrm{COMP},l}(\mathbf{h}_l, \mathbf{a}_l^j). \tag{5.4}$$

As can be seen from (5.4), $\hat{\mathbf{a}}_l^j$ is only determined by $\mathbf{h}_l$. The channels between all the nodes are assumed to be quasi-static, and the instantaneous CSI of $h_l$ remains unchanged during the entire exchange process. Therefore, the maximized computation rate $R_{\mathrm{COMP},l}(\mathbf{h}_l, \hat{\mathbf{a}}_l^j)$ for decoding the linear combination $t_l^j$ at relay $N_l$ remains the same during the entire exchange process. Thus, the maximized computation rate at relay $N_l$ given by (5.3) can be rewritten as

$$R_{\mathrm{COMP},l}\big(\mathbf{h}_l, \hat{\mathbf{a}}_l\big) = \log^+\left(||\hat{\mathbf{a}}_l||^2 - \frac{P|\hat{\mathbf{a}}_l\mathbf{h}_l^\dagger|^2}{\sigma^2 + P||\mathbf{h}_l||^2}\right)^{-1}, \tag{5.5}$$

and

$$\hat{\mathbf{a}}_l^j \equiv \hat{\mathbf{a}}_l = \arg\max_{\mathbf{a}_l \neq 0} R_{\mathrm{COMP},l}(\mathbf{h}_l, \mathbf{a}_l), \tag{5.6}$$

where $\hat{\mathbf{a}}_l = [\vec{a}_l, \overleftarrow{a}_l]$. $\vec{a}_l$ and $\overleftarrow{a}_l$ are two complex integer coefficients corresponding to the two messages $t_{l-1}^{j-1}$ and $t_{l+1}^{j-1}$ in linear combination $t_l^j$. The linear combination corresponding to the maximized computation rate $R_{\mathrm{COMP},l}(\mathbf{h}_l, \hat{\mathbf{a}}_l)$ at relay node $N_l$ in time slot $j$ can be shown as

$$t_l^j = \hat{\mathbf{a}}_l\begin{bmatrix} t_{l-1}^{j-1} & t_{l+1}^{j-1}\end{bmatrix}^T = \vec{a}_l t_{l-1}^{j-1} + \overleftarrow{a}_l t_{l+1}^{j-1}. \tag{5.7}$$

It is noted that when the integer coefficients $\vec{a}_l$ and $\overleftarrow{a}_l$ in the above linear combination are both set to 1, the linear combination is equivalent to the modular-2 addition in the "standard" PNC [14], which is also implied in [92, Remark 4] and [25, Section II-B].

## 5.5 Finding the Best Coefficient Vector

In general, the choice of the integer coefficient vector $\hat{\mathbf{a}}_l$ at each relay depends on channel coefficient $\mathbf{h}_l$ and transmission power $P$. One simple greedy approach is to choose the coefficient vector with the highest computation rate. In [92, Lemma 1], the author proved that the computation rate $R_{\mathrm{COMP},l}\big(\mathbf{h}_l, \hat{\mathbf{a}}_l\big)$ given by (5.5) is zero if the coefficient vector $\hat{\mathbf{a}}_l$ satisfies

$$||\hat{\mathbf{a}}_l|| \geqslant 1 + ||\mathbf{h}_l||^2 P. \tag{5.8}$$

Therefore, the greedy approach for searching for the best coefficient vector $\hat{\mathbf{a}}_l$ can be simplified to

$$\hat{\mathbf{a}}_l = \arg \max_{\{\mathbf{a}_l \neq 0\} \cap \{||\mathbf{a}_l|| < 1 + ||\mathbf{h}_l||^2 P\}} R_{\mathrm{COMP},l}(\mathbf{h}_l, \mathbf{a}_l). \tag{5.9}$$

Coefficient vector $\mathbf{a}_l$ consists of two complex integer coefficients, which are further made up of two real parts and two imaginary parts. Therefore, four independent integer variables needed to be decided in this greedy search algorithm. For example, when the average SNR of the channel is 10 dB and the transmission power $P$ is set to 1, the number of iterations with the greedy search approach is $2.58e + 10$. Therefore, this greedy approach is apparently not applicable in practical communication systems. There has been much research on how to simplify the approach to find the best coefficient vector to maximize the computation rate. According to Theorem 1 in [32] and Proposition 1 in [33], the above maximization problem (5.6) amounts to the following SVP

$$\hat{\mathbf{a}}_l = \arg \min_{\mathbf{a}_l \neq 0} ||\mathbf{a}_l \mathbf{L}||, \tag{5.10}$$

where $\mathbf{L}$ is the Cholesky decomposition matrix of $I - \frac{P}{n_0 + P||\mathbf{h}_l||^2} \mathbf{h}_l^\dagger \mathbf{h}_l$, and $I$ is an $L$ by $L$ identity matrix.

For the above special two-dimensional case in Rayleigh fading channels, the following complex lattice reduction algorithm proposed in [146] can be applied to solve the above SVP and obtain the maximized computation rate efficiently.

**Complex lattice reduction algorithm to obtain $\hat{\mathbf{a}}_l$**

*Input:* Channel coefficient vector $\mathbf{h}_l = \{h_{l-1}, h_{l+1}\}$, transmit power $P$.
*Output:* Coefficient vector $\hat{\mathbf{a}}_l$.

$\mathbf{G} = I - \frac{P}{1+P\|\mathbf{h}\|^2}\mathbf{h}^\dagger\mathbf{h}$.
$\mathbf{L} = \mathbf{Cholesky\ decompositon}\,(\mathbf{G})$.
**if** $\mathbf{norm}\,(\mathbf{L}\,(1,:)) > \mathbf{norm}\,(\mathbf{L}\,(2,:))$ **then**
  $b_1 = \mathbf{L}\,(2,:)\,; b_2 = \mathbf{L}\,(1,:)\,.$
**else**
  $b_1 = \mathbf{L}\,(1,:)\,; b_2 = \mathbf{L}\,(2,:)\,.$
**end if**.
**while** $\mathbf{abs}\,(\mathbf{real}\,(\mathbf{dot}\,(b_1, b_2))) > \frac{\mathbf{norm}(b_1)^2}{2}$ &
  $\mathbf{abs}\,(\mathbf{imag}\,(\mathbf{dot}\,(b_1, b_2))) > \frac{\mathbf{norm}(b_1)^2}{2}$ **then**
  $n = \mathbf{round}\left(\mathbf{real}\left(\frac{\mathbf{dot}(b_1,b_2)}{\mathbf{dot}(b_1,b_1)}\right) + \mathbf{imag}\left(\frac{\mathbf{dot}(b_1,b_2)}{\mathbf{dot}(b_1,b_1)}\right)\right)$.
  $b_2 = b_2 - n * b_1$.
  **if** $\mathbf{norm}\,(b_1) >= \mathbf{norm}\,(b_2)$ **then**
    $\mathbf{swap}\,(b_1, b_2)$.
  **else**
    **if** $\mathbf{abs}\,(\mathbf{real}\,(\mathbf{dot}\,(b_1, b_2))) <= \frac{\mathbf{norm}(b_1)^2}{2}$ &
      $\mathbf{abs}\,(\mathbf{imag}\,(\mathbf{dot}\,(b_1, b_2))) <= \frac{\mathbf{norm}(b_1)^2}{2}$ **then**
      **break**.
    **end**.
  **end**.
**end**.
$\hat{\mathbf{a}}_l = b_1$

Figure 5.2 plots the maximized computation rates obtained by the above algorithm and the greedy search algorithm given by (5.9). From the figure, it is clear that the maximized computation rates obtained by the two algorithms are identical. On the other hand, the result also demonstrates that the maximized computation rate achieved by CPF is almost linearly increased with the transmission power in high power regions.

## 5.6 Recovering Messages

The decoded linear combinations received by each user node after time slot $L-1$ consist of both incoming and outgoing messages. For example, the decoded linear combinations $t_1^4$ and $t_1^6$ at user node $N_1$ in time slots 4 and 6 in the 5-node 2-

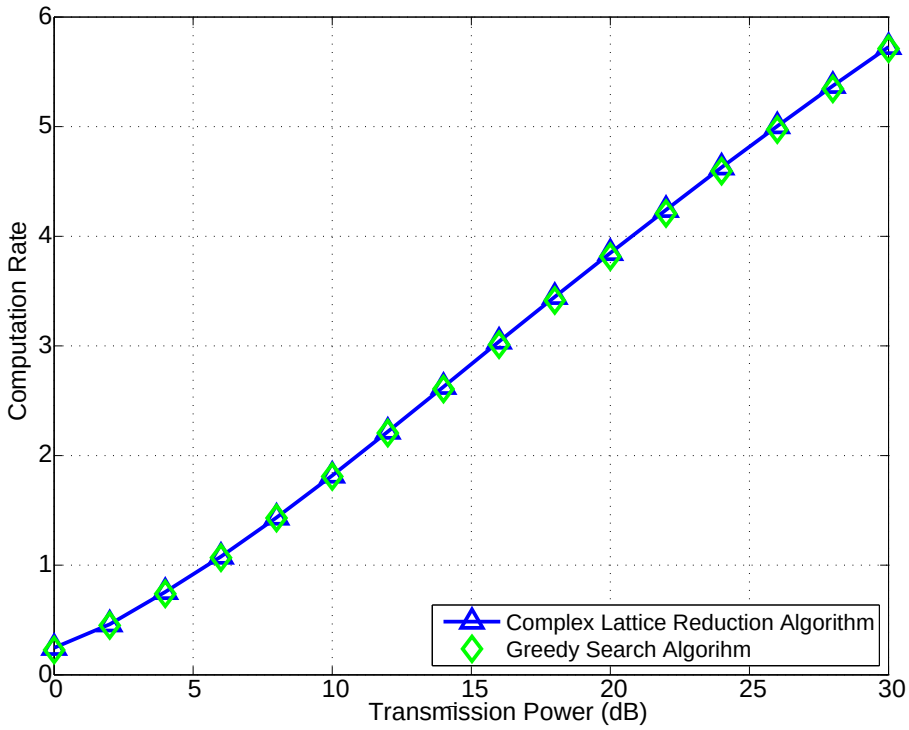


Figure 5.2: Maximized computation rate obtained by two different algorithms.

message MH-TRC can be obtained as

$$\begin{aligned} t_1^4 =& \vec{a}_2\hat{u}_2 + \overleftarrow{a}_2 t_3^2 \\ =& \vec{a}_2\hat{u}_2 + \overleftarrow{a}_2\left(\vec{a}_3 t_2^1 + \overleftarrow{a}_3 t_4^1\right) \\ =& \vec{a}_2\hat{u}_2 + \overleftarrow{a}_2\left(\vec{a}_3\hat{u}_1 + \overleftarrow{a}_3\hat{v}_1\right) \\ =& \vec{a}_2\hat{u}_2 + \overleftarrow{a}_2\vec{a}_3\hat{u}_1 + \overleftarrow{a}_2\overleftarrow{a}_3\hat{v}_1, \end{aligned} \tag{5.11}$$

$$\begin{aligned} t_1^6 =& \vec{a_3} t_2^3 + \overleftarrow{a}_3 t_4^3 \\ =& \vec{a_3}\left(\vec{a}_2\hat{u}_2 + \overleftarrow{a}_2 t_3^2\right) + \overleftarrow{a}_3\left(\vec{a}_4 t_3^2 + \overleftarrow{a}_4\hat{v}_2\right) \\ =& \vec{a_3}\left(\vec{a}_2\hat{u}_2 + \overleftarrow{a}_2\left(\vec{a}_3\hat{u}_1 + \overleftarrow{a}_3\hat{v}_1\right)\right) + \overleftarrow{a}_3\left(\vec{a}_4\left(\vec{a}_3\hat{u}_1 + \overleftarrow{a}_3\hat{v}_1\right) + \overleftarrow{a}_4\hat{v}_2\right) \\ =& \vec{a_3}\vec{a}_2\hat{u}_2 + (\vec{a}_3^2\overleftarrow{a}_2 + \overleftarrow{a}_3\vec{a}_4\vec{a}_3)\hat{u}_1 + (\vec{a}_3\overleftarrow{a}_2\overleftarrow{a}_3 + \overleftarrow{a}_3^2\vec{a}_4)\hat{v}_1 + \overleftarrow{a}_3\overleftarrow{a}_4\hat{v}_2. \end{aligned} \tag{5.12}$$

As can be seen from (5.11), the received linear combination in time slot 4 contains the outgoing messages $\hat{u}_1$ and $\hat{u}_2$, and also the incoming message $\hat{v}_1$. Knowing the complex integer coefficients passed from relay node $N_2$, the user node $N_1$ can extract its own messages $\hat{u}_1$ and $\hat{u}_2$ from the combination and recover

incoming messages $\hat{v}_1$. In time slot 6, since user node $N_1$ has the knowledge of message $\hat{u}_1$ and $\hat{u}_2$, and $\hat{v}_1$ recovered in time slot 4, it can extract these messages from the combination $t_1^6$ given by (5.12), and recover $\hat{v}_2$.

For the MH-CPF scheme in the generalized $L$-node $K$-message MH-TRC with the case $2K-1 \geqslant L-1$, $t_1^j$ can be given by

$$t_1^j = \sum_{l=1}^{\frac{j}{2}} \phi_l^j \hat{u}_l + \sum_{l=1}^{\frac{j-(L-1)}{2}} \psi_l^j \hat{v}_l + \prod_{l=2}^{L-1} \overleftarrow{a}_l \hat{v}_{\frac{j-L+3}{2}}, \quad j \in \{L-1, L+1, ..., 2K-2\}, \tag{5.13}$$

$$t_1^j = \sum_{l=1}^{K} \phi_l^j \hat{u}_l + \sum_{l=1}^{\frac{j-(L-1)}{2}} \psi_l^j \hat{v}_l + \prod_{l=2}^{L-1} \overleftarrow{a}_l \hat{v}_{\frac{j-L+3}{2}}, \quad j \in \{2K, 2K+2, ..., \mathcal{T}_{\text{MH-CPF}}\}, \tag{5.14}$$

and for the case $2K-1 < L-1$, $t_1^j$ can be given by

$$t_1^j = \sum_{l=1}^{K} \phi_l^j \hat{u}_l + \sum_{l=1}^{\frac{j-(L-1)}{2}} \psi_l^j \hat{v}_l + \prod_{l=2}^{L-1} \overleftarrow{a}_l \hat{v}_{\frac{j-L+3}{2}}, \quad j \in \{L-1, L+1, ..., \mathcal{T}_{\text{MH-CPF}}\}, \tag{5.15}$$

where $\phi_l^j$ and $\psi_l^j$ are two polynomials of $\{\vec{a}_l\}_{l=2}^{L-1}$ and $\{\overleftarrow{a}_l\}_{l=2}^{L-1}$ in time slot $j$. (5.13) describes the received linear combination between $\hat{v}_1$ reaches $N_1$ and $\hat{u}_K$ is sent from $N_1$, and (5.14) denotes the received linear combination after $\hat{u}_K$ is sent from $N_1$ until time slot $\mathcal{T}_{\text{MH-CPF}}$.

To solve the above linear equations for its required messages, user node $N_1$ has to know all the $\phi_l^j$ and $\psi_l^j$, the complexity of which increases exponentially with the numbers of hops and messages. The similar recursive approaches proposed in the last chapter for deriving the noise power can be applied here to obtain the linear combinations at the user nodes. The detailed derivation is presented in Appendix A.3, and the results are given by

$$\begin{aligned} t_1^j = {} & \vec{a}_1 \hat{u}_{\frac{j}{2}} + \sum_{i=1}^{\Psi(j)} \left[ (-1)^{i-1} \left( \overset{i}{\underset{K=1,l_1=2}{\overline{\otimes}}} \Phi\left(\frac{j}{2}\right) \right) t_1^{j-2i} \right] + \\ & \sum_{i=1}^{\Psi(j)} \left[ (-1)^{i-1} \left( \overset{i}{\underset{K=1,l_1=3}{\overline{\otimes}}} \Phi\left(\frac{j}{2}\right) \right) \left( t_1^{j-2i} - \vec{a}_1 \hat{u}_{\frac{j-2i}{2}} \right) \right] + \prod_{i=2}^{L-1} \overleftarrow{a}_i \hat{v}_{\frac{j-L+2}{2}}, \\ & j \in \{L, L+2, ..., 2K-2\} \end{aligned} \tag{5.16}$$

and

$$t_1^j = \sum_{i=1}^{\Psi(j)} \left[ (-1)^{i-1} \left( \bigotimes_{K=1,l_1=2}^{i} \Phi\left(\frac{j}{2}\right) \right) t_1^{j-2i} \right] + \sum_{i=1}^{\Psi(j)} \left[ (-1)^{i-1} \left( \bigotimes_{K=1,l_1=3}^{i} \Phi\left(\frac{j}{2}\right) \right) \left( t_1^{j-2i} - \vec{a}_1 \hat{u}_{\frac{j-2i}{2}} \right) \right] + \prod_{i=2}^{L-1} \overline{a}_i \hat{v}_{\frac{j-L+2}{2}}, \quad (5.17)$$
$$j \in \{2K, 2K+2, ..., \mathcal{T}_{\text{MH-CPF}}\}$$

where

$$\Psi(j) = \begin{cases} \lfloor \frac{L-1}{2} \rfloor & \frac{j}{2} \geq L-1 \\ \lfloor \frac{L}{4} \rfloor + \frac{j-L+2}{2} - 1 & \text{else} \end{cases}.$$

## 5.7 Outage Probability

For MH-CPF in the MH-TRC, each message follows a different transmission path, and failing to decode one message will affect the decoding of the following messages. The outage probabilities for these $K$ messages are different, and the outage probabilities of later messages are poorer than those of early messages. Due to the symmetrical property of the two-way transmission, the outage probabilities for the two messages $\hat{u}_k$ and $\hat{v}_k$ are identical.

Given a target end-to-end rate $R$, the average outage probability per message in the $L$-node $K$-message MH-TRC is defined as

$$\begin{aligned} p^{\text{out}}(R) &= \frac{1}{2K} \sum_{k=1}^{K} \left( p_{\hat{v}_k}^{\text{out}}(R) + p_{\hat{u}_k}^{\text{out}}(R) \right) \\ &= \frac{1}{K} \sum_{k=1}^{K} p_{\hat{v}_k}^{\text{out}}(R), \end{aligned} \quad (5.18)$$

where $p_{\hat{v}_k}^{\text{out}}(R)$ and $p_{\hat{u}_k}^{\text{out}}(R)$ are the outage probabilities of messages $\hat{v}_k$ and $\hat{u}_k$, respectively.

To meet a target end-to-end rate $R$ for the MH-TRC, each single transmission in the MH-TRC should achieve the following target message rate

$$R_{\text{MSG}} = \frac{R}{C}, \quad (5.19)$$

which implies that the more time units that are needed for exchanging one message, the higher the message rate required for a single transmission.

### 5.7.1 Non-Network Coding

The messages are transmitted one-by-one and hop-by-hop with the Non-NC scheme. With the "good" lattice codes suggested by Erez and Zamir in [90], the achievable message rate $R_l$ of hop $l$ is given by

$$R_l = \log_2(1+\gamma_l), \tag{5.20}$$

where

$$\gamma_l = \frac{P|h_l|^2}{\sigma^2} \tag{5.21}$$

is the received SNR at hop $l$, which is exponentially distributed with parameter $1/\bar{\gamma}_l$, with $\bar{\gamma}_l = \frac{2P\alpha_l^2}{\sigma^2}$ denoting the average SNR.

The outage event of a single-hop transmission is defined as when $R_l$ is below a target message rate

$$R_{\text{Non-NC}} = \frac{R}{C_{\text{Non-NC}}} = (L-1)R. \tag{5.22}$$

Therefore, the outage probability for the transmission at hop $l$ can be given by

$$\begin{aligned} p_l^{\text{out}}(R_{\text{Non-NC}}) &= \Pr\left[R_l < R_{\text{Non-NC}}\right] \\ &= 1 - \exp\left(-\frac{2^{(L-1)R}-1}{\bar{\gamma}_l}\right). \end{aligned} \tag{5.23}$$

For Non-NC in the MH-TRC, the transmission of message $\hat{u}_k$ is in outage if any transmission at the $L-1$ hops is in outage. The outage probability for each message is the same due to the same transmission procedure and the quasi-static channel at each hop. The average outage probability of Non-NC for the MH-TRC is equivalent to the outage probability of a single message $\hat{v}_k$, which can be derived as

$$\begin{aligned} p_{\text{Non-NC}}^{\text{out}}(R) &= p_{\text{Non-NC},\hat{v}_k}^{\text{out}}(R) \\ &= 1 - \prod_{l=1}^{L-1}\left(1 - p_l^{\text{out}}\big((L-1)R\big)\right) \\ &= 1 - \prod_{l=1}^{L-1}\exp\left(-\frac{2^{(L-1)R}-1}{\bar{\gamma}_l}\right). \end{aligned} \tag{5.24}$$

### 5.7.2 Multi-Hop Compute-and-Forward

In MH-CPF, signals are transmitted bi-directionally, and each single message will pass a series of intermediate relay nodes before it reaches the destination. The outage event for message $\hat{u}_k$ with MH-CPF occurs when any transmission that affects the transmission of the concerned message is in outage. Due to bi-directional transmission in MH-CPF, the transmission of message $\hat{v}_k$ is more complicated than the hop-by-hop transmission in the Non-NC scheme. In the following sections, the transmission events that affect the transmission of message $\hat{v}_k$ and the corresponding outage probabilities are analyzed.

First, denote by $f_l^j$ the transmission event when node $N_l$ receives a signal from one of its neighboring nodes, or an interference signal from both neighboring nodes in time slot $j$

$$f_l^j \triangleq \big\{N_{l-1} \xrightarrow{x} N_l\big\} \cup \big\{N_l \xleftarrow{y} N_{l+1}\big\} \cup \big\{N_{l-1} \xrightarrow{x} N_l \xleftarrow{y} N_{l+1}\big\}, \quad (5.25)$$
$$\forall l \in \{1,2,...,L\}, \forall j \in \{1,2,3,...\},$$

and $\mathcal{F}_{\hat{v}_k}$ as the set of all the transmission events that affect the transmission of message $\hat{u}_k$

$$\mathcal{F}_{\hat{v}_k} \triangleq \Big\{ \{f_l^j\}_{l\in\{1,2,...,L\}}^{j\in\{1,2,...,\mathcal{T}_k\}} \Big\}, \quad \forall k \in \{1,2,...,K\}, \quad (5.26)$$

where $\mathcal{T}_k = L - 1 + 2(k-1)$ is the total number of time slots used for exchanging $k$ messages.

**Transmission events for message $\hat{u}_k$ in the 5-node 2-message MH-TRC**: As can be observed from Figure 3.7 in Chapter 3, 12 transmission events occur with a total of 6 time slots. The entire set of transmission events can be obtained as

$$\big\{f_2^1, f_4^1, f_3^2, f_2^3, f_4^3, f_1^4, f_3^4, f_5^4, f_2^5, f_4^5, f_1^6, f_5^6\big\},$$

and the sets $\mathcal{F}_{\hat{v}_1}$ and $\mathcal{F}_{\hat{v}_2}$ for messages $\hat{v}_1$ and $\hat{v}_2$ are

$$\mathcal{F}_{\hat{v}_1} = \big\{f_2^1, f_4^1, f_3^2, f_2^3, f_1^4\big\}, \quad \text{and} \quad \mathcal{F}_{\hat{v}_2} = \big\{f_2^1, f_4^1, f_3^2, f_2^3, f_4^3, f_1^4, f_3^4, f_2^5, f_1^6\big\},$$

respectively.

Similar to WNC in the TWRC, the transmission with MH-CPF in the MH-TRC also consists of a series of multiple-access and broadcast phases. Accordingly, $f_l^j$ can be further divided into two sub-events, i.e., single-access transmission event, denoted by $f_{S,l}^j$, and multiple-access transmission event, denoted by $f_{M,l}^j$.

- **Single-access transmission event:** A single-access transmission event represents an event in which a node receives the signal from only one of two neighboring nodes,

$$N_{l-1} \xrightarrow{x} N_l \quad \text{or} \quad N_l \xleftarrow{y} N_{l+1}$$

In MH-CPF for the $L$-node $K$-message, the single access transmission event $f_{S,l}^j$ occurs

  - In the initial stages when relay nodes receive their first signals;
  - At relay nodes $N_2$ and $N_{L-1}$ in the odd time slots after user nodes finish sending all messages; and
  - At user nodes $N_1$ and $N_L$ during even time slots after $L-1$ time slots.

The achievable rate of the single-access transmission event is equivalent to the achievable rate of point-to-point transmission given by (5.20). Thus, the outage probability of the single-access transmission event $f_{S,l}^j$ can be given by

$$p_{f_{S,l}^j}^{\text{out}}(R_{\text{MH-CPF}})=1-\exp\left(-\frac{2^{\frac{L-1+2(K-1)}{2K}R}-1}{\bar{\gamma}_l}\right), \tag{5.27}$$

or

$$p_{f_{S,l}^j}^{\text{out}}(R_{\text{MH-CPF}})=1-\exp\left(-\frac{2^{\frac{L-1+2(K-1)}{2K}R}-1}{\bar{\gamma}_{l+1}}\right), \tag{5.28}$$

where

$$R_{\text{MH-CPF}}=\frac{R}{C_{\text{MH-CPF}}}=\frac{L-1+2(K-1)}{2K}R \tag{5.29}$$

is the target message rate for MH-CPF in the $L$-node $K$-message MH-TRC.

- **Multiple-access transmission event:** A multiple-access transmission event denotes an event in which a relay receives bi-directional signals from both neighboring nodes,

$$N_{l-1} \xrightarrow{x} N_l \xleftarrow{y} N_{l+1}$$

which occurs

  - At relay nodes $\{N_l\}_{l=3}^{L-2}$ in the time slots after the initial stages; and
  - At relay nodes $N_2$ and $N_{L-1}$ after the initial stage and before the user nodes finish sending all messages.

The outage probability of the multiple-access transmission event is the probability that the maximized computation rate $R_{\text{COMP},l}(\mathbf{h}_l, \hat{\mathbf{a}}_l)$ at relay node $N_l$ is less than the target message rate $R_{\text{MH-CPF}}$, given by

$$p_{f_{M,l}^j}^{\text{out}}(R_{\text{MH-CPF}}) = \Pr\left[R_{\text{COMP},l}(\mathbf{h}_l, \hat{\mathbf{a}}_l) < \frac{L-1+2(K-1)}{2K} R\right]. \quad (5.30)$$

The maximization of the computation rate $R_{\text{COMP},l}(\mathbf{h}_l, \hat{\mathbf{a}}_l)$ is an SVP problem, which has no closed-form solutions. Thus, the closed-form outage probability expression of $p_{f_{M,l}^j}^{\text{out}}(R_{\text{MH-CPF}})$ is unattainable. However, the complex lattice reduction algorithms can be applied to calculate the outage probability numerically.

Accordingly, the sets $\mathcal{F}_{\hat{v}_1}$ and $\mathcal{F}_{\hat{v}_2}$ for the transmission of messages $\hat{v}_1$ and $\hat{v}_2$ in the 5-node 2-message MH-TRC can be rewritten as

$$\begin{aligned}\mathcal{F}_{\hat{v}_1} &= \left\{f_{S,2}^1, f_{S,4}^1, f_{M,3}^2, f_{M,2}^3, f_{S,1}^4\right\}, \quad \text{and}\\ \mathcal{F}_{\hat{v}_2} &= \left\{f_{S,2}^1, f_{S,4}^1, f_{M,3}^2, f_{M,2}^3, f_{M,4}^3, f_{S,1}^4, f_{M,3}^4, f_{S,2}^5, f_{S,1}^6\right\}.\end{aligned}$$

The outage probability of message $\hat{v}_k$ occurs when any transmission event in the set $\mathcal{F}_{\hat{v}_k}$ is in outage. Thus, the outage probability of message $\hat{v}_k$ can be given by

$$\begin{aligned}p_{\text{MH-CPF},\hat{v}_k}^{\text{out}}(R) =& 1 - \prod_{f_{S,l}^j \in \mathcal{F}_{\hat{v}_k}} \left(1 - p_{f_{S,l}^j}^{\text{out}}(R_{\text{MH-CPF}})\right)\\ & \prod_{f_{M,l}^j \in \mathcal{F}_{\hat{v}_k}} \left(1 - p_{f_{M,l}^j}^{\text{out}}(R_{\text{MH-CPF}})\right). \quad (5.31)\end{aligned}$$

For simplicity, it is assumed that all channels $h_l$ are independently identically distributed [137], i.e., $\bar{\gamma}_l = \bar{\gamma}$. Therefore, the outage probabilities of the same type of sub-events in set $\mathcal{F}_{\hat{v}_k}$ are the identical.

Let $A_k$ and $B_k$ be the numbers of sub-event $f_{S,l}^j$ and $f_{M,l}^j$ in set $\mathcal{F}_{\hat{v}_k}$, respectively. Following the MH-CPF scenarios at each node given in Section 3.6, $A_k$ and $B_k$ can be readily obtained as

$$\begin{aligned} A_k=& \mathcal{T}_k + \frac{L-3}{2} - K, \quad B_k = (L-3)(k-1) + 1 + \sum_{i=2}^{K} \left( \frac{L+1}{2} - i \right), \\ & 2K - 1 < L - 1, \quad \forall k \in \{1, 2, ..., K\}, \end{aligned} \tag{5.32}$$

and

$$A_k= \begin{cases} \mathcal{T}_k - k & k \in \{1, 2, ..., C\} \\ \mathcal{T}_k - C & k \in \{C+1, ..., K\} \end{cases}, \tag{5.33}$$

$$B_k= \begin{cases} (L-2)(k-1) + 1 + \sum\limits_{i=1}^{\frac{L-3}{2}} i & k \in \{1, 2, ..., C\} \\ (L-3)(k-1) + C + \sum\limits_{i=1}^{\frac{L-3}{2}} i & k \in \{C, ..., K\} \end{cases} \tag{5.34}$$

$$C = \frac{2K - (L-3)}{2}, 2K - 1 > L - 1$$

Thus, the outage probability of message $\hat{v}_k$ given by (5.31) can be derived as

$$\begin{aligned} p_{\text{MH-CPF},\hat{v}_k}^{\text{out}}(R) =& 1 - \underbrace{\left(1 - p_{f_{S,i}^j}^{\text{out}}(R_{\text{MH-CPF}})\right)^{A_k}}_{A} \underbrace{\left(1 - p_{f_{M,i}^j}^{\text{out}}(R_{\text{MH-CPF}})\right)^{B_k}}_{B} \\ =& 1 - \exp\left( -\frac{2^{\frac{L+2(K-1)}{2K}R} - 1}{\bar{\gamma}} \right)^{A_k} \\ & \left(1 - \Pr\left[ R_{\text{COMP},l}(\mathbf{h}_l, \hat{\mathbf{a}}_l) < \frac{L-1+2(K-1)}{2K} R \right] \right)^{B_k} \end{aligned} \tag{5.35}$$

Substituting (5.35) into (5.18), the outage probability for MH-CPF can be given as

$$\begin{aligned} p_{\text{MH-CPF}}^{\text{out}}(R) =& \frac{1}{K} \sum_{k=1}^{K} p_{\text{MH-CPF},\hat{v}_k}^{\text{out}}(R) \\ =& 1 - \frac{1}{K} \sum_{k=1}^{K} \left[ \exp\left( -\frac{2^{\frac{L+2(K-1)}{2K}R} - 1}{\bar{\gamma}} \right)^{A_k} \right. \\ & \left. \left(1 - \Pr\left[ R_{\text{COMP},l}(\mathbf{h}_l, \hat{\mathbf{a}}_l) < \frac{L-1+2(K-1)}{2K} R \right] \right)^{B_k} \right] \end{aligned} \tag{5.36}$$

## 5.8 Effective Network Throughput

In the "standard" PNC, the relay uses PNC mapping [14] to decode the modular-2 sum of transmitted messages, where PNC mapping was proven to have the same BER as the traditional decode and forward (DF) strategy. However, the analysis of the achievable rate of the "standard" PNC established in [14] is a challenging task since it depends on the specific modulation method. For the BSC with the error probability $P_e$, the authors in [95] calculated the achievable rate of PNC as $R \leqslant \frac{1}{2}(1 - H(P_e))$.

For fading channels, the BER for PNC is intractable due to the multiple information in the collided signal and random channel state information (CSI). As far as the literature review suggests, no BER analyse of PNC in fading channels have been established in published work to date. Therefore, the analytical expression of the BER is computationally intractable for the MH-CPF scheme. However, note that the probability of the successful transmission $1 - p^{\text{out}}$ is the upper-bound of the symbol error rate. Therefore, using bounding technique, the upper-bound effective network throughput can be given by

$$\hat{C}^e \triangleq C(1 - P^{\text{out}}) \tag{5.37}$$

## 5.9 Numerical Results

In this section, the outage probabilities of the Non-NC and MH-CPF schemes for the $L$-node $K$-message MH-TRC are compared. The target end-to-end rate for the MH-TRC $R$ is set to 1 bit/sec/Hz for all comparisons.

The outage probability versus the average SNR per hop $\bar{\gamma}$ for the 5-node MH-TRC is plotted in Figure 5.3. As can be observed from the figure, MH-CPF can achieve an approximately 6 dB gain in comparison with Non-NC at the outage probability of $10^{-2}$ when the number of messages is 2. Moreover, MH-CPF has better outage performance than Non-NC in the 5-node MH-TRC with less than 9 messages, while the outage probability of MH-CPF is worse than that of Non-NC when the number of messages is larger than 9. In comparison with the MH-ANC for non-regenerative MH-TRC in [35], MH-CPF has an approximately 3 dB gain at the outage probability of $10^{-2}$ for the 5-node 2-message MH-TRC.

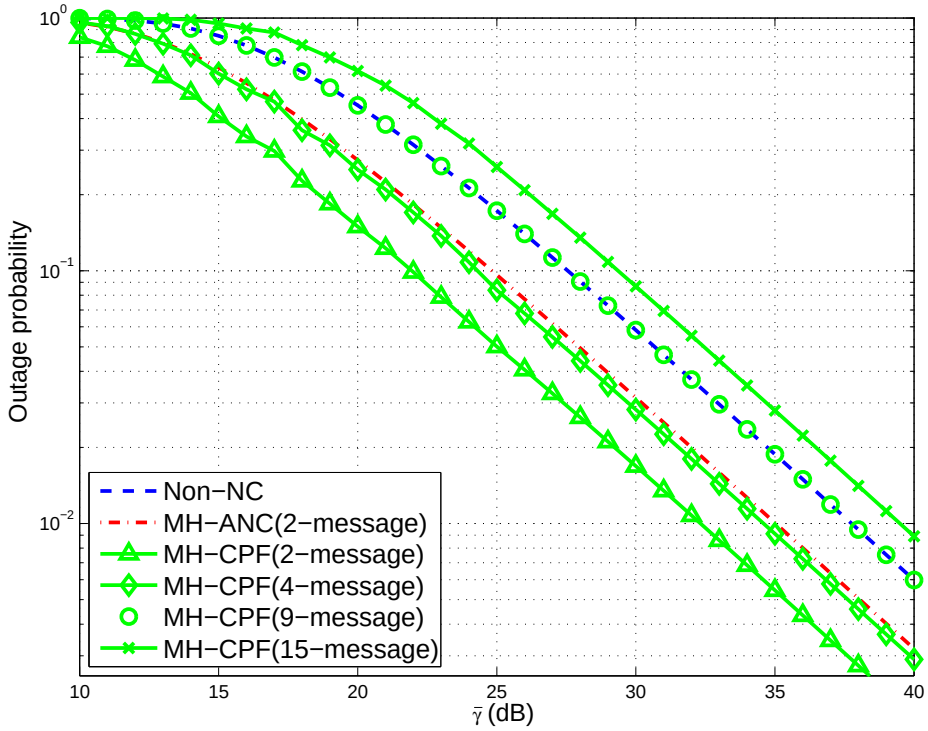


Figure 5.3: Outage probability versus the average SNR per hop for the 5-node MH-TRC.

Figure 5.4 shows the outage probability versus the number of messages for 7-node, 11-node, and 15-node MH-TRCs. The average SNR per hop is set to 40 dB. As can be seen from (5.24), the outage probability of the Non-NC scheme is not affected by the number of messages.

However, the outage probability of MH-CPF is affected by the numbers of both nodes and messages. On one hand, the network throughput of MH-CPF increases with the increased number of messages, making the MH-CPF target message rate $R_{\text{MH-CPF}}$ smaller as can be seen from (5.29). As a result, the outage probabilities $p^{\text{out}}_{f^j_{S,l}}(R_{\text{MH-CPF}})$ and $p^{\text{out}}_{f^j_{M,l}}(R_{\text{MH-CPF}})$ decrease with the increase of the number of messages, causing the bases of terms $A$ and $B$ in (5.35) increase.

On the other hand, the numbers of transmissions events $A_k$ and $B_k$ (which are the powers of term $A$ and $B$) increase with the increased number of messages. It should be noted that the bases of terms $A$ and $B$ are both smaller than 1. According to the property of exponentiations, when the base is smaller than 1, the exponentiation is a decreasing function of the power. As a result, the bases of

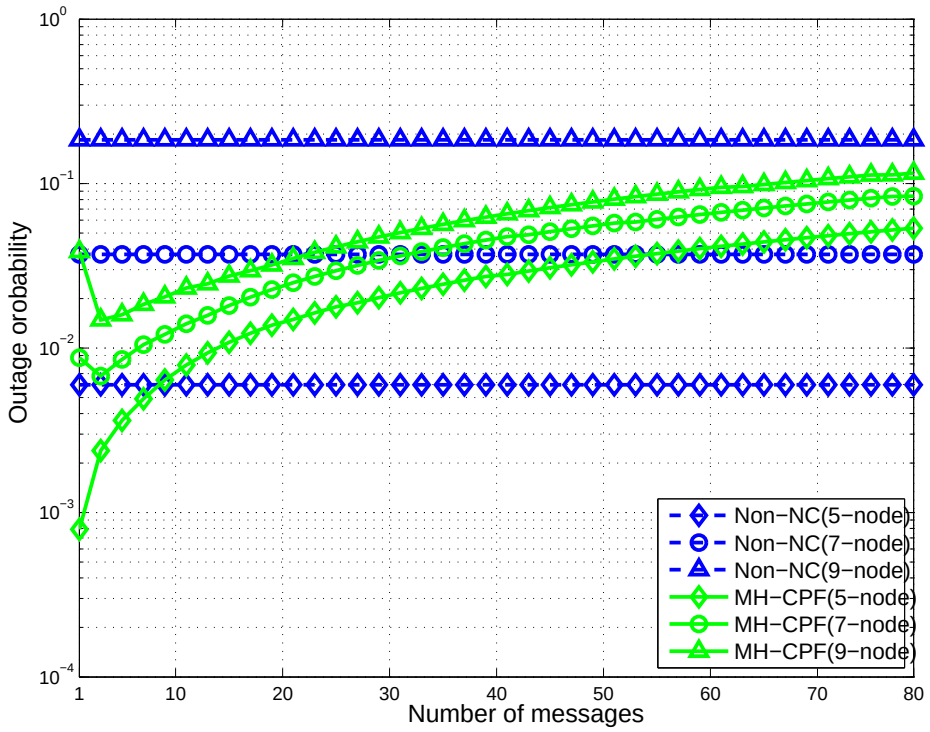


Figure 5.4: Outage probability versus the number of messages for the generalized MH-TRC.

terms $A$ and $B$ in (5.35) (the values are between $[0, 1]$) increase with the increase of the number of messages, and the powers of term $A$ and $B$ also increase with the number of messages. The relationship between the outage probability of MH-CPF given by (5.36) and the number of messages is difficult to determine analytically. As indicated in Figure 5.4, each outage probability curve has a valley point, denoting the minimum outage probability that MH-CPF can achieve in the MH-TRC with a specific number of nodes.

Moreover, it can be demonstrated that there exists an optimal number of messages for different scale MH-TRCs, where MH-CPF can achieve the best outage performance. This optimal number of messages increases with the number of nodes. For example, the number of messages for the 7-node, 11-node and 15-node MH-TRCs are 1, 3 and 9, respectively.

It can also be observed from Figure 5.4, that MH-CPF has a better outage performance than Non-NC when the number of messages is under 31 for the 7-node MH-TRC. Moreover, it is clearly demonstrated that for the 11-node and 15-node MH-TRCs, the outage probabilities of MH-CPF are always superior to

those of Non-NC for the number of messages up to 80, as shown in the figure.

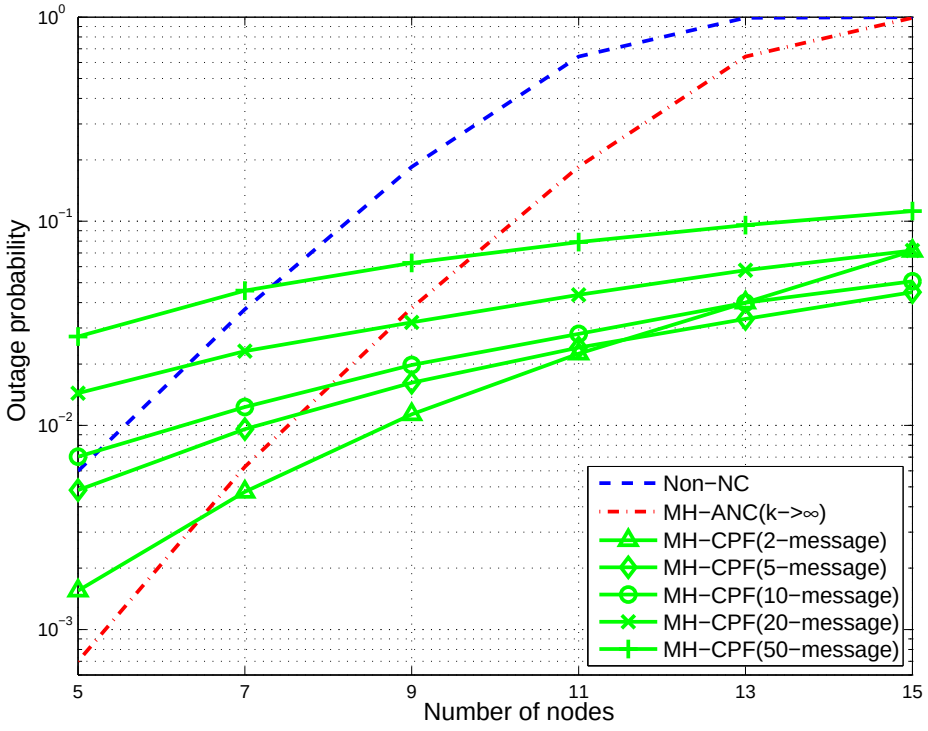


Figure 5.5: Outage probability versus the number of nodes for the generalized MH-TRC.

The outage probability versus the number of nodes is plotted in Figure 5.5. The average SNR per hop is also set to 40 dB. It can be seen from the figure that, the outage performance of MH-CPF is always better than Non-NC when the number of messages is 2 or 5 in all the MH-TRCs with number of nodes larger than 5. With the increase in the number of messages, MH-CPF can achieve a better outage performance than Non-NC with a relatively large number of nodes. For example, for the MH-TRC with more than 7 nodes, the outage performance of MH-CPF is always better than Non-NC when the number of messages is less than 50, as can be seen from Figure 5.5. Similarly, MH-ANC has better outage performance than MH-CPF when the number of hops is small, while MH-CPF performs better in the MH-TRC with a relatively large number of nodes.

Figure 5.6 plots the effective network throughput for the generalized MH-TRC with both schemes when the number of messages $K \gg L$. It is assumed that the average SNR per hop $\bar{\gamma}'$ is 40 dB. The figure demonstrates that MH-CPF is superior to the Non-NC scheme in all-scale MH-TRCs, and the gain increases

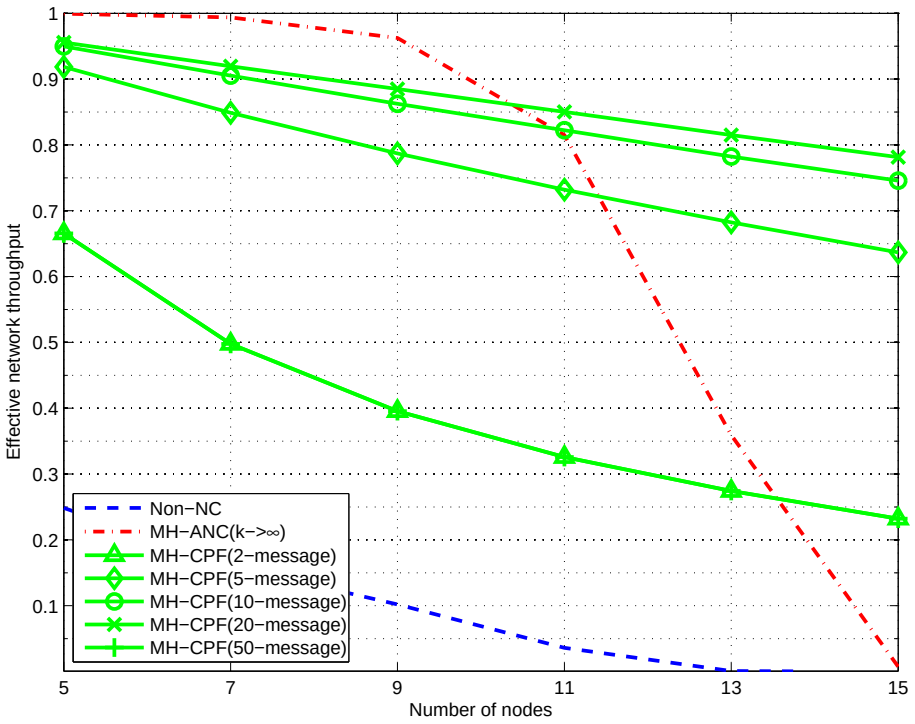


Figure 5.6: Effective network throughput versus the number of nodes for the generalized MH-TRC.

with the increase in the number of messages. Moreover, it can be seen that the effective network throughput of the MH-CPF scheme is not better than MH-ANC when the number of nodes is relatively small. However, when the numbers of nodes and messages are large, MH-CPF can always achieve better effective network throughput than MH-ANC.

## 5.10 Summary

In this chapter, the original CPF is extended to MH-CPF with application to the generalized MH-TRC. To maximize the computation rates at each relay node during the whole exchange process, the complex lattice reduce algorithm is applied to find the best coefficient vector. The result demonstrates that the computation rate obtained by the complex lattice reduce algorithm is well matched to the result obtained by the greedy search algorithm. Due to the exponentially increase complexity of the received linear combinations at user nodes, the conventional approach for recovering messages in the original CPF scheme is inapplicable to

MH-CPF. The forward and backward recursive approaches proposed in Chapter 4 is applied to obtain the linear combinations at the user nodes.

Furthermore, the outage performance for the proposed MH-CPF is analyzed. The outage probabilities for both Non-NC and MH-CPF schemes are derived. The numerical results show that for the MH-TRC with a relatively small number of nodes, MH-CPF can achieve better outage performance than Non-NC. Moreover, it is also demonstrated that for the MH-TRC with a large number of nodes, MH-CPF can always have a better outage probability compared to Non-NC when the number of message is large.

To summarize, the outage probability of each message in MH-CPF depends on the numbers of single-access and multi-access transmission events that interfere with the transmission of the messages. Due to bi-directional transmission, the transmission of early messages interferes with the transmission of later messages. Therefore, the outage probability of MH-CPF increases with the number of messages. However, the outage probability of MH-CPF converges a stable value when the number of messages is far larger than the number of nodes, and increases slowly with the increase in the number of nodes.

On one hand, when the numbers of nodes and messages are small, the network throughput of MH-CPF is only slightly greater than that of Non-NC, while the number of transmissions that interfere the transmission of a single message of MH-CPF is far worse than that of Non-NC. Therefore, the outage probability of MH-CPF is worse than that of Non-NC when the numbers of nodes and messages are small. On the other hand, when the numbers of nodes and messages are large, the network throughput of MH-CPF is significantly better than that of Non-NC. The network throughput of Non-NC decreases quickly with the increase in the number of nodes, while the network throughput of MH-CPF remains constant regardless of the numbers of messages and nodes. As a result, the outage probability of Non-NC increase fast with the increase of the number of nodes, while the outage probability of MH-CPF increase slowly with the number of nodes when the number of messages is large. Although the MH-CPF scheme cannot outperform Non-NC in outage performance when the number of nodes is small, it can achieve a better outage performance when the number nodes is large.

# Chapter 6

# Optimal Wireless Network Coding for Multi-Hop Two-Way Relay Channels

## 6.1 Introduction

The work presented in the previous two chapters have demonstrated that the proposed MH-WNC with fixed two time intervals is not able to outperform Non-NC in all-scale MH-TRCs. In view of this fact, this project aims to design an optimal MH-WNC that can achieve the best outage performance for all scale MH-TRCs. More specifically, a multiple-time-interval (Multi-TI) MH-WNC scheme is proposed. It uses multiple time intervals, instead of two at the user nodes. To obtain the optimal MH-WNC, the outage performance for the MH-WNC schemes with different time intervals is to be investigated. It should be noted that the transmission scenario for the Multi-TI MH-WNC scheme differs from each other due to the different transmission time intervals. Therefore, the results from the last two chapters are directly inapplicable. In this case, a generalized transmission scheme is designed, and performance analysis for Multi-TI MH-WNC is presented. The results of network throughput, received SNR and outage probability will be presented to show the relationship between the number of nodes, messages and time intervals with them. Finally, the findings are discussed, then the optimal MH-WNC for all scale MH-TRCs is summarized.

The contributions in this chapter can be summarized as follows:

1. Design of the generalized $I$-TI MH-WNC ($I$ represents the number of transmission time intervals at user nodes) for the generalized $L$-node $K$-message MH-TRC;

2. Analysis of the performance of $I$-TI MH-WNC by converting the transmission model to a special binary tree model joined with the corresponding characteristic matrices;

3. The design of a postorder traverse algorithm to obtain the received signal-to-noise-ratio (SNR) of each message for the $I$-TI MH-ANC scheme, and the outage probability for the $I$-TI MH-CPF obtained with the converted transmission matrices.

4. Evaluation of the relationships between the number of nodes, messages and time intervals with the network throughput, received SNR and outage probability, and determination of an optimal MH-WNC for all scale MH-TRCs with the best outage probability. Moreover, the obtained optimal MH-WNC scheme is proven to be superior to Non-NC in outage performance in all scale MH-TRCs.

## 6.2 Problem Statement

In the last two chapters, the performance of MH-WNC with fixed two time intervals is analyzed (which is referred to as the 2-TI MH-WNC scheme in this chapter) for both non-regenerative and regenerative MH-TRCs. In the 2-TI MH-WNC scheme, each node works once every two time slots, i.e., odd-numbered nodes work in odd time slots, and even-numbered nodes work in even time slots. It is proven that this $I$-TI MH-WNC scheme can achieve a significantly improved network throughput compared to the Non-NC scheme, i.e., $L-1$ times larger than Non-NC when $K \gg L$. However, it is also demonstrated that MH-ANC cannot provide better outage performance than Non-NC in large scale non-regenerative MH-TRCs, while MH-CPF is unable to outperform Non-NC in small scale regenerative MH-TRCs.

It is later found that the MH-WNC scheme with fixed two time intervals is not the only transmission scheme to implement network coding in the MH-TRC. In the 2-TI MH-WNC scheme, network coding is performed at all the relay nodes in all time slots. However, when the number of time intervals (TIs) in MH-WNC is increased to $\{4, 6, 8, ...\}$ (odd numbers do not work due to the swapping transmission scheme for even-numbered and odd-numbered nodes), the network coding is performed at relay nodes in different patterns.

It should be noted that the $I$-TI MH-WNC scheme with a larger number of TIs has poorer network throughput than the 2-TI MH-WNC scheme. Moreover, the signal collision occurs when the forward signal meets the backward signal in MH-WNC. The number of signal collisions at each relay node is determined by the number of nodes, the number of messages, and the number of time intervals. For example, it can be seen that for the 2-TI MH-WNC in the 5-node 2-message MH-TRC, the first signal collision occurs at relay nodes $N_2$ and $N_{L-1}$ immediately after the user nodes send out their second message in time slot 3, and the signal collision continues at all the relay nodes until the central node broadcasts the final signal. On the other hand, when the number of TIs equals the number of hops ($I = L - 1$), the signal collision only occurs at central relay node $N_{(L+1)/2}$. Therefore, the number of signal collisions equals the number of messages $K$.

On one hand, the increase of the number of TIs reduces the network throughput. On the other hand, it also reduces the number of signal collisions, the noise propagation and the number of compute-and-forward processes. The aim of the work in this chapter is to determine the optimal MH-WNC that achieves the best outage performance for all-scale MH-TRCs with the best outage probability, which amounts to investigating the relationship between the number of TIs and the received SNR, the network throughput and the outage probability.

## 6.3 Assumptions

To simplify the analysis, it is assumed that the power per node per transmission is equalized to one for all the nodes during the entire exchange process in the 2-TI MH-WNC scheme. The number of transmissions at each relay node is reduced

due to the transmission overlap between messages. Thus, compared to Non-NC schemes, the MH-WNC scheme reduces the number of transmissions at the relay nodes, thus reducing the overall power consumption. Similarly, due to the reduction of the number of signal collisions, the $I$-TI MH-WNC schemes with a larger number of TIs consumes more power than the 2-TI MH-WNC scheme.

In this chapter, the overall system transmission power is assumed to be the same for both Non-NC and $I$-TI MH-WNC schemes. Each node is assigned with a unit power $P$ for one message exchange. The greater the number of transmissions required at a node, the smaller the power per transmission will be. For example, for a $L$-node $K$-message MH-TRC, each node is equipped with the same transmission power $2KP$. Denote by $n_l$ the total number of transmissions required at relay node $N_l$, the power per transmission for $N_l$ per is given by

$$P_l = \frac{2KP}{n_l}. \tag{6.1}$$

For the Non-NC scheme, one transmission is required for one message at each node. The number of transmission is $K$ for both user nodes, and $2K$ for all the relay nodes. Therefore, the power per transmission for both user nodes is $2P$, and $P$ for the relay nodes.

For $I$-TI MH-WNC, the relay nodes have different transmission patterns due to their different locations in the MH-TRC. Thus, the power per transmission is not identical for all the nodes. For example, for a 9-node 3-message MH-TRC, the number of transmission $n_l$ and the power per transmission $P_l$ for all the nodes can be shown in Table 6.1.

Table 6.1: Transmission powers of the nodes in the 9-node 3-message MH-TRC

| TI | Number of time slot | Number of | Nodes | | | | | | | | |
|---|---|---|---|---|---|---|---|---|---|---|---|
| ($I$) | ($T = L - 1 + I(K-1)$) | transmissions | $N_1$ | $N_2$ | $N_3$ | $N_4$ | $N_5$ | $N_6$ | $N_7$ | $N_8$ | $N_9$ |
| 2 | 12 | $n_l$ | 3 | 6 | 5 | 4 | 3 | 4 | 5 | 6 | 3 |
| | | $P_l$ | $2P$ | $P$ | $6P/5$ | $3P/2$ | $2P$ | $3P/2$ | $6P/5$ | $P$ | $2P$ |
| 4 | 16 | $n_l$ | 3 | 6 | 4 | 6 | 3 | 6 | 4 | 6 | 3 |
| | | $P_l$ | $2P$ | $P$ | $3P/2$ | $P$ | $2P$ | $P$ | $P/4$ | $P$ | $2P$ |
| 6 | 20 | $n_l$ | 3 | 4 | 6 | 6 | 3 | 6 | 6 | 4 | 3 |
| | | $P_l$ | $2P$ | $3P/2$ | $P$ | $P$ | $2P$ | $P$ | $P/6$ | $3P/2$ | $2P$ |
| 8 | 24 | $n_l$ | 3 | 6 | 6 | 6 | 3 | 6 | 6 | 6 | 3 |
| | | $P_l$ | $2P$ | $P$ | $P$ | $P$ | $2P$ | $P$ | $P/6$ | $P$ | $2P$ |

As can be seen from the table, the number of transmissions for user nodes and central relay nodes are both equivalent to $K$ regardless of the number of time intervals. However, the number of transmissions for the other relay nodes changes with the number of time intervals.

## 6.4 System Model

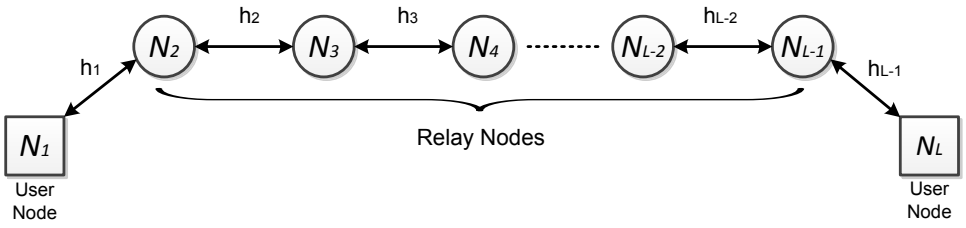


Figure 6.1: The $L$-node $K$-message multi-hop two-way relay network.

The same $L$-node $K$-message MH-TRC model discussed in the previous chapters, as shown in Figure 6.1, is considered. Instead of sending their messages every two time slots, the two user nodes $N_1$ and $N_L$ send one message every $I$ time slots simultaneously. Similarly, the transmission scenario for the generalized $I$-TI MH-WNC can be extrapolated as follows:

- User nodes send their messages very $I$ time slots in odd time slots, until they complete sending all the $K$ messages; and then they begin receiving messages from their neighboring relay nodes from time slot $L-1$ every $I$ time slots, until the end of the entire transmission; and they remain silent in the rest time slots; and

- Relay nodes transmit each forward and backward message once every $I$ time slots.

Following the transmission scenario, the transmission modes for each node in different time slots with MH-WNC can be summarized as:

- For user nodes $N_1$ and $N_L$,
  $\mathbb{S}_1^j = \mathbb{S}_L^j = \mathbb{T}$, $j \in \{1, I+1, 2I+1, ..., (K-1)I+1\}$.

$\mathbb{S}_1^j = \mathbb{S}_L^j = \mathbb{R}$, $j \in \{L-1, L-1+I, L-1+2I, ..., L-1+I(K-1)\}$.
$\mathbb{S}_1^j = \mathbb{S}_L^j = \ominus$, other.

- For relay nodes $\{N_l\}_{l=2}^{L-1}$,
  $\mathbb{S}_l^j = \mathbb{T}$, $j \in \{L-l+1, L-l+I+1, L-l+2I+1, ..., L-l+(K-1)I+1\} \cup \{l+1, l+I+1, l+2I+1, ..., l+(K-1)I+1\}$.
  $\mathbb{S}_l^j = \mathbb{R}$, if $\mathbb{S}_{l-1}^j = \mathbb{T} \cup \mathbb{S}_{l+1}^j = \mathbb{T}$.
  $\mathbb{S}_l^j = \ominus$, other.

where $\mathbb{R}$, $\mathbb{T}$ and $\ominus$ are the receiving, sending and silent modes of the nodes, respectively. $\mathbb{S}_l^j$ is the operation mode for node $N_l$ in time slot $j$.

The grid chart of the transmission pattern for the $I$-TI MH-WNC can be depicted with the platform in Chapter 3. For example, the grid chart for the 5-node 3-message MH-TRC with the 4-TI MH-WNC is shown in Figure 6.2.

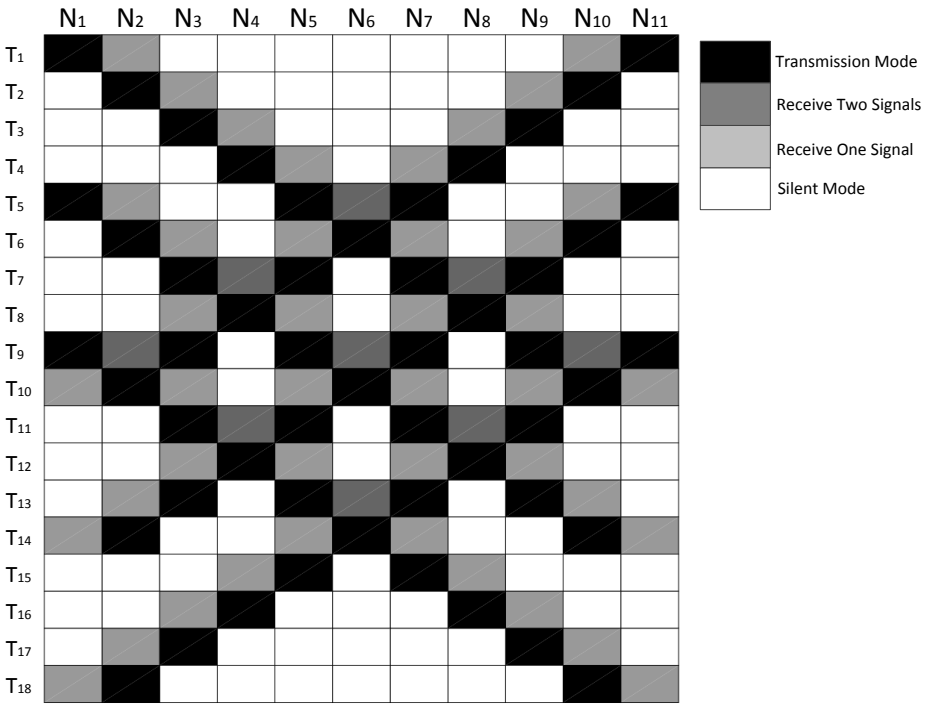


Figure 6.2: Grid chart for the transmission scheme of the 11-node 3-message MH-TRC with 4-TI MH-WNC.

It can be seen that the grid chart shown in Figure 6.2 is different from that of 2-TI MH-WNC shown in Figure 3.8(a). The number of time slots is more than

that of 2-TI MH-WNC, however it can seen that the distribution of gray grids is looser, representing less interference. Moreover, the number of silent nodes is more than that of the 2-TI MH-WNC scheme, meaning less channel use rate and network throughput.

With $I$-TI MH-WNC, the total number of time slots used is $\mathcal{T}_{\text{MH-WNC}} = L - 1 + I(K-1)$. The network throughput is

$$C_{\text{MH-WNC}} = \frac{2K}{L-1+I(K-1)} \quad \text{(message/time slot)}. \tag{6.2}$$

When the number of messages $K$ is far larger than the number of nodes $L$, an upper limit of $C_{\text{MH-WNC}}$ can be obtained as

$$\hat{C}_{\text{MH-WNC}} = \lim_{K>>L} \frac{2K}{L-1+I(K-1)} = \frac{2}{I} \quad \text{(message/time slot)}. \tag{6.3}$$

The network throughput decreases with the increase of the transmission time intervals, as can be seen from (6.3).

## 6.5 Methodologies

In this section, the methodologies for the performance analysis of $I$-TI MH-WNC will be presented, including the received SNR for the non-regenerative system and outage probability for the generalized MH-TRC.

Before delving into details, Table 6.2 which defines the terms used in the rest of the chapter is presented to the reader.

The transmission pattern of $I$-TI MH-WNC can be represented by a $\mathcal{T}$ by $L$ matrix. For example, the pattern matrix for message $u_1$ and $v_1$ in the 5-node 3-message MH-TRC with the 2-TI MH-WNC can be expressed as

$$\mathbf{T}_1 = \begin{bmatrix} 1 & -1 & 0 & -1 & 1 \\ 0 & 1 & -2 & 1 & 0 \\ 1 & -2 & 1 & -2 & 1 \\ -1 & 1 & -2 & 1 & -1 \end{bmatrix} \tag{6.4}$$

where the element $t_{j,i}$ represents the mode of node $N_i$ at time slot $j$. By converting the corresponding the transmission gird chart, it can be found that the yellow-colored elements in the above matrix do not affect the transmission of message $v_1$.

Table 6.2: Definitions of terms used in this chapter.

| Notation | Term | Definition |
|---|---|---|
| $\mathbf{T}_k$ | **Pattern matrix** | The matrix representing the transmission pattern of MH-WNC |
| $\mathbf{T}_{v_k}$ | **Transmission matrix** | The matrix representing the transmission pattern for message $v_k$ |
| $\mathbf{N}_{v_k}$ | **Noise matrix** | The matrix only containing the transmission events of the transmission matrix $\mathbf{T}_{v_k}$ |
| $\tilde{\mathbf{N}}_{v_k}$ | **Noise power matrix** | The matrix displaying the received noise power propagation at each node of message $v_k$ |
| $\mathbf{S}_{v_k}$ | **Signal matrix** | The matrix displaying the transmission events that participates the transmission of message $v_k$ |
| $\tilde{\mathbf{S}}_{v_k}$ | **Signal power matrix** | The matrix displaying the weight of each element in the signal characteristic matrix $\mathbf{S}_{v_k}$ |
| $\mathbb{S}_{v_k}$ | **Single access transmission matrix** | The matrix displaying the single access transmission events that affect the transmission of message $v_k$ |
| $\tilde{\mathbb{S}}_{v_k}$ | **Single access transmission power matrix** | The matrix displaying the powers of each event in the single access transmission matrix $\mathbb{S}_{v_k}$ |
| $\mathbb{C}_{v_k}$ | **CPF matrix** | The matrix displaying the CPF events that affect the transmission of message $v_k$ |
| $\tilde{\mathbb{C}}_{v_k}$ | **CPF power matrix** | The matrix that displays the power-pairs of each event in the CPF matrix $\mathbb{C}_{v_k}$ |
| $W_i$ | **Weight** | The weight of links from a specific node to its left and right child nodes in the binary tree structure |

Therefore, setting these yellow-colored elements to zero, the transmission matrix for message $v_1$ can be given by

$$\mathbf{T}_{v_1} = \begin{bmatrix} 1 & -1 & 0 & -1 & 1 \\ 0 & 1 & -2 & 1 & 0 \\ 1 & -2 & 1 & 0 & 0 \\ -1 & 1 & 0 & 0 & 0 \end{bmatrix}. \tag{6.5}$$

The transmission matrix for each message in generalized $L$-node $K$-message MH-TRC with $I$-TI MH-WNC can be obtained similarly. The following received SNR and outage probability analysis can be carried out based on the transmission matrix.

### 6.5.1 Analog Network Coding

The end-to-end SNR for the $I$-TI MH-ANC is defined as the average SNR of each message $v_k$, which can be given by

$$\gamma_{\text{MH-ANC},v_k} = \frac{\mathcal{S}_{\text{MH-ANC},v_k}}{\mathcal{N}_{\text{MH-ANC},v_k}}, \tag{6.6}$$

where the $\mathcal{S}_{\text{MH-ANC},v_k}$ and $\mathcal{N}_{\text{MH-ANC},v_k}$ are the signal and noise power of message $v_k$, respectively. Similar to the performance analysis in Chapter 4, the noise propagation through different paths needs to be determined in order to derive the received SNR of each message. It is difficult to implement an universal recursive approach for the generalized $I$-TI MH-ANC. Therefore, in the following sections, the transmission pattern is converted into a binary tree model, and a postorder traversal approach is proposed for analyzing the noise and signal powers ($\mathcal{N}_{\text{MH-ANC},v_k}$ and $\mathcal{S}_{\text{MH-ANC},v_k}$) numerically.

#### 6.5.1.1 Noise Power

The noise propagation model for message $v_1$ and $v_2$ in the 5-node 3-message MH-TRC with 2-TI MH-WNC can be illustrated by Figure 6.3.

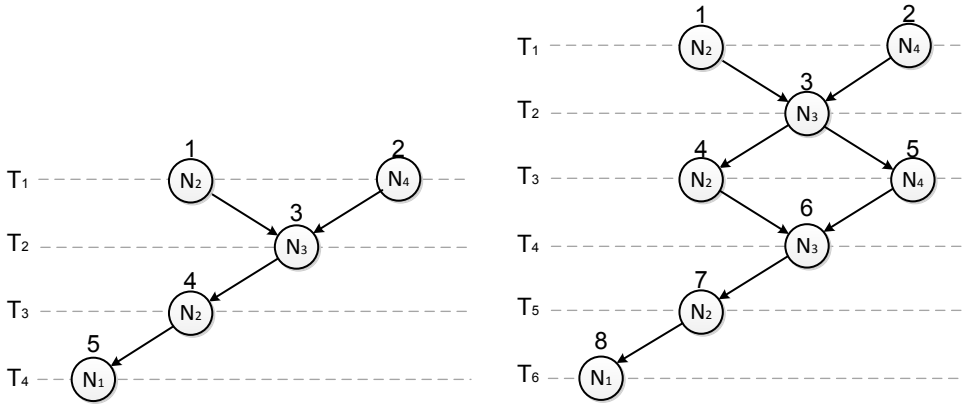


**(a)** $v_1$. **(b)** $v_2$.

Figure 6.3: Noise propagation model in the 5-node 3-message MH-TRC with 2-TI MH-WNC.

As can be seen from the above two figures, the received noise at user node $N_1$ for message $v_1$ consists of the noise propagation from 4 nodes, while each noise

term only consists of one propagation path. On the other hand, the received noise for $v_2$ consists of the noise propagation from 7 nodes, where noise terms from node 4, 5, 6 and 7 consist of one propagation path, and the other noise terms are made up of 2 paths.

It is interesting to find that the above Figure 6.3 is a binary-tree-like structure, while the only difference from the canonical binary tree is that child nodes may have two parent nodes. It is well known that there are a number of numerical solutions for the binary tree traversal problem. Therefore, by converting the noise power derivation to the binary tree problem, the derivation can be simplified.

To illustrate the algorithm, the converted binary tree for the transmission pattern presented in Figure 4.3 in Section 4.4.1 is shown in Figure 6.4.

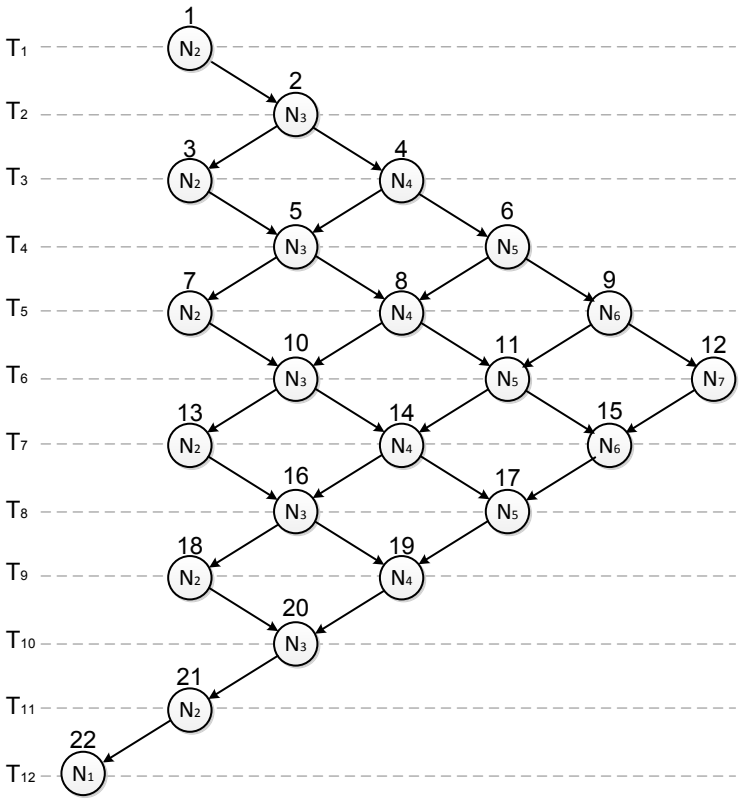


Figure 6.4: Binary tree structure for Figure 4.2.

There are 22 nodes in this binary tree, and each node represents a node in the MH-TRC in a specific time slot. Node 22 is the end of the transmission at user node $N_1$, which is also the bottom node of the binary tree. The received noise at each node in the figure propagates via different paths to end node 22. Therefore,

the final noise power at node 22 is a combination of 22 terms, which contain the propagation power of the received noise at each node. Denote by $N_i'$ the term of received noise power plus the propagated noise power from the previous nodes at node $i$ in the above figure. The noise power at node 22 can be expressed as

$$\mathcal{N}_{22} = \mathcal{N}_1' + \mathcal{N}_2' + \mathcal{N}_i' + ... + \mathcal{N}_{22}' = \sum_{i=1}^{22} \mathcal{N}_i',$$

For the general case, the received noise at node $N_1$ in time slot $j$ can be given by

$$\mathcal{N}_j = \sum_{i \in \mathcal{U}_j} \mathcal{N'}_i, \tag{6.7}$$

where $\mathcal{U}_j$ is the set of the nodes for the converted binary tree in time slot $j$.

Consider the link from $i$ to $i+1$, the transmission between two nodes can be expressed as

$$y_{i+1} = \sqrt{P_i} G_i h_i y_i + w_{i+1}. \tag{6.8}$$

It can be noticed that the noise term in $y_i$ is multiplied by an amplification factor $\sqrt{P_i} G_i h_i$. Denote by $W_i$ the weight of the link from node $i$ to $i+1$, each term $\mathcal{N'}_i$ can then be calculated by traversing the binary tree from the node $i$. The weight at this link is the power of the amplification factor, given by

$$W_i = P_i {G_i}^2 |h_i|^2. \tag{6.9}$$

To simplify the analysis, it is assumed that all the channels are identically distributed, i.e., $|h_i|^2 = |h|^2$. Therefore, the amplification factor $G_i$ can be accordingly simplified to

$$G_i = \sqrt{\frac{1}{(P_{i-1} + P_{i+1})|h|^2 + \sigma^2}} \tag{6.10}$$

for the multiple access transmission, and

$$\overleftarrow{G}_i = \sqrt{\frac{1}{P_{i+1}|h|^2 + \sigma^2}}, \text{ or } \vec{G}_i = \sqrt{\frac{1}{P_{i-1}|h|^2 + \sigma^2}} \tag{6.11}$$

for the single access transmission. The weights corresponding to the three amplification factors can be obtain as

$$W_i^1 = \frac{P_i |h|^2}{P_{i-1}|h|^2 + \sigma^2}, \quad W_i^2 = \frac{P_i |h|^2}{P_{i+1}|h|^2 + \sigma^2},$$

$$W_i^3 = \frac{P_i|h|^2}{(P_{i-1}+P_{i+1})|h|^2+\sigma^2}.$$

Dividing $\sigma^2$ on the numerators and denominators, the three weights can be upper-bounded in high SNR regions as

$$W_l^1 = \frac{P_l|h|^2}{P_{l-1}|h|^2+\sigma^2} = \frac{\frac{2KP\gamma}{n_l}}{\frac{2KP\gamma}{n_{l-1}}+1} \approx \frac{n_{l-1}}{n_l},$$

$$W_l^2 \approx \frac{n_{l+1}}{n_l}, \quad W_l^3 \approx \frac{n_{l-1}n_{l+1}}{n_l(n_{l-1}+n_{l+1})}.$$

It is noted that the weights on links of node $i$ to the left and right child nodes are the same. The channel is assumed to be quasi-static and constant throughout the exchange process, therefore the weight on the same node $\{N_l\}_{l=1}^L$ in the MH-TRC is the same at different layers of the converted binary tree. Denote by the weight vectors $\mathbf{W}^i, i = \{1,2,3\}$, which are made up of the three different weights at each node in the MH-TRC. The three types of weight vectors can be constructed as follows

$$\mathbf{W}^1 = \left[W_1^1\ W_2^1\ \cdots\ W_L^1\right], \tag{6.12}$$

$$\mathbf{W}^2 = \left[W_1^2\ W_2^2\ \cdots\ W_L^2\right], \tag{6.13}$$

$$\mathbf{W}^3 = \left[W_1^3\ W_2^3\ \cdots\ W_L^3\right]. \tag{6.14}$$

Since only the transmission event affects noise propagation, the transmission matrix for each message can be further converted into a characteristic matrix that only contains transmission event elements. For example, by setting the receiving elements to 0, the noise matrix for $v_1$ can be obtained as

$$\mathbf{N}_{v_1} = \begin{bmatrix} 0 & 0 & 0 & 0 & 0 \\ 0 & 2 & 0 & 1 & 0 \\ 0 & 0 & 3 & 0 & 0 \\ 0 & 3 & 0 & 0 & 0 \end{bmatrix}, \tag{6.15}$$

where 1 represents the single access transmission to left neighboring node with weight $W_l^1$, 2 represents the single access transmission to the right neighboring node with weight $W_l^2$, and 3 represents the broadcast transmission to both neighboring nodes with weight $W_l^3$,

Corresponding to the three types of weights, the above noise matrix can be further divided into three sub-noise matrices. For example, the noise matrix given by (6.15) can be divided into

$$\mathbf{N}_{v_1}^1 = \begin{bmatrix} 0 & 0 & 0 & 0 & 0 \\ 0 & 0 & 0 & 1 & 0 \\ 0 & 0 & 0 & 0 & 0 \\ 0 & 0 & 0 & 0 & 0 \end{bmatrix}, \mathbf{N}_{v_1}^2 = \begin{bmatrix} 0 & 0 & 0 & 0 & 0 \\ 0 & 1 & 0 & 0 & 0 \\ 0 & 0 & 0 & 0 & 0 \\ 0 & 0 & 0 & 0 & 0 \end{bmatrix}, \mathbf{N}_{v_1}^3 = \begin{bmatrix} 0 & 0 & 0 & 0 & 0 \\ 0 & 0 & 0 & 0 & 0 \\ 0 & 0 & 1 & 0 & 0 \\ 0 & 1 & 0 & 0 & 0 \end{bmatrix}. \tag{6.16}$$

Therefore, the final noise power matrix can be calculated by

$$\tilde{\mathbf{N}}_{v_k} = \sum_{i=1}^{3} \left( \mathbf{N}_{v_k}^i \circ \mathbf{W}^i \right). \tag{6.17}$$

where $\circ$ represents the following operation

$$A \circ B = \begin{bmatrix} a_{11} & a_{12} & \cdots & a_{1n} \\ a_{21} & a_{22} & \cdots & a_{2n} \\ \vdots & \vdots & \ddots & \vdots \\ a_{m1} & a_{m2} & \cdots & a_{mn} \end{bmatrix} \circ \begin{bmatrix} b_1 \\ b_2 \\ \vdots \\ b_n \end{bmatrix} = \begin{bmatrix} a_{11}b_1 & a_{12}b_2 & \cdots & a_{1n}b_n \\ a_{21}b_1 & a_{22}b_2 & \cdots & a_{2n}b_n \\ \vdots & \vdots & \ddots & \vdots \\ a_{m1}b_1 & a_{m2}b_2 & \cdots & a_{mn}b_n \end{bmatrix}, \tag{6.18}$$

For example, the noise power matrix for message $v_1$ in the 5-node 3-message MH-TRC with 2-TI MH-ANC can be obtained as

$$\tilde{\mathbf{N}}_{v_1} = \begin{bmatrix} 0 & 0 & 0 & 0 & 0 \\ 0 & 0.7500 & 0 & 0.7500 & 0 \\ 0 & 0 & 0.6667 & 0 & 0 \\ 0 & 0.3750 & 0 & 0 & 0 \end{bmatrix}, \tag{6.19}$$

The noise power then can be calculated by traversing the binary tree built by the noise power matrix as

$$\mathbf{Trv}\left( \tilde{\mathbf{N}}_{v_k} \right). \tag{6.20}$$

where the $\mathbf{Trv}(\cdot)$ stands for the traversal function, which can be explained as follows.

**Postorder traversal algorithm**: The propagation of the noise power is simply the traversal of the weight at each non-zero node in the matrix. Therefore, instead of using the pro-order traversal method, the following postorder traversal approach for the noise power matrix is proposed

1. The starting point of the postorder traversal method is the end node where the last transmission travels. For example, for the matrix given by (6.19), the starting point is element $\tilde{\mathbf{N}}_{v_1}(4,2) = 0.3750$. A new matrix **Nn** with the same dimension is constructed, and element $\mathbf{Nn}(i,j)$ represents the propagation power of the received noise at $N_j$ in time slot $i$;

2. For the element in the noise power matrix that has only one child node, the value of the corresponding element in **Nn** equals the value of its child node multiplied by its weight. For the element which has two child nodes, the value equals the summation of the values of its two child nodes multiplied by its weight; and

3. The postorder traversal runs until it reaches the top element in the characteristic matrix. The final noise power equals the summation of all the elements of **Nn** plus $\sigma^2$ (which is the received noise at the end user node without propagation).

The Postorder traversal algorithm for the characteristic matrix $\tilde{\mathbf{N}}_{v_1}$ is described as follows

**Algorithm: Postorder traversal algorithm for $\mathbf{N}_{v_k}$**

*Input:* Noise power matrix $\mathbf{N}_{v_k}$.
*Output:* Noise power $\mathcal{N}_{v_k}$.

1.**Nn** =**ZEROS**$(\mathcal{T}_i \times L)$
2.**for** i=1 to $\mathcal{T}_i$ **do**
3. **for** j=1 to $L$ **do**
4. **if** $\mathbf{C}_{v_i}(i,j) = 0$ **then**
5. $\mathbf{Nn}(i,j) \leftarrow 0$
6. **end if**
7. **if** $\mathbf{C}_{v_i}(i,j) \neq 0$ **then**
8. $\mathbf{Nn}(i,j) \leftarrow (\mathbf{Nn}(i+1,j-1) + \mathbf{Nn}(i+1,j+1)) \times \mathbf{C}_{v_i}(i,j)$
9. **end if**
10. **end for**
11.**end for**
12.**return** $\mathcal{N}_{v_k} \leftarrow$ **SUM**$(\mathbf{Nn}) + 1$

#### 6.5.1.2 Signal Power

Each signal may have different signal powers although they all go through the same path with $I$-TI MH-WNC. The similar approach for calculating the noise characteristic power matrix can be applied to obtain the signal characteristic power matrix. The signal matrix of message $v_1$ for the 5-node 3-message MH-TRC with the 2-TI MH-ANC scheme can be obtained as

$$\mathbf{S}_{v_1} = \begin{bmatrix} 0 & 0 & 0 & 4 \\ 0 & 0 & 1 & 0 \\ 0 & 3 & 0 & 0 \\ 3 & 0 & 0 & 0 \end{bmatrix}, \tag{6.21}$$

where 1, 2 and 3 represent the same transmission events at those in the noise matrix given by (6.15). The element 4 represents the transmission from the user node, the weight of which is

$$W_l^4 = P_l, \tag{6.22}$$

and the corresponding weight vector can be given by

$$\mathbf{W}^4 = \left[ W_1^4 \; W_2^4 \; \cdots \; W_L^4 \right]. \tag{6.23}$$

Therefore, the final signal power matrix can be obtained as

$$\tilde{\mathbf{S}}_{v_k} = \sum_{i=1}^{4} \left( \mathbf{S}_{v_k}^i \circ \mathbf{W}^i \right). \tag{6.24}$$

For example, the signal power matrix for message $v_1$ in the 5-node 3-message MH-TRC with 2-TI MH-ANC can be obtained as

$$\tilde{\mathbf{S}}_{v_1} = \begin{bmatrix} 0 & 0 & 0 & 1 \\ 0 & 0 & 0.7500 & 0 \\ 0 & 0.6667 & 0 & 0 \\ 0.3750 & 0 & 0 & 0 \end{bmatrix}. \tag{6.25}$$

It can be found that the transpose of the signal power matrix is a diagonal matrix, thus the signal power can be obtained by calculating the determinant of the transpose of the matrix, shown as

$$\det\left( \left[ \tilde{\mathbf{S}}_{v_k} \right]^T \right). \tag{6.26}$$

#### 6.5.1.3 Received SNR

To this end, the received SNR of message $v_k$ can be calculated by dividing the signal power in (6.26) with the noise power in (6.20), given by

$$\gamma_{v_k} = \frac{\det\left(\left[\tilde{\mathbf{S}}_{v_k}\right]^T\right)}{\mathbf{Trv}\left(\tilde{\mathbf{N}}_{v_k}\right)}. \tag{6.27}$$

For example, the upper bound received SNR of message $v_1$ in the 5-node 3-message MH-TRC with 2-TI MH-ANC can be obtained as

$$\gamma_{v_1} = \frac{0.19|h|^2}{6.33\sigma^2} = 0.03\gamma, \tag{6.28}$$

where $\gamma = \frac{|h|^2}{\sigma^2}$ is the average SNR per hop.

It can be further found that the upper bound received SNR for message $v_k$ can be expressed as a scaled version of the average SNR per hop $\gamma$, given by

$$\gamma_{v_k} = f_k\gamma, \tag{6.29}$$

where $f_k$ is the scaled factor.

#### 6.5.1.4 Outage Probability

Following the definition, the outage probability of the $I$-TI MH-ANC can be derived by

$$\begin{aligned} p^{\text{out}}_{\text{MH-ANC}}(R) &= \Pr\left[\frac{2K}{\mathcal{T}_{\text{MH-ANC}}}\log(1+\gamma_{\text{MH-ANC}}) < R\right] \\ &= \Pr\left[\frac{2K}{\mathcal{T}_{\text{MH-ANC}}}\log\left(1+\frac{1}{K}\sum_{k=1}^{K} f_k\gamma'\right) < R\right] \\ &= F_{\gamma'}\left(\gamma' < \frac{2^{\frac{\mathcal{T}_{\text{MH-ANC}}}{2K}R}-1}{\frac{1}{K}\sum\limits_{k=1}^{K} f_k}\right) \\ &= 1-\exp\left(\frac{2^{\frac{\mathcal{T}_{\text{MH-ANC}}}{2K}R}-1}{\frac{1}{K}\sum\limits_{k=1}^{K} f_k\bar{\gamma}'}\right). \end{aligned} \tag{6.30}$$

Given a target rate, the two variables in the outage probability are network throughput $C$ and average received SNR factor $f_k$.

### 6.5.2 Compute-and-Forward

The outage event of each message occurs when any of the transmissions that affect the transmission of the message is in outage in MH-CPF, which can be given by

$$p_{v_k}^{\text{out}} = 1 - \underbrace{\prod_{f_{S,i}^j \in \mathcal{F}_{v_k}} \left(1 - \mathbf{p}_{f_{S,i}^j}^{\text{out}}\right)}_{A} \underbrace{\prod_{f_{M,i}^j \in \mathcal{F}_{v_k}} \left(1 - \mathbf{p}_{f_{M,i}^j}^{\text{out}}\right)}_{B}. \tag{6.31}$$

In order to calculate the outage probability for MH-CPF, the number of the single access events $f_{S,l}^j$ and multiple access events $f_{M,l}^j$ in set $\mathcal{F}_{v_k}$ need to be obtained, as well as the achievable rate of each single access transmission $R_l$, and the computation rate at each multiple access transmission $R_{\text{COMP},l}(\mathbf{h}_l, \hat{\mathbf{a}}_l)$.

As can be seen from the outage probabilities given by (5.30) and (5.28), the outage probability is determined by the average SNR $\bar{\gamma}_l$, which is further determined by the transmission power $P_l$, channel gain $|h|^2$ and the noise power $\sigma^2$. The two parameters $|h|^2$ and $\sigma^2$ can be considered as constant values. Therefore, the only variable in the outage probability of the single access transmission is the transmission power $P_l$.

Moreover, it can be seen from (5.5) that the computation rate at relay node $N_l$ is determined by the channel coefficient vector $\mathbf{h}_l$, and the best integer coefficient vector $\hat{\mathbf{a}}_l$. It is noted that $\hat{\mathbf{a}}_l$ is determined by the transmission power $P_l$ and channel coefficient vector $\mathbf{h}_l$. Therefore, considering that all the channels are identically distributed and CSI remains constant during the entire exchange process, the computation rate $R_{\text{COMP},l}(\mathbf{h}_l, \hat{\mathbf{a}}_l)$ is also determined by $\mathbf{P}_l = [P_{l-1}\ P_{l+1}]$.

#### 6.5.2.1 Single Access Transmission

The single transmission event matrix $\mathbb{S}_{v_k}$ can be extracted from the transmission matrix of message $v_k$, by setting the corresponding elements (whose left or right neighboring element in the transmission matrix $\mathbf{T}_{v_k}$ is $-1$) to 1. For example, the single access transmission matrix of message $v_1$ for the 5-node 3-message

MH-TRC with 2-TI MH-CPF scheme can be obtained as

$$\mathbb{S}_{v_1} = \begin{bmatrix} 1\ 0\ 0\ 0\ 1 \\ 0\ 0\ 0\ 0\ 0 \\ 0\ 0\ 0\ 0\ 0 \\ 0\ 1\ 0\ 0\ 0 \end{bmatrix}. \tag{6.32}$$

The transmission power vector can be represented as

$$\mathbf{P} = [P_1 \quad P_2 \quad P_3 \cdots P_l \cdots \quad P_L], \tag{6.33}$$

where $P_l$ is the power per transmission of node $N_l$ given by (6.1).

Multiplying the single access transmission matrix with the power vector, the single access transmission power matrix can be obtained as

$$\tilde{\mathbb{S}}_{v_k} = \mathbb{S}_{v_k} \circ \mathbf{P}^T. \tag{6.34}$$

Given a target rate $R$, the single access transmission outage probability matrix (the element of which is the outage probability of each single access transmission) can then be obtain by

$$\mathbb{P}^{\text{out}}_{S,v_k} = 1 - \exp\left(-\frac{(2^{\frac{R}{C}} - 1)}{\bar{\gamma}}. * \tilde{\mathbb{S}}_{v_k}\right), \tag{6.35}$$

where $C$ is the network throughput for the $I$-TI MH-CPF in the $L$-node $K$-message MH-TRC, $(.*)$ represents element multiplication operation.

The element in $\mathbb{P}^{\text{out}}_{S,v_k}$ is the outage probability for all the single access transmission events given by $\mathbf{T}_{v_k}$. Therefore, term $A$ in (6.31) can then be obtained as

$$A = \mathbf{Prod}\left(\mathbf{I} - \mathbb{P}^{\text{out}}_{S,v_k}\right), \tag{6.36}$$

where Prod$(\cdot)$ represents the product of all the non-zero elements in the matrix, and $\mathbf{I}$ is the matrix of ones.

#### 6.5.2.2 Multiple Access Transmission

The received signal at relay node $N_l$ can be given by

$$\begin{aligned} y_l^j &= \sqrt{P_{l-1}} h_{l-1} v_{l-1}^{j-1} + \sqrt{P_{l+1}} h_{l+1} v_{l+1}^{j-1} + w_l^j \\ &= \mathbf{D}_l \left[v_{l-1}^{j-1}\ v_{l+1}^{j-1}\right]^T + w_l^j, \end{aligned} \tag{6.37}$$

where $\mathbf{D}_l = [\sqrt{P_{l-1}}h_{l-1}\ \sqrt{P_{l+1}}h_{l+1}]$. The corresponding maximized computation rate with the coefficient vector $\hat{\mathbf{a}}_l$ can be given by

$$R_{\mathrm{COMP},l}(\mathbf{P}_l, \mathbf{h}_l, \hat{\mathbf{a}}_l) = \log^+\left(||\hat{\mathbf{a}}_l||^2 - \frac{|\hat{\mathbf{a}}_l\mathbf{D}_l^\dagger|^2}{n_0 + ||\mathbf{D}_l||^2}\right)^{-1}. \tag{6.38}$$

The computation rate at node $N_l$ is determined by the transmission powers of the neighboring nodes. Therefore, the power-pair vector can be built as

$$\mathbf{P}_M = [P_{M,1} \quad P_{M,2} \quad P_{M,3}\cdots P_{M,l}\cdots P_{M,L}], \tag{6.39}$$

where each element $P_{M,l} = (P_{l-1}, P_1)$ contains the transmission powers of the two neighboring nodes of $N_l$. $P_{M,1} = P_{M,L} = (0, 0)$ are the power-pairs at the two user nodes since there is no multiple access transmission on them.

The CPF matrix $\mathbb{C}_{v_k}$ can be extracted from the transmission matrix of message $v_k$, by setting the corresponding elements (whose value in the transmission matrix $\mathbf{T}_{v_k}$ is 2) to 1. Multiplying the CPF matrix $\mathbb{C}_{v_k}$ with the power vector, the CPF power matrix can be obtained as

$$\tilde{\mathbb{C}}_{v_k} = \mathbb{C}_{v_k} \circ \mathbf{P}_M^T. \tag{6.40}$$

For a given target rate $R$, the CPF outage probability matrix (the element of which is the outage probability of each CPF process) can then be obtain by

$$\mathbb{P}^{\mathrm{out}}_{M,v_k} = \mathbf{CPF}\left(\tilde{\mathbb{C}}_{v_k}\right), \tag{6.41}$$

where $\mathbf{CPF}(\cdot)$ represents the function that calculates the outage probability of each non-zero element with the complex lattice reduction method given in Section 5.5.

The element in $\mathbb{P}^{\mathrm{out}}_{M,v_k}$ is the outage probability for all the multiple access transmission events given by $\mathbf{T}_{v_k}$. Therefore, term $B$ in (6.31) can then be obtained as

$$B = \mathbf{Prod}\left(\mathbf{I} - \mathbb{P}^{\mathrm{out}}_{M,v_k}\right). \tag{6.42}$$

To this end, the outage probability for message $v_k$ with the MH-CPF scheme can be given by

$$p^{\mathrm{out}}_{v_k} = \mathbf{I} - \mathbf{Prod}\left(\mathbf{I} - \mathbb{P}^{\mathrm{out}}_{S,v_k}\right)\mathbf{Prod}\left(\mathbf{I} - \mathbb{P}^{\mathrm{out}}_{M,v_k}\right). \tag{6.43}$$

## 6.6 Numerical Results

The numerical results for the generalized $I$-TI MH-WNC are presented in this section. In order to analyze the relationship between the network throughput, average received SNR and outage probability, the average received SNR, outage probability of the $I$-TI MH-WNC scheme can be plotted using the proposed algorithms.

### 6.6.1 Network Throughput

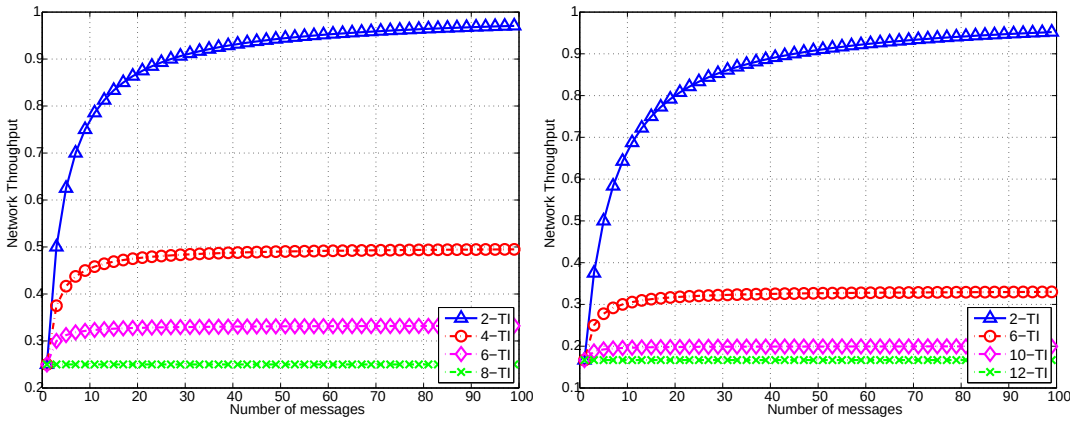


**(a) 9-*node*.** **(b) 13-*node*.**

Figure 6.5: Network throughput versus the number of messages for different scale MH-TRCs.

Figure 6.5 shows the network throughput versus the number of messages for different scale MH-TRCs. As can be seen from the figure, the network throughput increases with the increase of the number of messages, and reaches its upper limit when the number of the messages is far larger than the number of nodes. Moreover, it can be found that the network throughput of the MH-WNC does not change with the increase of the number of messages when the number of time intervals equals the number of hops, i.e., $I = L - 1$.

Figure 6.6 illustrates the network throughput versus the number of time intervals for different scale MH-TRCs. The network throughput for the MH-WNC decreases with the increased number of time intervals in all scale MH-TRCs. It

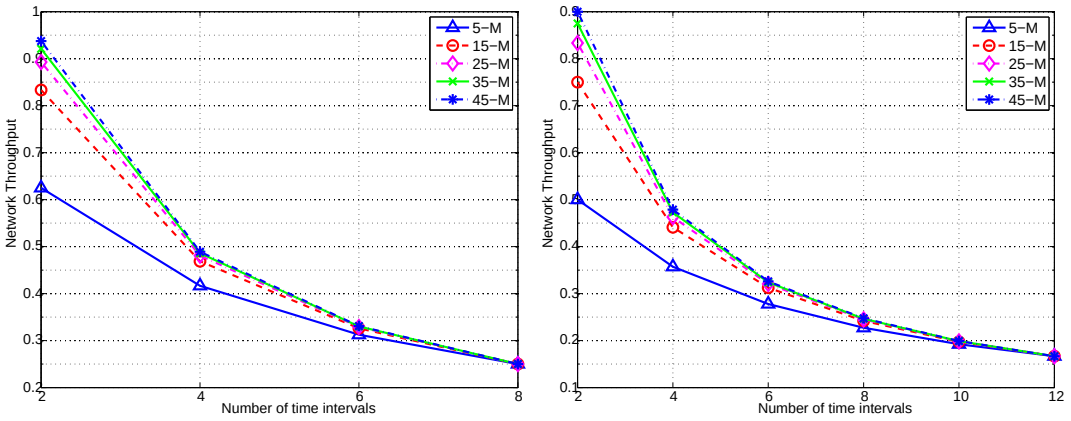


**(a) 9-*node.*** **(b) 13-*node.***

Figure 6.6: Network throughput versus the number of time intervals for different scale MH-TRCs.

can be observed that the network throughput of MH-WNC is closer to each other when the number of messages or the number of time intervals is large.

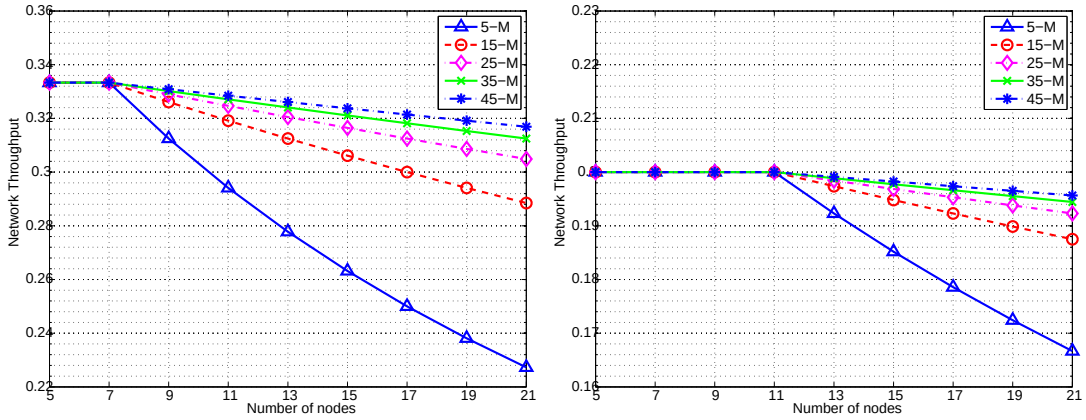


**(a) 6-*TI.*** **(b) 10-*TI.***

Figure 6.7: Network throughput versus the number of nodes for the MH-ANC schemes with different time intervals.

Figure 6.7 plots the network throughput versus the number of nodes for the MH-WNC scheme with different time intervals. For the MH-WNC scheme with large number of time intervals, all the curves remain constant when $L-1 \leqslant I$. For example, the network throughput remains unchanged for the 5-node and 7-node MH-TRCs with the 6-TI MH-WNC scheme disregards the change of the number

of messages.

### 6.6.2 Average Received SNR

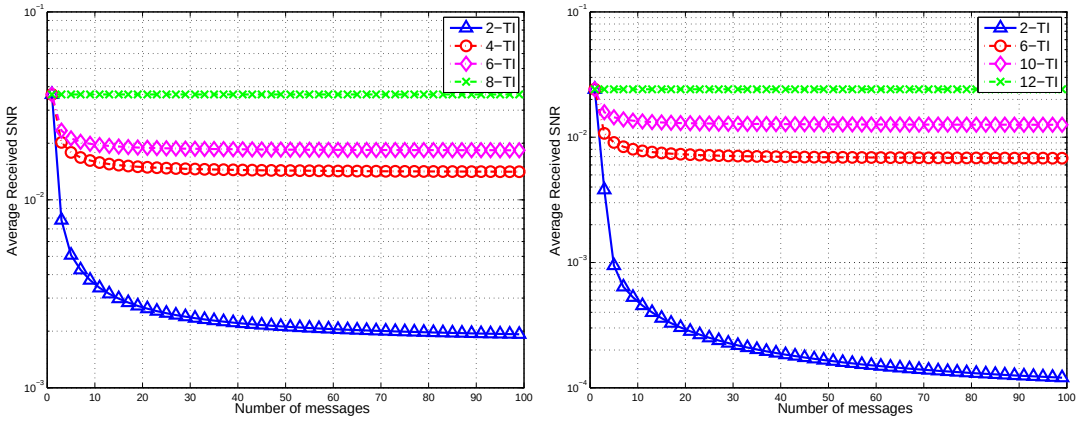


**(a)** 9-***node.*** **(b)** 13-***node.***

Figure 6.8: Average received SNR versus the number of messages for different scale MH-TRCs.

Figure 6.8 plots the average received SNR for $I$-TI MH-ANC versus the number of messages for different scale MH-TRCs. As can be seen from the figure, the average received SNR decreases with the increase in the number of messages. Moreover, the curve starts with a very steep drop, and becomes steady when the number of messages is large. As can be found in the noise power matrix given by (6.19), the elements are all smaller than 1. The noise power propagation at each node is the traversal of the binary tree, that is the product of all the non-zero elements. The number of nodes in the binary tree increases with the increase of the number of messages. Therefore, when the postorder traversal algorithm runs up to a certain layer, the value of the noise power propagation becomes trivial compared to the signal power. Therefore, the received SNR decreases slowly and remains constant when the number of messages reaches a certain value. Moreover, as can be seen from the figure, when the number of time intervals $I = L-1$, the average received SNR remains constant despite the change in the number of messages. The figure also demonstrates that the average received SNR of the MH-ANC with larger time intervals is larger than the $I$-TI MH-ANC scheme

with a smaller number of time intervals.

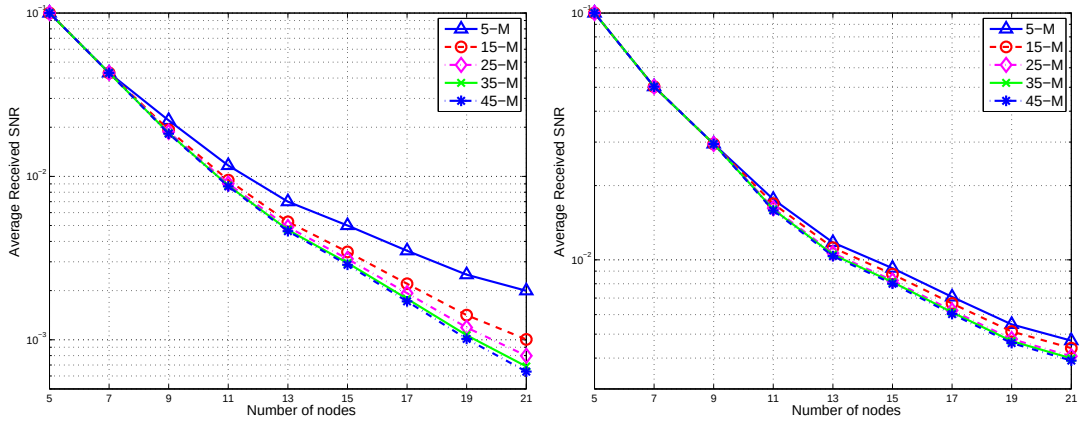


**(a) 6-*TI*.** **(b) 10-*TI*.**

Figure 6.9: Average received SNR versus the number of nodes for the MH-ANC schemes with different number of time intervals.

Figure 6.9 shows the average received SNR versus the number of nodes for the MH-ANC schemes with different numbers of time intervals. The average received SNR decreases with the increase of the number of nodes. It can be found that when the number of time intervals is larger than the hops, i.e., $I > L - 1$, the transmission of later messages is not affected by the transmission of early messages. As a result, the noise propagation from the early messages does not affect the received SNR of the later messages. Therefore, it can be seen from the figure that the average received SNR remains unchanged despite the increase in the number of messages. Moreover, it can observed from the figure, that the average received SNR for the large number of messages are almost identical to each other, which is consistent to the findings in Figure 6.8.

### 6.6.3 Outage Probability

This section presents the outage probability results for the MH-WNC schemes with two different relaying strategies. More specifically, the outage probability of the MH-ANC scheme is determined by the network throughput and average received SNR. Therefore, with the numerical results presented in the last two sections, the outage probability of MH-ANC can be plotted readily. For the MH-

CPF scheme, the outage probability can be calculated by the algorithm proposed in the Section 6.5.2.

#### 6.6.3.1 Multi-Hop Analog Network Coding

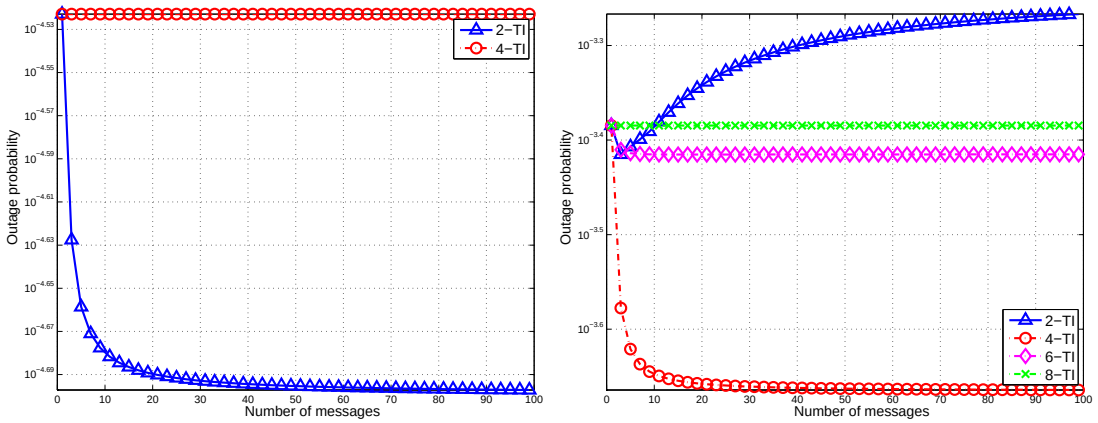


**(a) 5-*node.*** **(b) 9-*node.***

Figure 6.10: Outage probability versus the number of messages for different scale MH-TRCs.

Figure 6.10 shows the outage probability versus the number of messages for different scale MH-TRCs. As can be seen from the figure, for the 5-node MH-TRC, the outage probability curve of the MH-ANC scheme is similar to that of the average received SNR. The outage probability for 2-TI MH-ANC decreases with the increasing number of messages. For 4-TI MH-ANC in the 5-node MH-TRC, the outage probability remains constant as the outages of early messages do not affect that of later messages. However, for the 9-node MH-TRC shown in the figure, the outage probability of the 2-TI MH-ANC scheme drops with the increase in the number of messages before a certain value, i.e., $K = 4$, then reaches the lowest outage probability. The outage probability returns increasing after this certain value (similar observations can be found in Chapter 4 Section 4.9). It can be found that for the MH-ANC scheme with a larger number of time intervals, the outage probability keeps decreasing with the increased number of messages, and reaches a constant value when the number of messages is large.

It can also be found from the figure that the 2-TI MH-ANC scheme has

significantly better outage performance than the 4-TI MH-ANC scheme in the 5-node MH-TRC. The $I$-TI MH-ANC scheme with $I > L-1$ has the same received SNR as $(L-1)$-TI MH-ANC, but a lower network throughput. Therefore, it can be deduced that the $I$-TI MH-ANC scheme with $I > L-1$ has poorer outage performance than the $(L-1)$-TI MH-ANC scheme. As a result, it is concluded that the optimal MH-ANC for the 5-node MH-TRC is the 2-TI MH-ANC scheme. Similarly, it can be found that the optimal MH-ANC for the 9-node MH-TRC is the 4-TI MH-ANC scheme.

As can be seen from the figure that the outage probability of the $I$-TI MH-ANC with $I > 2$ decreases with the number of messages, and reaches a stable value when the number of messages is far larger than the number of nodes, i.e., $K \gg L$.

In Figure 6.11, the outage probability versus the number of time intervals when $K = 400$ is plotted. Figure 6.11 illustrates the relationship between the

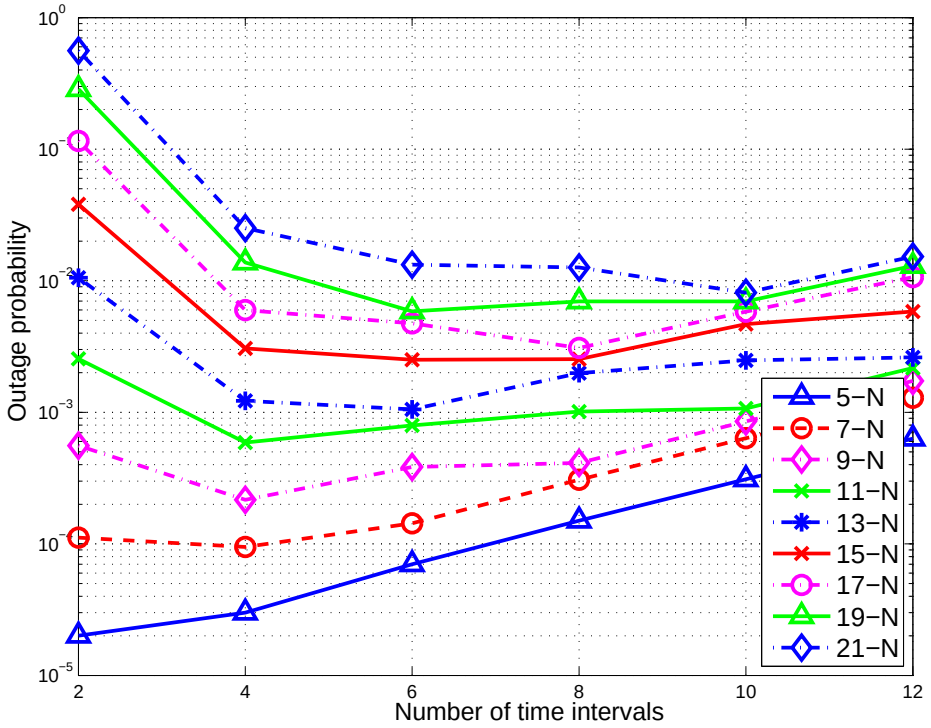


Figure 6.11: Outage probability versus the number of time intervals for different scale MH-TRCs.

numbers of time intervals and nodes. As can be seen from the figure, all the outage probability curves follow almost the same distribution. The outage probability

decreases with the increase in the number of time intervals when the number of time intervals is below a certain value, and starts to increase when the number of time intervals keeps increasing. Each curve has a corresponding valley point with the lowest outage probability. The figure clearly shows that there exists an optimal MH-ANC scheme that can achieve the best outage performance for all-scale MH-TRCs. The number of time intervals corresponding to the optimal MH-CPF scheme for all scale MH-TRCs can be summarized as the following Table 6.3.

Table 6.3: Optimal MH-ANC for different scale MH-TRCs.

| Number of nodes (L) | Number of time intervals (I) |
|---|---|
| 5 | 2 |
| 7 | 4 |
| 9 | 4 |
| 11 | 4 |
| 13 | 6 |
| 15 | 8 |
| 17 | 8 |
| 19 | 6 |
| 21 | 10 |

Generally, the number of time intervals for the optimal MH-ANC scheme increases with the number of nodes. However, the optimal number of time intervals has a drop when the number of nodes is 19. It is difficult to generalize a pattern for the optimal MH-ANC from Table 6.3. However, the outage probability obtained with the optimal MH-ANC can be plotted with the table, as shown in Figure 6.12. As demonstrated in Chapter 4, the outage performance gain for the 2-TI MH-ANC to the Non-NC scheme disappears when the number of nodes is large. However, as shown by Figure 6.12, the outage probability of the optimal MH-ANC scheme is significantly better than that of the Non-NC scheme, and the gain increases with the increased number of nodes.

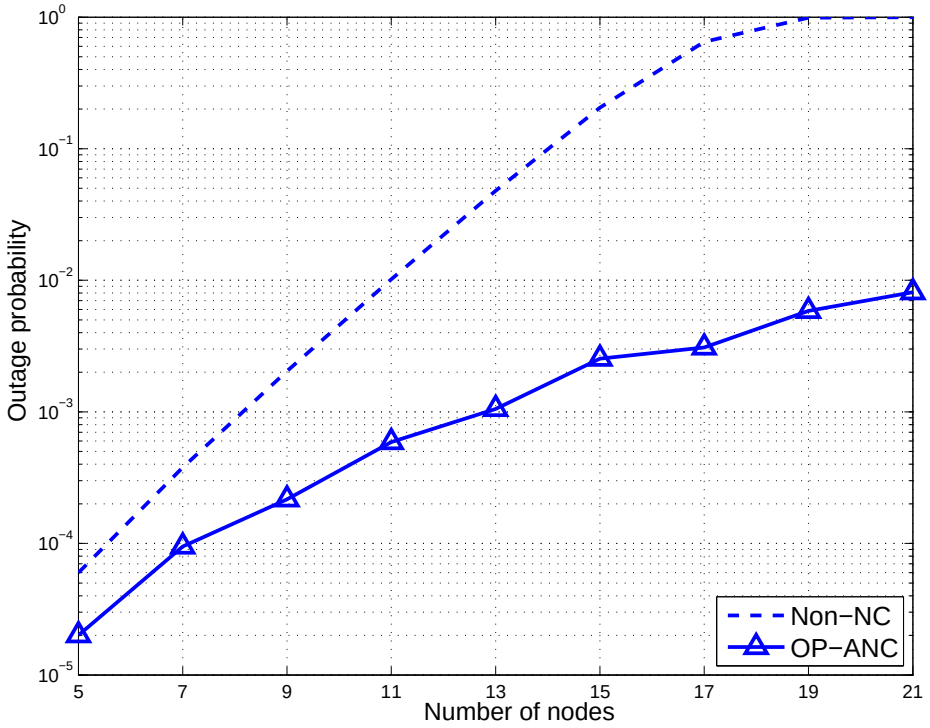


Figure 6.12: Outage probability for the optimal MH-ANC scheme versus the number of nodes.

#### 6.6.3.2 Multi-Hop Compute-and-Forward

In this section, the outage probability for the MH-CPF schemes with different time intervals is presented.

Figure 6.13 shows the outage probability versus the number of messages for different scale MH-TRCs. It can clearly be seen from the figure that the outage probability for the $I$-TI MH-CPF with $I < L - 1$ generally increases with the number of messages, except some curves might have a drop when the number of messages is small.

The 2-TI MH-CPF scheme is superior to the other $I$-TI MH-CPF schemes with $I < L - 1$ in outage probability when the number of messages is smaller than 400 as shown in the figure. It can also be observed that the increased rate of the outage probability for different $I$-TI MH-CPF schemes with $I < L - 1$ gets slower with the increase in the number of messages. Moreover, the larger the number of time intervals $I$ is, the slower the increase rate will be, as shown in the four figures.

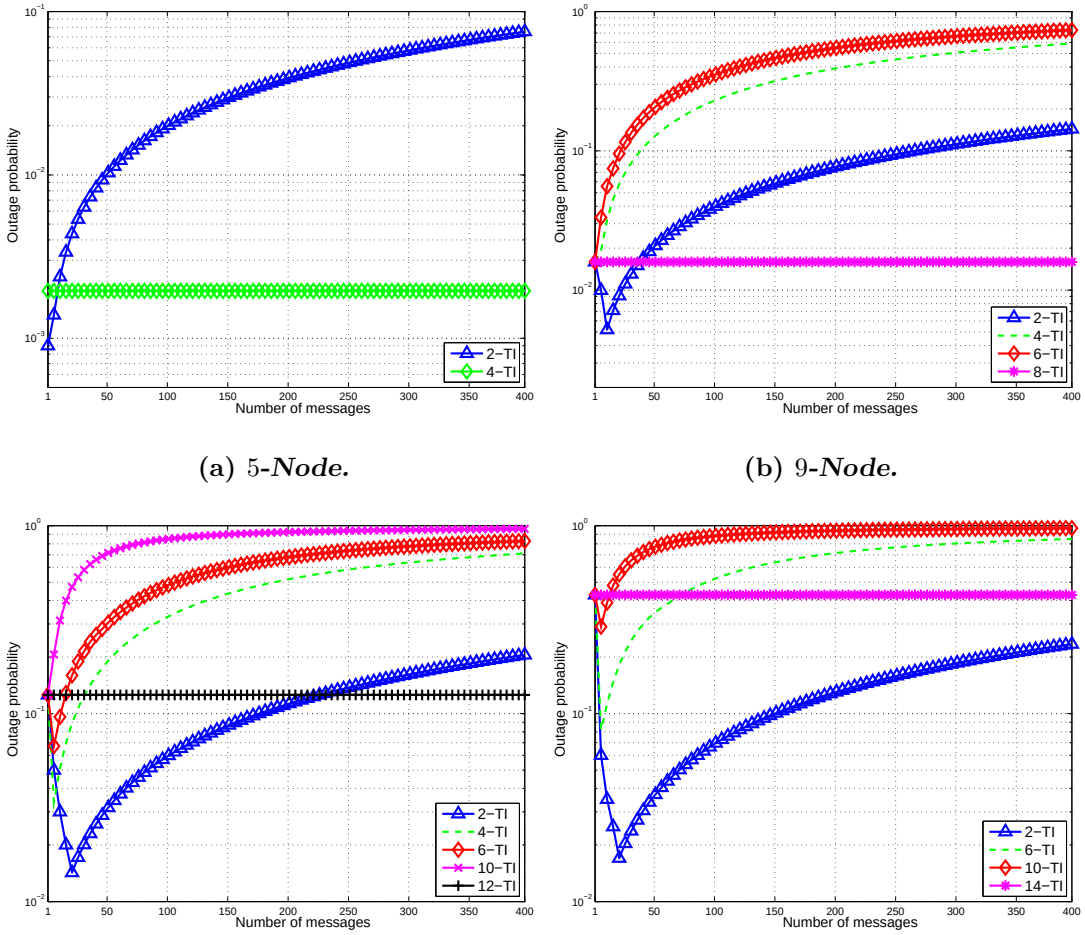


**(a)** 5-***Node.*** **(b)** 9-***Node.***

**(c)** 13-***Node.*** **(d)** 15-***Node.***

Figure 6.13: Outage probability versus the number of messages for different scale MH-TRCs.

On the other hand, when the number of time intervals is equivalent to the number of hops $I = L - 1$, the transmission of each message is independent to each other. Therefore, the outage probability remains unchanged despite the increased number of messages. From the first three figures, it can seen that the outage probability of the $(L-1)$-TI MH-CPF scheme is larger than the $I$-TI MH-CPF schemes with smaller number of time intervals when the number of messages is small. However, with the increase in the number of messages, the outage probability of other $I$-TI MH-CPF schemes increases quickly. As a result, the $(L-1)$-TI MH-CPF scheme has better outage performance than the other schemes when the number of messages is large.

On the other hand, as can be observed from Figure 6.13(d), the 2-TI MH-

CPF scheme is always superior to the 14-TI MH-CPF scheme in the 15-node MH-TRC when the number of messages is smaller than 400 as shown in the figure. However, the outage probability of 2-TI MH-CPF keeps increasing when the number of messages is larger than 400. Therefore, it can be interpreted that the outage probability of 2-TI MH-CPF will exceed the outage probability of 14-TI MH-CPF when the number of message reaches a certain value (the number is 620 as the experiment results suggest).

To this end, it can be concluded that when the number of messages is relatively small (the threshold is different for different scale MH-TRCs, e.g., 9-message for 5-node MH-TRC, 40-message for 9-node MH-TRC, and 250-message for 13-node MH-TRC), the 2-TI MH-CPF is the optimal MH-CPF scheme for all scales MH-TRCs. On the other hand, when the number of messages exceeds this threshold, the optimal MH-CPF scheme the MH-TRC is the $(L-1)$-TI MH-CPF scheme, where the number of time intervals equals to the number of hops.

**Optimal MH-CPF scheme at the number of messages** 400. When the number of messages is 400, the outage probability versus the number time intervals, the outage probability versus the number nodes, and the outage probability of the optimal MH-CPF are plotted in the following Figures.

Figure 6.14 plots the outage probability versus the number of time intervals for the MH-CPF schemes with different time intervals. As can be seen from the figure, all the other outage probability curves follow the same distribution except the outage probability curve for the 5-node. The outage probability decreases when the number of TIs increases from 2 to 4, and starts to increase when the number of TIs is larger than 4. However, the outage probabilities of the MH-TRC with a larger number of nodes increase when then number of TIs is below a certain value, i.e., 4-TI for the 7-node MH-TRC, and 8-TI for the 11-node MH-TRC. Then the outage probability curves for these MH-TRCs suddenly drop to a valley point when $I = L - 1$, and start to rise again. It can be found that the valley point move rightwards with an increase of the number of nodes. Moreover, the figure also suggests that the valley point is not the lowest outage probability of the MH-TRC when the number of nodes is larger than 13. On the other hand, the outage probability of the 2-TI MH-CPF has the lowest outage probability in

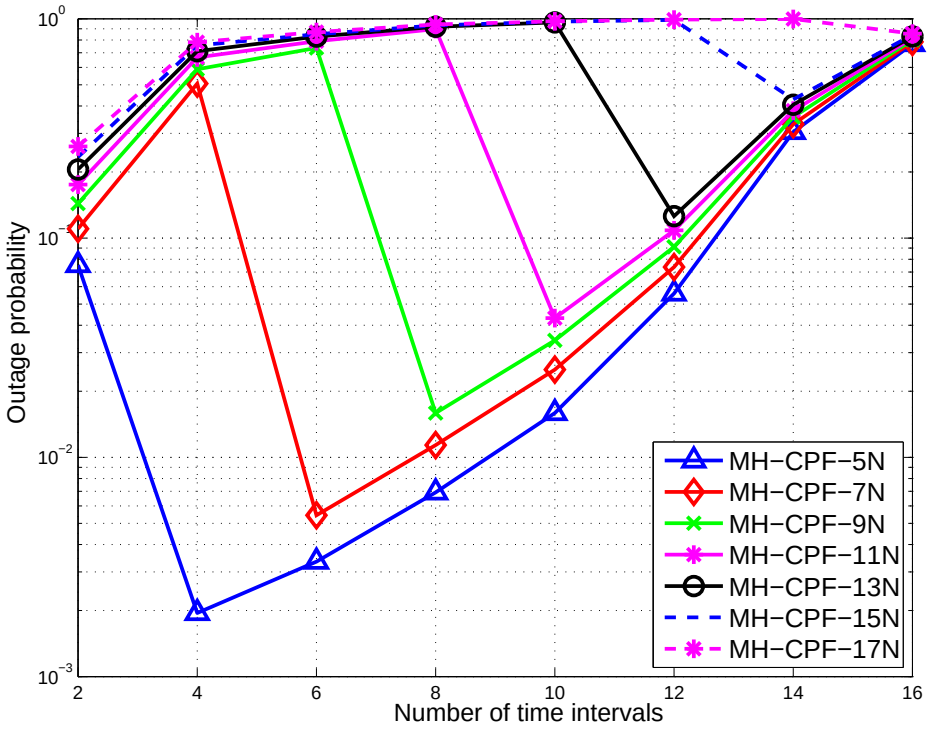


Figure 6.14: Outage probability versus the number of time intervals for different scale MH-TRCs.

the MH-TRC with more than 13 nodes. The figure clearly shows that there exist an optimal MH-CPF for all scale MH-TRCs that can achieve the best outage performance.

To demonstrate the optimal MH-CPF for different scale MH-TRCs, the outage probability versus the number of nodes for the MH-CPF scheme with the different time intervals is plotted in Figure 6.15. It can be seen from the figure that the outage probabilities for the MH-CPF schemes with different time intervals increase with the number of nodes. Moreover, for the 2-TI MH-CPF scheme, the outage probability increases steadily with the increased number of nodes, which is consistent with the result shown in the last chapter. However, the outage probability for the $I$-TI MH-CPF with larger number of TIs suddenly rises when $L-1>I$, i.e., for the 6-TI MH-CPF, the outage probability has a sudden jump when the number of nodes increases from 7 to 9.

Moreover, the figure shows the optimal MH-CPF scheme from another perspective. It shows that, when the number of nodes is smaller than 15, the number of time intervals for the optimal MH-CPF scheme increases with the number of

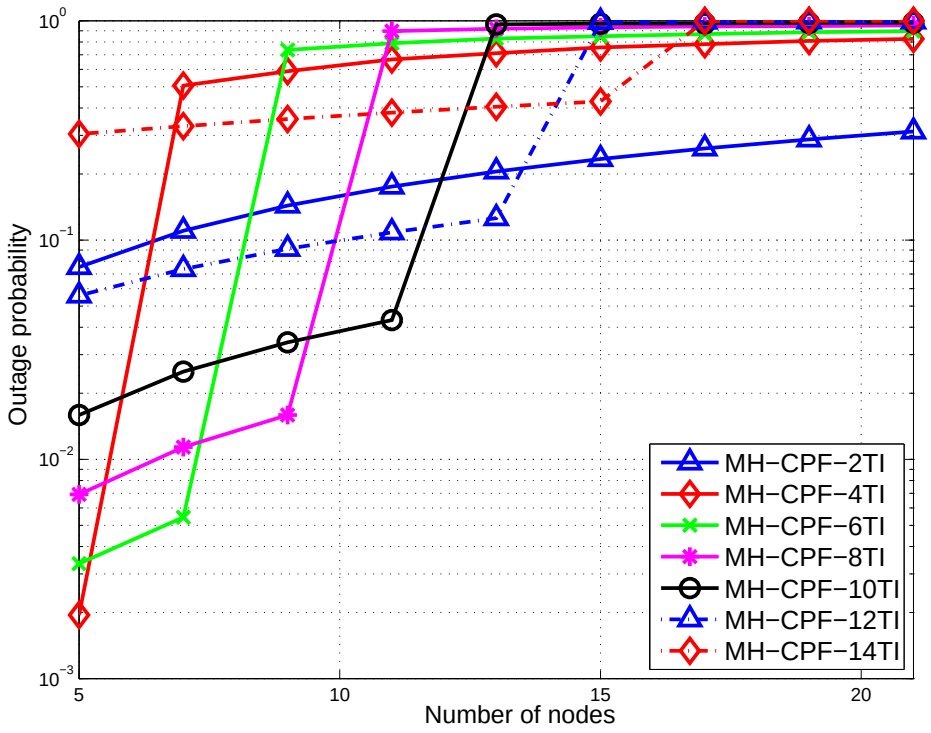


Figure 6.15: Outage probability versus the number of nodes for the MH-CPF schemes with different time intervals.

nodes. However, when the number of nodes is larger than 15, the 2-TI MH-CPF scheme achieves the best outage probability of all the MH-CPF schemes.

Moreover, Figure 6.16 plots the outage probability comparison between the Non-NC scheme and the optimal MH-CPF scheme when the number of messages is 400. The numerical results in the last chapter showed that the 2-TI MH-CPF scheme can only achieve a better outage performance when the number of nodes is large. However, the optimal MH-CPF scheme has overcome this issue, as can be seen from Figure 6.16. The optimal MH-CPF scheme can achieve a significant improvement in outage performance over Non-NC in all-scale MH-TRCs. It can also be found that the outage probability of the optimal MH-CPF scheme has the largest gain to the Non-NC scheme in the 9-node MH-TRC.

## 6.7 Summary

In this chapter, the original 2-TI MH-WNC scheme is extended to the $I$-TI MH-WNC scheme with multiple transmission time intervals. To generalize the perfor-

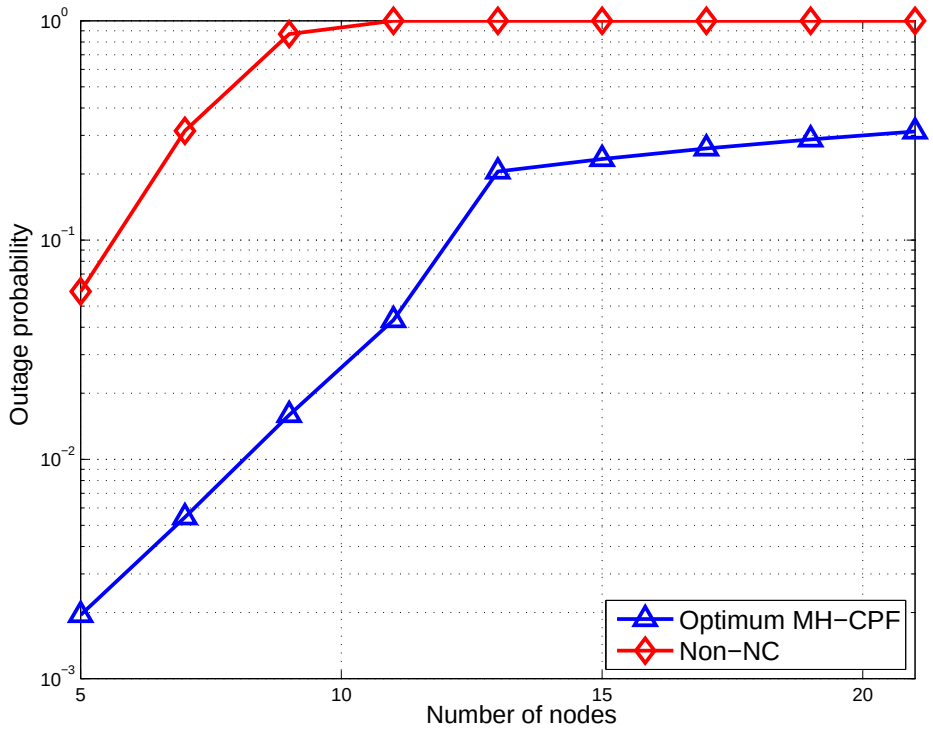


Figure 6.16: Outage probability versus the number of nodes for the optimal MH-CPF scheme.

mance analysis, the transmission model is convert to a special binary tree model, and build the corresponding characteristic matrices. The postorder traverse algorithm is designed to obtain the received SNR of each message in $I$-TI MH-ANC. The outage probability of $I$-TI MH-CPF is calculated by the corresponding characteristic matrices. The results of network throughput, received SNR and outage probability are demonstrated to show the relationship between the number of nodes, messages and time intervals with them.

The numerical results prove that there exists an optimal MH-ANC scheme for all-scale non-regenerative MH-TRCs. The number of time intervals of the optimal MH-ANC scheme generally increases with the number of nodes, but drops when the number of nodes is 19. It is also shown that the outage performance of the optimal MH-ANC scheme has significantly better outage performance than the Non-NC scheme in all-scale MH-TRCs. Moreover, the outage probability gain with the optimal MH-ANC scheme to Non-NC increases with the number of nodes.

Furthermore, the outage probability results obtained by the proposed algo-

rithm show that there is also an optimal MH-CPF scheme for all scale regenerative MH-TRCs. For the MH-TRC with a small number of messages, the optimal MH-CPF scheme is the 2-TI MH-CPF scheme, while the $L-1$-TI MH-CPF scheme is the optimal MH-CPF when the number of messages is large. It is also proven that the optimal MH-CPF scheme is able to outperform the Non-NC scheme when the number of messages is large in all scale MH-TRCs.

# Chapter 7

# Compute-and-Forward for Generalized Multi-Way Relay Channels

## 7.1 Introduction

The two-user two-way relay channel is the simplest and most popular network to implement WNC. However, when extending the two-user case to the multi-user case, most exiting WNC schemes are not directly applicable for the mRC (such as ANC, "standard" PNC and FFNC). Recently, the advent of the CPF scheme offered an opportunity to apply reliable wireless network coding into multi-user networks, and the established "computation rate" has been proven to achieve significant improvements over the traditional relaying strategies. However, as far as the literature review suggests, there are no published research results on the implementation of CPF to the TWRC, let alone the mRC.

In this chapter, the research on WNC is moved a step forward, and the original CPF scheme is extended from TWRC to the mRC. To ensure that all the user nodes can recover their required messages successfully, the user nodes have to receive at least $L-1$ linear independent equations (assuming that there are $L$ user nodes in the mRC). In the mean time, the overall computation rate should be maximized in order to exploit the advantage of CPF. Different from the multi-user multi-relay network which the original CPF scheme was based on, there is only

one relay in the mRC. Therefore, to successfully extend the original CPF scheme to the mRC, one important issue is to ensure the linear independent condition while maximizing the overall computation rate with the single received signal.

This study tackles the challenges and successfully extends CPF to the mRC. The contributions can be summarized as follows:

1. The transmission scheme of extended CPF in the mRC is presented, and it is proven to double the network throughput compared to the Non-NC scheme.

2. A dominated solution for maximizing the overall computation rate in the mRC is proposed to ensure that all the user nodes can recover their required messages successfully.

3. The outage performance of extended CPF for the mRC is analyzed. It is proven by the numerical results that the extended CPF scheme joint with the proposed dominated solution, has a significantly better outage performance than the Non-NC and ANC schemes in the single relay TWRC. Moreover, it is also demonstrated that the extended CPF scheme has better outage probability than Non-NC in the mRC with a relatively small number of users.

## 7.2 Related Work

It has been widely demonstrated that ANC and "standard" PNC can be applied to two-way relay channels [14], cooperative relay networks [99,147], user-cooperative relay networks [99, 148], and multi-hop two-way relay channels [35]. However, when extending the two-user case to the multi-user case, the conventional ANC and "standard" PNC are not directly applicable to the multi-user network:

- For the ANC in two-user relay channels, the relay receives an interference signal with two messages, and then amplifies and forwards it to users or destinations. The users or destinations can cancel the signals they already have, and extract the targeted signal. However, multiple signals might collide in the multiple access channel of the mRC, and the interference signal

is made up of multiple messages. The resulting signal after canceling its known signal is still a combination of multiple unknown signals. Therefore, the users or destinations are unable to obtain the desired individual messages. Moreover, since the cancelation is in an analog field, even if the users or destinations receive multiple interference signals, they still cannot extract their required individual messages.

- Relays decode an XOR summation of the messages from two users in the "standard" PNC for the two-user relay channels, i.e., $m_a \oplus m_b$. In the broadcast phase, relays broadcast the combination back to the two users. The users can easily extract its required message from this combination by performing another XOR addition with its own message. However, for the multi-user case in the mRC, the combination becomes $\{m_a \oplus m_b \oplus m_c \oplus ...\}$. Since each user has only the knowledge of its own message, it can recover the combination of other messages but not the individual messages (e.g., user $U_A$ owns message $m_A$, it can recover $\{m_b \oplus m_c \oplus ...\}$).

### 7.2.1 Finite-Field Network Coding

For the traditional network coding scheme, a simple $\oplus$ addition in GF(2) field is applied [19, 149, 150] in the single relay TWRC. However, when this network is extended to multi-user multi-relay networks, the diversity gain is still 2 [151] if the GF(2) field network coding is applied. Regarding this, FFNC was proposed in [104] for a two-user two-relay network. Instead of using binary addition in GF(2) field, the two relays add the two messages in GF(4) field and generate different linear independent codewords. A diversity gain of 3 can be achieved in the two-user two-relay network with FFNC.

In a full data exchange mRC where users want to obtain the messages from all the other users, each user sends its messages to the relay either through orthogonal channels or in different time slots. Different from the FFNC in the multi-relay network, there is only one relay in the mRC. In order to assure that all the users can recover their required messages from the combinations passed from the relay successfully, the users have to receive at least $L-1$ linear independent equations. Therefore, the relay has to add those messages in $GF(2^L)$ and generate $L-1$

linear independent equations, where the $L-1$ by $L$ coefficient matrix $\mathbf{A}$ built by these $L-1$ equations should satisfy the following *Coefficient Matrix Constraint*:

> $\mathbf{A}(:,i), i \in \{1,2,...,L\}$ — denoted as the (L-1)×(L-1) submatrix of $\mathbf{A}$ after removing the $i$-th column from $\mathbf{A}$ — should be full rank.

It can be found that $L$ time slots are required for the users to send all the messages to the relay, and another $L-1$ time slots are required for the relay to broadcast the $L-1$ linear independent equations to the users. Therefore, a total number of $2L-1$ time slots are required for the FFNC in the $L$-user mRC, while the number of time slots with the Non-NC scheme is $2L$. It can be seen that the network throughput improvement over Non-NC with FFNC decreases with the increased number of users. In the numerical results Section 7.6.2, the outage performance analysis of the FFNC scheme in the mRC will be presented.

### 7.2.2 Compute-and-Forward for Multi-Way Channels

With the proposed CPF by Nazer and Gastpar [92], the relay can decode successive linear equations and pass them back to the users. However, the original CPF was proposed for a cooperative multi-user multi-relay network, where the multiple users wish to transmit their messages to a destination via multiple relays. In the proposed CPF, each relay receives the messages from all the users via a shared MAC, and decodes a linear combination of the messages, then passes it to the destination. Upon receiving enough linear combinations, the destination is able to recover all the messages. It should be noted that the success of recovering messages at the destination relies on the fact that the linear equations have only one unique solution, the condition of which is that the coefficient vectors of the linear combinations from different relays are mutual linear independent. In another words, representing the linear equations by $\mathbf{AX} = \mathbf{B}$ (the row vectors of $\mathbf{A}$ is made of the linear combinations from different relays, $\mathbf{X}$ is the user message vector, and $\mathbf{B}$ is the decoded codeword at the destination from different relays), $R(\mathbf{A}) = R(\mathbf{B})$ ($R(\cdot)$ represents the rank of the matrix) is the necessary and sufficient condition.

Moreover, it should be noted that the coefficients chosen by the relays are based on the observation of the channels. If the channels between users and

relays are correlated with each other, the chosen coefficients will be correlated to each other, making the mutual linear independent condition dissatisfied. Different from the multi-user multi-relay network which the original CPF was based on, there is only one relay in the mRC. Therefore, in the application with CPF to mRC, there comes the issue of how to ensure the linear independent condition while maximizing the overall computation rate with the single received signal.

## 7.3 System Model

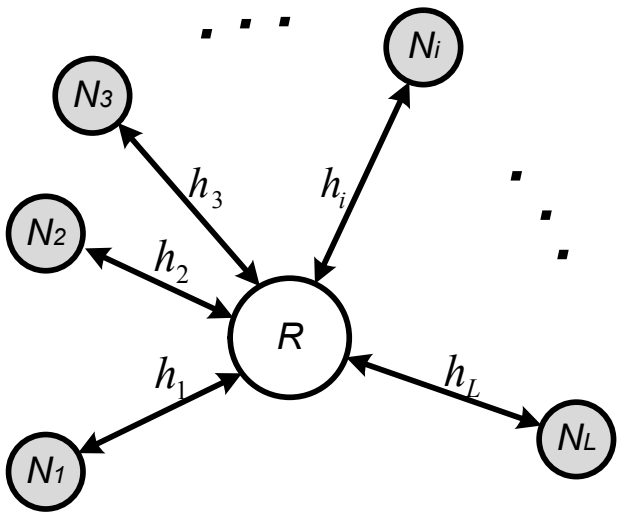


Figure 7.1: The multi-way relay channel.

Consider a generalized mRC shown in Figure 7.1, where $L$ users, denoted by $N_i \in \{N_1, N_2, ..., N_L\}$, communicate via a single relay $R$. In this model, users cannot receive the transmission from each other. User $N_i$ requires for the messages from other $L-1$ users

$$\bigcup_{j\in\{1,2,...,L\},j\neq i} \{s_j\}. \tag{7.1}$$

Each user is equipped with a nested lattice encoder [90], which maps message $s_i$ over the finite field to a length-$n$ complex-valued codeword, $x_i = \varepsilon(s_i)$ [92], which is subject to a power constraint $||x_i||^2 \leqslant nP$.

In addition, it is assumed that the channels are quasi-static, constant across time, and reciprocal in both directions, i.e, $h_{R-N_i} = h_{N_i-R}$. The Rayleigh fading

channel between user $N_i$ and the relay is denoted by $h_i \sim \mathcal{CN}(0, 2\alpha_i^2)$, which is modeled as a zero-mean, independent, circularly symmetric complex Gaussian random variable with variance $\alpha_i^2$ per dimension. Let $w$ be the received noise at the relay, which is a zero mean, independent, circularly symmetric, complex Gaussian random variable with a variance of $\sigma^2$. Denoted by $\gamma_i = \frac{P|h_i|^2}{\sigma^2}$ the instantaneous signal-to-noise ratio (SNR) of $h_i$, which is exponentially distributed with parameter $1/\bar{\gamma}_i$, with $\bar{\gamma}_i = \frac{2P\alpha_i^2}{\sigma^2}$ denoting the mean SNR of $h_i$.

For the conventional Non-NC scheme, each user transmits its message individually in different time slots. Two time slots are used for exchanging one message, and a total number of $2L$ time slots are required for $L$ messages exchange. The network throughput is defined as the number of messages transmitted in a time unit. Thus, the network throughput for Non-NC in this mRC is

$$C_{\text{Non-NC}} = \frac{\text{Number of messages}}{\text{Number of time slots}} = \frac{1}{2} \quad \text{(message/time slot)}. \tag{7.2}$$

## 7.4 Computation Rate

The CPF scheme for the mRC is shown in Figure 7.2, where the communication takes place in two phases, i.e., a multiple-access (MA) phase and a broadcast phase.

In the MA phase, $L$ users transmit simultaneously. It is assumed that all the transmission is perfectly synchronized. Thus, the received signal at the relay is

$$y_R = h_1 x_1 + h_2 x_2 + \cdots + h_L x_L + w. \tag{7.3}$$

The relay's role is to compute linear combinations and forward to the destination. Given enough linear combinations, the users can recover their required messages.

In this $L$-user mRC, to make sure that each user can recover the required $L-1$ messages, the relay should decode at least $L-1$ linearly combined equations

$$v_m = a_{m1} x_1 + a_{m2} x_2 + \cdots + a_{mL} x_L, \tag{7.4}$$

where $a_{ml} \in \{\mathbb{Z} + \mathbb{Z}j\}, l \in \{1, 2, ..., L\}$.

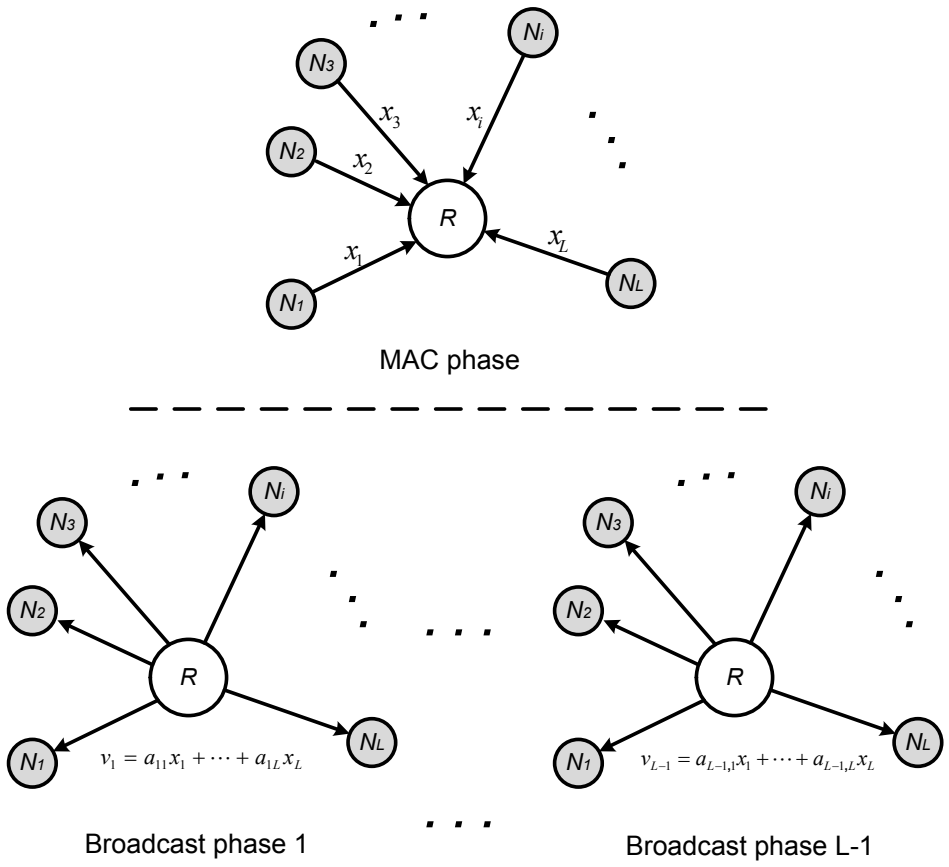


Figure 7.2: Compute-and-forward for the multi-way relay channel.

In the broadcast phase, the relay broadcasts the $L-1$ linear combinations to all the users one at a time slot. With these linearly combined equations and integer coefficients passed from the relay, the users can recover the required messages.

A total number of $L$ time slots is used for $L$ messages exchange. Thus, the network throughput for CPF in the mRC

$$C_{\text{CPF}} = 1 \quad \text{(message/time slot)}. \tag{7.5}$$

In comparison with the network throughput of Non-NC, CPF doubles the network throughput.

Nazer and Gastpar show that the relay can recover any set of linear combinations with the coefficient vector $\mathbf{a}_m = [a_{m1} a_{m2} \cdots a_{mL}]$ as long as the message rates are less than the following computation rate [92]

$$R_{\text{COMP}}(\mathbf{h}, \mathbf{a}_m) = \max_{\mathbf{a} \neq \mathbf{0}} \log^+ \left( ||\mathbf{a}||^2 - \frac{P|\mathbf{a}\mathbf{h}^\dagger|^2}{1 + P||\mathbf{h}||^2} \right)^{-1}, \tag{7.6}$$

where $\log^+(x) \triangleq \max\big(\log(x), 0\big)$ and $\mathbf{h} = [h_1 h_2 \cdots h_L]$.

For a given $\mathbf{h} \in \mathbb{C}^L$, the maximization of the computation rate in (7.6) amounts to the following SVP according to Theorem 1 in [32] and Proposition 1 in [34]

$$\mathbf{a}_m = \arg\min_{\mathbf{a}\neq\mathbf{0}} ||\mathbf{aL}||, \tag{7.7}$$

where $\mathbf{L}$ is the Cholesky decomposition of

$$\mathbf{G} = I - \frac{P}{1 + P||\mathbf{h}||^2}\mathbf{h}^\dagger\mathbf{h}, \tag{7.8}$$

where $I$ is an $L$ by $L$ identity matrix.

In original CPF, multiple relays decode multiple linear combinations, then pass them to the destination. However, there is only one relay in the mRC. It is noted that the relay is not limited to decode a single combination upon one reception. It can run the decoding step on its observed signal several times to extract successive linear combinations. For $M$ linearly combined equations, the selected network coding coefficient matrix is given by

$$\mathbf{A} = \begin{bmatrix} \mathbf{a}_1 \\ \mathbf{a}_2 \\ \vdots \\ \mathbf{a}_M \end{bmatrix} = \begin{bmatrix} a_{11} & a_{12} \cdots a_{1L} \\ a_{21} & a_{22} \cdots a_{2L} \\ \vdots & \vdots \ \ddots \ \vdots \\ a_{M,1} a_{M,2} \cdots a_{M,L} \end{bmatrix}. \tag{7.9}$$

It is suggested in [92] that the relay can successfully decode the $M$ linear combinations if and only if the message rates are less than

$$\min_{m\in\{1,2,\ldots,M\}} \big\{R_{\text{COMP}}(\mathbf{h}, \mathbf{a}_m)\big\}. \tag{7.10}$$

In the original CPF scheme, $L$ linearly independent equations are required for the destination to recover $L$ messages. However, since each user has the knowledge of its own message, they can also obtain the $L$ messages by $L-1$ linearly independent equations, providing that the dominated solution [34, Theorem 8]

- $\mathbf{a}_1 = \arg\min\{||\mathbf{aL}|| \mid \mathbf{a} \text{ is nonzero}\}$
  $\mathbf{a}_2 = \arg\min\{||\mathbf{aL}|| \mid \mathbf{a}, \mathbf{a}_1 \text{ are linearly independent}\}$
  $\vdots$
  $\mathbf{a}_M = \arg\min\{||\mathbf{aL}|| \mid \mathbf{a}, \mathbf{a}_1, ..., \mathbf{a}_{M-1} \text{ are linearly independent}\};$

satisfies the following *Coefficient Matrix Constraint*

- $\mathbf{A}(:,i), i \in \{1,2,...,L\}$ — denoted as the (L-1)×(L-1) submatrix of $\mathbf{A}$ after removing the $i$-th column from $\mathbf{A}$ — should be full rank.

It should be noted that the computation rates corresponding coefficient vectors $\{\mathbf{a}_1, \mathbf{a}_2, ..., \mathbf{a}_{L-1}\}$ are ordered descendingly. Therefore, the minimum computation rate given by (7.10) is actually the computation rate $R_{\text{COMP}}(\mathbf{h}, \mathbf{a}_{L-1})$.

*Algorithm for constructing coefficient matrix* $\mathbf{A}$: The algorithm for constructing the coefficient matrix $\mathbf{A}$ consists of following four steps

1. Use the complex lattice reduction algorithm in [152] to find an array of shortest non-zero vectors (or reduced basis) $\{\mathbf{b}_1, \mathbf{b}_2, ..., \mathbf{b}_L\}$ with the minimum norm in vector space $V$, the basis of which are the row vectors of $\mathbf{L}$;

2. Calculate the corresponding $\mathbf{Q} = [\mathbf{q}_1\ \mathbf{q}_2 \cdots \mathbf{q}_L]$ with $\mathbf{Q} = \mathbf{B}^T\mathbf{L}^{-1}$, where $\mathbf{B}$ is the matrix constructed with the column vectors $\{\mathbf{b}_1, \mathbf{b}_2, ..., \mathbf{b}_L\}$ ;

3. Reconstruct the matrix $\mathbf{Q}$ with the column vectors ordered descendingly by their norms; and

4. Take the first $L-1$ column vectors of $\mathbf{Q}$ as the column vectors of coefficient matrix $\mathbf{A}$.

The table below gives the detailed description of the algorithm.

**Algorithm: Construction of coefficient matrix A**

*Input:* Channel coefficient vector $\mathbf{h} = \{h_1, h_2, .., h_L\}$, transmit power $P$.
*Output:* Coefficient matrix $\mathbf{A}$.

1. $\mathbf{G} = I - \frac{P}{1+P||\mathbf{h}||^2}\mathbf{h}^\dagger\mathbf{h}$.
2. $\mathbf{L}$ = Cholesky decompositon($\mathbf{G}$).
3. $\mathbf{B}$ = CLLL($\mathbf{L}^T$) (Complex lattice reduction algorithm, see [152] for detail).
4. $\mathbf{Q} = \mathbf{B}^T\mathbf{L}^{-1}$.
5. $\mathbf{A} = \mathbf{Q}(:, 1 : L-1)$.

Figure 7.3 shows the maximized computation rate obtained with the above algorithm for different scale mRCs. It can be seen from the figures that the computation rate decreases with the increased number of users. Moreover, the computation rates corresponding to the coefficient vectors $\{\mathbf{a}_1, \mathbf{a}_2, ..., \mathbf{a}_{L-1}\}$ are

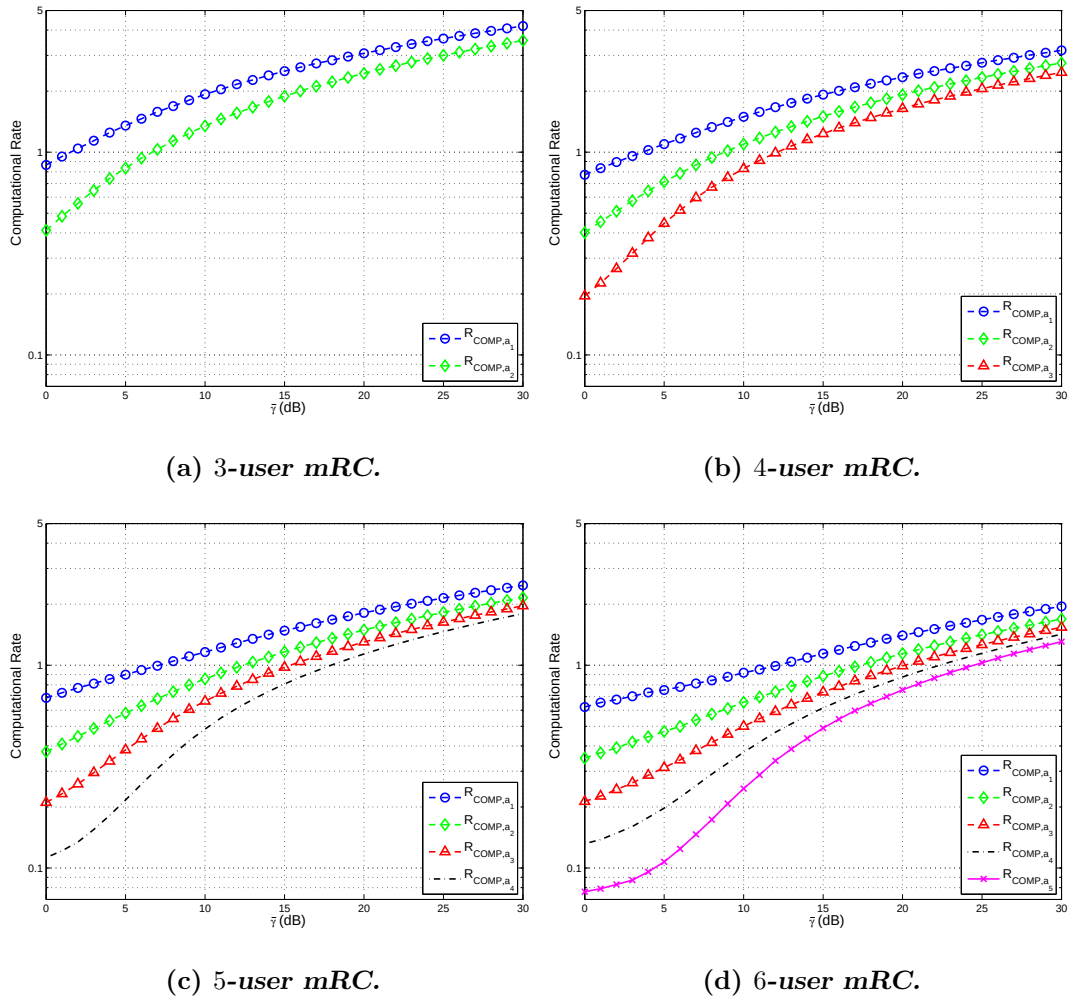


**(a) 3-*user mRC*.** **(b) 4-*user mRC*.**

**(c) 5-*user mRC*.** **(d) 6-*user mRC*.**

Figure 7.3: Computation rates versus the average SNR in different scale mRCs.

ordered descendingly. However, it can also be observed from the figures that the gap between the lowest computation rate $R_{\text{COMP}}(\mathbf{h}, \mathbf{a}_{L-1})$ and highest computation rate $R_{\text{COMP}}(\mathbf{h}, \mathbf{a}_1)$ (which is the maximized computation rate given in [92] at each relay) decreases with the increase of the average SNR per channel. Therefore, the proposed algorithm can achieve a relatively maximized computation rate and assure that each user can solve the linear equations for their required messages successfully.

## 7.5 Outage Probability

The proposed CPF is able to double the network throughput in comparison with the traditional Non-NC scheme according to (7.2) and (7.5). Although the overall

computation rate achieved by the relay decreases with the increase in the number of users, the computation rates for decoding different linear combinations are close to each other in high SNR regions. The outage probability of CPF is determined by both the network throughput and the achievable rate. This section presents the outage probability analysis of CPF for the mRC.

The transmission between users and the relay in the traditional Non-NC scheme is the single access transmission, and the broadcast transmission in the CPF scheme can also be considered as $L$ single access transmission. With the "good" lattice code proposed by Erez and Zamir [90], the information rate for each single transmission $N_i - R$ or $R - N_i$ in the $L$-user mRC is given by

$$R_i = \mathcal{D} \log_2 (1 + \gamma_i), \tag{7.11}$$

where $\mathcal{D}$ is the normalization factor defined as the number of messages divided by the number of time slots, which is equivalent to the network throughput.

Denote by $p_i^{\text{out}}(R)$ the outage probability of user $N_i$ in the mRC, which is defined as the probability of the event when $N_i$ cannot successfully receive all the required $L-1$ messages. For simplicity, it is assumed that all the channels $h_i$ are identically distributed, i.e., $\bar{\gamma}_i = \bar{\gamma}$. Thus, the outage probability for each user $N_i$ is identical. The average outage probability for the mRC can be given as

$$p^{\text{out}}(R) = \frac{1}{L} \sum_{i=1}^{L} p_i^{\text{out}}(R) = p_i^{\text{out}}(R). \tag{7.12}$$

### 7.5.1 Non-Network Coding

For the traditional Non-NC scheme, the transmission to user $N_i$ is in outage when any exchange transmission with the other $L-1$ users is in outage, including the transmission $\{N_j\}_{j \neq i} - R$ and $R - N_i$. Therefore, the outage probability for $N_i$ with Non-NC can be given by

$$p_{\text{Non-NC},i}^{\text{out}}(R) = 1 - \Big(1 - p_i^{\text{out}}\big(R\big)\Big)^{L-1} \prod_{j=1, j\neq i}^{L} \Big(1 - p_j^{\text{out}}\big(R\big)\Big), \tag{7.13}$$

where

$$p_i^{\text{out}}\big(R\big) = \Pr\big[R_i < R\big] \quad \textit{and} \quad p_j^{\text{out}}\big(R\big) = \Pr\big[R_j < R\big]$$

denote the outage probabilities of the single point-to-point transmission $R \to N_i$ and $N_j \to R$, respectively.

Substituting (7.11) into (7.13), the outage probability of Non-NC can be derived as

$$p^{\text{out}}_{\text{Non-NC}}(R)=1-\underbrace{\exp\left(-\frac{2^{2R}-1}{\bar{\gamma}}\right)}_{A}^{2L-2}. \tag{7.14}$$

At high SNR regions, the above outage probability can be approximated according to [105, Eq. (2)] as

$$p^{\text{out}}_{\text{Non-NC}}(R) \approx \frac{(2L-2)(2^{2R}-1)}{\bar{\gamma}}. \tag{7.15}$$

### 7.5.2 Compute-and-Forward

The outage event for $N_i$ with CPF occurs when either the MA phase or any single transmission $R \to N_i$ in the broadcast phase is in outage. Thus, given a target end-to-end rate $R$, the outage probability for user $N_i$ with CPF is

$$p^{\text{out}}_{\text{CPF},i}(R) = 1-\Big(1-p^{\text{out}}_{\text{CPF}}\big(R\big)\Big)\Big(1-p^{\text{out}}_{i}(R)\Big)^{L-1}, \tag{7.16}$$

where $p^{\text{out}}_{\text{CPF}}\big(R\big)$ is the outage probability of CPF in the MA phase, which is defined as the probability when the computation rate given by (7.10) is below the target message rate $R$. Thus, the outage probability of CPF in the MA phase can be given as

$$p^{\text{out}}_{\text{CPF}}(R) = \Pr\Big[\mathcal{D}_{\text{CPF}}\min_{m\in\{1,2,\ldots,L-1\}}\big\{R_{\text{COMP}}(\mathbf{h},\mathbf{a}_m)\big\} < R\Big]. \tag{7.17}$$

The maximization of the computation rate $R_{\text{COMP}}(\mathbf{h},\mathbf{a}_m)$ is an SVP problem, which has no closed-form solutions. Thus, the closed-form outage probability expression of $p^{\text{out}}_{\text{CPF}}(R)$ is unattainable. However, the complex lattice reduction algorithms proposed in [152] can be applied to numerically calculate the outage probability.

For the broadcast phase, the outage probability for $N_i$ can be given by

$$p^{\text{out}}_{\text{BR},i}(R)= 1-\exp\left(-\frac{2^{R}-1}{\bar{\gamma}}\right)^{L-1}. \tag{7.18}$$

Substituting (7.18) and (7.17) into (7.16), the outage probability of CPF for the generalized mRC can be derived as

$$p_{\mathrm{CPF}}^{\mathrm{out}}(R) = 1 - \underbrace{\exp\left(-\frac{2^R-1}{\bar{\gamma}}\right)}_{B}^{L-1} \underbrace{\Pr\left[\min_{m\in\{1,2,\ldots,L-1\}}\left\{R_{\mathrm{COMP}}(\mathbf{h},\mathbf{a}_m)\right\} \geqslant R\right]}_{C} \quad (7.19)$$

# 7.6 Numerical Results

This section presents the numerical result of the outage probability of the two schemes for the mRC. As mentioned earlier in Section 7.2, the FFNC scheme proposed in [104] is also applicable for the mRC. Before presenting the numerical analysis of the proposed scheme, the outage probability of the FFNC scheme in the mRC and the comparison with the traditional Non-NC scheme are first presented.

## 7.6.1 Finite-Field Network Coding

A total number of $2L-1$ time slots are required for the FFNC scheme in the $L$-user mRC. Therefore, given a target end-to-end rate $R$, the outage probability for user $N_l$ with FFNC can be given by

$$\begin{aligned} p_{\mathrm{FFNC}}^{\mathrm{out}}(R) &= 1 - \left(1 - \Pr\left[\frac{L}{2L-1}\log_2(1+\gamma) < R\right]\right)^{2L-1} \\ &= 1 - \underbrace{\exp\left(-\frac{2^{\frac{2L-1}{L}R}-1}{\bar{\gamma}}\right)}_{D}^{2L-1}. \end{aligned} \quad (7.20)$$

As can be observed from the above two equations, term $D$ of (7.20) is smaller than term $A$ in (7.14). On the other hand, the exponent of term $D$ is slightly bigger than that of term $A$. It is difficult to determine which outage probability is analytically superior. The outage probability comparison between these two schemes is plotted in the following Figure 7.4 and Figure 7.5.

The success of FFNC at one of the users in the single relay TWRC depends on the successful transmission of the three phases over the entire exchange process, i.e., $N_1 - R$, $N_2 - R$, and $R - N_1$ or $R - N_2$. However, in the Non-NC scheme, only two phases affect the transmission of one message exchange. On one hand, FFNC has a 50% improvement over Non-NC in the network throughput. On

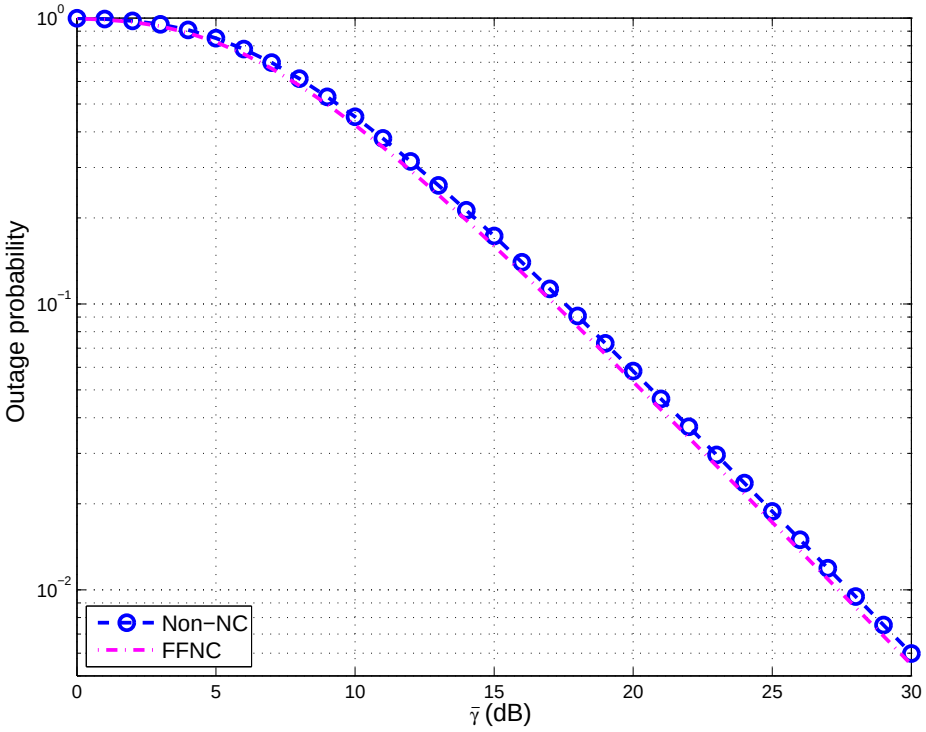


Figure 7.4: Outage probability versus the average SNR for the single relay TWRC.

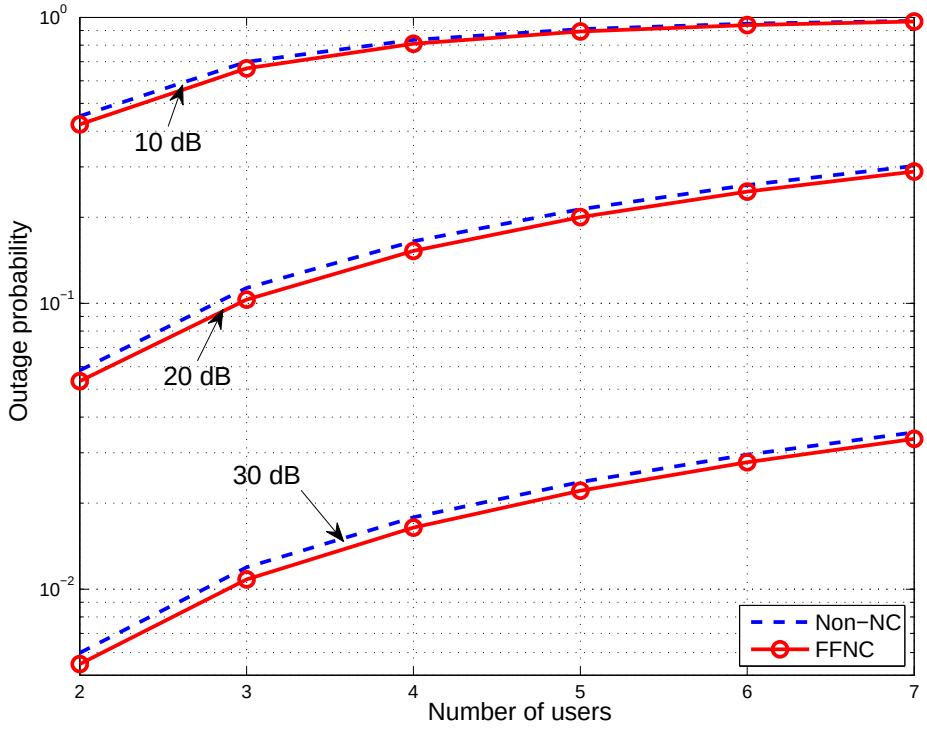


Figure 7.5: Outage probability versus the number of users for the mRC.

the other hand, the number of transmission events that affect the outage of one message exchange increases from 2 to 3. It can be seen from Figure 7.4, the outage performance improvement of FFNC over Non-NC is less than 1 dB in the single relay TWRC. Moreover, this outage probability improvement diminishes with the increase in the number of users as shown in Figure 7.5.

In summary, although the FFNC scheme is applicable to the mRC, it cannot provide a markedly increased outage performance compared to the Non-NC scheme. In the following sections, the outage performance comparison between the proposed extended CPF and Non-NC schemes is shown to demonstrate the superiority of the CPF scheme in outage performance.

### 7.6.2 Compute-and-Forward

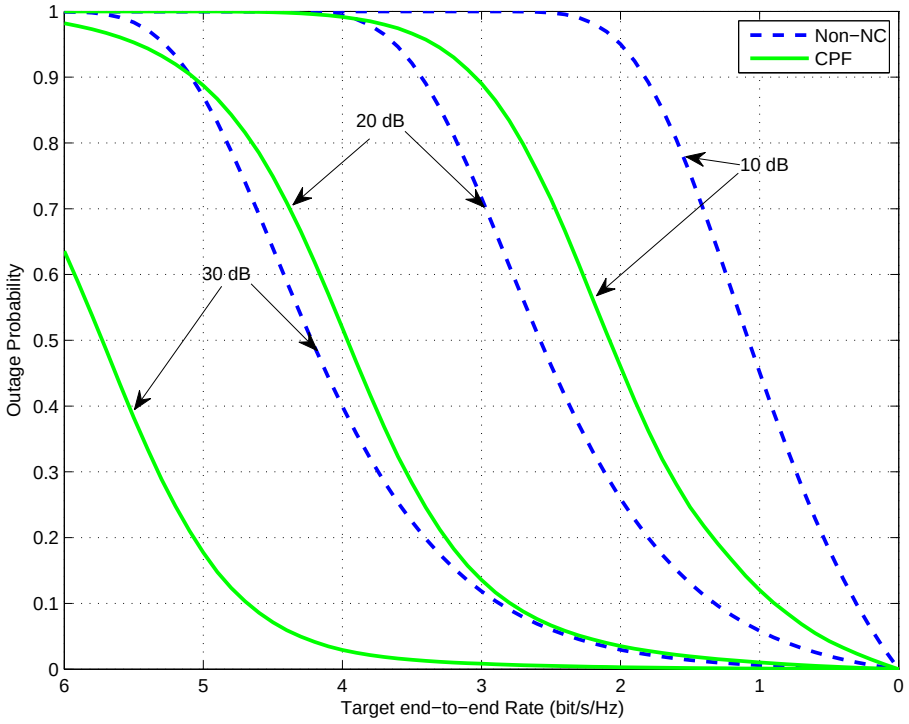


Figure 7.6: Outage probability versus the target end-to-end rate for the single relays TWRC.

The outage probability versus the target end-to-end rate for the 2-user mRC (also known as single relay TWRC) is shown in Figure 7.6. It can be observed from the figure that the outage improvement of CPF over Non-NC increases with

the increase of the target end-to-end rate and average SNR of the single relay TWRC. However, when the target rate reaches certain values, e.g., 4 bit/s/Hz at 10 dB, the outage probabilities of both schemes become poor, and there is no outage performance gain for CPF over Non-NC.

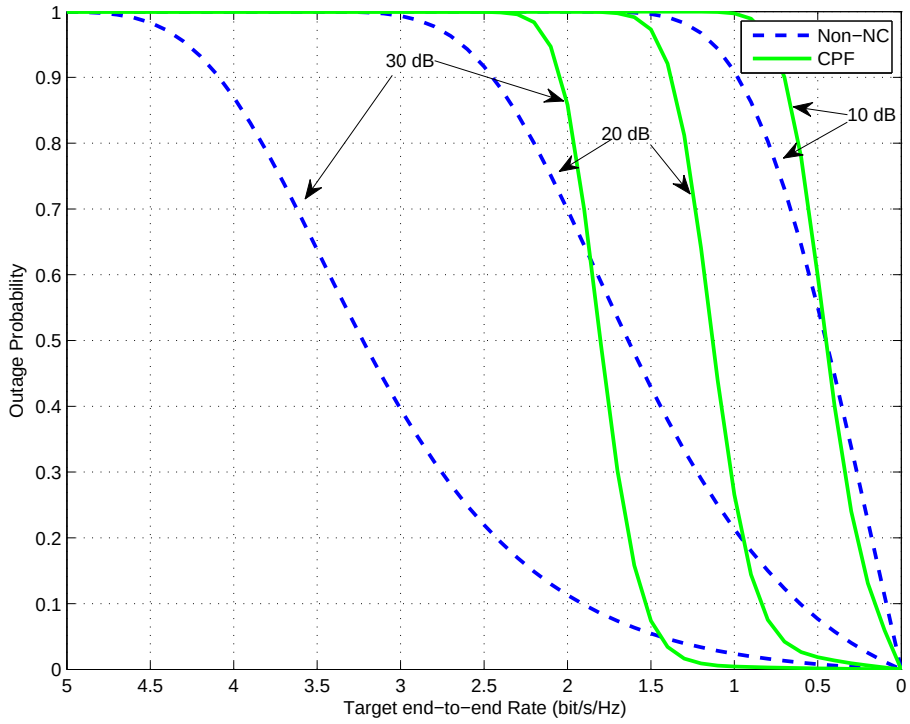


Figure 7.7: Outage probability versus the target end-to-end rate for the 5-user mRC.

Figure 7.7 shows the outage probability versus the target end-to-end rate for the 5-user mRC. It can be found that in the mRC with relatively large number of users, the outage performance gain of the CPF scheme over the Non-NC scheme collapses in the low SNR and high target rate regions.

As can be seen from these two figures, the CPF scheme has a significantly better outage performance than the Non-NC scheme in the single relay TWRC, and the gain improves with the increase of the average SNR. However, the CPF scheme is poorer in outage probability than the Non-NC scheme in high rate regions when the number of users in the mRC is larger. The following parts present the comparison between their outage probabilities from a different perspective. The target rate is set to 1 bit/sec/Hz in the following comparisons.

The outage probabilities for CPF, Non-NC and ANC for the single relay

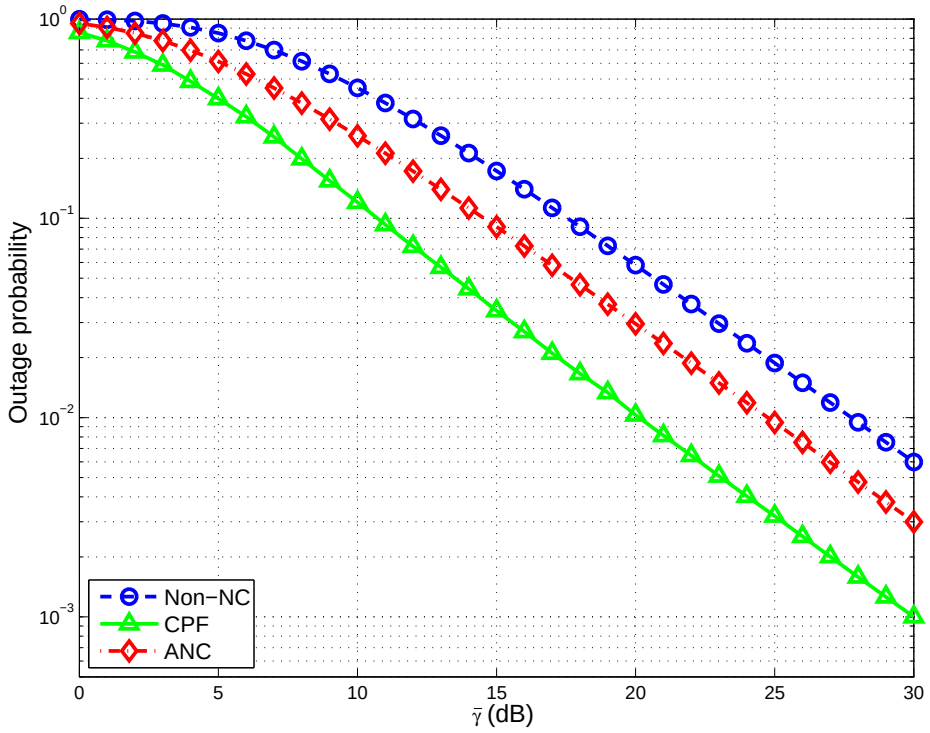


Figure 7.8: Outage probability versus the average SNR for the single relay TWRC.

TWRC are plotted in Figure 7.8. From the figure, it can be seen that CPF can achieve a 7 dB gain in comparison with Non-NC at the outage probability of $10^{-2}$. Moreover, it is also demonstrated that CPF is superior to ANC in outage performance, and a 5 dB gain can be achieved by CPF at the outage probability of $10^{-2}$.

For the generalized mRC, the outage probability versus average SNR $\bar{\gamma}$ for 2-user, 4-user and 5-user mRCs are plotted in Figure 7.9. As shown in the figure, CPF has the largest SNR gain in comparison with Non-NC in the 2-user mRC. The SNR gain for the 4-user mRC is 6 dB at the outage probability of $2 \times 10^{-2}$, and 4 dB for the 5-user mRC at the outage probability of $2.5 \times 10^{-2}$. It is demonstrated that the outage probability improvement of CPF decreases with the increased number of users.

The outage probability versus the number of users is plotted in Figure 7.10. The average SNR $\bar{\gamma}$ is set to 10, 20, and 30 dB. The outage probabilities for both schemes increase with the number of users. In addition, term $A$ in (7.14) is determined by the target rate $R$ and average SNR $\bar{\gamma}$, and not affected by the number of users $L$. Thus, the outage probability of Non-NC given by (7.14)

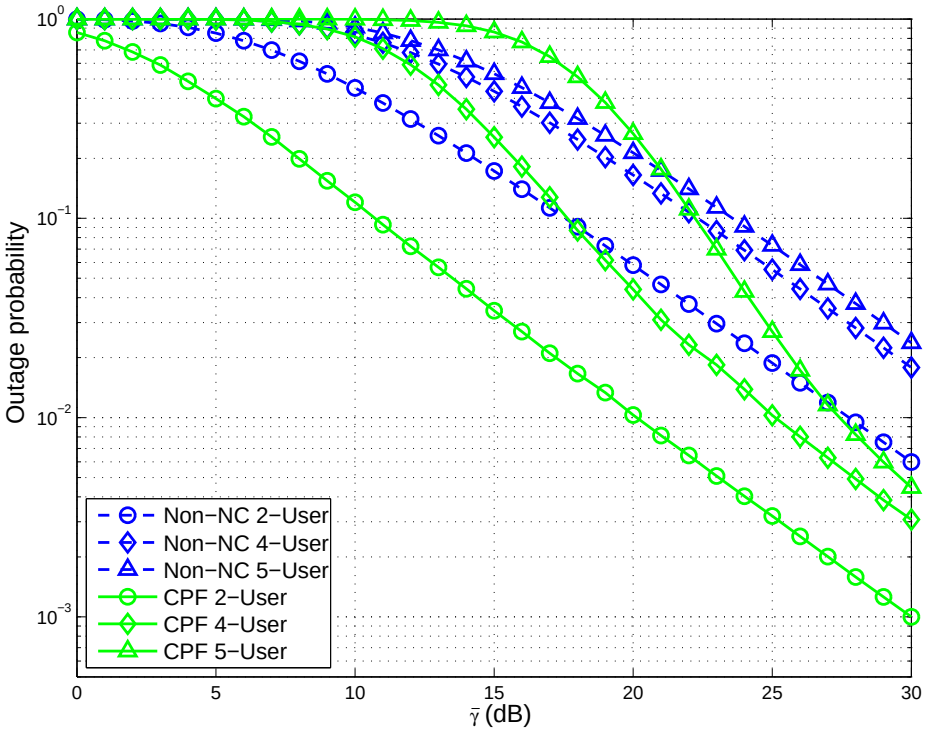


Figure 7.9: Outage probability versus the average SNR for the mRC.

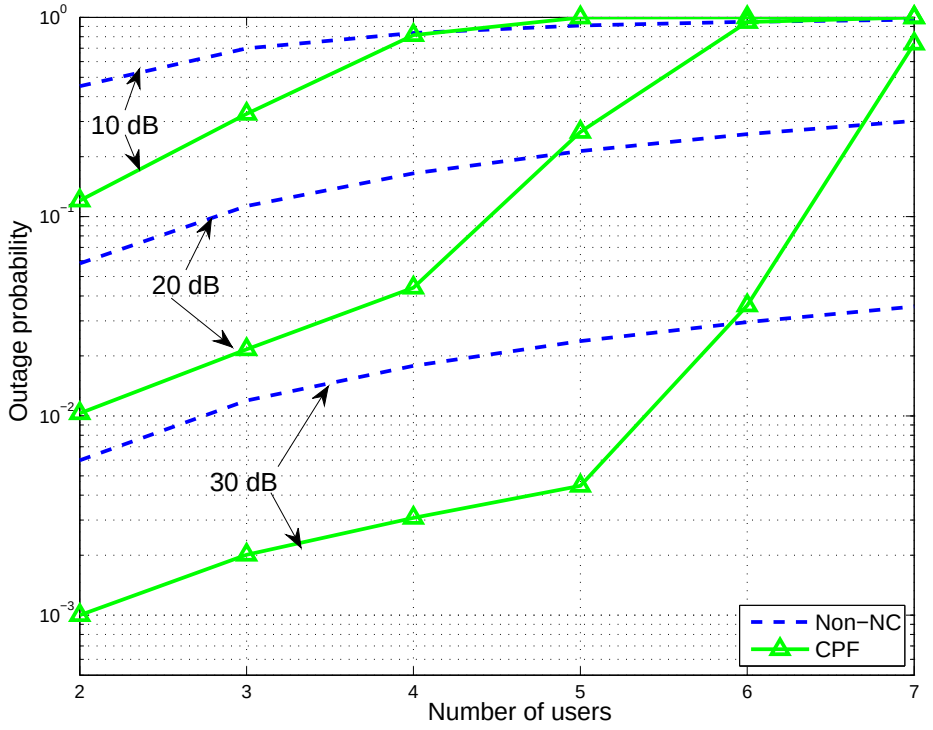


Figure 7.10: Outage probability versus the number of users for the mRC.

increases with the number of users $L$ exponentially. Similarly, term $B$ in (7.19) is also determined only by $R$ and $\bar{\gamma}$. However, the computation rate $R_{\text{COMP}}(\mathbf{h}, \mathbf{a}_m)$ decreases with the increase of $L$ as can be observed from the proposed algorithm for $\mathbf{A}$, thus making term $C$ in (7.19) decrease with the increase of $L$. As a result, the outage probability of CPF in (7.19) deteriorates faster than that of Non-NC in (7.14). It can be observed from Figure 7.10 that the intersection point of the two outage curves shifts rightward with the increase of the number of users. It is demonstrated that CPF has better outage performance than Non-NC in the mRCs with a relatively small number of users.

Finally, a 3-dimension figure shown in Figure 7.11 visually represents the outage performance comparison between CPF and Non-NC versus the number of users and average SNR $\bar{\gamma}$, and demonstrates the results demonstrated in the previous figures.

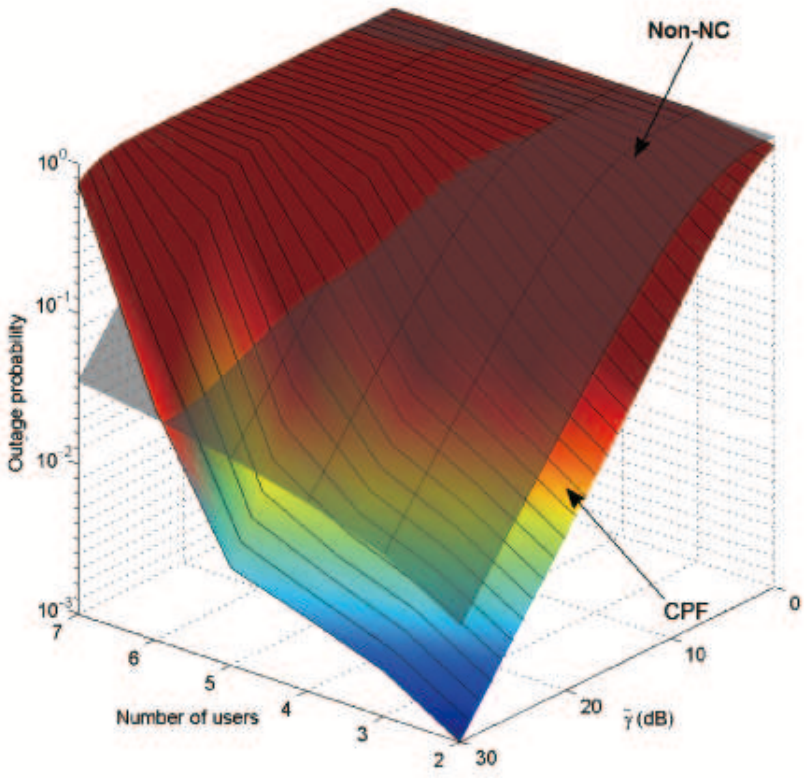


Figure 7.11: Outage probabilities versus the number of users and mean SNR for the mRC.

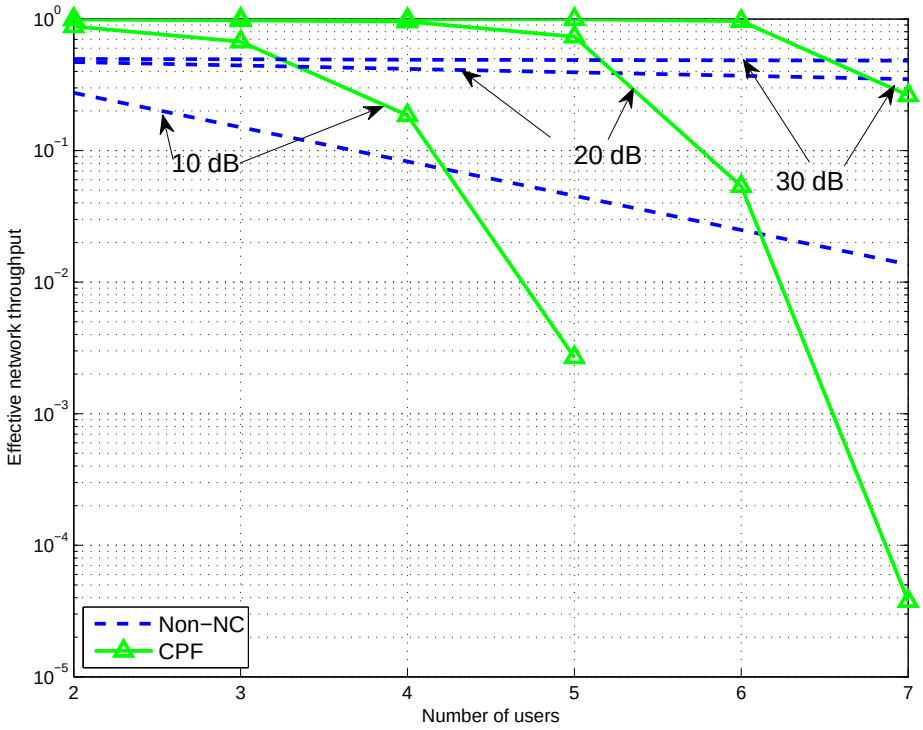


Figure 7.12: Effective network throughput versus the number of users for the mRC.

Figure 7.12 plots the effective network throughput versus the number of users for the mRC. The average SNR $\bar{\gamma}$ is set to 10, 20, and 30 dB. The outage probabilities for both schemes decrease with the number of users. When the number of users is small, CPF have better effective network throughput than Non-NC. However, the effective network throughput of CPF deteriorates rapidly with the increase of the number of users. It is demonstrated that CPF has better effective network throughput than Non-NC in the mRCs with a relatively small number of users.

## 7.7 Summary

The study presented in this chapter moves the research a step forward and extends the WNC scheme to the mRC. Due to the presence of multiple users in the mRC, most exiting WNC schemes are either not directly applicable (such as the traditional ANC and "standard" PNC schemes), or cannot provide a markedly increased network throughput and outage performance (such as FFNC). Inspired by the advantage of CPF, the transmission scheme of extended CPF for the mRC

is designed. It is proven to double the network throughput in comparison with the traditional Non-NC scheme. Moreover, the single relay case in the mRC is different from the multi-relay network where the original CPF scheme was proposed. Therefore, in order to solve the issue of how to ensure the linear independent condition while maximizing the overall computation rate upon one reception, a dominated solution is proposed to calculate the coefficient matrix. The obtained coefficient matrix is able to meet the linear independent requirement to ensure that all users can solve the $L-1$ linear equations for their required messages. In the mean time, the overall computation rate obtained by the proposed dominated solution is close to the maximized computation rate obtained with the original CPF in high SNR regions.

The outage probability of both CPF and Non-NC schemes is also derived in this study. As demonstrated by the numerical results, the CPF scheme has significantly better outage performance compared to the Non-NC and ANC schemes in the single relay TWRC. It is also demonstrated that CPF has a better outage probability over Non-NC in the mRC with a relatively small number of users. However, in the mRC with a relatively large number of users, CPF can only achieve a better outage performance over the Non-NC scheme in high SNR regions, while the outage performance gain of the CPF scheme over the Non-NC scheme collapses in the low SNR and high target rate regions in large scale mRCs.

To summarize, while most of the exiting network coding scheme is not directly applicable, the extended CPF scheme joined with the proposed dominated solution can be applied to the mRC. Not only does the extended CPF scheme provides a doubled network throughput improvement, it also provides a better outage performance over Non-NC in small scale mRCs.

# Chapter 8

# Conclusion

This thesis focuses on exploiting WNC in multi-hop two-way relay channels, and further mRCs. The transmission scheme along with the performance analysis are presented for the proposed schemes. The proposed WNC scheme for the MH-TRC and mRC is proven to be superior to the Non-NC scheme not only in the network throughput, but also in the outage performance.

Particularly, a generalized MH-WNC scheme is designed, and the transmission pattern is presented in grid charts with the built simulation platform. The proposed MH-WNC is proven to have a significant network throughput and communication delay improvement in comparison with the traditional hop-by-hop straightforward relaying schemes.

For the non-regenerative and regenerative MH-TRC, the outage performance for both MH-ANC and MH-CPF schemes are analyzed. Specifically, to circumvent the exponentially increased complexity with the increase of the numbers of nodes and messages, two recursive approaches are proposed to derive the received SNR for MH-ANC and the received linear combinations at the user nodes for MH-CPF. Moreover, a complex lattice reduction method is designed to find the best integer coefficients to maximize the computation rate.

The outage probability results demonstrate that the proposed MH-ANC has better outage performance over the traditional Non-NC scheme when the number of nodes is relatively small. Due to the noise propagation in the ANC scheme, the outage performance of MH-ANC deteriorates quickly with the increased number of nodes. Therefore, the MH-ANC scheme cannot outperform Non-NC schemes

in large-scale MH-TRCs. On the other hand, the re-mapping process at the relay node eliminates the noise propagation with the MH-CPF scheme. As a result, MH-CPF can outperform Non-NC in outage performance for the MH-TRC with large number of nodes.

Due to the fact that the proposed MH-WNC with fixed two time intervals cannot always provide better outage performance than Non-NC in all scale MH-TRCs, a Multi-TI MH-WNC is further proposed to investigate the relationship between the outage probability and number of time intervals. The MH-WNC with larger numbers of time intervals has less interference, thus less noise propagation for MH-ANC and less CPF processes for MH-CPF. By converting the transmission pattern to a binary-tree structure and building the corresponding characteristic matrices, the optimal MH-WNC which can achieve the best outage performance for all scale MH-TRCs is determined. The optimal MH-ANC and MH-CPF scheme are proven to have better outage performance over Non-NC in all scale MH-TRCs.

Finally, this project moves the research on WNC a step forward and extend the original CPF to the mRC. A dominated solution to maximize the overall computation rate and ensure all the users can successfully recover the required messages is proposed. The CPF joined with the proposed dominated solution is proven to double the network throughput and has better outage probability than the Non-NC scheme in the mRC with a relatively small number of users.

## 8.1 Future Work

This discussion concludes with recommendations of future works that are natural extensions of the problems considered in this thesis:

- **Adaptive Wireless Network Coding for Rate-Mismatch Multi-Hop Relay Networks:** The performance of WNC is limited by several factors such as packet length mismatch, traffic rate mismatch and transmit rate mismatch. The last factor is always neglected in most previous works, the network-coded packet is intended to be received by all the nodes in the multi-hop network, thus the minimal rate is chosen for the transmission. In

this way, the transmission at a low rate on the link supporting a high rate wastes its channel bandwidth. While network coding is applied to multi-hop networks, the effect of rate mismatch becomes more obvious, which is a crucial factor limiting the throughput of wireless networks. There has been some work on network coding modulation to solve the rate-mismatch issue [102, 103]. However, the work is limited to the three-phase network coding [24]. In view of this fact, an adaptive MH-WNC integrated with network-coded modulation could be an effective solution to overcome the rate-mismatch problem in the MH-TRC;

- **Optimal Compute-and-Forward for Multi-Way Relay Channels:** It is pointed out that the CPF scheme cannot be superior to Non-NC in all scale mRCs for all target rate and average SNR settings. However, similar to the optimal MH-WNC obtained in Chapter 6, there should exist an optimal CPF scheme for the mRC, which can achieve better outage performance in all scale mRCs. The optimal CPF scheme for the mRC can be realized by optimizing the transmission scheme or computation rate, which is an interesting topic and opened for further research; and

- **Wireless Network Coding for Multi-User Multi-Hop Relay Channels:** The work presented in Chapter 7 is a step forward in the network coding application from two-user to multi-user networks. In practical wireless communication networks, multiple users may communicate with each other through multiple relays and multiple hops, such as Mobile ad hoc networks (MANETS). This kind of network is usually classified as multi-user multi-hop relay channels or multi-user multi-relay channels. The improvement of spectrum efficiency in this network is in high demand. In this dissertation and some previous work, wireless network coding has been proven to be able to improve the spectrum efficiency significantly in multi-hop network, multi-user network, and multi-relay network [137]. It is quite natural to consider the case of WNC being applied to more complicated and random networks to improve the spectrum efficiency. The application of WNC to this kind of network is more than the combination of the existing schemes. However, with the pioneering work in this dissertation, it is quite possible

to find a solution for applying WNC to multi-user multi-hop relay channels or multi-user multi-relay channels.

Overall, the aim of this project has been implementing the wireless network coding to multi-hop two-way relay networks. The generalized MH-WNC scheme is designed for the MH-TRC, and the results demonstrate that the proposed MH-WNC can not only achieve a significantly better network throughput, it can also outperform Non-NC in outage performance. Furthermore, the extended work to the mRC provides a glimpse of the application of CPF in multi-user single relay networks. Last but not least, there still exists much work to be investigated, such as adaptive WNC for rate-mismatch multi-hop networks, WNC for multi-user multi-hop relay channels.

# References


[1] P. Kolios, V. Friderikos, and K. Papadaki, "Future wireless mobile networks," *IEEE Veh. Technol. Mag.*, vol. 6, pp. 24 – 30, Mar. 2011.

[2] J. N. Laneman and G. W. Wornell, "Exploiting distributed spatial diversity in wireless networks," in *Proc. Allerton Conf. Communications, Control, and Computing*, Monticello, IL, Oct. 2000, pp. 1 – 10.

[3] I. F. Akyildiz, W. Su, Y. Sankarasubramaniam, and E. Cayirci, "A survey on sensor networks," *IEEE Commun. Mag.*, vol. 40, pp. 102 – 114, Aug. 2002.

[4] I. F. Akyildiz and X. Wang, "A survey on wireless mesh networks," *IEEE Commun. Mag.*, vol. 43, pp. 23 – 30, Sep. 2005.

[5] T. Camp, J. Boleng, and V. Davies, "A survey of mobility models for ad hoc network research," *Wireless Communications & Mobile Computing: Special issue on Mobile Ad Hoc Networking: Research, Trends and Applications*, vol. 2, pp. 483 – 502, Sep. 2002.

[6] H. Hartenstein and K. Laberteaux, "A tutorial survey on vehicular ad hoc networks," *IEEE Commun. Mag.*, vol. 46, pp. 164 – 171, Jun. 2008.

[7] C. Zhang, S. Ariyavisitakul, and M. Tao, "Lte-advanced and 4g wireless communications," *IEEE Commun. Mag.*, vol. 50, pp. 102 – 103, Feb. 2012.

[8] ——, "Lte-advanced and 4g wireless communications: Part 2," *IEEE Commun. Mag.*, vol. 50, p. 26, Jun. 2012.

[9] R. Ghosh, Amitava Ratasuk, B. Mondal, N. Mangalvedhe, and T. A.

Thomas, "Lte-advanced: next-generation wireless broadband technology," *IEEE Wireless Communications*, vol. 17, pp. 10 – 22, Jun. 2010.

[10] W. Hoymann, Christian Chen, J. I. Montojo, A. Golitschek, C. Koutsimanis, and X. Shen, "Relaying operation in 3gpp lte: challenges and solutions," *IEEE Commun. Mag.*, vol. 50, pp. 156 – 162, Feb. 2012.

[11] H. Ju, E. Oh, and D. Hong, "Catching resource-devouring worms in next-generation wireless relay systems: Two-way relay and full-duplex relay," *IEEE Commun. Mag.*, vol. 47, pp. 58 – 65, Sep. 2009.

[12] R. Ahlswede, N. Cai, S.-Y. Li, and R. Yeung, "Network information flow," *IEEE Trans. Inf. Theory*, vol. 47, pp. 1204 – 1216, Jul. 2000.

[13] S. Katti, S. Gollakota, and D. Katabi, "Embracing wireless interference: Analog network coding," in *Proc. ACM SIGCOMM*, Kyoto, Japan, Aug. 2007, pp. 397 – 408.

[14] S. Zhang, S. C. Liew, and P. P. Lam, "Hot topic: physical-layer network coding," in *Proc. International conference on Mobile computing and networking*, Los Angeles, CA, Sep. 2006, pp. 23 – 29.

[15] S. Katti, H. Rahul, W. Hu, D. Katabi, M. Medard, and J. Crowcroft, "XORs in the air: Practical wireless network coding," *IEEE/ACM Trans. Netw.*, vol. 21, pp. 497–510, Mar. 2008.

[16] I. Byun and K. S. Kim, "Cooperative communication strategies using network coding for two-way relay channel with arq," *Telecomm. Rev.*, vol. 17, pp. 996 – 1008, Jun. 2007.

[17] Y. Lang, D. Wubben, and K.-D. Kammeyer, "An improved physical layer network coding scheme for two-way relay systems," in *Proc. International ITG Workshop on Smart Antennas (WSA)*, Bremen, Germany, Feb. 2010, pp. 107 – 114.

[18] P. Popovski and H. Yomo, "Physical network coding in two-way wireless relay channels," in *Proc. IEEE International Conference on Communications*, Glasgow,UK, Jun. 2007, pp. 707 – 712.

[19] P. Larsson, N. Johansson, and K. E. Sunell, "Coded bi-directional relaying," in *Proc. IEEE VTC*, Melbourne, Australia, May 2006, pp. 851 – 855.

[20] S. Zhang, S.-C. Liew, and P. Lam, "On the synchronization of physical-layer network coding," in *Proc. IEEE Information Theory Workshop*, Chengdu,China, Oct. 2006, pp. 404 – 408.

[21] C. Hausl and J. Hagenauer, "Iterative network and channel decoding for the two-way relay channel," in *Proc. IEEE International Conference on Communications*, Istanbul, Turkey, Jun. 2006, pp. 1568 – 1573.

[22] J. Li and W. Chen, "Physical layer network coding for wireless cooperative multi-cast flows," *IEICE Transactions on Communications*, vol. 92, pp. 2559 – 2567, Aug. 2009.

[23] M. Ju and I.-M. Kim, "Error performance analysis of BPSK modulation in physical-layer network-coded bidirectional relay networks," *IEEE Trans. Commun.*, vol. 58, pp. 2770 – 2775, Oct. 2010.

[24] R. Louie, Y. Li, and B. Vucetic, "Practical physical layer network coding for two-way relay channels: performance analysis and comparison," *IEEE Trans. Wireless Commun.*, vol. 9, pp. 764 – 777, Feb. 2010.

[25] T. Yang, T. Huang, J. Yuan, and Z. Chen, "Distance spectrum and performance of channel-coded physical-layer network coding for binary-input gaussian two-way relay channels," *IEEE Trans. Commun.*, vol. 60, pp. 1499 – 1510, Jun. 2012.

[26] M. Park, I. Choi, and I. Lee, "Exact BER analysis of physical layer network coding for two-way relay channels," in *Proc. IEEE Vehicular Technology Conference (VTC Spring)*, Budapest, Hungary, May 2011, pp. 1 – 5.

[27] C. Jiang, Y. Shi, Y. Hou, and S. Kompella, "On the asymptotic capacity of multi-hop MIMO ad hoc networks," *IEEE Trans. Wireless Commun.*, vol. 10, pp. 1032 – 1037, Apr. 2011.

[28] W. Ren, Q. Zhao, and A. Swami, "On the connectivity and multihop delay of ad hoc cognitive radio networks," *IEEE J. Sel. Areas Commun.*, vol. 29, pp. 805 – 818, Apr. 2011.

[29] H. Gacanin and F. Adachi, "Broadband analog network coding," *IEEE Trans. Wireless Commun.*, vol. 2, pp. 1577 – 1583, May 2010.

[30] A. Argyriou and A. Pandharipande, "Cooperative protocol for analog network coding in distributed wireless networks," *IEEE Trans. Wireless Commun.*, vol. 9, pp. 3112 – 3119, Oct. 2010.

[31] B. Nazer and M. Gastpar, "Reliable physical layer network coding," *Proceedings of the IEEE*, vol. 99, pp. 438 – 460, Mar. 2011.

[32] A. Osmane and J.-C. Belfiore, "The compute-and-forward protocol: Implementation and practical aspects," *submitted to IEEE Communication Letters*.

[33] C. Feng, D. Silva, and F. Kschischang, "Design criteria for lattice network coding," in *Proc. Annual Conference on Information Sciences and Systems*, Baltimore, MD, Mar. 2011, pp. 1 – 6.

[34] ——, "An algebraic approach to physical-layer network coding," *arXiv:1108.1695[cs.IT], submitted to IEEE Transactions on Information Theory*.

[35] G. Wang, W. Xiang, J. Yuan, and T. Huang, "Outage analysis of non-regenerative analog network coding for two-way multi-hop networks," *IEEE Commun. Lett.*, vol. 15, pp. 662 – 664, May 2011.

[36] G. Wang, W. Xiang, and J. Yuan, "Multi-hop compute-and-forward for generalized two-way relay channels," *submitted to Transactions on Emerging Telecommunications Technologies*.

[37] D. Gunduz, A. Yener, A. Goldsmith, and H. Poor, "The multi-way relay channel," in *Proc. IEEE International Symposium on Information Theory*, Seoul, Korea, Jul. 2009, pp. 339 – 343.

[38] R. Pabst, B. Walke, D. Schultz, P. Herhold, H. Yanikomeroglu, S. Mukherjee, H. Viswanathan, M. Lott, W. Zirwas, M. Dohler, H. Aghvami, D. Falconer, and G. Fettweis, "Relay-based deployment concepts for wireless and mobile broadband radio," *IEEE Commun. Mag.*, vol. 42, pp. 80 – 89, 2004.

[39] M. Dohler and Y. Li, *Cooperative Communications: Hardward, Channel & PHY*. New York: John Wiley and Sons, 2010.

[40] H. M.O. and A. M.-S., "A performance study of dualhop transmissions with fixed gain relays," *IEEE Trans. Wireless Commun.*, vol. 3, pp. 1963–1968, Jun. 2004.

[41] Y. Li, "Distributed coding for cooperative wireless networks: An overview and recent advances," *IEEE Commun. Mag.*, vol. 47, pp. 71 – 77, Aug. 2009.

[42] B. J., F. D.D., and Y. H., "Multihop diversity in wireless relaying channels," *IEEE Trans. Commun.*, vol. 52, pp. 1820–1830, Oct. 2004.

[43] K. G.K., "Performance bounds of multihop wireless communications with blind relays over generalized fading channels," *IEEE Trans. Wireless Commun.*, vol. 5, pp. 498–503, Mar. 2006.

[44] J. N. Laneman, "Cooperative diversity in wireless networks: Algorithms and architectures," Ph.D. dissertation, M.I.T. Doctoral Dissertation, Sep. 2002.

[45] A. El Gamal, N. Hassanpour, and J. Mammen, "Relay networks with delays," *IEEE Trans. Inf. Theory*, vol. 53, pp. 3413 – 3431, Oct. 2007.

[46] S. Borade, L. Zheng, and R. Gallager, "Amplify-and-forward in wireless relay networks: Rate, diversity and network size," *IEEE Trans. Inf. Theory*, vol. 53, pp. 3302 – 3318, Oct. 2007.

[47] M. Gastpar and M. Vetterli, "On the capacity of large gaussian relay networks," *IEEE Trans. Inf. Theory*, vol. 51, pp. 765 – 779, Mar. 2005.

[48] R. Dabora and S. Servetto, "On the role of estimate-and-forward with time sharing in cooperative communication," *IEEE Trans. Inf. Theory*, vol. 54, pp. 4409 – 4431, Oct. 2008.

[49] S. Salehkalaibar, L. Ghabeli, and M. Aref, "An achievable rate for relay networks based on compress-and-forward strategy," *IEEE Commun. Lett.*, vol. 14, pp. 279 – 281, Apr. 2010.

[50] M. Uppal, Z. Liu, V. Stankovic, and Z. Xiong, "Compress-forward coding with bpsk modulation for the half-duplex gaussian relay channel," *IEEE Commun. Lett.*, vol. 57, pp. 4467 – 4481, Nov. 2009.

[51] Y. Lee, M. hung Tsai, and S. lan Sou, "Performance of decode-and-forward cooperative communications with multiple dual-hop relays over nakagami-m fading channels," *IEEE Trans. Wireless Commun.*, vol. 8, pp. 2853 – 2859, Jun. 2009.

[52] M. Khormuji and E. Larsson, "Cooperative transmission based on decode-and-forward relaying with partial repetition coding," *IEEE Trans. Wireless Commun.*, vol. 8, pp. 1716 – 1725, Apr. 2009.

[53] E. Soljanin, P. Gupta, and G. Kramer, "Network coding for efficient network multi-cast," *Bell Labs Technical Journal*, vol. 14, pp. 157 – 166, Nov. 2009.

[54] S.-Y. R. Li, R. W. Yeung, and N. Cai, "Linear network coding," *IEEE Trans. Inf. Theory*, vol. 11, pp. 782 – 795, Oct. 2003.

[55] T. Ho, M. Medard, R. Koetter, K. D. R, M. Effros, J. Shi, and B. Leong, "A random linear network coding approach to multi-cast," *IEEE Trans. Inf. Theory*, vol. 52, Oct.

[56] C. Fragouli, J. Widmer, and J.-Y. L. Boudec, "Efficient broadcasting using network coding," *IEEE/ACM Trans. Netw.*, vol. 16, pp. 450 – 463, 2008.

[57] K. Lu, S. Fu, and Y. Qian, "On capacity of random wireless networks with physical-layer network coding," *IEEE J. Sel. Areas Commun.*, vol. 27, pp. 763 – 772, Jun. 2009.

[58] D. Lun, M. Medard, R. Koetter, and M. Efiros, "Further results on coding for reliable communication over packet networks," in *Proc. IEEE ISIT*, Adelaide, Australia, Sep. 2005, pp. 1848 – 1852.

[59] Z. Ding, D. Leung, K.K.and Goeckel, and D. Towsley, "On the study of network coding with diversity," *IEEE Trans. Wireless Commun.*, vol. 8, pp. 1247 – 1259, Mar. 2009.

[60] Y. Wu, P. A. Chou, and S.-Y. Kung, "Information exchange in wireless networks with network coding and physical-layer broadcast," in *Proc. CISS*, Baltimore, MD, Mar. 2005, pp. 1 – 5.

[61] F. Yang, Q. Zhang, W. Zhu, and Y.-Q. Zhang, "An efficient transport scheme for multimedia over wireless internet," in *Proc. Int. Conf. Third Generation Wireless and Beyon*, San Francisco, CA, May 2001, pp. 1 – 8.

[62] R. Gallager, "A perspective on multiaccess channels," *IEEE Trans. Inf. Theory*, vol. 31, pp. 124 – 142, Mar. 1985.

[63] P. Gupta and P. Kumar, "The capacity of wireless networks," *IEEE Trans. Inf. Theory*, vol. 46, pp. 388 – 404, Mar. 2000.

[64] T. Ojanpera and R. Prasad, "An overview of air interface multiple access for imt-2000/umts," *IEEE Commun. Mag.*, vol. 36, pp. 82 – 95, Sep. 1998.

[65] D. Falconer, F. Adachi, and B. Gudmundson, "Time division multiple access methods for wireless personal communications," *IEEE Commun. Mag.*, vol. 33, pp. 50 – 57, Jan. 1995.

[66] H. Sari and G. Karam, "Orthogonal frequency-division multiple access and its application to CATV networks," *Eur. Trans. Commun.*, vol. 45, pp. 507 – 516, Nov. 1998.

[67] M. Morelli, C.-C. Kuo, and M.-O. Pun, "Synchronization techniques for orthogonal frequency division multiple access (OFDMA): A tutorial review," *Proceedings of the IEEE*, vol. 95, pp. 1394 – 1427, Jul. 2007.

[68] J. Salehi, "Code division multiple-access techniques in optical fiber networks. i. fundamental principles," *IEEE Trans. Commun.*, vol. 27, pp. 824 – 833, Aug. 1989.

[69] D. Umehara, T. Hirano, S. Denno, M. Morikura, and T. Sugiyama, "Wireless network coding in slotted aloha with two-hop unbalanced traffic," *IEEE J. Sel. Areas Commun.*, vol. 27, p. 647, Jun. 2009.

[70] J. Le, J. Lui, and D.-M. Chiu, "On the performance bounds of practical wireless network coding," *IEEE Trans. Mobile Comput.*, vol. 9, pp. 1536 – 1233, Aug. 2010.

[71] R. Koetter and M. Medard, "An algebraic approach to network coding," *IEEE/ACM Trans. Netw.*, vol. 11, pp. 782 – 795, Oct. 2003.

[72] C. Fragouli, D. Katabi, A. Markopoulou, M. Medard, and H. Rahul, "Wireless network coding: Opportunities & challenges," in *Proc. IEEE MILCOM*, Orlando, FL, Oct. 2007, pp. 1 – 8.

[73] P. Popovski and N. Yomo, "Bi-directional amplification of throughput in a wireless mutli-hop network," in *Proc. IEEE Vehicular Technology Conference*, Melbourne, Australia, May 2006, pp. 588 – 593.

[74] B. Rankov and A. Wittneben, "Spectral efficient protocols for half-duplex fading relay channels," *IEEE J. Sel. Areas Commun.*, vol. 25, pp. 379 – 389, Feb. 2007.

[75] T. M. Cover and J. A. Thomas, *Elements of Information Theory.* New York: John Wiley and Sons, 1991.

[76] S. Zhang, S.-C. Liew, and P. P.Lam, "Physical-layer network coding," *IEEE J. Sel. Areas Commun.*, vol. 27, pp. 763 – 772, Jun. 2009.

[77] E. Peh, Y.-C. Liang, and Y. L. Guan, "Power control for physical-layer network coding in fading environments," in *Proc. IEEE International Symposium on Personal, Indoor and Mobile Radio Communications*, Cannes, France, 2008, pp. 1 – 5.

[78] T. K. Akino, P. Popovski, and V. Tarokh, "Denoising maps and constellations for wireless network coding in two-way relaying system," in *Proc. IEEE Global Telecommunications Conference*, New Orleans,US, Nov. 2008, pp. 1 – 5.

[79] S. Zhang and S.-C. Liew, "Channel coding and decoding in a relay system operated with physical-layer network coding," *IEEE J. Sel. Areas Commun.*, vol. 27, pp. 788 – 796, Jun. 2009.

[80] D. Divsalar, H. Jin, and R. J. McEliece, "Coding theorems for turbolike codes," in *Proc. 36th Allerton*, Allerton, Illinois, Sep. 1998, pp. 201 – 210.

[81] A. Zhan and C. He, "Joint design of channel coding and physical network coding for wireless networks," in *Proc. International Conference on Neural Networks and Signal Processing*, Nanjing, China, Jun. 2008, pp. 512 – 516.

[82] J. Proakis, *Digital Communications, 4th ed.* New York: McGraw-Hill, 2000.

[83] A. Goldsmith, *Wireless Communications*. New York: Cambridge, 2005.

[84] R. de Buda, "The upper error bound of a new near-optimal code," *IEEE Trans. Inf. Theory*, vol. 21, pp. 441 – 445, Jul. 1975.

[85] S. Wilson and R. Gaus, "Power spectra of multi-h phase codes," *IEEE Trans. Commun.*, vol. 29, pp. 250 – 256, Mar. 1981.

[86] E. Viterbo and J. Boutros, "A universal lattice code decoder for fading channels," *IEEE Trans. Inf. Theory*, vol. 45, pp. 1639 – 1642, Jul. 1999.

[87] R. Zamir, S. Shamai, and U. Erez, "Nested linear/lattice codes for structured multiterminal binning," *IEEE Trans. Inf. Theory*, vol. 45, pp. 1250 – 1276, Jun. 2002.

[88] R. Zamir, "Lattice are everywhere," in *Proc. 4th Ann. Workshop on Inf. Theory and Its Appl. (ITA 2009)*, La Jolla, CA, Feb. 2009, pp. 3 – 11.

[89] J. H. Conway and N. J. A. Sloane, *Sphere Packings, Lattices and Groups*. New York: Springer-Verlag, 1988.

[90] U. Erez and R. Zamir, "Achieving 1/2 log (1+SNR) on the AWGN channel with lattice encoding and decoding," *IEEE Trans. Inf. Theory*, vol. 50, pp. 2293 – 2314, Oct. 2004.

[91] B. Nazer and M. Gastpar, "Compute-and-forward: A novel strategy for cooperative networks," in *Proc. Asilomar Conference on Signals, Systems and Computers*, Pacific Grove, CA, Oct. 2008, pp. 69 – 73.

[92] ——, "Compute-and-forward: Harnessing interference throught strucutred codes," *IEEE Trans. Inf. Theory*, vol. 57, pp. 6463 – 6486, Oct. 2011.

[93] Y. Wu, P. A. Chou, and S.-Y. Kung, "Minimum-energy multi-cast in mobile ad hoc networks using network coding," *IEEE Trans. Commun.*, vol. 53, pp. 1906 – 1918, Nov. 2005.

[94] C. Fragouli, J. Widmer, and J.-Y. L. Boudec, "A network coding approach to energy efficient broadcasting: From theory to practice," in *Proc. IEEE Infocom*, Barcelona, Spain, Apr. 2006, pp. 1 – 4.

[95] Y. Hao, D. Goeckel, Z. Ding, D. Towsley, and K. K. Leung, "Achievable rates for network coding on the exchange channel," in *Proc. IEEE MILCOM*, Orlando, FL, Oct. 2007, pp. 1 – 7.

[96] D. Wang, S. Fu, and K. Lu, "Channel coding design to support asynchronous physical layer network coding," in *Proc. IEEE Global Telecommunications Conference*, Honolulu, US, Nov. 2009, pp. 1 – 6.

[97] F. Rossetto and M. Zorzi, "On the design of practical asynchronous physical layer network coding," in *Proc. IEEE SPAWC*, Perugia, Rome, Jun. 2009, pp. 469 – 473.

[98] L. Lu and S. C. Liew, "Asynchronous physical-layer network coding," *IEEE Trans. Wireless Commun.*, vol. 11, pp. 819 – 832, Feb. 2012.

[99] Y. Wang, C. Hu, H. Liu, M. Peng, and W. Wang, "Network coding in cooperative relay networks," in *Proc. IEEE International Symposium on Personal, Indoor and Mobile Radio Communications*, Cannes, France, Sep. 2008, pp. 1 – 5.

[100] Y. Li, R. Louie, and B. Vucetic, "Relay selection with network coding in two-way relay channel," *IEEE Trans. Veh. Technol.*, vol. 59, pp. 4489 – 4499, Nov. 2010.

[101] M. Ju and I.-M. Kim, "Relay selection with physical-layer network coding," in *Proc. IEEE GLOBECOM*, Miami, FL, Dec. 2010, pp. 1 – 5.

[102] J. M. Park, S.-L. Kim, and J. Choi, "Hierarchically modulated network coding for asymmetric two-way relay systems," *IEEE Trans. Veh. Technol.*, vol. 59, pp. 2179 – 2184, Jun. 2010.

[103] W. Chen, L. Hanzo, and Z. Cao, "Network coded modulation for two-way relaying," in *Proc. IEEE WCNC*, Cancun, Mexico, Mar. 2011, pp. 1765 – 1770.

[104] M. Xiao and M. Skoglund, "Design of network codes for multiple-user multiple-relay wireless networks," in *Proc. IEEE ISIT*, Seoul, Korea, Jul. 2009, pp. 2562 – 2566.

[105] ——, "Multiple-user cooperative communications based on linear network coding," *IEEE Trans. Commun.*, vol. 58, pp. 3345 – 3351, Dec. 2010.

[106] Q. You, Z. Chen, Y. Li, and B. Vucetic, "Multi-hop bi-directional relay transmission schemes using amplify-and-forward and analog network coding," in *Proc. IEEE International Conference on Communications*, Kyoto, Japan, Jun. 2011, pp. 1 – 6.

[107] E. Fasolo, F. Rossetto, and M. Zorzi, "Network coding meets MIMO," in *Proc. IEEE NetCod*, Hong Kong, China, Jan. 2008, pp. 1 – 6.

[108] H.-Q. Lai and K. Liu, "Space-time network coding," *IEEE Trans. Signal Process.*, vol. 59, pp. 1706 – 1718, Apr. 2011.

[109] Y.-C. Liang and R. Zhang, "Optimal analogue relaying with multi-antennas for physical layer network coding," in *Proc. IEEE ICC*, Beijing, China, May 2008, pp. 3893 – 3897.

[110] S. Zhang and S. Liew, "Physical layer network coding with multiple antennas," in *Proc. IEEE WCNC*, Sydney, Australia, Apr. 2010, pp. 1 – 6.

[111] S. Zhang, Y. Zhu, S.-C. Liew, and K. B. Letaief, "Joint design of network coding and channel decoding for wireless networks," in *Proc. IEEE Wireless Communications and Networking Conference*, Kowloon,Hongkong, Mar. 2007, pp. 780 – 785.

[112] J. Castura and Y. Mao, "Rateless coding and relay networks," *IEEE Signal Process. Mag.*, vol. 24, p. 27, Sep. 2007.

[113] M. Luby, "Lt codes," in *Proc. IEEE Symposium of Foundations of Computer Science*, Rome, Italy, Oct. 2004, pp. 271 – 280.

[114] A. Shokrollahi, "Raptor codes," *IEEE Trans. Inf. Theory*, vol. 52, pp. 2551–2567, Jun. 2006.

[115] M. Grangetto, R. Gaeta, and M. Sereno, "Rateless codes network coding for simple and efficient P2P video streaming," in *Proc. IEEE ICME*, New York, NY, Jun. 2009, pp. 1500 – 1503.

[116] Y. Liu, Y. Guo, and C. Liang, "A survey on peer-to-peer video streaming systems," *Journal of Peer-to-Peer Networking and Applications*, vol. 1, pp. 18 – 28, Mar. 2008.

[117] E. Kurniawan, S. Sun, K. Yen, and K. Chong, "Application of network coding in rateless transmission over wireless relay networks," *IEEE Trans. Commun.*, vol. 59, p. 507, Feb. 2011.

[118] E. Kurniawan, S. Sun, and K. Yen, K. ; Chong, "Network coded transmission of fountain codes over cooperative relay networks," in *Proc. IEEE Wireless Communications and Networking Conference*, Sydney, Australia, Apr. 2010, p. 1.

[119] S. Zhang, S. C. Liew, and L. Lu, "Physical layer network coding schemes over finite and infinite fields," in *Proc. IEEE Global Telecommunications Conference*, New Orleans, LA, Nov. 2008, p. 1.

[120] X. Zhang, H. Zhu, and J. Zhang, "RANC: Relay-aided network coding in multi-hop wireless networks," *Computer Communications*, vol. 32, pp. 974 – 984, Mar. 2009.

[121] F. Ono and K. Sakaguchi, "MIMO spatial spectrum sharing for high efficiency mesh network," *IEICE Trans. Commun.*, vol. E91-B, pp. 62 – 70, Jan. 2008.

[122] ——, "Space time codedmimo network coding," in *Proc. IEEE PIMRC2008*, Cannes, French, Sep. 2008, pp. 1 – 5.

[123] M. O. Hasna and M. S. Alouini, "Harmonic mean and end-to-end performance of transmission systems with relays," *IEEE Trans. Commun.*, vol. 52, pp. 130 – 135, Jan. 2004.

[124] M. O. Hasna and M.-S. Alouini, "A performance study of dual-hop transmissions with fixed gain relays," *IEEE Trans. Wireless Commun.*, vol. 3, pp. 1963 – 1968, Nov. 2004.

[125] M. Hasna and M.-S. Alouini, "End-to-end performance of transmission systems with relays over rayleigh-fading channels," *IEEE Trans. Wireless Commun.*, vol. 2, pp. 1126 – 1131, Nov. 2003.

[126] ——, "Outage probability of multihop transmission over Nakagami fading channels," *IEEE Commun. Lett.*, vol. 7, pp. 216 – 218, May 2003.

[127] M. O. Hasna, "Average BER of multihop communication systems over fading channels," in *Proc. IEEE ICECS*, Sharjah, UAE, Dec. 2003, pp. 723 – 726.

[128] X. Zhao, J.-B. Wang, J.-Y. Wang, M. Chen, M. Feng, and M. Sheng, "System outage probability analysis in uplink multi-hop cellular systems over composite channels," *EURASIP Journal on Wireless Communications and Networking*, vol. 35, pp. 35 – 40, Jul. 2011.

[129] C. Conne and I.-M. Kim, "Outage probability of multi-hop amplify-and-forward relay systems," *IEEE Trans. Wireless Commun.*, vol. 9, pp. 1139 – 1149, Mar. 2010.

[130] I. Maric, A. Goldsmith, and M. Medard, "Analog network coding in the high-SNR regime," in *Proc. WiNC*, Bostn, MA, Jun. 2010, pp. 1 – 6.

[131] B. Liu and N. Cai, "Analog network coding in the generalized high-SNR regime," in *Proc. IEEE ISIT*, St. Petersburg, Russia, Jul. 2011, pp. 74 – 78.

[132] S. Agnihotri, S. Jaggi, and M. Chen, "Analog network coding in general SNR regime," in *Proc. IEEE ISIT*, Cambridge, MA, Jul. 2012, pp. 2052 – 2056.

[133] S. Wang, Q. Song, X. Wang, and A. Jamalipour, "Rate and power adaptation for analog network coding," *IEEE Trans. Veh. Technol.*, vol. 60, pp. 2302 – 2313, Jun. 2011.

[134] H.-M. Wang, X.-G. Xia, and Q. Yin, "Full diversity achieving analog network coding for asynchronous two-way relay networks with linear receivers," in *Proc. IEEE ICC*, Kyoto, Japan, Jun. 2011, pp. 3630 – 3637.

[135] ——, "A linear analog network coding for asynchronous two-way relay networks," *IEEE Trans. Wireless Commun.*, vol. 9, pp. 3630 – 3637, Dec. 2010.

[136] J. Laneman, D. Tse, and G. Wornell, "Cooperative diversity in wireless networks: Efficient protocols and outage behavior," *IEEE Trans. Inf. Theory*, vol. 50, pp. 3062 – 3080, Dec. 2004.

[137] Y. Li, B. Vucetic, Z. Chen, and J. Yuan, "An improved relay selection scheme with hybrid relaying protocols," in *Proc. IEEE GLOBECOM*, Washington, DC, Nov. 2007, pp. 3704 – 3708.

[138] H. Cohen, *A Course in Computational Algebraic Number Theory.* New York: Springer-Verlag, 1993.

[139] W. H. Mow, "Maximum likelihood sequence estimation from the lattice viewpoint," Master's thesis, Chinese University of Hong Kong, Jun. 1991.

[140] C. Windpassinger, R. Fischer, and J. Huber, "Lattice-reduction-aided broadcast precoding," *IEEE Trans. Commun.*, vol. 52, pp. 2057 – 2060, Dec. 2004.

[141] U. Fincke and M. Phost, "Improved methods for calculating vectors of short length in a lattice, including a complexity analysis," *Mathematics of Computation*, vol. 44, pp. 103 – 105, Apr. 1985.

[142] Y. H. Gan, C. Ling, and W. H. Mow, "Complex lattice reduction algorithm for low-complexity full-diversity mimo detection," *IEEE Trans. Signal Process.*, vol. 57, pp. 2701 – 2710, Jul. 2009.

[143] U. Niesen and P. Whiting, "The degrees of freedom of compute-and-forward," *IEEE Trans. Inf. Theory*, vol. 58, pp. 5214 – 5232, Aug. 2012.

[144] B. Hassibi and B. M. Hochwald, "How much training is needed in multiple-antenna wireless links," *IEEE Trans. Inf. Theory*, vol. 49, pp. 951 – 963, Apr. 2003.

[145] C. Feng, D. Silva, and F. Kschischang, "Blind compute-and-forward," in *Proc. IEEE ISIT*, Cambridge, MA, Jul. 2012, pp. 403 – 407.

[146] H. Yao and G. Wornell, "Lattice-reduction-aided detectors for mimo communication systems," in *Proc. IEEE Global Commun. Conf.*, Taipei, Taiwan, R.O.C., Nov. 2002, pp. 424 – 428.

[147] L.-C. Wang, W.-C. Liu, and S.-H. Wu, "Diversity-multiplexing tradeoff analysis of a cooperative network coding system," in *Proc. IEEE Sarnoff Symposium*, Princeton,US, Mar. 2009, pp. 1 – 5.

[148] G. Menghwar and C. Mecklenbrauker, "Outage performance of two users cooperative network coding," in *Proc. International Symposium on Communications and Information Technology*, Icheon,South Korea, Sep. 2009, pp. 1180 – 1184.

[149] S. Yang and R. Koetter, "Network coding over a noisy relay : a belief propagation approach," in *Proc. IEEE International Symposium on Information Theory*, Nice, France, Jun. 2007, pp. 801 – 804.

[150] M. Xiao and T. Aulin, "Optimal decoding and performance analysis of a noisy channel network with network coding," *IEEE Trans. Commun.*, vol. 57, pp. 1402 – 1412, May 2009.

[151] Y. Chen, S. Kishore, and J. Li, "Wireless diversity through network coding," in *Proc. IEEE Wireless Communications and Networking Conference*, Las Vegas, US, Apr. 2006, pp. 1681 – 1686.

[152] Y. H. Gan and W. H. Mow, "Complex lattice reduction algorithms for low-complexity MIMO detection," in *Proc. IEEE GLOBECOM*, St. Louis, MO, Dec. 2005, pp. 2953 – 2957.

[153] I. S. Gradshteyn and I. M. Ryzhik, *Table of Integrals, Series, and Products, 5th ed.* San Diego: CA: Acdemic, 1994.

[154] M. Abramowitz and I. A. Stegun, *Handbook of Mathematical Functions With Formulas, Graphs, and Mathematical Tables, 9th ed.* New York: Dover, 1970.

[155] F. Oberhettinger and L. Badii, *Tables of Laplace Transforms.* Berlin: New York: Springer-Verlag, 1973.

# Appendix A

# Proofs

## A.1 End-to-End SNR of Non-NC in the Non-Regenerative MH-TRC

The end-to-end SNR for the Non-NC scheme is

$$\gamma_{y_{\hat{v}_k}} = \frac{\prod_{l=1}^{L-1} |h_l|^2 \prod_{i=2}^{L-1} G_l^2}{\sum_{l=1}^{L-1} \sigma^2 \prod_{z=1}^{l-1} |h_z|^2 \prod_{z=2}^{l} G_z^2}. \tag{A.1}$$

Dividing both the numerator and denominator by

$$\prod_{l=1}^{L-1} \sigma^2 \prod_{i=2}^{L-1} G_l^2,$$

the numerator (signal power) is now given by

$$\mathcal{S}_{y_{\hat{v}_k}} = \prod_{l=1}^{L-1} \gamma'_l, \tag{A.2}$$

where $\gamma'_l = |h_l|^2/\sigma^2$ is the SNR of hop $l$. The denominator (noise power) can be derived as

$$
\begin{aligned}
\mathcal{N}_{y_{\hat{v}_k}} &= \frac{\sum_{l=1}^{L-1} \sigma^2 \prod_{j=1}^{i-1} |h_j|^2 \prod_{j=2}^{i} G_j^2}{\prod_{l=1}^{L-1} \sigma^2 \prod_{i=2}^{L-1} G_l^2} \\
&= \sum_{l=1}^{L-1} \frac{\sigma^2 \prod_{j=1}^{i-1} |h_j|^2 \prod_{j=2}^{i} G_j^2}{\prod_{j=1}^{L-1} \sigma^2 \prod_{j=2}^{L-1} G_j^2} \\
&= \sum_{l=1}^{L-1} \frac{\prod_{j=1}^{i-1} |h_j|^2 \prod_{j=2}^{i} G_j^2}{\prod_{j=2}^{L-1} \sigma^2 \prod_{j=2}^{L-1} G_j^2} \\
&= \sum_{l=1}^{L-1} \frac{\prod_{j=1}^{i-1} |h_j|^2 \prod_{j=2}^{i} G_j^2}{\prod_{j=2}^{i} \sigma^2 \prod_{j=i+1}^{L-1} \sigma^2 \prod_{j=2}^{i} G_j^2 \prod_{j=i+1}^{L-1} G_j^2} \\
&= \sum_{l=1}^{L-1} \frac{\prod_{j=1}^{i-1} |h_j|^2 \prod_{j=2}^{i} G_j^2}{\prod_{j=1}^{i-1} \sigma^2 \prod_{j=i+1}^{L-1} \sigma^2 \prod_{j=2}^{i} G_j^2 \prod_{j=i+1}^{L-1} G_j^2} \\
&= \sum_{l=1}^{L-1} \frac{\prod_{j=1}^{i-1} \gamma_j'}{\prod_{j=i+1}^{L-1} \prod_{j=i+1}^{L-1} G_j^2 \sigma^2} \\
&= \sum_{l=1}^{L-1} \frac{\prod_{j=1}^{i-1} \gamma_j'}{\prod_{j=i+1}^{L-1} \prod_{j=i+1}^{L-1} \frac{\sigma^2}{|h_j|^2+\sigma^2}} \\
&= \sum_{l=1}^{L-1} \frac{\prod_{j=1}^{i-1} \gamma_j'}{\prod_{j=i+1}^{L-1} \prod_{j=i+1}^{L-1} \frac{1}{\gamma_j'+1}} \\
&= \sum_{l=1}^{L-1} \prod_{j=1}^{i-1} \gamma_j' \prod_{j=i+1}^{L-1} \gamma_j' + 1.
\end{aligned} \tag{A.3}
$$

Therefore, the received SNR of $y_{\hat{v}_k}$ with the Non-NC scheme can be derived

as

$$\begin{aligned}
\gamma_{\mathrm{T},y_{\hat{v}_k}} &= \frac{\prod_{l=1}^{L-1}\gamma'_l}{\sum_{l=1}^{L-1}\prod_{j=1}^{i-1}\gamma'_j\prod_{j=i+1}^{L-1}\gamma'_j+1} \\
&= \left[\frac{\sum_{l=1}^{L-1}\prod_{j=1}^{i-1}\gamma'_j\prod_{j=i+1}^{L-1}\gamma'_j+1}{\prod_{l=1}^{L-1}\gamma'_l}\right]^{-1} \\
&= \left[\sum_{l=1}^{L-1}\frac{\prod_{j=1}^{i-1}\gamma'_j\prod_{j=i+1}^{L-1}\gamma'_j+1}{\prod_{j=1}^{i-1}\gamma'_j\prod_{j=i}^{L-1}\gamma'_j}\right]^{-1} \\
&= \left[\sum_{l=1}^{L-1}\frac{\prod_{j=i+1}^{L-1}\gamma'_j+1}{\prod_{j=i}^{L-1}\gamma'_j}\right]^{-1} \\
&= \left[\sum_{l=1}^{L-1}\frac{1}{\gamma'_l}\frac{\prod_{j=i+1}^{L-1}\gamma'_j+1}{\prod_{j=i+1}^{L-1}\gamma'_l}\right]^{-1} \\
&= \left[\sum_{l=1}^{L-1}\frac{1}{\gamma'_l}\prod_{j=i+1}^{L-1}\left(1+\frac{1}{\gamma'_j}\right)\right]^{-1},
\end{aligned} \tag{A.4}$$

which then can be rewritten to

$$\gamma_{\mathrm{T},y_{\hat{v}_k}} = \left[\prod_{l=1}^{L-1}\left(1+\frac{1}{\gamma'_l}\right)-1\right]^{-1}. \tag{A.5}$$

## A.2 CDF of the End-to-End SNR of Non-NC in the Non-Regenerative MH-TRC

A new random variable $Z$ is defined as

$$Z = \frac{1}{X} = \prod_{l=1}^{L-1} \frac{\mu_l}{\gamma'_l} \tag{A.6}$$

where $X$ is defined as $\left[\prod_{l=1}^{L-1} \frac{\mu_l}{\gamma'_l}\right]^{-1}$. Due to the independence between $\gamma'_l$, the moment generating function (MGF) of $X$ can be written just simply the product of the MGF of $Y = \mu_l/\gamma'_l$. The MGF of $Y$ can be evaluated with the aid of [153, eq. (3.471.9)] and the modified Bessel function given in [153, eq. (8.486.16)] as

$$\mathcal{M}_Y(s) = 2\sqrt{\frac{\mu_l s}{\bar{\gamma}'_l}} K_1\left(2\sqrt{\frac{\mu_l s}{\bar{\gamma}'_l}}\right). \tag{A.7}$$

Hence, the MGF of $Z$ can be given by

$$\mathcal{M}_Z(s) = \prod_{l=1}^{L-1} 2\sqrt{\frac{\mu_l s}{\gamma'_l}} K_1\left(2\sqrt{\frac{\mu_l s}{\gamma'_l}}\right). \tag{A.8}$$

The CDF of $X$ is given by

$$\begin{aligned} F_X(x) &= \Pr(X < x) = \Pr\left(\frac{1}{Z} < x\right) = \Pr\left(Z > \frac{1}{x}\right) \\ &= 1 - \Pr\left(Z < \frac{1}{x}\right) = 1 - F_Z\left(\frac{1}{x}\right) \end{aligned} \tag{A.9}$$

where $F_Z(\cdot)$ is the CDF of $Z$. Using the differentiation property of Laplace transform, $F_Z(\cdot)$ can be written as

$$F_Z(z) = \mathcal{L}^{-1}\left(\frac{\mathcal{M}_Z(s)}{s}\right). \tag{A.10}$$

where $K_1(\cdot)$ is the first order modified Bessel function of the second kind

defined in [154, eq. (9.6.22)]. The derivation of the CDF of $X$ can be shown as

$$\begin{aligned}
F_X(x)=&1-F_Z\left(\frac{1}{x}\right)\\
=&1-\mathcal{L}^{-1}\left(\frac{\mathcal{M}_X(s)}{s}\right)\\
=&1-\mathcal{L}^{-1}\left(\frac{\prod_{l=1}^{L-1}2\sqrt{\frac{\mu_l s}{\bar{\gamma}'_l}}K_1(2\sqrt{\frac{\mu_l s}{\bar{\gamma}'_l}})}{s}\right)\\
=&1-\prod_{l=1}^{L-1}2\sqrt{\frac{\mu_l}{\bar{\gamma}'_l}}\mathcal{L}^{-1}\left(\frac{1}{s}\prod_{l=1}^{L-1}\sqrt{s}K_1\left(2\sqrt{\frac{\mu_l s}{\bar{\gamma}'_l}}\right)\right)\\
=&1-\prod_{l=1}^{L-1}2\sqrt{\frac{\mu_l}{\bar{\gamma}'_l}}\left(\int_0^t\left(f_1\circledast f_2\circledast\cdots\circledast f_{L-1}\right)(\tau)d\tau\right)\\
=&1-\prod_{l=1}^{L-1}2\sqrt{\frac{\mu_l}{\bar{\gamma}'_l}}\left(\prod_{l=1}^{L-1}\int_0^t f_i(\tau)d\tau\right)\\
=&1-\prod_{l=1}^{L-1}2\sqrt{\frac{\mu_l}{\bar{\gamma}'_l}}\left(\prod_{l=1}^{L-1}\frac{1}{2}e^{-\frac{\mu_l}{t\bar{\gamma}'_l}}\sqrt{\frac{\bar{\gamma}'_l}{\mu_l}}\right)\\
=&1-\exp\left(-\sum_{l=1}^{L-1}\frac{\mu_l}{t\bar{\gamma}'_l}\right)_{|t=\frac{1}{x}}\\
=&1-\exp\left(-x\sum_{l=1}^{L-1}\frac{\mu_l}{\bar{\gamma}'_l}\right)
\end{aligned}\tag{A.11}$$

where $\mathcal{L}^{-1}(\cdot)$ denotes the inverse Laplace transform and $\circledast$ represents convolution. $f_i(\tau)$ is defined as

$$f_i(\tau)=\mathcal{L}^{-1}\left(\sqrt{s}K_1\left(2\sqrt{\frac{\mu_l s}{\bar{\gamma}'_l}}\right)\right).\tag{A.12}$$

It follows from (A.12) with the help of [155, eq. (13.42)] that

$$f_i(\tau)=2\sqrt{\frac{\mu_l}{\bar{\gamma}'_l}}(2t)^{-2}\exp\left(\frac{-\mu_l}{\bar{\gamma}'_l t}\right).\tag{A.13}$$

The CDF given by (4.49) can be obtained by substituting $\mu_l=1$ into (A.11).

## A.3 Received Linear Combinations at the User Node $N_1$ for MH-CPF

The transmission scheme of the MH-CPF is the same as the MH-WNC scheme described in Chapter 3. To solve the final linear combination for the required messages, the user nodes have to know the coefficients of each variable in the combination.

The forward recursive approach is quite straightforward, following the same procedure of deriving the received linear combinations in the 5-node 2-message MH-TRC given by (5.11) and (5.12), the received linear combinations for the MH-TRCs with small numbers of nodes and messages can be intuitively obtained. However, the complexities of the polynomials $\phi_l^j$ and $\varphi_l^j$ increase with the numbers of nodes and messages. In order to circumvent the complexity issue, the backward recursive approach was proposed in Chapter 4 to solve the noise power. The same approach can be applied here to derive the received linear combination $t_1^j$.

First, denote by $N_i^j$ the relay $N_i$ in time slot $j$. Let $w_i[j]$ be the received linear combination at $N_i^j$, which can be derived as

$$w_1[j]=t_1^{j+1}, \tag{A.14}$$

$$w_2[j]=\frac{w_1[j+1]-\vec{a}_1\hat{u}_{\frac{j+2}{2}}}{\overleftarrow{a}_1}, \tag{A.15}$$

$$w_i[j]=\frac{w_{i-1}[j+1]-\vec{a}_{i-1}w_{i-2}[j]}{\overleftarrow{a}_{i-1}}, \quad \forall i \neq 1,2, \forall j \tag{A.16}$$

and $t_1^j$ can be obtained using $w_i[j]$ as

$$\begin{aligned} t_1^j=&\vec{a}_1\hat{u}_{\frac{j}{2}}+w_1[j-3]\vec{a}_2\overleftarrow{a}_1+w_2[j-4]\vec{a}_3\overleftarrow{a}_2\overleftarrow{a}_1+...+w_{\frac{j-2}{2}}\left[\frac{j-2}{2}\right]\vec{a}_{\frac{j}{2}}\overleftarrow{a}_{\frac{j}{2}-1}\overleftarrow{a}_{\frac{j}{2}-2}...\overleftarrow{a}_1 \\ =&\vec{a}_1\hat{u}_{\frac{j}{2}}+\sum_{i=1}^{\frac{j-2}{2}}w_i[j-(i+2)]\vec{a}_{i+1}\prod_{l=1}^{i}\overleftarrow{a}_l. \end{aligned} \tag{A.17}$$

For instance, the received linear combination $t_1^{10}$ can be given by

$$\begin{aligned}
t_1^{10} &= \vec{a}_1\hat{u}_5 + \sum_{i=1}^{4} w_i[10-(i+2)]\vec{a}_{i+1}\prod_{l=1}^{i}\overleftarrow{a}_l \\
&= \vec{a}_1\hat{u}_5 + w_1[7]\vec{a}_2\overleftarrow{a}_1 + w_2[6]\vec{a}_3\overleftarrow{a}_2\overleftarrow{a}_1 + w_3[5]\vec{a}_4\overleftarrow{a}_3\overleftarrow{a}_2\overleftarrow{a}_1 + w_4[4]\vec{a}_5\overleftarrow{a}_4\overleftarrow{a}_3\overleftarrow{a}_2\overleftarrow{a}_1 \\
&= \vec{a}_1\hat{u}_5 + t_1^8\vec{a}_2\overleftarrow{a}_1 + \frac{t_1^8-\vec{a}_1\hat{u}_4}{\overleftarrow{a}_1}\vec{a}_3\overleftarrow{a}_2\overleftarrow{a}_1 \\
&\quad + \frac{w_2[6]-\vec{a}_2w_1[5]}{\overleftarrow{a}_2}\vec{a}_4\overleftarrow{a}_3\overleftarrow{a}_2\overleftarrow{a}_1 + \frac{\frac{w_2[6]-\vec{a}_2w_1[5]}{\overleftarrow{a}_2}-\vec{a}_3w_2[4]}{\overleftarrow{a}_3}\vec{a}_5\overleftarrow{a}_4\overleftarrow{a}_3\overleftarrow{a}_2\overleftarrow{a}_1 \\
&= \vec{a}_1\hat{u}_5 + t_1^8\vec{a}_2\overleftarrow{a}_1 + (t_1^8-\vec{a}_1\hat{u}_4)\vec{a}_3\overleftarrow{a}_2 \\
&\quad + \frac{\frac{t_1^8-\vec{a}_1\hat{u}_4}{\overleftarrow{a}_1}-\vec{a}_2\hat{u}_1[6]}{\overleftarrow{a}_2}\vec{a}_4\overleftarrow{a}_3\overleftarrow{a}_2\overleftarrow{a}_1 + \frac{\frac{t_1^8-\vec{a}_1\hat{u}_4}{\overleftarrow{a}_1}-\vec{a}_2\hat{u}_1[6]}{\overleftarrow{a}_2}-\vec{a}_3\frac{t_1^6-\vec{a}_1\hat{u}_3}{\overleftarrow{a}_1}}{\overleftarrow{a}_3}\vec{a}_5\overleftarrow{a}_4\overleftarrow{a}_3\overleftarrow{a}_2\overleftarrow{a}_1 \\
&= \vec{a}_1\hat{u}_5 + t_1^8\vec{a}_2\overleftarrow{a}_1 + (t_1^8-\vec{a}_1\hat{u}_4)\vec{a}_3\overleftarrow{a}_2 + (t_1^8-\vec{a}_1\hat{u}_4)\vec{a}_4\overleftarrow{a}_3 \\
&\quad - t_1^6\vec{a}_4\overleftarrow{a}_3\vec{a}_2\overleftarrow{a}_1 + (t_1^8-\vec{a}_1\hat{u}_4)\vec{a}_5\overleftarrow{a}_4 - t_1^6\vec{a}_5\overleftarrow{a}_4\vec{a}_2\overleftarrow{a}_1 - (t_1^6-\vec{a}_1\hat{u}_3)\vec{a}_5\overleftarrow{a}_4\vec{a}_3\overleftarrow{a}_2 \\
&= \vec{a}_1\hat{u}_5 + t_1^8a_2^2 + (t_1^8-\vec{a}_1\hat{u}_4)a_3^2 + (t_1^8-\vec{a}_1\hat{u}_4)a_4^2 \\
&\quad - t_1^6a_4^2a_2^2 + (t_1^8-\vec{a}_1\hat{u}_4)a_5^2 - t_1^6a_5^2a_2^2 - (t_1^6-\vec{a}_1\hat{u}_3)a_5^2a_3^2,
\end{aligned}$$

which consists of the linear combinations of $t_1^6$ and $t_1^8$, where $a_i^2 = \vec{a}_i\overleftarrow{a}_{i-1}$. The number of the linear combinations used for deriving $t_1^j$ is $\lfloor\frac{j}{4}\rfloor$, where $\lfloor x\rfloor$ is the largest integer no more than $x$.

Furthermore, $t_1^{10}$ in (A.18) can be simplified to

$$\begin{aligned}
t_1^{10} =& \vec{a}_1\hat{u}_5 + t_1^8a_2^2 - t_1^6(a_2^2a_4^2 + a_2^2a_5^2) + (t_1^8-\vec{a}_1\hat{u}_4)\sum_{i=3}^{5}a_i^2 - (t_1^6-\vec{a}_1\hat{u}_3)a_3^2a_5^2 \\
=& \vec{a}_1\hat{u}_5 + \sum_{i=1}^{2}\left[(-1)^{i-1}\left(\overset{i}{\underset{K=1,l_1=2}{\boxtimes}}\Phi(5)\right)t_1^{10-2i}\right] \\
&+ \sum_{i=1}^{2}\left[(-1)^{i-1}\left(\overset{i}{\underset{K=1,l_1=3}{\boxtimes}}\Phi(5)\right)\left(t_1^{10-2i}-\vec{a}_1\hat{u}_{\frac{10-2i}{2}}\right)\right], \qquad \text{(A.18)}
\end{aligned}$$

where $\overset{i}{\underset{K=1,l_1=m}{\boxtimes}}\Phi(l_K) \triangleq \sum_{l_1=m}^{l}a_{l_1}^2\left(\sum_{l_2=l_1+2}^{l}a_{l_2}^2\left(\ldots\left(\left(\ldots\sum_{l_K=l_{K-1}+2}^{l}a_{l_K}^2\right)\right)\right)\right)$.

Following this approach, the received linear combinations $t_1^j$ can be obtained as given by (5.16) and (5.17).